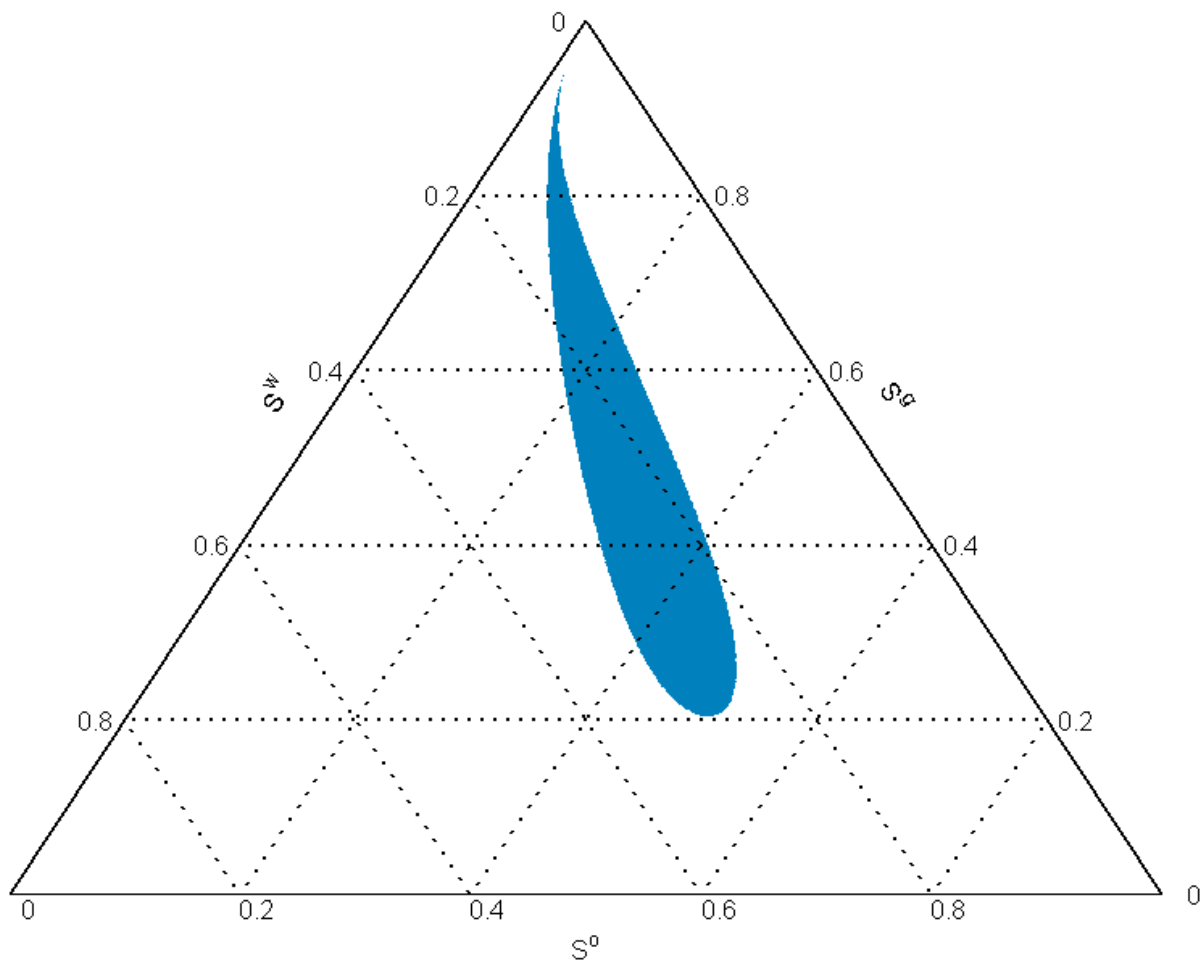# Elliptic regions in porous media flow

Effect of relative permeability on loss of strict hyperbolicity in three-phase porous media flow

A.S. Markensteijn

# Elliptic regions
# in porous media flow

## Effect of relative permeability on loss of strict hyperbolicity in three-phase porous media flow

by

# A.S. Markensteijn

A thesis submitted to the
Delft Institute of Applied Mathematics
at the faculty EEMCS of the TU Delft
in partial fulfilment of the requirements

for the degree

## MASTER OF SCIENCE

## in

## APPLIED MATHEMATICS

in the specialisation of Computational Science and Engineering,
to be defended publicly on September 28, 2016.

Delft, The Netherlands
September 2016

**TU**Delft
Delft
University of
Technology

# Elliptic regions in porous media flow

Effect of relative permeability on loss of strict hyperbolicity in three-phase porous media flow

by

## A.S. Markensteijn

Abstract: Reservoir simulation is a widely used means for prediction and optimization of oil recovery from a reservoir and it is based on the multiphase porous media flow model. For one dimensional, incompressible, immiscible three-phase flow in a homogeneous medium without gravity and capillary pressure, loss of strict hyperbolicity can occur for certain relative permeability models causing problems when solving the three-phase flow model numerically. To avoid loss of strict hyperbolicity, a set of three curves is used to determine the existence of an elliptic region and modelling three-phase relative permeability is seen as an interpolation problem between two two-phase relative permeabilities. This results in a new type of three-phase relative permeability model where the relative permeabilities of all three phases depend on both the water and gas saturation. The new relative permeability models are able to avoid loss of strict hyperbolicity in some cases where the existing relative permeability models resulted in an elliptic region, however, the new relative permeability models do not guarantee strict hyperbolicity for all situations. This leads to the view that a relative permeability model must be chosen for each situation separately.

Keywords: Elliptic region, loss of strict hyperbolicity, three-phase porous media flow, three-phase relative permeability, system of conservation laws of mixed type

**TU**Delft
Delft
University of
Technology

# Preface

Before you lies my master thesis, the summary of my work of the past nine months. During these nine months I learned that there is always a new line of investigation to be found if the previous one leads to a dead end. This project also showed me the richness of systems of conservation laws and Riemann problems and it helped me appreciate the complexity that non-linearity brings to a problem.

I would like to thank my supervisors Johan Romate and Cor van Kruijsdijk for giving me the opportunity to conduct my research and write my thesis at Shell and for helping me see the practical value of some of the more abstract results. And, I would like to thank Johan for always taking the time and having the patience to answer all my questions. I would also like to thank the other colleagues and interns at Shell for making me feel welcome and helping me with my project

Naturally, I would like to thank my family and friends for supporting me during these nine months. Special thanks go to Wouter for always helping me when I came home frustrated because things did not go as fast I wanted or because the results were not what I would have liked them to be.

Finally, I would like to thank you, the reader, for taking the time and effort to read my thesis. I hope you can find the same enthusiasm about loss of strict hyperbolicity as I developed during the course of the project.

*A.S. Markensteijn*
*September 20, 2016*

# Contents

# List of Figures

# Nomenclature

**Abbreviations**

| | |
|---|---|
| *R* | Rarefaction wave |
| *S* | Shock wave |
| *SR* | Shock-rarefaction wave |
| BL | Buckley-Leverett |
| EOR | Enhanced oil recovery. |
| FIM | Fully implicit method. |
| G | Gas |
| O | Oil |
| OG | Oil-gas |
| OW | Oil-water |
| W | Water |
| WG | Water-gas |

**Greek symbols**

| | | |
|---|---|---|
| $\eta$ | Eigenvalue of the Jacobian matrix of the linearized fractional flow equations. | |
| $\lambda$ | Mobility | $\frac{\mathrm{m\,s}}{\mathrm{kg}}$ |
| $\mu$ | Viscosity | $\frac{\mathrm{kg}}{\mathrm{m\,s}}$ |
| $\phi$ | Rock porosity | |
| $\rho$ | Density | $\frac{\mathrm{kg}}{\mathrm{m}^3}$ |
| $\sigma$ | Speed of shock wave | |

**Roman symbols**

| | | |
|---|---|---|
| R | Radius of the circle used for interpolation II. | |
| *A* | Phase accumulation | kg |
| *c* | Grid cell | |
| *D* | Diffusion of viscosity term. | |
| *F* | Flux function of FIM | |
| *f* | Fractional flow function | |
| *J* | Jacobian matrix | |
| *K* | Absolute permeability | $\mathrm{m}^2$ |
| $K_r$ | Endpoint of the relative permeability for a Corey-correlation. | |

| | | |
|---|---|---|
| $k_r$ | Relative permeability | |
| $N$ | Total number of grid cells | |
| $n$ | Corey-coefficient | |
| $p$ | Pressure | Pa |
| $R$ | Residual | |
| $r$ | Right eigenvector of the Jacobian matrix of the linearized fractional flow equations. | |
| $S$ | Saturation | |
| $S_{org}$ | Residual oil saturation in a water-gas system. | |
| $S_{orw}$ | Residual oil saturation in a water-oil system. | |
| $S_{or}$ | Residual oil saturation | |
| $S_{wc}$ | Connate or residual water saturation | |
| $T$ | Saturation triangle or ternary diagram | |
| $V$ | Volume | $m^3$ |
| $v$ | Velocity | $\frac{m}{s}$ |
| $Y$ | Primary variables of FIM | |

**Superscripts**

| | |
|---|---|
| $\alpha$ | Phase $\alpha$. Either o for oil, w for water or g for gas. |
| $\alpha_1 \alpha_2$ | Phase $\alpha_1$ in a $\alpha_1$-$\alpha_2$ system. |
| $g$ | Gas phase |
| $I$ | Interpolation I |
| $II$ | Interpolation II |
| $III$ | Interpolation III |
| $k$ | Iteration index of Netwon-Rapshon. |
| $n$ | Discrete time level |
| $o$ | Oil phase |
| $T$ | Transpose |
| $w$ | Water phase |

**Subscripts**

| | |
|---|---|
| $\alpha$ | Partial differentiation with respect to the saturation $S$ of phase $\alpha$, which is either o for oil, w for water or g for gas. |
| $\alpha_1 \alpha_2$ | Phase $\alpha_1$ in a $\alpha_1$-$\alpha_2$ system. |
| $d$ | Downstream state |
| $f$ | Fast-family |
| $i$ | Index of grid cell. |
| $m$ | Middle state |

$p$                     Family $p$. Either $f$ for fast-family or $s$ for slow-family.

$s$                     Slow-family

$T$                     Total, i.e. the sum over all phases.

$t$                     Partial differentiation with respect to time $t$.

$u$                     Upstream state

$x$                     Partial differentiation with respect to space $x$.

$p$                     Family $p$. Either $f$ for fast-family or $s$ for slow-family.

$s$                     Slow-family

$T$                     Total, i.e. the sum over all phases.

# 1

# Introduction

Reservoir simulation is a widely used means for prediction and optimization of oil recovery from a reservoir. The reservoir simulators are based on multiphase porous media flow models which describe the flow of a gaseous phase, an aqueous phase and a hydrocarbon phase through porous rock. These models are based on conservation of mass of the fluids and on a generalization of Darcy's law from one phase to multiphase. This extension of Darcy's law is of questionable validity and requires the use of a relative permeability, which describes the interaction between a phase and the rock and describes how easily a phase can flow through the rock in presence of other phases. When there are only two phases present, relative permeability can be measured relatively easy and mathematical models used in general are satisfactory and perform well. On the other hand, measuring three-phase relative permeabilities is complicated, time consuming and expensive (Alizadeh and Piri, 2014). This means that three-phase relative permeability data is scarce and that in general relative permeabilities are modelled. The way this is done greatly influences the resulting multiphase porous media flow model and, in contrast to two-phase flow, incorrectly modelling the relative permeability can lead to an ill-posed multiphase flow model and to subsequent simulation problems. The cause of this ill-posedness is the loss of strict hyperbolicity of the linearized system which is characterized by the existence of an elliptic region or an umbilic point in the linearized system. In general, loss of strict hyperbolicity is considered to be an unwanted feature of a three-phase porous media flow model, as the resulting nature of the solution is deemed unphysical. Hence, it seems reasonable to investigate how loss of strict hyperbolicity can be avoided.

Usually, water or gas is injected into the reservoir in order to displace the oil towards the producer well. In enhanced oil recovery (EOR) other materials are injected into the reservoir, see e.g. Lake et al. (2014) for examples of the materials used. These materials change properties of the phases present in the reservoir and change how the phases interact with the rock. This means that the relative permeability can change drastically throughout the reservoir, making it especially important in EOR to model the relative permeabilities correctly in order to avoid loss of strict hyperbolicity.

A lot of research has already been done concerning the effect of the relative permeability model on the strict hyperbolicity of the linear system. Bell et al. (1986) showed that an elliptic region can exist for a Stone-type relative permeability model, i.e. if the oil relative permeability depends on both the water and gas saturations, when gravity and capillary pressure are ignored and that the system with capillary pressure is weakly stable. Fayers (1989) derived sufficient conditions on the fractional flow functions for the system to be strictly hyperbolic when using Stone-type models. Trangenstein (1989) showed that a system including gravity is hyperbolic if and only if the relative permeability model is of Corey-type, i.e if the relative permeability of a phase only depends on the saturation of that phase. He also showed that for Stone-type models, given viscosity, it is always possible to find density and gravity coefficients such that the linear system with gravity has an elliptic region. Shearer and Trangenstein (1989) showed that a system without gravity and capillary pressure has at least one point inside the saturation triangle for which the system is non-strictly hyperbolic when using a certain class of Stone-type models. They also showed that every corner of the saturation triangle is an umbilic point for the relative permeabilities they consider. Falls and Schulte (1992) showed that loss of hyperbolicity can only occur in the region where all three phases are mobile, i.e. for one- and two-phase flow the system is strictly hyperbolic for all saturations. Juanes and Patzek (2004a) derived necessary conditions

for the three-phase relative permeability on the edges of the saturation triangle for the system to be strictly hyperbolic everywhere inside the saturation triangle. They also gave an example of a relative permeability model for which the system is indeed strictly hyperbolic for all saturations. Despite all this research a relative permeability model that results in a strictly hyperbolic system while at the same time matching all available data has still not been found and commonly used three-phase relative permeability models generally give rise to loss of strict hyperbolicity. Therefore the question is how loss of strict hyperbolicity can be recognized, but more importantly the question still remains whether loss of strict hyperbolicity can be avoided by choosing the right relative permeability model.

This thesis is structured as follows. In the rest of this chapter the mathematical model describing three-phase porous media flow is derived. In Chapter 2 the solution to the Buckley-Leverett problem, which describes two-phase porous media flow, is given. In Chapter 3 three-phase flow and the occurrence of loss of strict hyperbolicity is discussed. Furthermore, the effect of loss of strict hyperbolicity on the numerical solution is investigated. In Chapter 4 multiple existing three-phase relative permeability models are discussed and three new models are introduced. In Chapter 5 the construction of the Riemann solution for strictly hyperbolic three-phase flow models is described and the issues with this construction when loss of strict hyperbolicity occurs are discussed. In Chapter 6 the effect of the new three-phase relative permeability models on the occurrence of loss of strict hyperbolicity is investigated. Numerical experiments to investigate the effect of the new relative permeability models on the numerical solution of the three-phase porous media flow model are given in Chapter 7. Finally, the conclusions are given and discussed in Chapter 8.

## 1.1. Multiphase porous media flow model

Reservoir simulators model the flow of multiple phases through a reservoir. Most of these simulators are designed to be able to model a wide variety of problems, e.g. a different number of phases or dimensions, or a heterogeneous medium. However, in this thesis a simple one dimensional homogeneous reservoir with an injection well at one side of the reservoir and a production well at the other end of the reservoir will be looked at, see Figure 1.1. Inside the reservoir, the flow is described by a multiphase porous media flow model. For
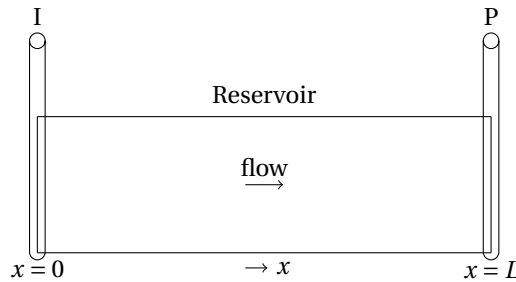


Figure 1.1: Simple reservoir with one injection well I at the left and one production well P at the right. The direction of flow is from the injector to the producer.

the simplified one dimensional model considered in this thesis, the direction of flow will always be from the injector to the producer, i.e. there is no back flow, and the injector can be identified as upstream and the producer as downstream. The boundary conditions enter the multiphase flow model by assuming a constant total flow rate throughout the entire reservoir, including the injector well and the producer well. Therefore, a constant injection rate and an equal constant production rate will be assumed.

The equations governing three phase flow in a porous medium are derived from conservation of mass and from an extension of Darcy's law. For a more detailed derivation of the governing equation than the one given below see e.g. Aziz and Settari (1979). One dimensional, immiscible incompressible flow of three phases - oil, water and gas - in a homogeneous porous medium will be assumed. Furthermore, the effects due to gravity and capillary pressure will be ignored. For one dimensional, immiscible flow without gravity and capillary pressure the conservation of mass for each phase is given by:

$$\frac{\partial \phi \rho^\alpha S^\alpha}{\partial t} + \frac{\partial}{\partial x}\left(\rho^\alpha v^\alpha\right) = 0 \quad \text{for } \alpha \in \{o, w, g\} \tag{1.1}$$

Here, $\phi$ is the rock porosity and $\rho^\alpha$ is the density of phase $\alpha$. $S^\alpha$ is the saturation of phase $\alpha$ which is defined as the the volume fraction of pores in the medium occupied by phase $\alpha$. Finally, $v^\alpha$ is the velocity of phase $\alpha$ which is defined as the volume of phase $\alpha$ flowing per unit time and per unit area. Since incompressible flow is assumed the density for each phase is constant and assuming constant rock porosity the conservation of mass can be rewritten as:

$$\phi \frac{\partial S^\alpha}{\partial t} + \frac{\partial}{\partial x}\left(v^\alpha\right) = 0 \quad \text{for } \alpha \in \{o, w, g\} \tag{1.2}$$

Darcy's law was originally determined experimentally for the flow of one phase, namely water, through sand and gives the relation between flow rate and the pressure difference. It is the equivalent of Fick's law for diffusion and Fourier's law for heat conduction. Darcy's law can be extended from one phase to multiphase flow by introducing a relative permeability $k_r^\alpha$ for each phase $\alpha$. This extension is given by:

$$v^\alpha = -\frac{K k_r^\alpha}{\mu^\alpha} \frac{\partial p^\alpha}{\partial x} \quad \text{for } \alpha \in \{o, w, g\} \tag{1.3}$$

where $\mu^\alpha$ is the viscosity of phase $\alpha$ and $p^\alpha$ is the pressure of phase $\alpha$. $K$ is the absolute permeability which is assumed to be independent of the phase and which is the permeability of the porous medium in single-phase flow. Finally $k_r^\alpha$ is the relative permeability of phase $\alpha$ which determines how easily a phase flows through the medium. Relative permeability is a dimensionless number between 0 and 1. The higher the relative permeability the easier the phase will flow. If the relative permeability of a phase is zero that phase can no longer flow and the phase is called immobile.

It will be assumed that the available pore space in the porous medium is completely filled, meaning that:

$$S^o + S^w + S^g = 1 \tag{1.4}$$

Due to this relation, every saturation triple $(S^w, S^o, S^g)$ can be expressed as a saturation pair $(S^w, S^g)$ and it can be represented in a ternary diagram or saturation triangle $T$ given by:

$$T = \left\{(S^w, S^g) \quad | \quad S^w \in [0, 1], S^g \in [0, 1], S^w + S^g \leq 1\right\} \tag{1.5}$$

A general ternary diagram is depicted in Figure 1.2. Note that on the edges of the ternary diagram the saturation of one of the phases will be zero, meaning that the edges of the ternary diagram represent two-phase flow. Similarly, in the corners of the ternary diagram only one phase is present. Since capillary pressure is
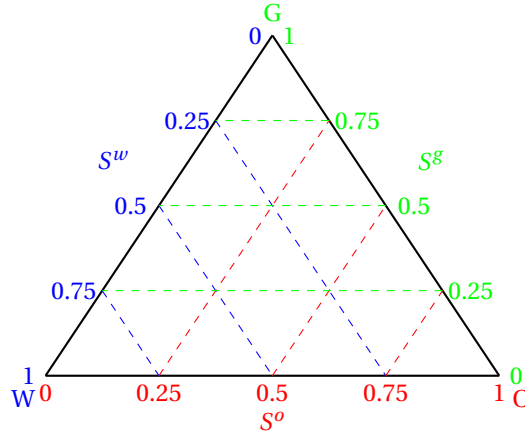


Figure 1.2: Ternary diagram. The corners represent points in the saturation space where only one phase is present. On the edge of the triangle opposite a corner, the saturation of that phase is zero and only the other two phases are present. Along the dashed lines the saturation of one of the phases is constant, e.g. along the blue lines the water saturation is constant.

ignored the pressure of each phase is the same, i.e. $p^o = p^w = p^g \equiv p$. Summing the conservation of mass (1.2) over all three phases and using Darcy's law (1.3) and equation (1.4) leads to the pressure equation or flow equation:

$$\frac{\partial v_T}{\partial x} = \frac{\partial}{\partial x}\left(-K\lambda_T \frac{\partial p}{\partial x}\right) = 0 \tag{1.6}$$

Here, $v_T = v^o + v^w + v^g$ is the total velocity and $\lambda_T = \lambda^o + \lambda^w + \lambda^g$ is the total mobility with $\lambda^\alpha := \frac{k_r^\alpha}{\mu^\alpha}$ the mobility of phase $\alpha$. From the pressure equation (1.6) it follows that $v_T$ is a function of time only, i.e. $v_T$ is constant in space. For the analysis in this thesis $v_T$ will be assumed constant in time as well. This means that the pressure equation reduces to:

$$v_T = -K\lambda_T \frac{\partial p}{\partial x} \tag{1.7}$$

Using Darcy's law (1.3), the conservation of mass (1.2) can be rewritten to obtain the saturation equation or transport equation:

$$\phi \frac{\partial S^\alpha}{\partial t} - \frac{\partial}{\partial x}\left(K\lambda^\alpha \frac{\partial p}{\partial x}\right) = 0 \quad \text{for } \alpha \in \{o, w, g\} \tag{1.8}$$

Substituting the expression of the total velocity (1.7) in the saturation equation (1.8) and using equation (1.4) to eliminate the equation for oil the fractional flow equations are obtained:

$$\begin{cases} \phi \frac{\partial S^w}{\partial t} + v_T \frac{\partial f^w}{\partial x} = 0 \\ \phi \frac{\partial S^g}{\partial t} + v_T \frac{\partial f^g}{\partial x} = 0 \end{cases} \tag{1.9}$$

where $f^\alpha := \frac{\lambda^\alpha}{\lambda_T}$ is the fractional flow of phase $\alpha$. Note that the fractional flows of all phases sum up to one, i.e. $\sum_\alpha f^\alpha = 1$. Rewriting the fractional flow equation (1.9) in matrix form results in the following $2 \times 2$ system:

$$S_t + \frac{v_T}{\phi} f_x = 0 \tag{1.10}$$

with $S = \left(S^w\ S^g\right)^T$ and $f = \left(f^w\ f^g\right)^T$, where $[\cdot]^T$ denotes the transpose. In general, the relative permeabilities are non-linear functions of the saturation of one or two phases, meaning that the system (1.10) is non-linear. System (1.10) can be linearized to obtain the quasilinear form:

$$S_t + \frac{v_T}{\phi} \frac{\partial f}{\partial S} S_x = 0 \tag{1.11}$$

with $\frac{\partial f}{\partial S}$ the Jacobian matrix given by:

$$\frac{\partial f}{\partial S} := \begin{pmatrix} f_w^w & f_g^w \\ f_w^g & f_g^g \end{pmatrix} = \frac{1}{\lambda_T^2} \begin{pmatrix} \lambda_T \lambda_w^w - \lambda^w \lambda_{T,w} & \lambda_T \lambda_g^w - \lambda^w \lambda_{T,g} \\ \lambda_T \lambda_w^g - \lambda^g \lambda_{T,w} & \lambda_T \lambda_g^g - \lambda^g \lambda_{T,g} \end{pmatrix} \tag{1.12}$$

Here, $[\cdot]_{\alpha_2}^{\alpha_1}$ is used to denote $\frac{\partial [\cdot]^{\alpha_1}}{\partial S^{\alpha_2}}$ with $\alpha_1, \alpha_2 \in \{w, g\}$ and $\lambda_{T,\alpha}$ is used to denote $\frac{\partial \lambda_T}{\partial S^\alpha}$ with $\alpha \in \{w, g\}$. The fractional flow equation (1.10) can be made dimensionless by introducing the dimensionless time $t$ and dimensionless space $x$ given by:

$$t = \frac{v_t}{L\phi} t_D \quad x = \frac{x_D}{L} \tag{1.13}$$

where $L$ is the length of the reservoir, $t_D$ is the time with dimension and $x_D$ is space with dimension. The dimensionless form of the fractional flow equation is then given by:

$$S_t + f_x = 0 \tag{1.14}$$

In the same way, the dimensionless quasilinear form of the fractional flow equation is given by:

$$S_t + \frac{\partial f}{\partial S} S_x = 0 \tag{1.15}$$

This dimensionless linearized system will be used to investigate the loss of strict hyperbolicity in chapter 3 and the structure of the solutions in chapter 5. To help understand the behavior of the numerical solutions to the three-phase flow problem, two-phase porous media flow will first be discussed.

# 2

# Two-phase flow through porous media

The analytical solution to the two-phase porous media flow problem with Riemann initial data was first obtained by Buckley and Leverett. An oil-water system will be considered, but the same analysis holds for any two-phase system. This means the gas saturation will be assumed zero and that the water and oil saturations sum up to one, i.e. $S^w + S^o = 1$. Therefore, the gas equation can be removed from the dimensionless fractional flow equations (1.15) leaving only one equation to describe two-phase flow:

$$S^w + f_w^w S^w = 0 \tag{2.1}$$

with $f_w^w = \frac{\partial f^w}{\partial S^w}$. This equation is known as the Buckley-Leverett (BL) equation.

## 2.1. Two-phase relative permeability

In order to obtain a solution for the Buckley-Leverett equation, the fractional flow function $f^w$ must be specified. Recall from Section 1.1 that the fractional flow function is defined as the ratio between the phase mobility and the total mobility such that $f^w = \frac{\lambda^w}{\lambda_T}$ with the mobility given by $\lambda^\alpha = \frac{k_r^\alpha}{\mu^\alpha}$ and $\lambda_T = \lambda^w + \lambda^o$, so by specifying the relative permeability for both oil and water the fractional flow function will be specified.

Relative permeability is the representation of pore-level displacement physics, fluid-fluid properties and rock-fluid properties (Alizadeh and Piri, 2014; Juanes and Patzek, 2004a; Lake et al., 2014). An example of such a property is wettability, which describes the degree to which a liquid maintains contact with a solid surface. When looking at two-phase flow the endpoint of the relative permeability of the wetting phase will in general be smaller than the endpoint of the non-wetting phase (Lake et al., 2014). The pore-level displacement physics, fluid-fluid properties and rock-fluid properties determine the shape of the relative permeability curve. Relative permeabilities are usually modelled as functions of saturation alone and the effect of the fluid-fluid properties, rock-fluid properties and pore-scale physics on the shape of the curve is incorporated through one or more parameters. The most used model for two-phase relative permeabilities is a Corey-correlation, which is an empirical model and for a water-oil system it is given by (Lake et al., 2014):

$$
\begin{aligned}
k_r^w(S^w) &= K_r^w \left( \frac{S^w - S_{wc}}{1 - S_{wc} - S_{or}} \right)^{n_w} \\
k_r^o(S^w) &= K_r^o \left( \frac{1 - S^w - S_{or}}{1 - S_{wc} - S_{or}} \right)^{n_o}
\end{aligned}
\tag{2.2}
$$

Here, $k_r^w$ and $k_r^o$ are the relative permeabilities of water and oil respectively, $K_r^w$ and $K_r^o$ are the endpoints of the relative permeabilities, $n_w$ and $n_o$ are the Corey-coefficients, $S_{wc}$ is the connate water saturation and $S_{or}$ is the residual oil saturation. Typical relative permeabilities for a water-oil system are shown in Figure 2.1a. From equation (2.2) it follows that using Corey-correlation results in a fractional flow function of water that is a function of the water saturation only. In general the fractional flow function shows an S-shape which is also the case when using a Corey-correlation for the relative permeability, see Figure 2.1b.

(a) Relative permeabilities                                      (b) Fractional flow function
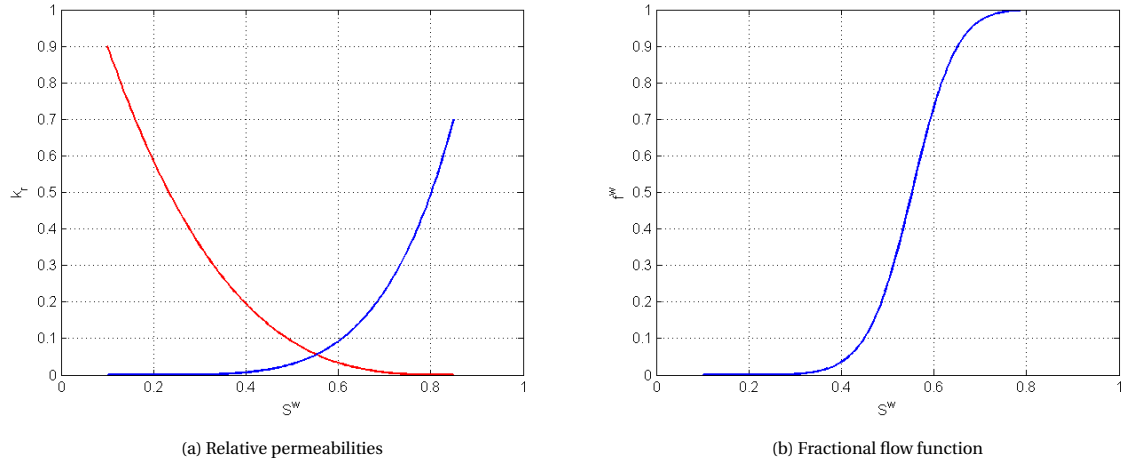
Figure 2.1: Typical relative permeabilities (a) for water (blue) and oil (red) for a water-oil system and corresponding typical fractional flow function for water (b).

## 2.2. Buckley-Leverett problem

In order to find a solution $S^w(x, t)$ to the BL equation (2.1) an initial condition must be specified, for which Riemann initial data will be used. This means that the saturation is assumed constant throughout the entire reservoir and that from time $t = 0$ water is injected at a constant rate at position $x$ is zero:

$$S^w(x,0) = \begin{cases} S_u^w & \text{if } x < 0 \\ S_d^w & \text{if } x > 0 \end{cases} \tag{2.3}$$

Here, $S_u^w$ is the upstream or injection state and $S_d^w$ is the downstream or reservoir state. Looking at the BL equation it can be seen that it is the quasilinear form of a scalar conservation law with the fractional flow function as flux function (LeVeque, 2002). If the fractional flow function $f^w$ would be convex or concave, i.e. if $f_{ww}^w = \frac{\partial^2 f^w}{\partial S^{w2}}$ would have the same sign for all $0 \leq S^w \leq 1$, the solution is straightforward and can be obtained using the method of characteristics. Depending on the sign of $f_{ww}^w$ and on whether $S_u^w > S_d^w$ or $S_u^w < S_d^w$ the solution consists of either a rarefaction wave traveling with speed $f_w^w(S)$ or a shock wave from $S_u^w$ to $S_d^w$ (LeVeque, 2002). Nonlinear scalar conservation laws for which the flux function is convex or concave are called genuinely nonlinear problems. The difficulty with the BL problem arises from the fact that the
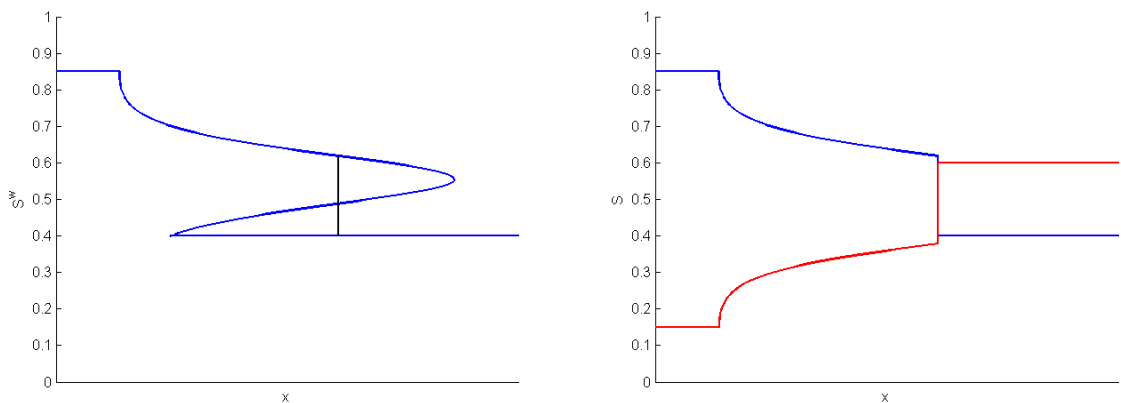


(a) Triple valued solution $S^w(x, t)$ for a certain time $t > 0$. The triple valued solution is shown in blue and the shock that replaces it is shown in black.

(b) Buckley-Leverett solution for a certain time $t > 0$. The oil saturation is shown in red and the water saturation is shown in blue.

Figure 2.2: Triple valued solution (a) and Buckley-Leverett solution (b) of the two-phase porous media flow model with Riemann initial data for a certain time $t > 0$.

fractional flow function is S-shaped and is therefore not convex or concave but contains an inflection point.

At the inflection point the derivative of the fractional flow function has a maximum, meaning that the second derivative changes sign. Nonlinear scalar conservation laws for which the flux function has one or more inflection points are called non-genuinely nonlinear problems. The method of characteristics fails for non-genuinely nonlinear problem. To see this, suppose that the inflection point occurs at $S^w = S^{\text{infl}}$ such that $f^w_{ww}(S^{\text{infl}}) = 0$. If $S^w_u, S^w_d < S^{\text{infl}}$ or $S^w_u, S^w_d > S^{\text{infl}}$ the problem behaves as if it is genuinely nonlinear and the solution consists of either a shock wave or rarefaction wave. If however $S^w_u < S^{\text{infl}} < S^w_d$ or $S^w_u > S^{\text{infl}} > S^w_d$ the method of characteristics would result in a triple valued solution since $f^w_w$ has a maximum at $S^{\text{infl}}$ (LeVeque, 2002). This triple valued part of the solution is not physical and is replaced by a shock, see Figure 2.2a. For the example shown in Figure 2.2a the relative permeabilities and fractional flow function as shown in Figure 2.1 are used and as reservoir state $S^w_d = 0.4$ is assumed and pure water is injected. From Figure 2.1a it follows that the residual oil saturation is $S_{or} = 0.15$, which means that the upstream state will be $S^w_u = 0.85$ even though pure water is injected. Replacing the triple valued part of the solution by a shock wave results in the solution as shown in Figure 2.2b. From this figure it can be concluded that the solution to the Buckley-Leverett problem, when looking from downstream to upstream, consists of a shock wave directly followed by a rarefaction wave simply called a shock-rarefaction wave. Such a combination of a shock and a rarefaction is called a composite wave.

### 2.2.1. Convex-hull construction
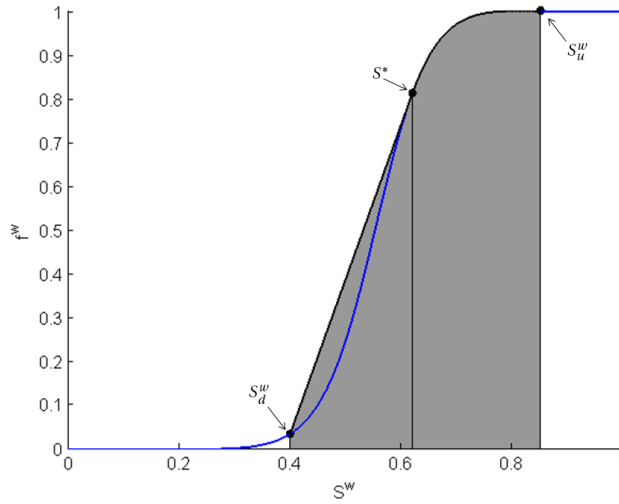


Figure 2.3: The convex-hull (grey) of the water fractional flow function (blue) from the downstream state $S^w_d$ (left black point) to the upstream state $S^w_u$ (right black point). The middle black point gives the state $S^*$ just after the shock.

The complete BL solution, including the correct shock to replace the region where the solution becomes triple valued, can be constructed using the convex-hull of the fractional flow function, see Figure 2.3. The convex-hull is the smallest convex set containing the set $\{(S^w, F) \mid S^w_d \le S^w \le S^w_u, F \le f^w(S^w)\}$ (LeVeque, 2002). The shock wave must be a weak solution of the BL equation (2.1) and to determine if it is a physically admissible solution it must satisfy an entropy condition. For non-genuinely nonlinear scalar conservation laws this admissibility condition was determined by Oleinik and is an extension of the Lax entropy condition, which is used for genuinely nonlinear problems (LeVeque, 2002). A weak solution $S(x, t)$ of the BL equation satisfies the Oleinik entropy condition if:

$$\frac{f^w(S) - f^w(S^w_l)}{S - S^w_l} \ge \sigma \ge \frac{f^w(S) - f^w(S^w_r)}{S - S^w_r} \tag{2.4}$$

for all $S$ between $S_l$ and $S_r$. Here, $S_l$ is the state directly behind the discontinuity and $S_r$ the state directly before the discontinuity and $\sigma$ is the speed of the discontinuity $S(x, t)$, which is given by the Rankine-Hugoniot condition (LeVeque, 2002):

$$\sigma = \frac{f^w(S_r) - f^w(S_l)}{S_r - S_l} \tag{2.5}$$

Since in the BL solution the shock wave is directly followed by the rarefaction wave, the speed of both waves at the point where the two waves connect must be equal. Denoting the saturation where they join by $S^*$ and using that the speed of the rarefaction wave is equal to $f_w^w$ this means that:

$$f_w^w(S^*) = \sigma = \frac{f^w(S^*) - f^w(S_d^w)}{S^* - S_d^w} \tag{2.6}$$

The solution to equation (2.6) is a straight line passing through $(S_d^w, f^w(S_d^w))$ with slope $f_w^w(S^*)$, which means that it is tangent to the fractional flow function $f^w$ at the point $S^*$, see the straight line segment between $S_d^w$ and $S^*$ in Figure 2.3. This straight line correspond to the shock wave of the BL solution. The convex-hull is completed by the the fractional flow function $f^w$ itself for $S^* < S^w < S_u^w$ and this part corresponds to the rarefaction wave of the BL solution. Note that this convex-hull construction also holds for a genuine nonlinear scalar conservation law. In that case the convex-hull would either consist of only a single straight line, which corresponds to a single shock wave, or it would consist of the flux function itself, which corresponds to a single rarefaction wave.

From the convex-hull construction it follows that the fractional flow function and its derivative determine the wave speeds of the Buckley-Leverett solution. The wave speeds are always real and positive, meaning that the BL equation is a strictly hyperbolic equation. Therefore, loss of strict hyperbolicity does not occur for two-phase flow.

# 3

# Loss of strict hyperbolicity in three-phase flow

From the previous section it follows that loss of strict hyperbolicity does not occur for two-phase flow. This was also shown by Falls and Schulte (1992), who found that loss of strict hyperbolicity can only occur in the region where all three phases are mobile. Therefore, three-phase flow will be considered throughout the rest of this thesis.

In order to determine if loss of strict hyperbolicity occurs a definition of when the system is called strictly hyperbolic is needed. First recall from Section 1.1 that the dimensionless quasilinear form of the fractional flow equations is given by:

$$S_t + \frac{\partial f}{\partial S} S_x = 0 \tag{3.1}$$

with $S = \left(S^w \ S^g\right)^T$, $f = \left(f^w \ f^g\right)^T$ and $\frac{\partial f}{\partial S}$ the Jacobian matrix $J$ given by:

$$J = \frac{\partial f}{\partial S} = \frac{1}{\lambda_T^2} \begin{pmatrix} \lambda_T \lambda_w^w - \lambda^w \lambda_{T,w} & \lambda_T \lambda_g^w - \lambda^w \lambda_{T,g} \\ \lambda_T \lambda_w^g - \lambda^g \lambda_{T,w} & \lambda_T \lambda_g^g - \lambda^g \lambda_{T,g} \end{pmatrix} \tag{3.2}$$

Then, in a point $(S^w, S^g) \in T$, the linearized system (3.1) is called:

- Strictly hyperbolic if the eigenvalues of the Jacobian matrix are real and distinct.

- Non-strictly hyperbolic if the eigenvalues of the Jacobian matrix are real and equal.

- Elliptic if the eigenvalues of the Jacobian matrix are complex.

Loss of strict hyperbolicity occurs if the system (3.1) is non-strictly hyperbolic or elliptic in at least one point inside the saturation triangle. The complete linearized system (3.1) is called strictly hyperbolic if the linearized system is strictly hyperbolic in every point $(S^w, S^g) \in T$ and it is called non-strictly hyperbolic if the system is not strictly hyperbolic, i.e. if loss of strict hyperbolicity occurs. The subdomain of the saturation triangle $T$ for which the system is elliptic is called the elliptic region. A single saturation value for which the system is non-strictly hyperbolic is called an umbilic point. An example of an elliptic region is given in Figure 3.1. Note that the boundary of the elliptic region consists of a line of umbilic points.

From the definition of loss of strict hyperbolicity it follows that the eigenvalues of the Jacobian matrix (3.2) must be looked at to determine if loss of strict hyperbolicity occurs. The eigenvalues are given by (Juanes and Patzek, 2004a):

$$\eta = \frac{f_w^w + f_g^g \pm \sqrt{(f_w^w + f_g^g)^2 - 4(f_w^w f_g^g - f_g^w f_w^g)}}{2}$$

$$= \frac{f_w^w + f_g^g \pm \sqrt{(f_w^w - f_g^g)^2 + 4 f_g^w f_w^g}}{2} \tag{3.3}$$
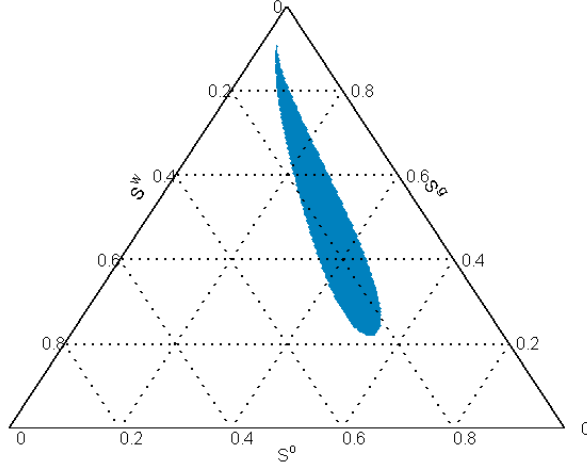
Figure 3.1: Example of an elliptic region (blue) within the ternary diagram.

If the term $(f_w^w - f_g^g)^2 + 4f_g^w f_w^g$ is negative, the eigenvalues $\eta$ will be complex conjugates. So the shape of fractional flow functions $f^\alpha$ determines whether there are saturations for which the linear system (3.1) is elliptic or non-strictly hyperbolic. But, just like for two-phase flow, the fractional flows are determined by the relative permeabilities. Therefore, the relative permeabilities determine whether loss of strict hyperbolicity occurs. Measuring three-phase relative permeabilities is complicated, time consuming and expensive (Alizadeh and Piri, 2014). For instance, hysteresis becomes more complicated in three-phase than in two-phase flow meaning that three-phase relative permeability is more difficult to measure than two-phase relative permeability. This means there is very little three-phase relative permeability data available and therefore three phase relative permeabilities are usually modelled. The existing three-phase relative permeability models can be classified as being either of Corey-type or of Stone-type. Note that Corey-type is not be confused with Corey-correlations as introduced in the previous chapter. Corey-type refers to a certain type of three-phase relative permeability model, which will be described below, whereas Corey-correlations refer to a specific functional form of two-phase relative permeabilities. Similarly, Stone-type is not be confused with normalized Stone interpolation, which will be described later in this section. Like Corey-type, Stone-type refers to a certain type of three-phase relative permeability model, whereas normalized Stone interpolation refers to a specific three-phase relative permeability model which can be of Corey-type or of Stone-type.
Corey-type models assume that the relative permeability of each phase depends only on the saturation of that phase, i.e:

$$k_r^w = k_r^w(S^w), \quad k_r^o = k_r^o(S^o), \quad k_r^g = k_r^g(S^g) \tag{3.4}$$

Stone-type models are based on the assumption that for a water-wet rock, the non-wetting phase (gas) occupies the largest pores, the wetting phase (water) occupies the smallest pores and the intermediate wetting phase (oil) occupies the pores of intermediate size (Holden, 1990; Stone, 1970). From this it follows that the relative permeability of water and gas only depend on their respective saturations, while the relative permeability of oil depends on both the water and gas saturations. So a Stone-type model is characterized by:

$$k_r^w = k_r^w(S^w), \quad k_r^o = k_r^o(S^w, S^g), \quad k_r^g = k_r^g(S^g) \tag{3.5}$$

For both a Corey-type and a Stone-type model the three-phase relative permeabilities of water and gas are the same as the relative permeabilities of the water and gas relative permeabilities in the two-phase water-oil and oil-gas systems respectively. A convenient way to picture three-phase relative permeability is by isoperms. Isoperms are lines in the ternary diagram along which the relative permeability is constant. Three main types of isoperms can be distinguished, namely concave, convex and linear, see Figure 3.2. A combination of these types is also possible, see for example Figure 3.3b where the isoperms are partly convex and partly concave. An example of the isoperms of three-phase oil relative permeability for a both Corey-type and a Stone-type model is shown in Figure 3.3. Note that the isoperms of a Corey-type model are parallel to the edge where the saturation is zero. For instance, the oil isoperms of a Corey-type model are parallel to

(a) Linear isoperms                      (b) Concave isoperms                      (c) Convex isoperms
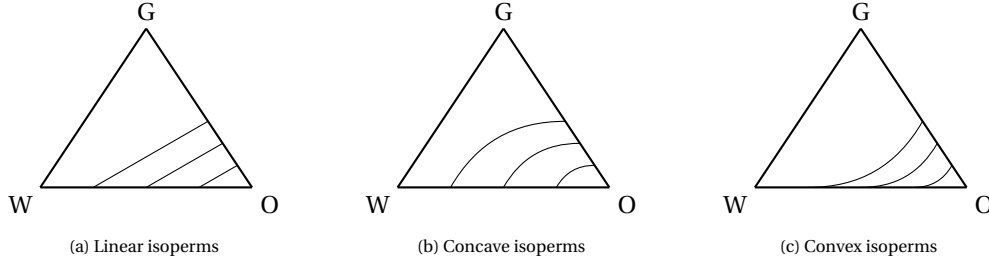
Figure 3.2: Three possible shapes of oil isoperms: Linear (a), concave (b) and convex (c)



(a) Corey-type model

(b) Stone-type model
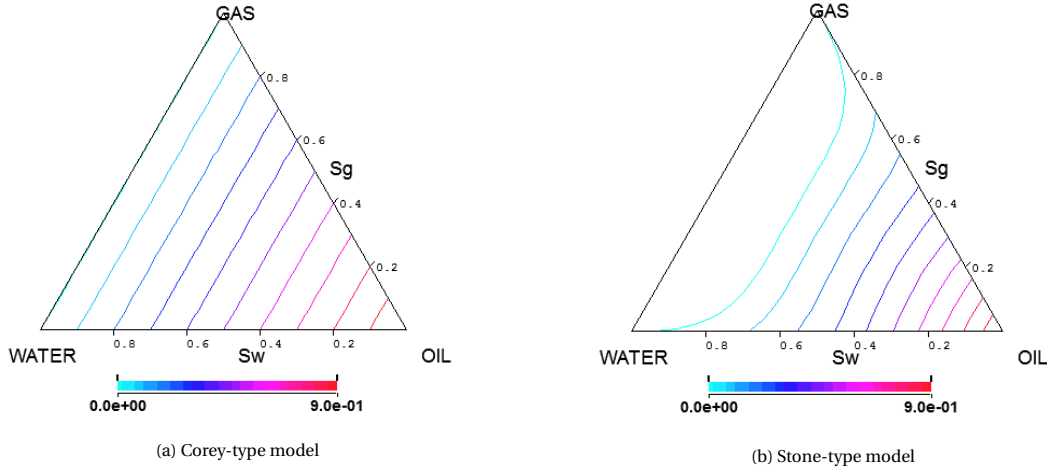
Figure 3.3: Oil isoperms obtained using normalized Stone interpolation. For the two-phase relative permeabilities, both models use a Corey-correlation with endpoints equal to one and zero residual saturations. The Corey-coefficients for the Corey-type model are $n_w = n_g = n_{ow} = n_{og} = 1$ and $n_w = n_g = n_{ow} = n_{og} = 2$ for the Stone-type model.

the water-gas (WG) edge, see Figure 3.3a. Also note that for both a Corey-type and a Stone-type model the isoperms of gas and water are always parallel to the oil-water (OW) and oil-gas (OG) edge respectively due to the assumption that $k_r^g = k_r^g(S^g)$ and $k_r^w = k_r^w(S^w)$. A multitude of three-phase relative permeabilities models exist, see e.g. Baker (1988), but in this section only one of the most used models in reservoir simulations, namely normalized Stone interpolation, is discussed. Some other three-phase relative permeability models are discussed in Chapter 4.

## 3.1. Normalized Stone interpolation

Since three-phase relative permeability data is scarce, two-phase relative permeabilities are used, which are relatively easy to measure. Three-phase relative permeability is then modelled by interpolating between these two-phase relative permeabilities. Since $k_r^w = k_r^w(S^w)$ and $k_r^g = k_r^g(S^g)$ interpolation is only used for the oil relative permeability. Therefore, interpolation is used between the water-oil and the oil-gas system. For the two-phase relative permeabilities in these systems a Corey-correlation is used, as was done for two-phase flow, see equation (2.2). For the water-oil system the Corey-correlations are given by:

$$
\begin{aligned}
k_r^w(S^w) &= K_r^w \left( \frac{S^w - S_{wc}}{1 - S_{wc} - S_{orw}} \right)^{n_w} \\
k_r^{ow}(S^w) &= K_r^{ow} \left( \frac{1 - S^w - S_{orw}}{1 - S_{wc} - S_{orw}} \right)^{n_{ow}}
\end{aligned}
\tag{3.6}
$$

And for the oil-gas system they are given by:

$$
\begin{aligned}
k_r^g(S^g) &= K_r^g \left( \frac{S^g - S_{gc}}{1 - S_{wc} - S_{gc}} \right)^{n_g} \\
k_r^{og}(S^g) &= K_r^{og} \left( \frac{1 - S^g - S_{org} - S_{wc}}{1 - S_{wc} - S_{gc} - S_{org}} \right)^{n_{og}}
\end{aligned}
\tag{3.7}
$$

Here, $k_r^w$ and $k_r^g$ are the relative permeabilities of water and gas, $k_r^{ow}$ and $k_r^{og}$ are the relative permeabilities of oil in a water-oil respectively oil-gas system, $K_r^w$, $K_r^{ow}$, $K_r^g$ and $K_r^{og}$ are endpoints of the relative permeabilities, $n_w$, $n_{ow}$, $n_g$ and $n_{og}$ are the Corey-coefficients, $S_{wc}$ and $S_{gc}$ are the connate water and connate gas saturations and $S_{orw}$ and $S_{org}$ are the residual oil saturations for the water-oil respectively oil-gas system. The connate water saturation $S_{wc}$ is incorporated in the relative permeabilities for the oil-gas system because relative permeabilities for the oil-gas system are usually measured in the presence of connate water saturation.

Stone interpolation was introduced by Stone (1970) and several variations have later been proposed (Aziz and Settari, 1979; Baker, 1988). The original model, StoneI (Stone, 1970), is based on probability and requires the estimation of the minimum value of the three-phase oil residual saturation. A second model, StoneII (Stone, 1973), is also based on probability but does not require the minimum value of the oil residual saturation. Therefore, StoneII is the preferred method.
The main assumption of StoneII is that the total relative permeability is equal to the product of the sum of the two-phase relative permeabilities:

$$k_r^o + k_r^g + k_r^w = \left(k_r^w + k_r^{ow}\right)\left(k_r^g + k_r^{og}\right) \tag{3.8}$$

or, rewritten:

$$k_r^o = \left(k_r^w + k_r^{ow}\right)\left(k_r^g + k_r^{og}\right) - k_r^g - k_r^w \tag{3.9}$$

In order to view the resulting relative permeability as a probability it must be between 0 and 1. Therefore a normalization is applied. Several ways of normalization have been proposed (Aziz and Settari, 1979; Baker, 1988), but the general form is given by:

$$k_r^o = k_{r,\max}^o \left[\left(\frac{k_r^w}{k_{r,\max}^w} + \frac{k_r^{ow}}{k_{r,\max}^o}\right)\left(\frac{k_r^g}{k_{r,\max}^g} + \frac{k_r^{og}}{k_{r,\max}^o}\right) - \frac{k_r^w}{k_{r,\max}^w} - \frac{k_r^g}{k_{r,\max}^g}\right] \tag{3.10}$$

In this thesis, the following normalization will be used:

$$k_{r,\max}^w = k_r^w(1 - S_{orw}) \tag{3.11}$$
$$k_{r,\max}^g = k_r^g(1 - S_{wc}) \tag{3.12}$$
$$k_{r,\max}^o = k_r^{ow}(S_{wc}) = k_r^{og}(S_{gc}) \tag{3.13}$$

Assuming all endpoints of the Corey-correlations to be one, all these normalisation factors will be equal to one.

Looking at equation (3.10) it follows that there might be values within the saturation triangle where $k_r^o$ can become negative. Since this has no physical meaning $k_r^o \equiv 0$ is used in this region, meaning that the oil is immobile in this region of the saturation triangle. Since the flow reduces to two-phase flow on the edges of the ternary diagram the oil is immobile on the WG edge. Therefore, the region were the oil is immobile is adjacent to the WG edge. In Figure 3.3b it can be seen that the region where $k_r^o = 0$ is located to the left of the zero, i.e. the lightest blue, isoperm which is indeed closest to the water-gas edge. Finally, note that using Corey-correlations (3.6) and (3.7) for the two-phase relative permeabilities means that normalised Stone interpolation can only lead to a Corey-type relative permeability model if $n_w = n_{ow} = n_{og} = n_g = 1$. These Corey-coefficients are only realistic if interfacial tension is negligible.

## 3.2. Numerical method
The three-phase flow model has not yet been solved analytically when loss of strict hyperbolicity occurs, except in very specific cases, e.g. (Azevedo et al., 2010). This means that the system (1.14) will be solved numerically. Furthermore, the effect of the existence of the elliptic region on the numerical solution obtained using an existing reservoir simulator is to be investigated. The reservoir simulator considered uses a fully implicit method (FIM). This means that a finite volume approach will be used for the spatial part combined with an implicit method for the time differentiation. Since gravity and capillary pressure are neglected, back flow is not possible, meaning that if the eigenvalues are real they are also positive (Guzmán and Fayers, 1997b). Therefore, information always travels in one direction, as was the case for two-phase flow. Again, the direction of flow is from the injector to the producer, meaning that the injector well is on the upstream side and

the producer well is on the downstream side, see Figure 1.1. The existing reservoir simulator is designed to be able to solve more complicated problems than the simplified model discussed in this thesis. Therefore, the reservoir simulator does not solve the fractional flow equations (1.14), which has the water and gas saturation as primary variables, but solves the saturation equation (1.8) and uses the pressure, the oil accumulation and the gas accumulation as primary variables. For comparison purposes an explicit upwind method will be used to solve the fractional flow equation (1.14).

### 3.2.1. Fully implicit method

For FIM the one dimensional reservoir, see Figure 1.1, is divided into grid cells $c_i$ with $i = 0, 1, \ldots, N$ using an equal spacing, i.e. every grid cell has length $\Delta x$, see Figure 3.4. Note that even though it is an one dimensional
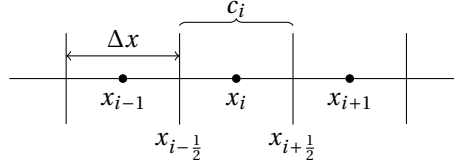


Figure 3.4: Grid cells $c_i$. The middle of grid cell $c_i$ is denoted as $x_i$ and the boundaries by $x_{i+\frac{1}{2}}$ and $x_{i-\frac{1}{2}}$.

problem, every grid cell must have a volume to use a finite volume method. Therefore, every grid cell has width $\Delta y$ and height $\Delta z$ such that every grid cell has a volume $V_{gc}$ of $\Delta x \Delta y \Delta z$. Then a finite volume method is used to approximate the spatial derivative in the saturation equation (1.8). First note that by including the phase density the saturation equation can be rewritten as:

$$\frac{\partial \rho^\alpha S^\alpha}{\partial t} = \frac{\partial}{\partial x}\left(K\frac{k_r^\alpha \rho^\alpha}{\mu^\alpha}\frac{\partial p}{\partial x}\right), \quad \text{for } \alpha \in \{w, o, g\} \tag{3.14}$$

The integral form of the saturation equation over one grid cell $c_i$ is then given by:

$$\int\limits_{V_{gc}} \frac{\partial \rho^\alpha S^\alpha}{\partial t} dx = \int\limits_{V_{gc}} \frac{\partial}{\partial x}\left(K\frac{k_r^\alpha \rho^\alpha}{\mu^\alpha}\frac{\partial p}{\partial x}\right) dx$$

$$\Delta y \Delta z \int\limits_{c_i} \frac{\partial \rho^\alpha S^\alpha}{\partial t} dx = \Delta y \Delta z \int\limits_{c_i} \frac{\partial}{\partial x}\left(K\frac{k_r^\alpha \rho^\alpha}{\mu^\alpha}\frac{\partial p}{\partial x}\right) dx, \quad \text{for } \alpha \in \{w, o, g\}, i = 0, 1, \ldots, N \tag{3.15}$$

Introducing the phase mass accumulation $A^\alpha$ and the flux $F^\alpha$ gives:

$$\frac{d}{dt} A_i^\alpha := \Delta y \Delta z \int\limits_{c_i} \frac{\partial \rho^\alpha S^\alpha}{\partial t} dx = \Delta y \Delta z \left[K\frac{k_r^\alpha \rho^\alpha}{\mu^\alpha}\frac{\partial p}{\partial x}\right]_{x_{i-\frac{1}{2}}}^{x_{i+\frac{1}{2}}} := F_{i+\frac{1}{2}}^\alpha - F_{i-\frac{1}{2}}^\alpha, \quad \text{for } \alpha \in \{w, o, g\}, i = 0, 1, \ldots, N \tag{3.16}$$

where $F_{i+\frac{1}{2}}^\alpha$ and $F_{i-\frac{1}{2}}^\alpha$ are the fluxes through the cell boundaries at $x_{i-\frac{1}{2}}$ and $x_{i+\frac{1}{2}}$ respectively. This equation still contains a time derivative which will be approximated implicitly:

$$\frac{d}{dt} A_i^\alpha = \frac{A_i^{\alpha, n+1} - A_i^{\alpha, n}}{\Delta t}, \quad \text{for } \alpha \in \{w, o, g\}, i = 0, 1, \ldots, N \tag{3.17}$$

Here, $A_i^{\alpha, n}$ is $A^\alpha$ at $x = x_i$ and at time $t^n = n\Delta t + t^0$ with $t^0$ the starting time and $n$ the discrete time level. The mass accumulation $A_i^{\alpha, n}$ is approximated by the midpoint rule:

$$A_i^{\alpha, n} = \Delta y \Delta z \int\limits_{c_i} \rho^\alpha S^{\alpha, n} dx \approx \Delta x \Delta y \Delta z \phi \rho^\alpha S_i^{\alpha, n}, \quad \text{for } \alpha \in \{w, o, g\}, i = 0, 1, \ldots, N \tag{3.18}$$

Combining equation (3.16) and equation (3.17) leads to the following discretized equations:

$$\frac{A_i^{\alpha, n+1} - A_i^{\alpha, n}}{\Delta t} = F_{i+\frac{1}{2}}^{\alpha, n+1} - F_{i-\frac{1}{2}}^{\alpha, n+1} \tag{3.19}$$

In order to find an expression for the fluxes $F^\alpha_{i+\frac{1}{2}}$ and $F^\alpha_{i-\frac{1}{2}}$ an upwind approach is used. Using the notation from Figure 3.4 and using the direction of flow as in Figure 1.1 the upwind value of $x_{i+1/2}$ is $x_i$ since the direction of flow is from $x_i$ to $x_{i+1}$. Note that the flux terms contain a pressure gradient, which will be approximated by a central difference scheme. The flux functions are then given by:

$$F^\alpha_{i+\frac{1}{2}} = \Delta y \Delta z K \frac{\rho^\alpha}{\mu^\alpha} k^\alpha_{r_i} \frac{p_{i+1} - p_i}{\Delta x} \tag{3.20}$$

Combining the discretized equations (3.19) with the expression for the fluxes (3.20) gives the full discretization of the saturation equation:

$$\frac{A^{\alpha,n+1}_i - A^{\alpha,n}_i}{\Delta t} = \Delta y \Delta z K \frac{\rho^\alpha}{\mu^\alpha} k^{\alpha,n+1}_{r_i} \frac{p^{n+1}_{i+1} - p^{n+1}_i}{\Delta x} - \Delta y \Delta z K \frac{\rho^\alpha}{\mu^\alpha} k^{\alpha,n+1}_{r_{i-1}} \frac{p^{n+1}_i - p^{n+1}_{i-1}}{\Delta x} \tag{3.21}$$

This expression only holds for the internal grid cells, for the boundary grid cells a boundary condition must be incorporated into the expression. For this, a constant injection rate and an equal constant production rate are assumed.

In section 1.1 one of the phases was eliminated using equation (1.4) which states that saturations must sum up to one. In order to be able to eliminate a phase from the discretized saturation equations (3.21) equation (1.4) is rewritten in terms of volumes and accumulations. From the definition of the accumulation (3.18) it follows that:

$$S^\alpha_i \approx \frac{A^\alpha_i}{\phi \Delta x \Delta y \Delta z \rho^\alpha}, \quad \text{for } \alpha \in \{w, o, g\} \tag{3.22}$$

Note that the sum of the saturation must be one in every grid cell, such that:

$$\sum_\alpha S^\alpha_i = \sum_\alpha \frac{A^\alpha_i}{\phi \Delta x \Delta y \Delta z \rho^\alpha}, \quad \text{for } \alpha \in \{w, o, g\}$$

$$1 = \frac{1}{\phi \Delta x \Delta y \Delta z} \sum_\alpha \frac{A^\alpha_i}{\rho^\alpha}$$

$$0 = \phi \Delta x \Delta y \Delta z - \sum_\alpha \frac{A^\alpha_i}{\rho^\alpha} \tag{3.23}$$

Since $\phi \Delta x \Delta y \Delta z$ gives the available pore volume in grid cell $c_i$, it follows that $\frac{A^\alpha_i}{\rho^\alpha}$ gives the pore volume occupied by phase $\alpha$ in grid cell $c_i$.

Equation (3.21) for all phases together with equation (3.23) gives the system of discretized equations. Note that equation (3.21) is nonlinear due to the relative permeability function. This means that at every time step a nonlinear system must be solved. In order to approximate the solution of this nonlinear system the Newton-Raphson method is used.

### Newton-Raphson

The discretized equations (3.23) and (3.21) can be rewritten in residual form as:

$$R_{V_i} = \phi \Delta x \Delta y \Delta z - \sum_\alpha \frac{A^{\alpha,n+1}_i}{\rho^\alpha} \tag{3.24}$$

$$R_{A^\alpha_i} = A^{\alpha,n+1}_i - A^{\alpha,n}_i - \frac{\Delta t}{\Delta x} \Delta y \Delta z K \rho^\alpha \frac{1}{\mu^\alpha} \left[ k^{\alpha,n+1}_{r_i}(p^{n+1}_{i+1} - p^{n+1}_i) - k^{\alpha,n+1}_{r_{i-1}}(p^{n+1}_i - p^{n+1}_{i-1}) \right] \tag{3.25}$$

This is a systems with four equations for every grid cell; one saturation equation for each phase and one phase volume equation. Due to the phase volume equation (3.24) one of the saturation equations can be eliminated, which leads to a system of three equations for every grid cell. In accordance with the existing reservoir simulator the water accumulation will be eliminated even though the oil saturation was eliminated in the continuous system (3.1). The elimination of the water phase is done by substituting the phase volume residual (3.24) in the transport residual (3.25) for the water phase, which gives the following residual (for the full derivation, see Appendix A.1):

$$R_{\tilde{A}^w_i} = -\rho^w \frac{A^{g,n+1}_i}{\rho^g} - \rho^w \frac{A^{o,n+1}_i}{\rho^o} + \rho^w \frac{A^{g,n}_i}{\rho^g} + \rho^w \frac{A^{o,n}_i}{\rho^o} - \frac{\Delta t}{\Delta x} \Delta y \Delta z K \frac{\rho^w}{\mu^w} \left[ k^{w,n+1}_{r_i}(p^{n+1}_{i+1} - p^{n+1}_i) - k^{w,n+1}_{r_{i-1}}(p^{n+1}_i - p^{n+1}_{i-1}) \right] \tag{3.26}$$

For both Corey-type and Stone-type models $k_{r_i}^w$ is a function of the water saturation only, but it can be expressed as a function of the oil and gas accumulations using equation (3.22) and $S^w = 1 - S^g - S^o$ as follows:

$$k_{r_i}^w = k_{r_i}^w \left( 1 - \frac{A_i^g}{\phi \Delta x \Delta y \Delta z \rho^g} - \frac{A_i^o}{\phi \Delta x \Delta y \Delta z \rho^o} \right), \quad \text{for } i = 0, 1, \ldots, N \tag{3.27}$$

The residuals $R_{\tilde{A}_i^w}$, $R_{A_i^o}$, and $R_{A_i^g}$ give a $3 \cdot N \times 3 \cdot N$ nonlinear system of equations with $N$ the number of grid cells. The primary variables of this system are:

$$Y = \left[ p_1^{n+1}, A_1^{o,n+1}, A_1^{g,n+1}, \ldots, p_i^{n+1}, A_i^{o,n+1}, A_i^{g,n+1}, \ldots, p_N^{n+1}, A_N^{o,n+1}, A_N^{g,n+1} \right]^T$$

At every time step the $3 \cdot N \times 3 \cdot N$ nonlinear system is solved using a Newton-Raphson approximation:

$$J^k dY^{k+1} = -R^k \tag{3.28}$$

with $k$ the iteration index, $J^k$ the Jacobian matrix and $R^k$ the residual vector given by

$$R = [R_{\tilde{A}_1^w}, R_{A_1^o}, R_{A_1^g}, \ldots, R_{\tilde{A}_i^w}, R_{A_i^o}, R_{A_i^g}, \ldots, R_{\tilde{A}_N^w}, R_{A_N^o}, R_{A_N^g}]^T \tag{3.29}$$

and $dY^{k+1}$ is the Newton update, i.e. the new iteration $Y^{k+1}$ is obtained from the old iteration $Y^k$ by $Y^{k+1} = Y^k + dY^{k+1}$. The final iteration of the Newton-Raphson method is then used as an approximation of the solution of the three-phase flow model at the new time level $n+1$.

Dropping the time level $n+1$ and the iteration index $k$ for notational simplicity, the Jacobian matrix can be written as:

$$J = \begin{pmatrix} J_{11} & J_{12} & \ldots & J_{1N} \\ J_{21} & J_{22} & & \vdots \\ \vdots & & \ddots & \\ J_{N1} & \ldots & & J_{NN} \end{pmatrix} \tag{3.30}$$

where every submatrix $J_{ij}$ is a $3 \times 3$ matrix, since three residuals and three primary variables are considered, given by:

$$J_{ij} = \begin{pmatrix} \frac{\partial R_{\tilde{A}_i^w}}{\partial p_j} & \frac{\partial R_{\tilde{A}_i^w}}{\partial A_j^o} & \frac{\partial R_{\tilde{A}_i^w}}{\partial A_j^g} \\ \frac{\partial R_{A_i^o}}{\partial p_j} & \frac{\partial R_{A_i^o}}{\partial A_j^o} & \frac{\partial R_{A_i^o}}{\partial A_j^g} \\ \frac{\partial R_{A_i^g}}{\partial p_j} & \frac{\partial R_{A_i^g}}{\partial A_j^o} & \frac{\partial R_{A_i^g}}{\partial A_j^g} \end{pmatrix} \tag{3.31}$$

For Corey-type and Stone-type relative permeability models the entries of the submatrices of the Jacobian matrix are given by the following matrices, for which the full derivation is given in Appendix A:

$$J_{ii-1} = \begin{pmatrix} -\frac{\Delta t}{\Delta x} \Delta y \Delta z K \rho^w \frac{1}{\mu^w} k_{r_{i-1}}^w & -\frac{\Delta t}{\Delta x^2} \frac{1}{\phi} K \frac{\rho^w}{\rho^o} \frac{1}{\mu^w} (p_i - p_{i-1}) \frac{\partial k_{r_{i-1}}^w}{\partial S_{i-1}^w} & -\frac{\Delta t}{\Delta x^2} \frac{1}{\phi} K \frac{\rho^w}{\rho^g} \frac{1}{\mu^w} (p_i - p_{i-1}) \frac{\partial k_{r_{i-1}}^w}{\partial S_{i-1}^w} \\ -\frac{\Delta t}{\Delta x} \Delta y \Delta z K \rho^o \frac{1}{\mu^o} k_{r_{i-1}}^o & -\frac{\Delta t}{\Delta x^2} \frac{1}{\phi} K \frac{1}{\mu^o} (p_i - p_{i-1}) \frac{\partial k_{r_{i-1}}^o}{\partial S_{i-1}^w} & \frac{\Delta t}{\Delta x^2} \frac{1}{\phi} K \frac{\rho^o}{\rho^g} \frac{1}{\mu^o} (p_i - p_{i-1}) \left( \frac{\partial k_{r_{i-1}}^o}{\partial S_{i-1}^g} - \frac{\partial k_{r_{i-1}}^o}{\partial S_{i-1}^w} \right) \\ -\frac{\Delta t}{\Delta x} \Delta y \Delta z K \rho^g \frac{1}{\mu^g} k_{r_{i-1}}^g & \frac{\Delta t}{\Delta x^2} \frac{1}{\phi} K \frac{\rho^g}{\rho^o} \frac{1}{\mu^g} (p_i - p_{i-1}) \frac{\partial k_{r_{i-1}}^g}{\partial S_{i-1}^g} & \frac{\Delta t}{\Delta x^2} \frac{1}{\phi} K \frac{1}{\mu^g} (p_i - p_{i-1}) \frac{\partial k_{r_{i-1}}^g}{\partial S_{i-1}^g} \end{pmatrix} \tag{3.32}$$

$$J_{ii} = \begin{pmatrix} \frac{\Delta t}{\Delta x} \Delta y \Delta z K \rho^w \frac{1}{\mu^w} (k_{r_i}^w + k_{r_{i-1}}^w) & -\frac{\rho^w}{\rho^o} + \frac{\Delta t}{\Delta x^2} \frac{K}{\phi} \frac{\rho^w}{\rho^o} \frac{1}{\mu^w} (p_{i+1} - p_i) \frac{\partial k_{r_i}^w}{\partial S_i^w} & -\frac{\rho^w}{\rho^g} + \frac{\Delta t}{\Delta x^2} \frac{K}{\phi} \frac{\rho^w}{\rho^g} \frac{1}{\mu^w} (p_{i+1} - p_i) \frac{\partial k_{r_i}^w}{\partial S_i^w} \\ \frac{\Delta t}{\Delta x} \Delta y \Delta z K \rho^o \frac{1}{\mu^o} (k_{r_i}^o + k_{r_{i-1}}^o) & 1 + \frac{\Delta t}{\Delta x^2} \frac{1}{\phi} K \frac{1}{\mu^o} (p_{i+1} - p_i) \frac{\partial k_{r_i}^o}{\partial S_i^w} & -\frac{\Delta t}{\Delta x^2} \frac{1}{\phi} K \frac{\rho^o}{\rho^g} \frac{1}{\mu^o} (p_{i+1} - p_i) \left( \frac{\partial k_{r_i}^o}{\partial S_i^g} - \frac{\partial k_{r_i}^o}{\partial S_i^w} \right) \\ \frac{\Delta t}{\Delta x} \Delta y \Delta z K \rho^g \frac{1}{\mu^g} (k_{r_i}^g + k_{r_{i-1}}^g) & -\frac{\Delta t}{\Delta x^2} \frac{1}{\phi} K \frac{\rho^g}{\rho^o} \frac{1}{\mu^g} (p_{i+1} - p_i) \frac{\partial k_{r_i}^g}{\partial S_i^o} & 1 - \frac{\Delta t}{\Delta x^2} \frac{1}{\phi} K \frac{1}{\mu^g} (p_{i+1} - p_i) \frac{\partial k_{r_i}^g}{\partial S_i^g} \end{pmatrix} \tag{3.33}$$

$$J_{ii+1} = \begin{pmatrix} -\frac{\Delta t}{\Delta x} \Delta y \Delta z K \rho^w \frac{1}{\mu^w} k_{r_i}^w & 0 & 0 \\ -\frac{\Delta t}{\Delta x} \Delta y \Delta z K \rho^o \frac{1}{\mu^o} k_{r_i}^o & 0 & 0 \\ -\frac{\Delta t}{\Delta x} \Delta y \Delta z K \rho^g \frac{1}{\mu^g} k_{r_i}^g & 0 & 0 \end{pmatrix} \tag{3.34}$$

$$J_{ij} \equiv 0, \quad \text{if } j \neq i-1, i, i+1 \tag{3.35}$$

Note that for both a Corey-type and a Stone-type relative permeability model the entries with $\frac{\partial k_r^g}{\partial S^o}$ are zero since both types of model assume that $k_r^g = k_r^g(S^g)$. Also note that, as for the discretized equations (3.21) and (3.23), these expressions for the submatrices only hold for the internal grid cells, i.e. the submatrices $J_{11}$ and $J_{NN}$ will have different entries due to boundary conditions.

### 3.2.2. Upwind method
An upwind method will be used to solve the fractional flow equation (1.15) in order to compare the results with the solution using the existing reservoir simulator. Recall that dimensionless form of the fractional flow equation is given by:

$$S_t + f_x = 0 \tag{3.36}$$

The same spatial discretization will be used as for FIM, see Figure 3.4. Using a standard upwind approach and explicit time discretization the following numerical scheme is obtained:

$$S_i^{n+1} = S_i^n - \frac{\Delta t}{\Delta x}\left[f_{i+\frac{1}{2}}^n - f_{i-\frac{1}{2}}^n\right] \tag{3.37}$$

with $f_{i+\frac{1}{2}}^n = f\left(S_i^n\right)$ and $f_{i-\frac{1}{2}}^n = f\left(S_{i-1}^n\right)$. Unlike FIM, this method is conditionally stable.

## 3.3. Effect of elliptic region on numerical solution
Now that the numerical schemes are derived the effect of an elliptic region on the numerical solution can be looked at. To show this effect more clearly Corey-coefficients are used that fall outside the range of physically realistic coefficients as described in chapter 4. For the water-oil and oil-gas relative permeabilities Corey-correlations (3.6) and (3.7) are used with the following Corey-coefficients:

$$n_{ow} = 2$$
$$n_w = 1.1$$
$$n_{og} = 2$$
$$n_g = 1.1$$

Furthermore, all residual saturations are assumed to be zero and all endpoints are asssumed to be one. This non-realistic choice of Corey-correlations results in larger than average elliptic region, see Figure 3.5a. Note



(a) Elliptic region
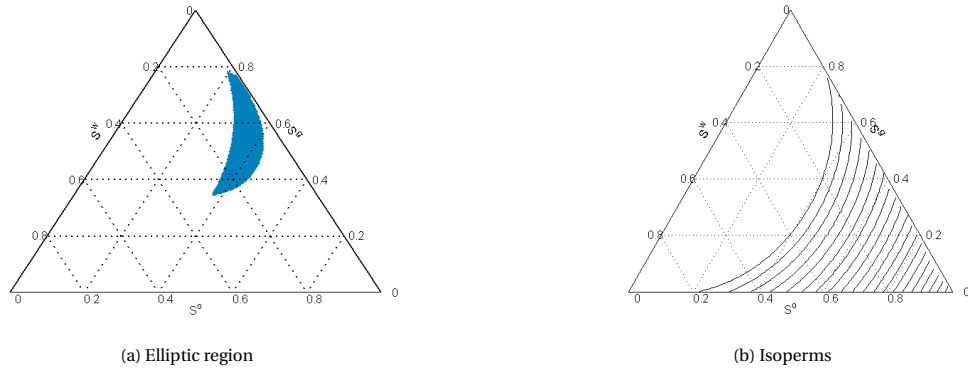


(b) Isoperms

Figure 3.5: Elliptic region (a) and oil isoperms (b) for normalized Stone with $n_{ow} = n_{og} = 2$ and $n_w = n_g = 1.1$ as Corey-coefficients. All residual saturations are zero and all endpoints are one.

that left of the isoperms in Figure 3.5b the oil relative permeability is zero, meaning that in this region the oil is immobile. This region is therefore governed by two-phase flow instead of three-phase flow, and the elliptic region indeed does not extent into this two-phase flow region. This was also shown by Falls and Schulte (1992), who stated that loss of strict hyperbolicity can only occur in the three-phase flow region.

In order to solve the three-phase flow model an initial condition must be given. As initial data $S(x,0) = \left(S^w(x,0) \quad S^g(x,0)\right)^T$ Riemann data will be assumed, as was done for two-phase flow:

$$S(x,0) = \begin{cases} S_u & \text{if } x < 0 \\ S_d & \text{if } x > 0 \end{cases} \tag{3.38}$$

Bell et al. (1986) showed that the elliptic region causes linear instability of the solution. They also showed that taking capillary pressure into account, which result in a diffusion term, damps the linear instability leading to what Bell et al. (1986) call a weakly stable system. Since both FIM and the first order upwind scheme result in some numerical diffusion the numerical solution is expected to be weakly stable. It will be shown, however, that there are situation for which the solution of the Riemann problem is influenced by the elliptic region. This behavior can be explained by the structure of the Riemann solution, which will be explained in Chapter 5. Furthermore, Isaacson et al. (1990) and Azevedo and Marchesin (1995) showed, amongst others, that uniqueness of the Riemann solution is not guaranteed if loss of strict hyperbolicity occurs, see Chapter 5.

### 3.3.1. Hyperbolic region

The first example takes both the initial state $S_d$ and injection state $S_u$ inside the hyperbolic region of the ternary diagram, and both in the three-phase flow region. Looking at figure 3.5a, choosing

$$S_u = \begin{pmatrix} 0.46 \\ 0.16 \end{pmatrix} \quad S_d = \begin{pmatrix} 0.2 \\ 0.3 \end{pmatrix} \tag{3.39}$$

means that both $S_u$ and $S_d$ lie in the hyperbolic region. Using this initial condition results in the the numeri-



(a) FIM



(b) Upwind scheme

Figure 3.6: Numerical solution after 7 years using FIM (a) and the upwind scheme (b) with both the initial and the injection state inside the hyperbolic region. The oil saturation is shown in red, the water saturation in blue and the gas saturation in green.



(a) FIM
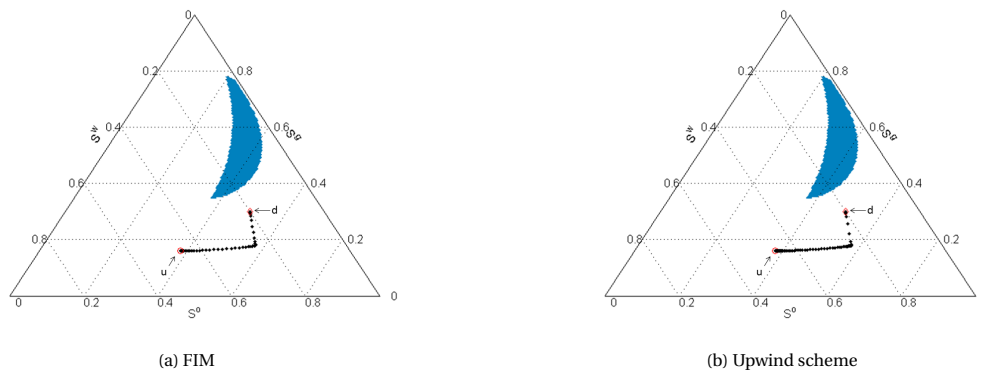


(b) Upwind scheme

Figure 3.7: Saturation path of point 1 (black dots) after 7 years using FIM (a) and the upwind scheme (b) with both the initial and the injection state inside the hyperbolic region. The red circle shows the injection or upstream state, also denoted by u, and the red diamond shows the initial or downstream state, also denoted by d. The elliptic region is shown in blue.

cal solution as shown in Figure 3.6 with corresponding saturation path as shown in Figure 3.7. The saturation path gives the saturations as a function of time for a single point $x_i$ in the reservoir. Two points are used to obtain saturation paths. Point 1 is located at 1/5 of the reservoir starting from the injector and point 2 is located at 4/5 of the reservoir. No instability can be seen in the numerical solution which is to be expected since the complete saturation path lies inside the hyperbolic region. Also note that both numerical schemes give the same solution, although the solution using FIM shows more diffusion than the solution using the upwind scheme.

As a second example both the injection and initial state are again chosen inside the hyperbolic region, but the injection state lies close to the boundary of the elliptic region:

$$S_u = \begin{pmatrix} 0.05 \\ 0.5 \end{pmatrix} \quad S_d = \begin{pmatrix} 0.46 \\ 0.16 \end{pmatrix} \tag{3.40}$$

Figure 3.8 shows the numerical solution for both FIM and the upwind method and Figure 3.9 shows the saturation path of point 1. These figures also show the numerical solution and saturation path when using the



(a) FIM        (b) Upwind scheme.        (c) Upwind scheme. Different $\frac{\Delta t}{\Delta x}$.
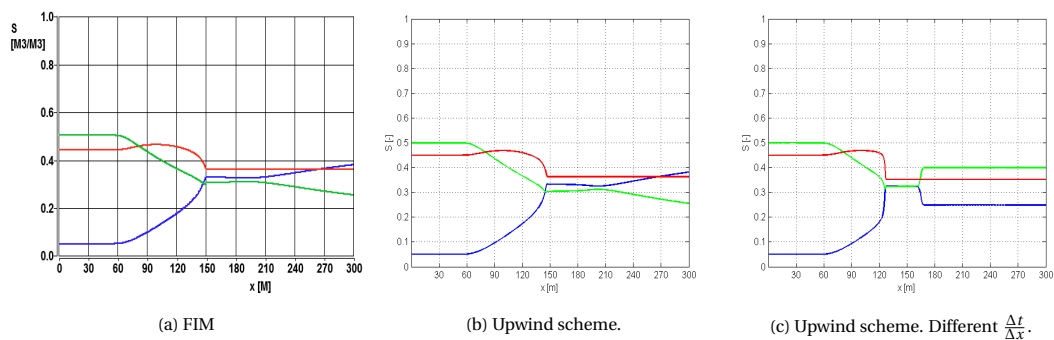
Figure 3.8: Numerical solution after 15 years using FIM (a), the upwind scheme (b) and the upwind scheme with different $\Delta t$ (c) with both the initial and the injection state inside the hyperbolic region. The oil saturation is shown in red, the water saturation in blue and the gas saturation in green.



(a) FIM        (b) Upwind scheme.        (c) Upwind scheme. Different $\frac{\Delta t}{\Delta x}$.

Figure 3.9: Saturation path of point 1 (black dots) after 15 years using FIM (a), the upwind scheme (b) and the upwind scheme with different $\frac{\Delta t}{\Delta x}$ (c) with both the initial and the injection state inside the hyperbolic region. The red circle shows the injection or upstream state, also denoted by u, and the red diamond shows the initial or downstream state, also denoted by d. The elliptic region is shown in blue.

upwind scheme but with a bigger $\frac{\Delta t}{\Delta x}$. It can be seen that changing this ratio changes the structure of the solution. Using the same $\frac{\Delta t}{\Delta x}$ as in Figure 3.9c for FIM did not result in a change in structure of the solution but resulted in the same structure as in Figure 3.9a. As was the case for the previous example, no instability occurs.

### 3.3.2. Elliptic region

In order to further investigate the effect of the elliptic region on the numerical solution, three different cases will be looked at. The first case has the initial state inside the elliptic region and the injection state outside the elliptic region. The second case has the initial state outside the elliptic region and the injection state inside

the elliptic region. Finally, a case with both states inside the elliptic region is looked at.

For the first case, the following states will be used:



(a) FIM                                                                                  (b) Upwind scheme

Figure 3.10: Numerical solution after 7 years using FIM (a) and the upwind scheme (b) with the initial state inside the elliptic region and the injection state outside the elliptic region. The oil saturation is shown in red, the water saturation in blue and the gas saturation in green.



(a) FIM                                                                                  (b) Upwind scheme.

Figure 3.11: Saturation path of point 1 (black dots) after 7 years using FIM (a) and the upwind scheme (b) with the initial state inside the elliptic region and the injection state outside the elliptic region. The red circle shows the injection or upstream state, also denoted by u, and the red diamond shows the initial or downstream state, also denoted by d. The elliptic region is shown in blue.

$$S_u = \begin{pmatrix} 0.46 \\ 0.16 \end{pmatrix} \quad S_d = \begin{pmatrix} 0.1 \\ 0.5 \end{pmatrix} \tag{3.41}$$

The numerical solution for both FIM and the upwind method are shown in Figure 3.10 and the corresponding saturation paths of point 1 are shown in Figure 3.11. There is no instability in the solution, and the solution shocks out of the elliptic region to a constant state. The solution shocks out of the elliptic region due to the integral curves and Rankine-Hugoniot locus of a state inside the elliptic region, which will be explained in chapter 5. Since the constant state and the injection state are both in the hyperbolic region, the wave between these two constant state also shows no instability. So in this example the elliptic region has no effect on the numerical solution, since the solution shocks out of the elliptic region and afterwards does not return to the elliptic region. Furthermore, note that the bend in the saturation path of FIM in Figure 3.11a is less sharp than the bend in the saturation path of the upwind scheme in Figure 3.11b. This is caused by the larger numerical diffusion of FIM compared to the numerical diffusion of the explicit upwind method.

For the second case the injection and initial states are interchanged such that:

$$S_u = \begin{pmatrix} 0.1 \\ 0.5 \end{pmatrix} \quad S_d = \begin{pmatrix} 0.46 \\ 0.16 \end{pmatrix} \tag{3.42}$$

The numerical solution for both FIM and the upwind method, with 12 years simulated, are shown in Figure 3.12 and the corresponding saturation paths of point 1 are shown in Figure 3.13. The numerical solution for

(a) FIM
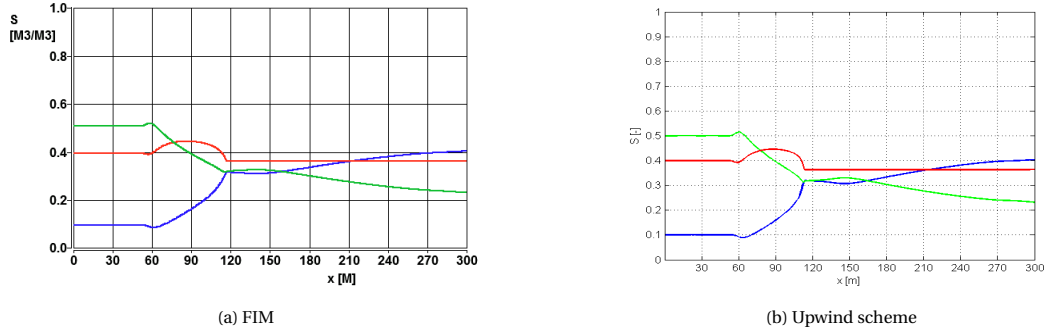


(b) Upwind scheme

Figure 3.12: Numerical solution after 12 years using FIM (a) and the upwind scheme (b) with the injection state inside the elliptic region and the initial state outside the elliptic region. The oil saturation is shown in red, the water saturation in blue and the gas saturation in green.



(a) FIM
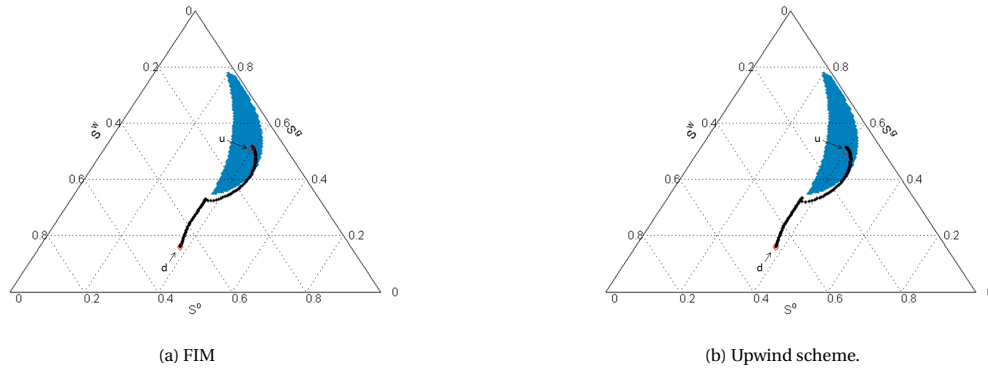


(b) Upwind scheme.

Figure 3.13: Saturation path of point 1 (black dots) after 12 years using FIM (a) and the upwind scheme (b) with the injection state inside the elliptic region and the initial state outside the elliptic region. The red circle shows the injection or upstream state, also denoted by u, and the red diamond shows the initial or downstream state, also denoted by d.



(a) FIM
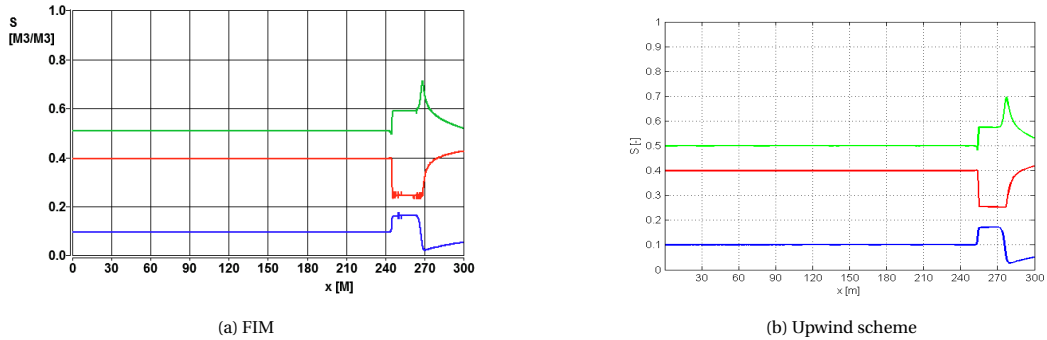


(b) Upwind scheme
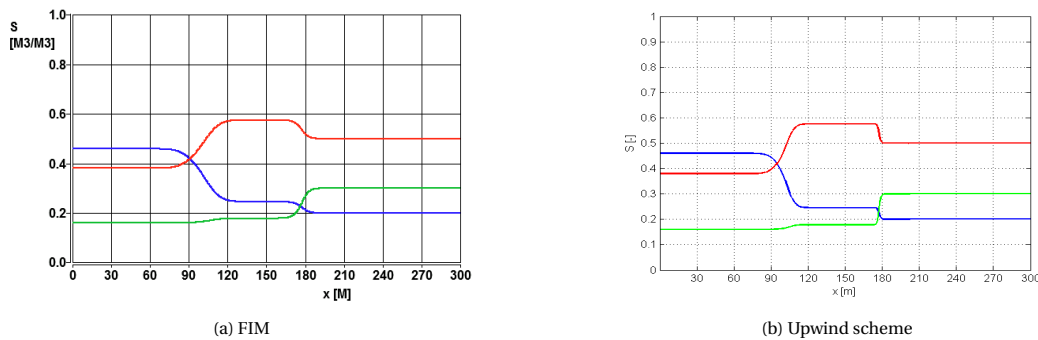
Figure 3.14: Numerical solution after 60 years using FIM (a) and the upwind scheme (b) with the injection state inside the elliptic region and the initial state outside the elliptic region. The oil saturation is shown in red, the water saturation in blue and the gas saturation in green.

both FIM and the upwind method, with 60 years simulated, are shown in Figure 3.14 and the corresponding saturation paths of point 2 are shown in Figure 3.15. Looking at Figures 3.12 and 3.13 there are no instabilities and the elliptic region does not seem to have any effect on the numerical solution to the Riemann problem. However, Figure 3.14a shows some oscillations which is an indication of linear instability. This linear instability is damped out by the numerical diffusion, resulting in small oscillations. Furthermore, comparing Figures 3.13 and 3.15 it can seen that the saturation path changes later in time, which means that the structure of the Riemann solution changes through time. Since point 2 is expected to have the same saturation path as point 1 once the injection state has also reached point 2, this change in structure is undesired behaviour. From this it can be concluded that the elliptic region does affect the numerical solution to the Riemann problem if the

(a) FIM
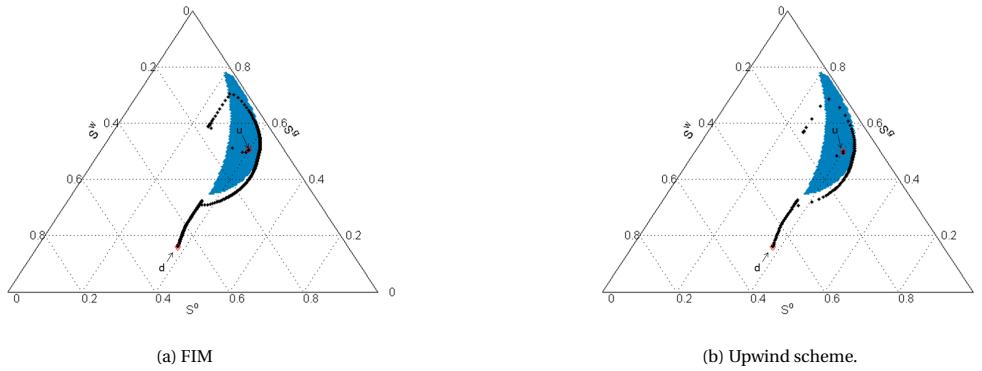
(b) Upwind scheme.

Figure 3.15: Saturation path of point 2 (black dots) after 60 years using FIM (a) and the upwind scheme (b) with the injection state inside the elliptic region and the initial state outside the elliptic region. The red circle shows the injection or upstream state, also denoted by u, and the red diamond shows the initial or downstream state, also denoted by d. The elliptic region is shown in blue.



(a) FIM
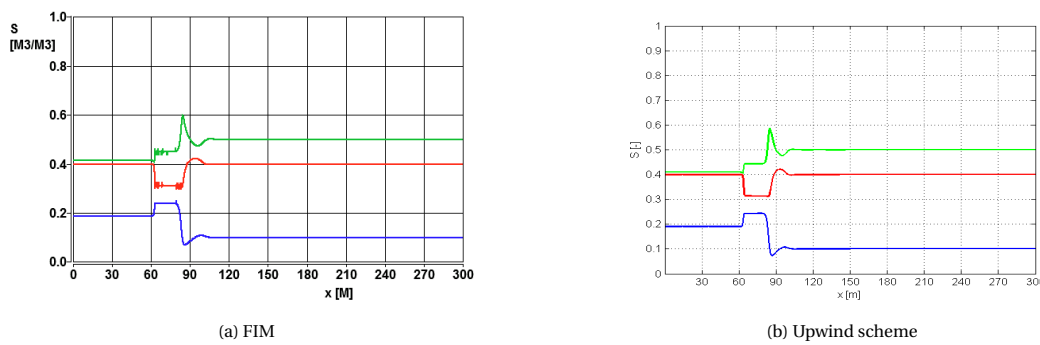
(b) Upwind scheme

Figure 3.16: Numerical solution after 14 years using FIM (a) and the upwind scheme (b) with both states inside the elliptic region. The oil saturation is shown in red, the water saturation in blue and the gas saturation in green.



(a) FIM
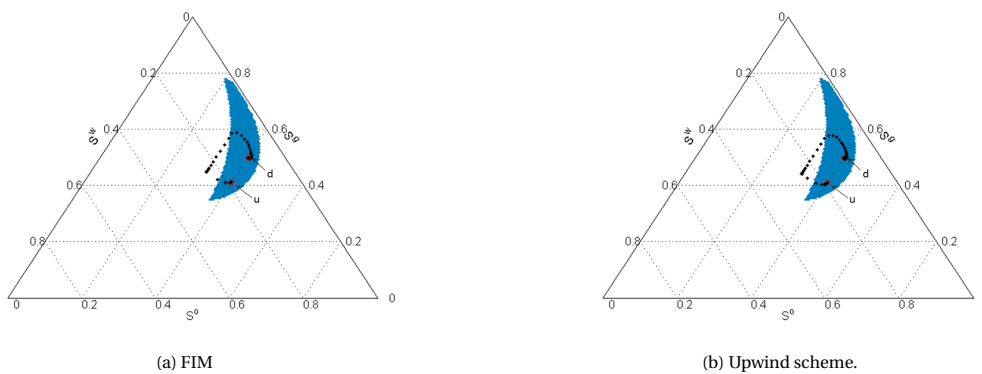
(b) Upwind scheme.

Figure 3.17: Saturation path of point 1 (black dots) after 14 years using FIM (a) and the upwind scheme (b) with both states inside the elliptic region. The red circle shows the injection or upstream state, also denoted by u, and the red diamond shows the initial or downstream state, also denoted by d. The elliptic region is shown in blue.

injection state lies inside the elliptic region.

For the last case, both the injection state and the initial state are taken inside the elliptic region. Holden (1990) showed that if both the initial and injection state lie inside the elliptic region, the solution must contain at least one state outside the elliptic region. This means there will be an intermediate state in the hyperbolic region while the injection state is in the elliptic region. From the previous example it follows that this will result in some effect on the numerical solution. As injection and initial states the following saturations are

(a) FIM
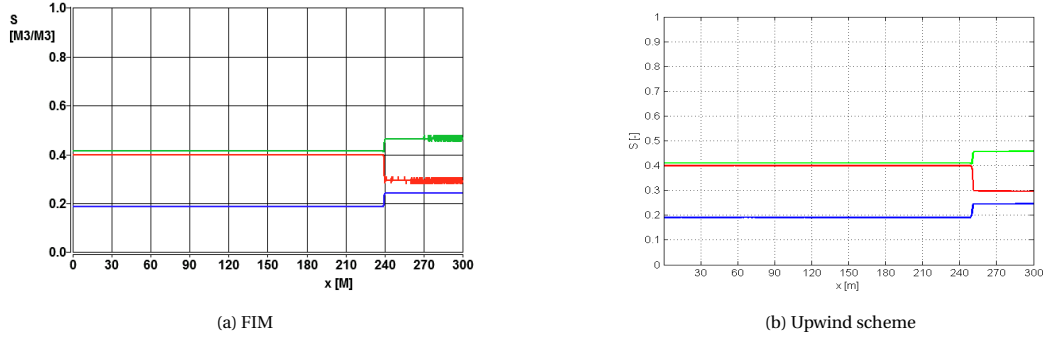


(b) Upwind scheme

Figure 3.18: Numerical solution after 65 years using FIM (a) and the upwind scheme (b) with both states inside the elliptic region. The oil saturation is shown in red, the water saturation in blue and the gas saturation in green.
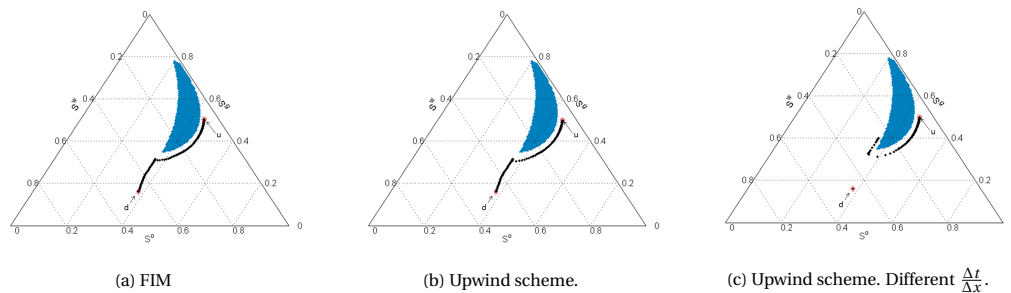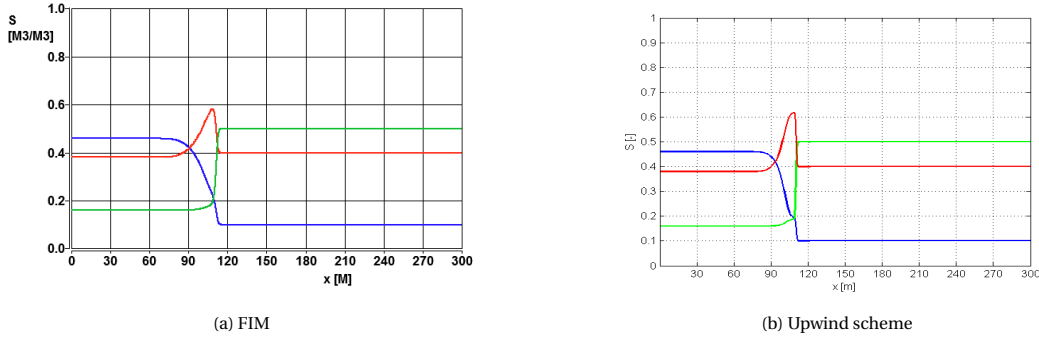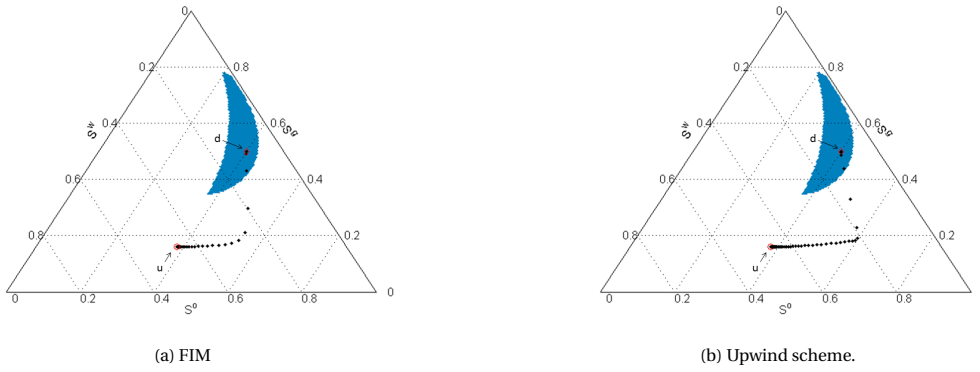


(a) FIM
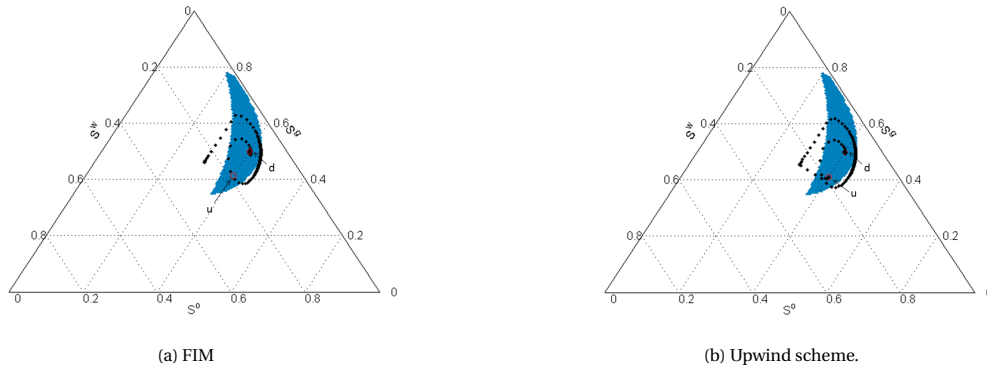


(b) Upwind scheme.

Figure 3.19: Saturation path of point 1 (black dots) after 65 years using FIM (a) and the upwind scheme (b) with both states inside the elliptic region. The red circle shows the injection or upstream state, also denoted by u, and the red diamond shows the initial or downstream state, also denoted by d. The elliptic region is shown in blue.

used:

$$S_u = \begin{pmatrix} 0.19 \\ 0.41 \end{pmatrix} \quad S_d = \begin{pmatrix} 0.1 \\ 0.5 \end{pmatrix} \tag{3.43}$$

The numerical solution for both FIM and the upwind method, with 14 years simulated, are shown in Figure 3.16 and the corresponding saturation paths of point 1 are shown in Figure 3.17. The numerical solution for both FIM and the upwind method, with 65 years simulated, are shown in Figure 3.18 and the corresponding saturation paths of point 2 are shown in Figure 3.19. Looking at Figures 3.17 and Figures 3.19 there is indeed at least on state outside the elliptic region. Comparing these two figures with each other shows that the numerical solution to the Riemann problem changes structure as time progresses. Finally, in Figure 3.16a and Figure 3.18a oscillations can be seen, just like for the previous example.

## 3.4. Analysis of Jacobian matrix

Choosing the injection state or both the injection and the initial state inside the elliptic region causes oscillations and unwanted changes in structure of the Riemann solution. It would therefore be convenient to detect if the solution is in the elliptic region or is entering the elliptic region during a simulation. One way to do this might be to look at the Jacobian matrix of the numerical scheme. The question is if it is possible to determine if the elliptic region is entered during simulation using the reservoir simulator, i.e. using FIM. This means that the Jacobian matrix of FIM, see equation (3.30), will be analysed. More specifically, it is investigated if the eigenvalues of the Jacobian matrix of FIM are a good indicator for the eigenvalues of the Jacobian of the continuous system (3.2). Looking at the submatrices $J_{ii-1}$ and $J_{ii}$ of the FIM Jacobian given by equation (3.32) and equation (3.33) it follows that they give the Jacobian matrix of the discretized equations (3.21) and (3.23) describing three-phase porous media flow. So the eigenvalues of these two submatrices in each grid cell will be compared with the eigenvalues of the continuous equation (3.3) using the saturation values in each grid cell. Note that the Jacobian matrix (3.2) of the continuous equation is a 2 × 2 matrix, thus it has 2

(a) Saturation profile



(b) Normalized imaginary part of the eigenvalues
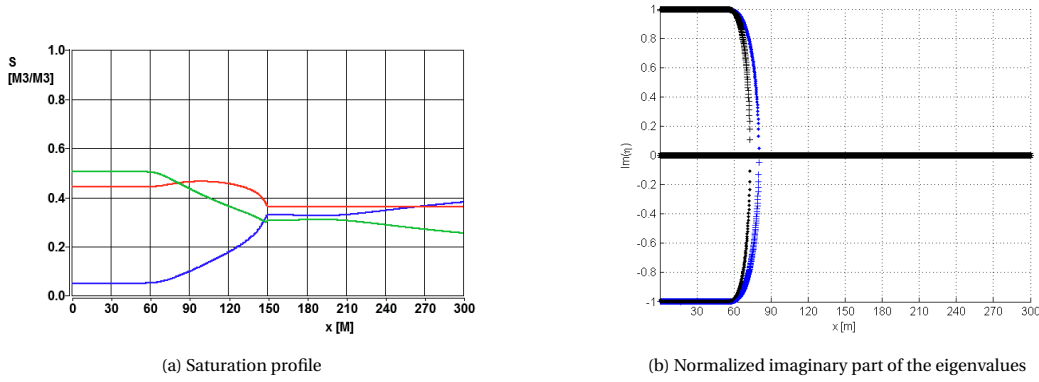
Figure 3.20: Saturation profile after 15 years (a) obtained from FIM. The oil saturation is shown in red, the water saturation in blue and the gas saturation in green. The normalized imaginary part of the eigenvalues (b) of the submatrices $J_{ii}$ (black) and $J_{ii-1}$ (blue) of the FIM Jacobian. The imaginary part of the eigenvalues of the Jacobian of the continuous systems is zero for each grid cell. Both injection and initial state are outside the elliptic region.



(a) Saturation profile



(b) Normalized imaginary part of the eigenvalues
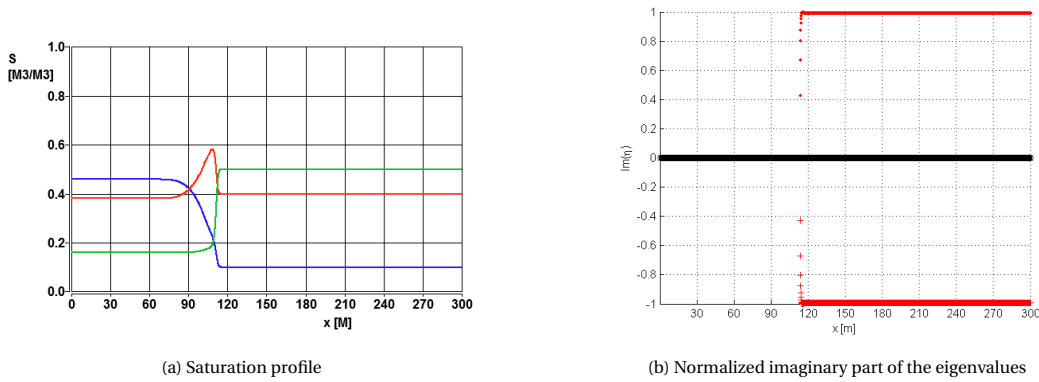
Figure 3.21: Saturation profile after 15 years (a) obtained from FIM. The oil saturation is shown in red, the water saturation in blue and the gas saturation in green. The normalized imaginary part of the eigenvalues (b) of the submatrices $J_{ii}$ (black) of the FIM Jacobian and of the eigenvalues of the Jacobian of the continuous systems (red) for each grid cell. The imaginary part of the eigenvalues of the submatrices $J_{ii-1}$ of the FIM Jacobian is zero for each grid cell. The initial state is inside the elliptic region.

eigenvalues. The submatrices of the FIM Jacobian on the other hand are $3 \times 3$ matrices, and the submatrices therefore have 3 eigenvalues but one of the eigenvalues always has zero imaginary part. Also note that, even if the eigenvalues of the submatrices of the Jacobian matrix of FIM give a good indication, it means that the eigenvalues must be calculated for each grid cell for each time step, which is computationally expensive.

Three examples will be looked at, namely case two from section 3.3.1 which has both states outside the elliptic region, case one from section 3.3.2 which has the initial state inside the elliptic region and case three from section 3.3.2 which has both states inside the elliptic region. For all examples the normalized imaginary part of the eigenvalues of the submatrices of the Jacobian of FIM and of the eigenvalues of the Jacobian of the continuous equation will be shown. This means that imaginary part of the eigenvalues of three different matrices will be plotted. As mentioned above, for each of the two submatrices of FIM one of the eigenvalues has zero imaginary part, and these eigenvalues are therefore plotted on top of each other. If the imaginary part of the eigenvalues of the Jacobian of the continuous system is also zero, these values will not be visible since they are plotted under the eigenvalues of the submatrices of FIM. For comparison purposes the saturation profile will also be shown even though they are already shown in the previous section.

The first example has both states inside the hyperbolic region. The saturation profile and the normalized imaginary part of the eigenvalues for each grid cell are shown in Figure 3.20. Figure 3.9 shows that all the saturations of the numerical solution stay outside the elliptic region. Therefore, all eigenvalues are expected to be real for all grid cells. Looking at Figure 3.20b it can be seen that the eigenvalues of the Jacobian of the continuous equations indeed have zero imaginary part. The eigenvalues of the two submatrices $J_{ii}$ and $J_{ii-1}$ on the other hand have non-zero imaginary part for the grid cells where the injection state is (almost) reached.

This means that complex eigenvalues of the submatrices of the FIM Jacobian do not necessarily indicate the presence of an elliptic region.

The second example has the initial state inside the elliptic region. The saturation profile and the normalized imaginary part of the eigenvalues for each grid cell are shown in Figure 3.21. Figure 3.11 shows that once the solution leaves the elliptic region, it does not return inside the elliptic region. This means that complex eigenvalues are expected on the producer side of the reservoir and real eigenvalues are expected on the injector side of the reservoir. Figure 3.21 shows that the eigenvalues of the Jacobian of the continuous equations indeed have non-zero imaginary part in the part of the reservoir where the saturations are (almost) equal to the initial state. The eigenvalues of the submatrices of the FIM Jacobian on the other hand have zero imaginary part throughout the entire reservoir. This means that real eigenvalues of the submatrices of the FIM Jacobian do not necessarily indicate the lack of elliptic region.

The final example has both the initial and the injection state inside the elliptic region. The saturation profile



(a) Saturation profile
(b) Normalized imaginary part of the eigenvalues
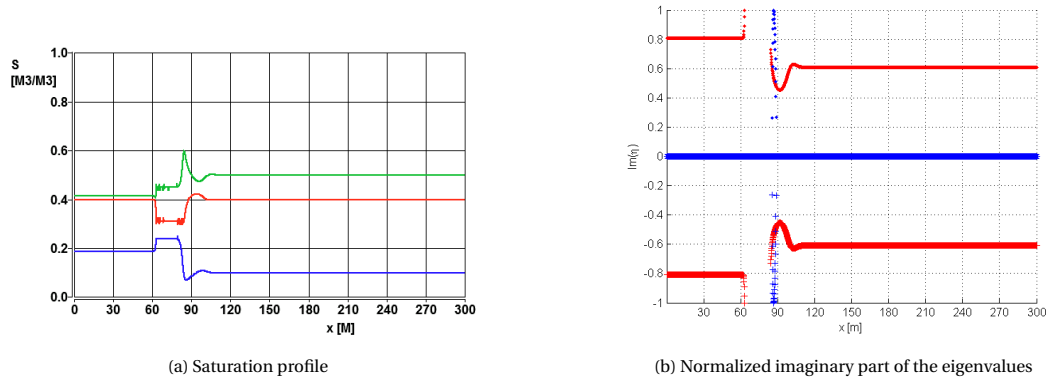
Figure 3.22: Saturation profile after 14 years (a) obtained from FIM. The oil saturation is shown in red, the water saturation in blue and the gas saturation in green. The normalized imaginary part of the eigenvalues (b) of the submatrices $J_{ii-1}$ (blue) of the FIM Jacobian and the eigenvalues of the Jacobian of the continuous systems (red) for each grid cell. The imaginary part of the eigenvalues of the submatrices $J_{ii}$ of the FIM Jacobian is zero for each grid cell. Both states are inside the elliptic region.



(a) Saturation profile
(b) Normalized imaginary part of the eigenvalues
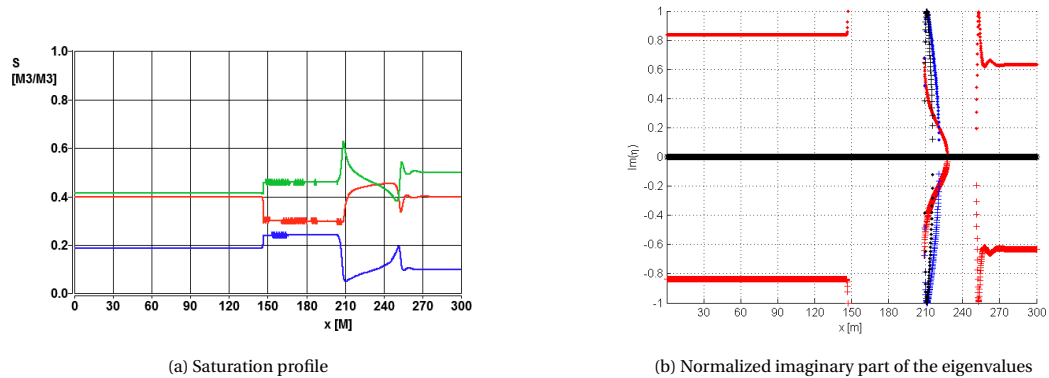
Figure 3.23: Saturation profile after 37 years (a) obtained from FIM. The oil saturation is shown in red, the water saturation in blue and the gas saturation in green. The normalized imaginary part of the eigenvalues (b) of the submatrices $J_{ii}$ (black) and $J_{ii-1}$ (blue) of the FIM Jacobian and the eigenvalues of the Jacobian of the continuous systems (red) for each grid cell. Both states are inside the elliptic region.

and the imaginary part of the eigenvalues for each grid cell are shown in Figure 3.22 for a simulation of 14 years and in Figure 3.23 for a simulation of 37 years. In both figures it can be seen that the eigenvalues of the Jacobian of the continuous equations indeed have non-zero part for the grid cells where the saturations are equal to the initial or injection state. From Figure 3.19 it can concluded that it is possible that the solution enters the elliptic region again after leaving it. Similar behavior is seen in Figure 3.23 where there are some complex eigenvalues close to 200m. Although the eigenvalues of the submatrices of the FIM Jacobian also

have non-zero imaginary part close to 200m, they do not have non-zero imaginary part for all the grid cells for which the Jacobian of the continuous equations has complex eigenvalues. Furthermore, the submatrices of the FIM Jacobian have real eigenvalues for the grid cell that have saturations equal to the injection or initial state. From this, and the previous examples, it can be concluded that the eigenvalues of the submatrices $J_{ii}$ and $J_{ii-1}$ do not provide enough information to conclude if the numerical solution enters the elliptic region or is in the elliptic region.

Since it is not so easy to determine if an elliptic region is encountered during a simulation and since computing the eigenvalues of the submatrices of the Jacobian matrix of FIM for every grid cell and time step is too expensive in practical applications, another approach can be to develop a way to avoid elliptic regions in the first place. For this some methods must be used to ensure that the solution does not enter the elliptic region. One option is to determine where the elliptic region is located inside the ternary diagram before starting a simulation. Since the eigenvalues are determined by the fractional flow functions, which are determined by the relative permeability, the relative permeability model determines if and where an elliptic region is located in the ternary diagram. Different three-phase relative permeability models will therefore be investigated.

# 4

# Three-phase relative permeability models

In Chapter 3 it was concluded that the existence of an elliptic region inside the ternary diagram can have a significant effect on the numerical solution of the three-phase porous media flow model. Furthermore, it is not easy to detect the presence of an elliptic region during a simulation. Therefore, the existence and location of the elliptic region will be looked at before the simulation is started. Since the existence and location of the elliptic region depends on the three-phase relative permeability model, different possible relative permeability models will be discussed. This chapter first describes some of the existing relative permeabilities models. Then, the available three phase relative permeability data is discussed. Finally some new three-phase relative permeability models will be introduced. The existence and location of the elliptic region based on a chosen relative permeability will be discussed in Chapter 6.

As mentioned in Chapter 2 relative permeability is usually modelled as a function of saturation alone, despite being a representation of pore-level displacements, fluid-fluid properties and rock-fluid properties. The effect of these properties or pore-level effects are generally incorporated through one or more parameters. All of the three-phase relative permeabilities models discussed are based on two-phase relative permeabilities, for which Corey-correlations will be assumed, see equations (3.6) and (3.7). The effect of the rock properties on the relative permeabilities can then be incorporated through the Corey-coefficients and through the endpoints of the relative permeabilities. In general the more wetting a phase the higher its Corey coefficient. Typical Corey-coefficients are $2.5 < n_w, n_{ow}, n_{og} < 6$ and $1.5 < n_g < 2.5$. For an intermediate-wet rock the Corey-coefficient for water and oil can become roughly equal and will be around 2.5 to 3. Since gas is the most non-wetting phase for both a water-wet and an intermediate-wet rock, the oil-gas system can be considered to be oil-wet in both cases. Therefore, the Corey-coefficient of oil $n_{og}$ is always higher than that of gas $n_g$.

## 4.1. Current models

Besides normalized Stone, described in Section 3.1, a wide variety of three-phase relative permeability models exists which are almost all Stone-type models, see e.g. Baker (1988). All these models use different physical aspects to determine their model, some of these aspects are hysteresis effects, wettability of the rock, or pore scale effects. Despite the research into relative permeability models, no model yet exists that is able to account for all the physical effects. Furthermore, most of the models are based on two-phase relative permeability data.

In this section two more existing three-phase relative permeability models will be discussed, namely linear isoperms and saturation weighted interpolation. Figure 4.1 shows the oil isoperms using normalized Stone, linear isoperms and saturation weighted for the same two-phase Corey-correlations.

### 4.1.1. Linear isoperms

Linear isoperms, assumes, as the name suggests, that the isoperms of the three-phase oil relative permeability are straight lines between the line of residual gas saturation and residual water saturation, see Figure 3.2a. In order to obtain the linear isoperms the water saturation $\tilde{S}^w$ on the OW edge and the gas saturation $\tilde{S}^g$ on the WG edge are determined such that the oil relative permeabilities of the two two-phase systems are equal, i.e.

(a) Normalized Stone        (b) Linear isoperms        (c) Saturation weighted
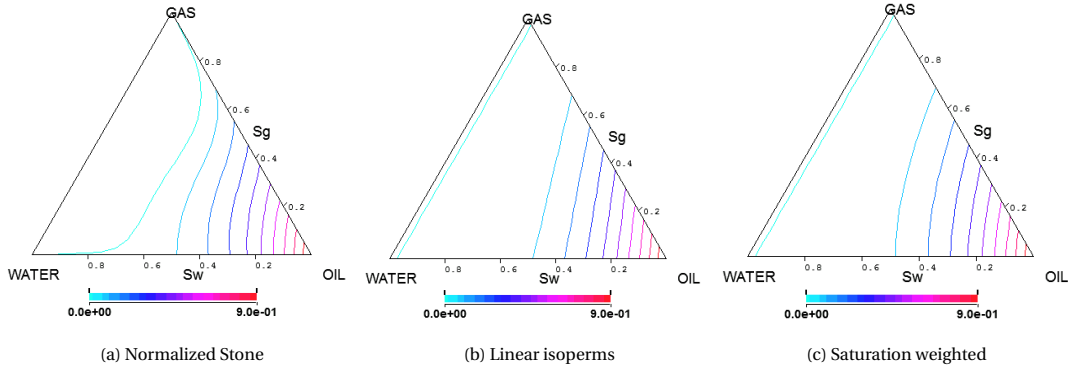
Figure 4.1: Oil isoperms for normalized Stone (a), linear isoperms (b) and saturation weighted (c). Two-phase relative permeabilities modelled with Corey-correlation with zero residuals and endpoints equal to one and $n_w = n_{ow} = 3.5$ and $n_g = n_{og} = 2$ as Corey-coefficients.

such that $k_r^{ow}(\tilde{S}^w) = k_r^{og}(\tilde{S}^g)$. Then the line between these two saturations is taken as an isoperm with the value of the three-phase oil relative permeability equal to that of the two two-phase relative permeabilities, i.e.:

$$k_r^o(S^w, S^g) = k_r^{ow}(\tilde{S}^w) = k_r^{og}(\tilde{S}^g) \quad \text{for each } (S^w, S^g) \text{ on the isoperm} \tag{4.1}$$

where each $(S^w, S^g)$ lies on the isoperm between $\tilde{S}^w$ and $\tilde{S}^g$ if:

$$\tilde{S}^g S^w + S^g \tilde{S}^w = S^g S^w \tag{4.2}$$

This construction is also shown in Figure 4.2. Equation (4.1) and equation (4.2) determine the oil relative
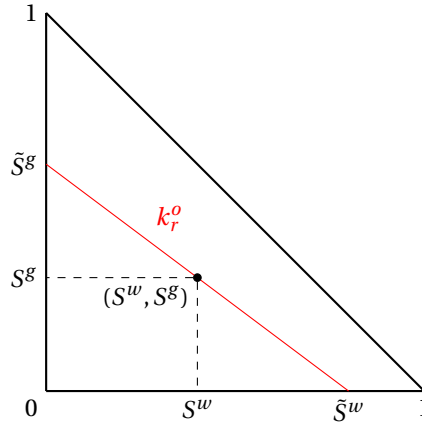


Figure 4.2: Linear isoperm (red) between $\tilde{S}^w$ and $\tilde{S}^g$. Along this isoperm the value of the oil relative permeability $k_r^o$ is constant and given by $k_r^o(S^w, S^g) = k_r^{ow}(\tilde{S}^w) = k_r^{og}(\tilde{S}^g)$.

permeability, but a closed expression for $k_r^o$ as a function of $S^w$ and $S^g$ can not be obtained. This means that linear isoperms is a more difficult method to implement and analyse then normalized Stone.

If Corey-correlations with residuals zero and endpoints one are assumed for the two two-phase systems, linear isoperms results in a Corey-type model if $n_{ow} = n_{og}$ since then $\tilde{S}^w = \tilde{S}^g$ meaning that the isoperms will be parallel to the WG edge. Conversely, linear isoperms results in a Stone-type model if $n_{ow} \neq n_{og}$, since then $\tilde{S}^w \neq \tilde{S}^g$ for $0 < \tilde{S}^w, \tilde{S}^g < 1$ meaning that the isoperms will not be parallel to the WG edge.

### 4.1.2. Saturation weighted interpolation
Saturation weighted interpolation is a near-linear interpolation between the two two-phase systems, and is given by (Baker, 1988):

$$k_r^o(S^w, S^g) = \frac{(S^w - S_{wc})k_r^{ow} + (S^g - S_{gc})k_r^{og}}{(S^w - S_{wc}) + (S^g - S_{gc})} \tag{4.3}$$

where $k_r^{ow}$ is taken at the actual oil saturation and $k_r^{og}$ is taken at the actual gas saturation. Furthermore, $k_r^{og}$ is assumed to be measured in the presence of irreducible water saturation $S_{wc}$. Saturation weighted interpolation will favor the two-phase system with the largest relative permeability. This means that the relative permeability in the interior of the ternary diagram will be dominated by the largest relative permeability of the two two-phase systems. This behaviour becomes stronger if the difference between the two two-phase relative permeabilities $k_r^{ow}$ and $k_r^{og}$ becomes greater, and is especially a problem if the residual oil saturation in both two-phase systems are not equal (Baker, 1988).

If Corey-correlations with residuals zero and endpoints one are assumed for the two two-phase systems, saturation weighted results in a Corey-type model if $n_{ow} = n_{og}$ and in a Stone-type model if $n_{ow} \neq n_{og}$.

## 4.2. Experimental data

Although measuring three-phase relative permeability is complicated, costly and time consuming some measurements have been carried out over the years. Alizadeh and Piri (2014) give a review of the experimental results concerning three-phase relative permeability between 1980 and 2013. They state that, despite recent interest in measuring three-phase relative permeabilities, common practice is still to model three-phase relative permeabilities. Furthermore, a lot of the experiments have been carried out under comparable conditions, e.g. most of the experiments have been conducted using water-wet rocks.

Baker (1988) compares the three-phase relative permeability models he describes with the available data at that time. He finds that all the models fit the available data well for large oil saturation, but that linear isoperms and saturation weighted generally give a better fit with the data than normalized Stone for small oil saturations. In a more recent paper Kianinejad and DiCarlo (2016) give experimental data for the oil relative permeability for two different types of rock and compare their results with a Corey-type model, saturation weighted interpolation and StoneI. For the Corey-type model, they assume a Corey-correlation for the oil relative permeability. They find that both the Corey-type model and the saturation weighted model fit the data well, but that the Corey-type model fits the data better. They find that StoneI fails for low oil saturations.

Alizadeh and Piri (2014) discuss one experiment where the effect of viscosity on the relative permeabilities was studied. In this experiment, not only the oil isoperms were concave, but the gas isoperms as well. The water isoperms on the other hand were straight lines parallel to the OG edge. Therefore, this experiment suggests that there is at least one case for which the gas and oil relative permeabilities depend on both the water and gas saturations. Akhlaghinia et al. (2014) investigate the effect of temperature on three-phase relative permeabilities for a system with water, gas and heavy oil. They find that all three phases show a curvature in their isoperms, meaning that the relative permeabilities of all three phases depend on both the water and gas saturation. Lü et al. (2012) investigate three-phase relative permeability in both a water-wet rock and oil-wet rock. They find that for the water-wet rock the isoperms of water are straight lines parallel to the OG edge while the isoperms of gas and oil are concave. This shows that the water relative permeability depends only on the water saturation whereas the oil and gas relative permeabilities depend on both the water and oil saturation. For the oil-wet rock, they find that the isoperms of all phases are concave, meaning the all three three-phase relative permeabilities depend on both the water and gas saturations. From the experiments above it can concluded that there are situations in which both Corey-type and Stone-type models will model the relative permeabilities incorrectly. Furthermore, the experiments show that, depending on the situation at hand, the isoperms of the three phases can show completely different behavior. Therefore, the best relative permeability model will most likely be a different model for each situation.

### 4.2.1. Three-phase relative permeability as an interpolation problem

The isoperms can be linear, concave, convex or a combination of two or three of these depending on the particular situation at hand. This means that for every situation the three-phase relative permeability should be chosen such that it matches the data, when available. Furthermore, Trangenstein (1989) showed that a Corey-type model will always result in an umbilic point inside the ternary diagram. He also showed that for a Stone-type model, given viscosity, it is always possible to find density and gravity coefficients such that there is an elliptic region inside the ternary diagram. This adds to the view that a relative permeability model should be chosen for each individual situation. Modelling relative permeability can thus be seen as an interpolation problem between two two-phase systems. For instance, if the measured isoperms of oil suggest that the oil relative permeability depends on both the water and gas saturations, interpolation must be done between

the water-oil and oil-gas system. Similarly, if the gas relative permeability depends on both the water and gas saturation, interpolation must be done between the water-gas and oil-gas systems. In Corey-type (3.4) and Stone-type models (3.5) only the oil relative permeability needs to be interpolated. In this thesis, the relative permeability models are extended to types where all three relative permeabilities depend on both the water and gas saturations and interpolation is needed for all three phases. Depending on the desired shape of the isoperms a different interpolation method can be chosen for each phase. For instance, oil relative permeability can be obtained using saturation weighted interpolation while gas relative permeability can be obtained using linear isoperms. Even though it is possible to use a different interpolation method for each phase, the same interpolation method will be used for all phases in this thesis. In order to use a interpolation method for the water and gas relative permeabilities, the two-phase relative permeabilities in the water-gas system must also be known. For this Corey-correlation with zero residual saturation and endpoint equal to one will be assumed as well. The two-phase relative permeabilities in all two-phase systems are then given by:

$$k_r^{wo} = k_r^{wo}(S^w) = (S^w)^{n_{wo}} \tag{4.4}$$

$$k_r^{ow} = k_r^{ow}(S^w) = (1 - S^w)^{n_{ow}} \tag{4.5}$$

$$k_r^{go} = k_r^{go}(S^g) = (S^g)^{n_{go}} \tag{4.6}$$

$$k_r^{og} = k_r^{og}(S^g) = (1 - S^g)^{n_{og}} \tag{4.7}$$

$$k_r^{wg} = k_r^{wg}(S^w) = (S^w)^{n_{wg}} \tag{4.8}$$

$$k_r^{gw} = k_r^{gw}(S^w) = (1 - S^w)^{n_{gw}} \tag{4.9}$$

Here $k_r^{\alpha_1 \alpha_2}$ is used to denote the relative permeability of phase $\alpha_1$ in a $\alpha_1$-$\alpha_2$ system with $n_{\alpha_1 \alpha_2}$ the corresponding Corey-coefficient. For example $k_r^{wg}$ denotes the relative permeability of water in a water-gas system with $n_{wg}$ the corresponding Corey-coefficient. Note that the two-phase relative permeabilities in the water-gas systems are chosen as functions of $S^w$, but they can be rewritten as functions of $S^g$ using that $S^w = 1 - S^g$ in the water-gas system.

## 4.3. New Models

In this section two new interpolation methods, interpolation I and interpolation II, will be introduced as well as a combination of these two methods called interpolation III. Interpolation I is introduced because it is the most simple method to interpolate between two two-phase systems. Interpolation II is introduced to construct isoperms that are more concave than the isoperms of interpolation I. Interpolation III is introduced to use the benefits of interpolation II, namely the concavity of the isoperms, without having its drawbacks. The interpolation to obtain the oil relative permeability for each interpolation method is given in detail. The interpolation to obtain the relative permeability of the other two phases is similar and can be found in detail in Appendix B.

### 4.3.1. Interpolation I

Interpolation I is the first of the three newly introduced interpolation methods. It is introduced with the idea to make the interpolation as simple as possible, without taking any physical arguments into account other than that the oil relative permeability should reduce to the two-phase relative permeability $k_r^{ow}$ on the WO and to $k_r^{og}$ on the OG edge. Therefore, for a point $(S^w, S^g)$ in the interior of the ternary diagram the points on the WO and OG edge that have the same oil-saturation as the interior point are determined and interpolation is done between these two points. These two points, called $\tilde{S}^w$ and $\tilde{S}^g$, are the endpoints of the oil isosaturation line, see Figure 4.3. Since $S^o = 1 - S^w - S^g$ for $S^o$ in the ternary diagram, and since $\tilde{S}^w$ and $\tilde{S}^g$ lie on the oil isosaturation and on the OW respectively OG edge, it follows that:

$$S^o = 1 - \tilde{S}^g \tag{4.10}$$

$$S^o = 1 - \tilde{S}^w \tag{4.11}$$

$$S^o = 1 - S^w - S^g \tag{4.12}$$

$$\tag{4.13}$$

Therefore,

$$\tilde{S}^w = \tilde{S}^g = S^w + S^g \tag{4.14}$$
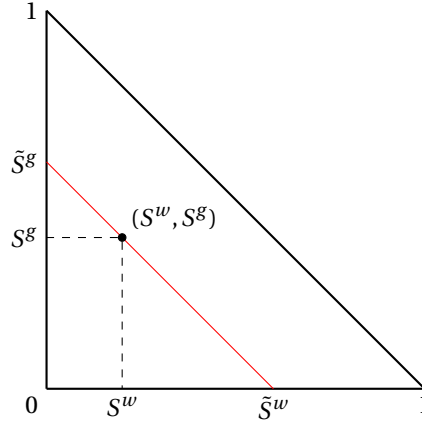
Figure 4.3: Oil isosaturion (red) for a point $(S^w, S^g)$. The oil relative permeability in $(S^w, S^g)$ is obtained by linear interpolation between the oil relative permeability in $\tilde{S}^w$ and the oil relative permeability in $\tilde{S}^g$

Then linear interpolation is used between the oil relative permeabilities in $\tilde{S}^w$ and $\tilde{S}^g$ to obtain the oil relative permeability for the interior points. Since $\tilde{S}^w$ and $\tilde{S}^g$ lie on the edge of the ternary diagram, the oil relative permeability is given by the two-phase relative permeability of each edge. This leads to the following expression for the three-phase oil relative permeability:

$$k_r^o(S^w, S^g) = \frac{S^w}{S^w + S^g} k_r^{ow}(S^w + S^g) + \frac{S^g}{S^w + S^g} k_r^{og}(S^w + S^g) \tag{4.15}$$

Comparing this interpolation method with the saturation weighted interpolation, see section 4.1.2, and assuming that all residual saturations are zero, it can seen that they are identical. Looking at equation (4.15) it follows that $k_r^o(S^w, 0) = k_r^{ow}(S^w)$ and $k_r^o(0, S^g) = k_r^{og}(S^g)$, meaning that the oil relative permeability indeed reduces to the two-phase oil relative permeability on the WO and OG edges. Furthermore, looking at the oil relative permeability when the oil saturation is zero, that is when $S^g = 1 - S^w$, gives:

$$k_r^o(S^w, 1 - S^w) = \frac{S^w}{S^w + 1 - S^w} k_r^{ow}(S^w + 1 - S^w) + \frac{1 - S^w}{S^w + 1 - S^w} k_r^{og}(S^w + 1 - S^w) \tag{4.16}$$

$$= S^w k_r^{ow}(1) + S^w k_r^{og}(1) \tag{4.17}$$

Since Corey-correlations with endpoints equal to one and zero residual saturation are assumed for the two-phase systems it holds that $k_r^o(S^w, 1 - S^w) = 0$. Therefore, this interpolation method also reduces to the expected two-phase behavior on the WG edge. Furthermore interpolation I will reduce to a Corey-type method if $n_{ow} = n_{og}$ if interpolation I is only used to obtain the oil relative permeability. Since $k_r^{ow}(S^w + S^g) = k_r^{og}(S^w + S^g)$ if $n_{ow} = n_{og}$ and since $S^w + S^g = 1 - S^o$, equation (4.15) gives $k_r^o = k_r^{ow}(1 - S^o)$ meaning that $k_r^o$ is only a function of the oil saturation.

Similarly, expressions for the three-phase water and gas relative permeabilities can be obtained:

$$k_r^w(S^w, S^g) = \frac{1 - S^w - S^g}{1 - S^w - S^g + S^g} k_r^{wo}(1 - (1 - S^w - S^g) - S^g) + \frac{S^g}{1 - S^w - S^g + S^g} k_r^{wg}(1 - (1 - S^w - S^g) - S^g)$$

$$= \frac{1 - S^w - S^g}{1 - S^w} k_r^{wo}(S^w) + \frac{S^g}{1 - S^w} k_r^{wg}(S^w) \tag{4.18}$$

$$k_r^g(S^w, S^g) = \frac{1 - S^w - S^g}{1 - S^w - S^g + S^w} k_r^{go}(1 - (1 - S^w - S^g) - S^w) + \frac{S^g}{1 - S^w - S^g + S^w} k_r^{gw}(1 - S^w - S^g + S^w)$$

$$= \frac{1 - S^w - S^g}{1 - S^g} k_r^{go}(S^g) + \frac{S^w}{1 - S^g} k_r^{gw}(1 - S^g) \tag{4.19}$$

Note that $k_r^w(S^w, 0) = k_r^{wo}$, $k_r^w(0, S^g) = 0$ and $k_r^w(S^w, 1 - S^w) = k_r^{wg}$, meaning that the water relative permeability reduces to the expected two phase behavior. This also holds for the gas relative permeability since $k_r^g(S^w, 0) = 0$, $k_r^g(0, S^g) = k_r^{go}$ and $k_r^w(S^w, 1 - S^g) = k_r^{gw}$. Furthermore, note that interpolation I will still reduce to a Corey-type model when interpolation I is used to obtain the relative permeability for all phases if

$n_{ow} = n_{og}$, $n_{wo} = n_{wg}$ and $n_{go} = n_{gw}$. It will reduce to a Stone-type model if $n_{go} = n_{gw}$, $n_{wo} = n_{wg}$ and $n_{ow} \neq n_{og}$.

### 4.3.2. Interpolation II

Just like interpolation I, interpolation II is not based on any physical assumptions other than that the oil relative permeability should reduce to the two-phase oil relative permeability at the WO and OG edge edge. However, a slightly more complex interpolation method is used to make the isoperms more concave. Instead of obtaining $\tilde{S}^w$ and $\tilde{S}^g$ from the oil isosaturation line as was done for interpolation I, $\tilde{S}^w$ and $\tilde{S}^g$ are now obtained by defining a circle through $(S^w, S^g)$. This circle takes the origin as centre and uses the distance from the origin to the point $(S^w, S^g)$ as radius, see Figure 4.4. This means that $\tilde{S}^w = \tilde{S}^g = R = \sqrt{(S^w)^2 + (S^g)^2}$.
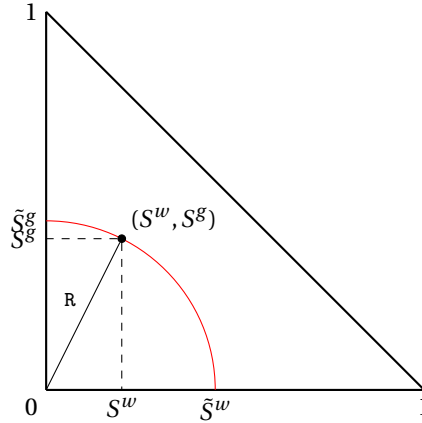
Figure 4.4: Circle (red) through $(S^w, S^g)$ with radius R and the origin as center. The oil relative permeability in $(S^w, S^g)$ is obtained by linear interpolation between the oil relative permeability in $\tilde{S}^w$ and the oil relative permeability in $\tilde{S}^g$

Again, linear interpolation is used between the oil relative permeabilities in $\tilde{S}^w$ and $\tilde{S}^g$ on the two edges to obtain the oil relative permeability for the interior point. This leads to the following expression for the three-phase oil relative permeability:

$$k_r^o(S^w, S^g) = \frac{S^w}{S^w + S^g} k_r^{ow}\left(\sqrt{(S^w)^2 + (S^g)^2}\right) + \frac{S^g}{S^w + S^g} k_r^{og}\left(\sqrt{(S^w)^2 + (S^g)^2}\right) \tag{4.20}$$

Note that, as for interpolation I, $k_r^o(S^w, 0) = k_r^{ow}(S^w)$ and $k_r^o(0, S^g) = k_r^{og}(S^g)$, meaning that the oil relative permeability indeed reduces to the two-phase oil relative permeability on the WO and OG edges. However, looking at the oil relative permeability when the oil saturation is zero, that is when $S^g = 1 - S^w$, it follows that:

$$\begin{aligned} k_r^o(S^w, 1 - S^w) &= \frac{S^w}{S^w + 1 - S^w} k_r^{ow}\left(\sqrt{(S^w)^2 + (1 - S^w)^2}\right) + \frac{1 - S^w}{S^w + 1 - S^w} k_r^{og}\left(\sqrt{(S^w)^2 + (1 - S^w)^2}\right) \\ &= S^w k_r^{ow}\left(\sqrt{2(S^w)^2 + 2S^w + 1}\right) + S^g k_r^{og}\left(\sqrt{2(S^w)^2 + 2S^w + 1}\right) \end{aligned} \tag{4.21}$$

For $0 < S^w < S^g$ it holds that $0 < \sqrt{2(S^w)^2 + 2S^w + 1} < \frac{1}{2}\sqrt{2}$ which gives that $1 > k_r^{ow}\left(\sqrt{(S^w)^2 + (S^g)^2}\right) > \frac{1}{2}\sqrt{2}$. Therefore, the oil relative permeability does not go to zero as the oil saturation tends to zero. This means that the oil phase would still be mobile even when there is no oil left. Hence, this interpolation method does not reduce to the expected two-phase flow behavior on the WG edge. Furthermore, interpolation II does not reduce to a Corey-type model if $n_{ow} = n_{og}$. As for interpolation I $k_r^{ow}(\tilde{S}^w) = k_r^{og}(\tilde{S}^w)$ if $n_{ow} = n_{og}$ such that $k_r^o = k_r^{ow}(\tilde{S}^w)$. But now $\tilde{S}^w = \sqrt{(S^w)^2 + (S^g)^2}$ which cannot be written as a function of $S^o$ alone. This means that interpolation II will always result in a Stone-type model if interpolation II is only used to obtain the oil relative permeability.

Similarly, expressions for the three-phase water and gas relative permeabilities can be obtained:

$$k_r^w(S^w, S^g) = \frac{1 - S^w - S^g}{1 - S^w - S^g + S^g} k_r^{wo} \left(1 - \sqrt{(S^o)^2 + (S^g)^2}\right) + \frac{S^g}{1 - S^w - S^g + S^g} k_r^{wg} \left(1 - \sqrt{(S^o)^2 + (S^g)^2}\right)$$

$$= \frac{1 - S^w - S^g}{1 - S^w} k_r^{wo} \left(1 - \sqrt{(S^o)^2 + (S^g)^2}\right) + \frac{S^g}{1 - S^w} k_r^{wg} \left(1 - \sqrt{(S^o)^2 + (S^g)^2}\right) \qquad (4.22)$$

$$k_r^g(S^w, S^g) = \frac{1 - S^w - S^g}{1 - S^w - S^g + S^w} k_r^{go} \left(1 - \sqrt{(S^o)^2 + (S^w)^2}\right) + \frac{S^w}{1 - S^w - S^g + S^w} k_r^{gw} \left(\sqrt{(S^o)^2 + (S^w)^2}\right)$$

$$= \frac{1 - S^w - S^g}{1 - S^g} k_r^{go} \left(1 - \sqrt{(S^o)^2 + (S^w)^2}\right) + \frac{S^w}{1 - S^g} k_r^{gw} \left(\sqrt{(S^o)^2 + (S^w)^2}\right) \qquad (4.23)$$

with

$$(S^o)^2 + (S^g)^2 = (1 - S^w - S^g)^2 + (S^g)^2$$
$$= 1 - 2S^w - 2S^g + 2S^w S^g + (S^w)^2 + 2(S^g)^2$$
$$(S^o)^2 + (S^w)^2 = (1 - S^w - S^g)^2 + (S^w)^2$$
$$= 1 - 2S^w - 2S^g + 2S^w S^g + 2(S^w)^2 + (S^g)^2$$

Note that $k_r^w(S^w, 0) = k_r^{wo}$ and $k_r^w(S^w, 1 - S^w) = k_r^{wg}$, meaning that the water relative permeability reduces to the expected two phase behavior on the OW and WG edge. The gas relative permeability reduces to the expected two phase behavior on the OG and WG edge since $k_r^g(0, S^g) = k_r^{go}$ and $k_r^g(S^w, 1 - S^w) = k_r^{gw}$. Both relative permeabilities, however, do not go to zero as the saturation goes to zero, i.e. $k_r^w(0, S^g) > 0$ and $k_r^g(S^w, 0) > 0$. This means that water is still mobile if the water saturation is zero and that gas is still mobile if the gas saturation is zero. This unphysical behavior means that interpolation II does not reduce to the expected two-phase flow behavior on the OG edge due to the water relative permeability and on OW edge due to the gas relative permeability. Furthermore, the relative permeability of all phases will depend on both the water and gas saturations if interpolation II is used to obtain the relative permeabilities of all phases. In other words, interpolation II will never result in a Corey-type or Stone-type model if interpolation II is used to obtain the relative permeability of all three phases.

### 4.3.3. Interpolation III
Interpolation III is the last of the new interpolation methods. This method is introduced to combine the concave isoperms of interpolation II with the reduction to two-phase behavior on all edges of interpolation I. To achieve this, interpolation III must reduce to interpolation II for large saturation values and to interpolation I for small saturation values. Therefore, the three-phase relative permeabilities are given by:

$$k_r^o(S^w, S^g) = S^o k_r^{o,II}(S^w, S^g) + (1 - S^o) k_r^{o,I}(S^w, S^g)$$
$$= (1 - S^w - S^g) k_r^{o,II}(S^w, S^g) + (S^w + S^g) k_r^{o,I}(S^w, S^g) \qquad (4.24)$$

$$k_r^w(S^w, S^g) = S^w k_r^{w,II}(S^w, S^g) + (1 - S^w) k_r^{w,I}(S^w, S^g) \qquad (4.25)$$

$$k_r^g(S^w, S^g) = S^g k_r^{g,II}(S^w, S^g) + (1 - S^g) k_r^{g,I}(S^w, S^g) \qquad (4.26)$$

Here $k_r^{\alpha,I}(S^w, S^g)$ and $k_r^{\alpha,II}(S^w, S^g)$ denote the relative permeability of phase $\alpha$ obtained using interpolation I and interpolation II respectively.

Note that using interpolation III for only the oil relative permeability will not reduce $k_r^o$ to a Corey-type model when $n_{ow} = n_{og}$ due to the influence of interpolation II. Interpolation III will therefore always result in a Stone-type model. Also note that, as for interpolation I, $k_r^o(S^w, 0) = k_r^{ow}(S^w)$ and $k_r^o(0, S^g) = k_r^{og}(S^g)$. So interpolation III reduces to the expected two-phase behavior on the OW and OG edge. Looking at the oil relative permeability when the oil saturation is zero, that is when $S^g = 1 - S^w$, it can be seen that $k_r^o(S^w, 1 - S^w) = 0$. So interpolation III also reduces to two-phase flow behavior on the WG edge, as expected.

Similar behavior holds for the water and gas relative permeabilities. This means that if interpolation III is used to obtain the relative permeabilities for all phases, the model will reduce to two-phase behavior on all edges due to the influence of interpolation I. Furthermore, it means that all three relative permeabilities depend on both the water and gas saturations due to the influence of interpolation II, such that interpolation III will never result in a Corey-type or Stone-type model if interpolation III is used to obtain the relative permeability of all three phases.

$$\Huge 5$$

# Three-phase Riemann problem

In order to investigate the effect that the different three-phase relative permeability models have on the solution of the three-phase porous media flow model, the structure of the solution to the Riemann problem will be looked at. Riemann problems play an important role in analysing hyperbolic systems of equations, since the solution to these relatively simple problems can help to understand the structure of the solutions for the system with more complicated initial data. In oil recovery they play an even more important role. If the reservoir initially has a constant distribution of phase saturations and if injection is done at a constant flow rate, Riemann initial data would be the way to model this situation. In chapter 2 the solution to the Riemann problem for two-phase flow was given. This solution consisted of either a single shock wave, a single rarefaction wave or a composite wave. The structure of the Riemann solution for a system of two equations is richer than that for the single two-phase flow equation, and can become quite complex when loss of strict hyperbolicity is involved. First the Riemann problem for a strictly hyperbolic problem will be looked at and the main steps to construct a solution in this case will be given. Then the effect of loss of strict hyperbolicity on the structure of the Riemann solution will be discussed.

## 5.1. Strictly hyperbolic system

For the strictly hyperbolic Riemann problem, the dimensionless system describing three phase flow (1.14) will be looked at and the fractional flow functions are assumed to be such that the system is strictly hyperbolic for all saturations in the saturation triangle $T$. As initial data the saturations are assumed constant throughout the entire reservoir and an injection of a constant mixture at the left of the reservoir is assumed. This means the following problem will be looked at:

$$S_t + f_x = 0 \tag{5.1}$$

with initial data

$$S(x,0) = \left\{ \begin{array}{ll} S_u & \text{if } x \leq 0 \\ S_d & \text{if } x > 0 \end{array} \right. \tag{5.2}$$

where $S_u$ is the upstream or injection state and $S_d$ is the downstream or reservoir state. For a strictly hyperbolic system, the solution is a self-similar solution, i.e. the solution $S$ is a function of $\frac{x}{t}$ only, e.g (Azevedo et al., 2010). The solution consists of one or more self-similar waves and there are several types of waves that can be distinguished, e.g. the trivial constant solution, a rarefaction wave and a discontinuity or shock.

### 5.1.1. Rarefaction waves

As mentioned above, a rarefaction wave is a self-similar solution. Therefore, a solution $S$ to the Riemann problem is written as $S = S(\frac{x}{t}) := S(\eta)$. Substituting this in the linear form of the system of equations (1.15) gives:

$$-\eta \frac{dS}{d\eta} + J(S) \frac{dS}{d\eta} = 0 \tag{5.3}$$

where $J(S) = \frac{\partial f}{\partial S}$ is the Jacobian matrix given by equation (1.12). This system can be rewritten as an eigenvalue problem as follows:

$$\left[ J(S) - \eta I \right] \frac{dS}{d\eta} = 0 \tag{5.4}$$

where, for a given $S$, $\eta$ is the eigenvalue given by equation (3.3) and $\frac{dS}{d\eta} := r(S) = \left( r^w \ r^g \right)^T$ the corresponding right eigenvector given by (Juanes and Patzek, 2004b):

$$\frac{r^w}{r^g} = \frac{f_g^w}{\eta - f_w^w} = \frac{\eta - f_g^g}{f_w^g} \tag{5.5}$$

Since the system is assumed to be strictly hyperbolic for all $S$ in the saturation space, the eigenvalues will be real and distinct. This means that the solution $S$ will travel with speed $\eta(S)$ along the integral curve obtained from $\frac{dS}{d\eta} = r(S)$. Since the eigenvalues are distinct, a slow-family rarefaction wave travelling with speed $\eta_s$ and a fast-family rarefaction wave travelling with speed $\eta_f$ where $\eta_s < \eta_f$ can be distinguished.

### Rarefaction curves
From the eigenvalue problem (5.4) it follows that:

$$\frac{dS}{d\eta} = r(S) \tag{5.6}$$

This ODE gives the integral curves in the saturation space. For each state $S$ there are two integral curves that cross each other; one integral curve for $\eta_s(S)$ and one for $\eta_f(S)$. Since the speed of the solution must increase from upstream to downstream the wave speed, i.e the eigenvalues, along an integral curve must increase when following the integral curve from an upstream to an downstream state. Therefore, a distinction is made between genuinely nonlinear problems and non-genuinely nonlinear problems. For genuinely nonlinear problems, the eigenvalues increase monotonically along the entire integral curve. This corresponds to a convex flux function for the scalar case, see Chapter 2. The system is genuinely nonlinear if (Juanes and Patzek, 2004b):

$$\nabla \eta_p(S) \cdot r_p(S) \neq 0, \quad \text{for all } S \in T, \quad p \in \{s, f\} \tag{5.7}$$

For a non-genuinely nonlinear system the eigenvalues do not increase monotonically along an integral curve, instead the eigenvalues reach an extreme value somewhere on the integral curve, say at state $S^*$. Therefore, the system is called non-genuinely nonlinear if there exists an $S^* \in T$ such that:

$$\nabla \eta_p(S^*) \cdot r_p(S^*) = 0, \quad \text{for } S^* \in T, \quad p \in \{s, f\} \tag{5.8}$$

The curve that connects all maxima or minima along the integral curves of one family, given by all $S \in T$ for which equation (5.8) holds, is called the inflection locus, e.g. (Juanes and Patzek, 2004b), or the fognal, e.g (Holden, 1987). The existence of an extreme value means that, for a non-genuinely nonlinear system, only part of the integral curve corresponds to a rarefaction wave. For an upstream state $S_u$ only that part of the slow-family integral curve of $S_u$ along which the eigenvalue increases is the rarefaction curve of $S_u$. Equivalently, for a downstream state $S_d$ the rarefaction curve of $S_d$ is only that part of the fast-family integral curve along which the eigenvalue decreases.

### 5.1.2. Shock waves
Another possibility for a self-similar solution is a discontinuity that travels with a speed $\sigma$. These discontinuities are weak solutions, meaning that they to do not satisfy the problem in differential form (1.14) but satisfy the corresponding integral equation. From this integral equation it is possible to obtain the Rankine-Hugoniot (RH) conditions, see e.g. LeVeque (2002):

$$- \sigma (S_d - S_u) + f(S_d) - f(S_u) = 0 \tag{5.9}$$

where $S_d$ denotes the state downstream of the discontinuity and $S_u$ denotes the state upstream of the discontinuity. This condition remains valid if the states $S_u$ and $S_d$ are interchanged (Azevedo et al., 2010). Therefore, for a discontinuity to be a shock, an additional physical admissibility condition must be satisfied. If the system is strictly hyperbolic and if the fractional flow functions are such that the problem is genuinely nonlinear, the Lax entropy condition determines which discontinuities are physical shocks. This condition ensures that,

for a p-shock, the p-characteristics impinge on the discontinuity while the other characteristics cross the discontinuity (LeVeque, 2002). The Lax entropy condition, for a $2 \times 2$ system, is given by (Azevedo et al., 2010):

$$\eta_s(S_d) < \sigma < \eta_s(S_u) \quad \text{and} \quad \sigma < \eta_f(S_d) \quad \text{for a slow-family shock wave}$$
$$\eta_f(S_d) < \sigma < \eta_f(S_u) \quad \text{and} \quad \sigma > \eta_s(S_u) \quad \text{for a fast-family shock wave}$$

(5.10)

For a non-genuinely nonlinear system, the number of characteristics impinging on a shock might be different (LeVeque, 2002) and the Lax entropy condition cannot be used to determined physical admissibility. Instead, the Liu entropy condition can be used. The Liu entropy condition, which is an extension of the Lax entropy condition and Oleinik's entropy condition which only holds for the scalar case, is given by (Liu, 1974):

$$\sigma_p(S_d, S_u) \le \sigma_p(S, S_u), \quad \text{for } p \in \{s, f\}$$

(5.11)

If the inflection loci are single connected curves, this condition is equivalent to (Juanes and Patzek, 2004b):

$$\eta_s(S_d) < \sigma \le \eta_s(S_u) \quad \text{and} \quad \sigma < \eta_f(S_d)$$
$$\eta_f(S_d) < \sigma \le \eta_f(S_u) \quad \text{and} \quad \sigma > \eta_s(S_u)$$

(5.12)

Note that the Liu entropy condition reduces to the Lax entropy condition in the case that the system is genuinely nonlinear.

Another option for an admissibility condition is the vanishing viscosity criterion which is sometimes also called the viscous profile criterion. For the vanishing viscosity criterion a small viscosity term is introduced to the system:

$$S_t + f_x = \varepsilon \left( D(S) S_x \right)_x$$

(5.13)

where $D(S)$ is a diffusion term. Taking $S_u$ and $S_d$ as boundary conditions the weak discontinuity $S$ joining $S_u$ and $S_d$ is a shock if it is a solution to equation (5.13) in the limit $\varepsilon \to 0$ (Isaacon et al., 1992).

### Rankine-Hugoniot loci
The Rankine-Hugoniot condition (5.9) together with the appropriate admissibility conditions determine the shock solution. If one state in the RH condition is fixed, say the upstream state $S_u$, then all downstream states $S_d$ for which the states $S_u$ and $S_d$ satisfy the RH condition describe a curve through saturation space. This curve is called the Rankine-Hugoniot locus. The part of this curve for which the admissibility condition is satisfied is called the shock curve and gives all the states $S_d$ that can be reached by a shock from state $S_u$. In a similar way, it is possible to determine a 'backward' Rankine-Hugoniot locus and shock curve, which is the curve given by all states $S_u$ that can shock to a state $S_d$ (Azevedo et al., 2010). If the system is strictly hyperbolic and non-genuinely nonlinear and if the Liu entropy condition is used to determine shock admissibility, then the shock curve through every state $S$ is connected to $S$ and consists of two continuous branches without self intersections (Holden, 1987). The RH-locus is tangent to the integral curve in the reference state, which means that one of these shock curves is tangent to the fast-family integral curve and the other one is tangent to the slow-family integral curve (LeVeque, 2002). This leads to a division of the shock curve in a fast-family curve and a slow-family curve.

### 5.1.3. Wave-curve method
In general the solution to the Riemann problem consists of a sequence of constant states, starting with the downstream state and ending with the upstream state, that are connected with rarefaction waves, shock waves or a combination thereof. Assuming a strictly hyperbolic system, which may be non-genuinely nonlinear, a slow-family wave $W_s$ connects the upstream state $S_u$ to a constant middle state $S_m$ which is subsequently connected to the downstream state $S_d$ by a fast-family wave $W_f$ (Juanes and Patzek, 2004b; Marchesin and Plohr, 2001), such that:

$$S_d \xrightarrow{W_f} S_m \xrightarrow{W_s} S_u$$

If the system is genuinely-nonlinear, such a slow- or fast-family wave is either a rarefaction wave or a shock wave. If the system is non-genuinely nonlinear such a wave is a rarefaction wave, a shock wave, or a composite wave. A fast-family composite wave consist of fast-family shock followed by a fast-family rarefaction and a slow-family composite wave consists of slow-family rarefaction followed by a slow-family shock (Holden, 1987). A composite wave of a family can only occur if the upstream and downstream states lie on opposite

sides of the inflection locus of that family (Juanes and Patzek, 2004b), see also the BL solution in Chapter 2. The shock speed is then equal to the speed of the rarefaction wave at the state where the rarefaction wave and the shock wave connect (Holden, 1987; Juanes and Patzek, 2004b). This means that there is no constant state between the shock wave and rarefaction wave that make up the composite wave.

In order to determine the solution to the Riemann problem, the middle state $S_m$ must be found. This is done by computing the rarefaction and shock curves through the upstream state $S_u$ and the 'backward' rarefaction and shock curves through the downstream state $S_d$. Recall that the wave speed must increase from upstream to downstream. This means that through state $S_u$ the slow-family rarefaction and shock curves are computed, while through state $S_d$ the fast-family rarefaction and shock curves are computed. The rarefaction and shock curves form a continuous curve, called a wave-curve (Azevedo et al., 2010), along which the wave speed increases when looking from upstream to downstream. The intersection between the slow-family wave-curve and fast-family wave-curve determine the middle state $S_m$. Following the slow-family wave-curve from the upstream state $S_u$ to the middle state $S_m$ and from there following the fast-family wave-curve to the downstream state $S_d$, the complete Riemann solution can be obtained. For a more detailed explanation see e.g. Azevedo et al. (2010).

An example is shown in Figure 5.1. This figure shows the integral curves through the upstream and downstream state, the RH locus of the middle state and the saturation path. First note that the saturation path follows the integral curves or the RH locus, as expected when using the wave curve method. Also note that the upstream state has not yet reached the point that was used to obtain the saturation path, meaning that the saturation path does not fully reach the upstream state. From Figure 5.1b combined with the value of the eigenvalues on the integral curves and the values of the shock speed of the RH locus it follows that the solution starts with the downstream state which is connected to the middle state with a fast-family shock-rarefaction wave. This middle state is then connected to the upstream state with a slow-family shock-rarefaction wave. Hence, the full solution has the following structure:

$$S_d \xrightarrow{SR_f} S_m \xrightarrow{SR_s} S_u \tag{5.14}$$

where $\xrightarrow{S}$ denotes a shock wave, $\xrightarrow{R}$ denotes a rarefaction wave and $\xrightarrow{SR}$ denotes a shock-rarefaction wave.



(a) Saturation profile

(b) Analysis of numerical solution

Figure 5.1: Saturation profile at half of the total simulation time (a) and analysis of numerical solution for the total simulation time (b) using interpolation I. In (a) the blue line shows the water saturation, the red line shows the oil saturation and the green line shows the gas saturation. In (b) the red line shows the fast integral curve through the downstream state and the blue line shows the RH locus of the downstream state. The pink line shows the slow integral curve through the upstream state. The green lines shows the RH locus of the middle state. The black crosses show the saturation path. The injection state, upstream state and complete saturation path are located inside the hyperbolic region.

## 5.2. Non-strictly hyperbolic system

The same problem described as in the beginning of Section 5.1 will be looked at, only now fractional flow functions are allowed such that the system becomes non-strictly hyperbolic. This means that the saturation triangle contains one or multiple umbilic points or one or multiple elliptic regions. One of the main

problems with the solution to the Riemann problem in case of loss of strict hyperbolicity is the existence and uniqueness of the Riemann problem. There are examples in which the Liu entropy conditions cannot guarantee existence, e.g. (Shearer et al., 1987), and at the same time there are examples in which the vanishing viscosity criterion fails to guarantee uniqueness, e.g. (Azevedo and Marchesin, 1995) or (Isaacson et al., 1990). Moreover, there are other examples in which the vanishing viscosity criterion fails to guarantee existence (Čanić, 2003). Therefore, none of the admissibility conditions for shocks used in the strictly hyperbolic case are sufficient to ensure existence and uniqueness of the solution to the Riemann problem in the case of loss of strict hyperbolicity. Since there is yet no admissibility condition that ensures uniqueness for a general 2x2 non-strictly hyperbolic system, one of these classical admissibility conditions must still be used. In multiphase porous media flow, the preferred method is the vanishing viscosity criterion, since this condition encompasses and generalizes the Lax and the Oleinik entropy condition (Azevedo and Marchesin, 1995). Furthermore, the vanishing viscosity criterion takes physical effects into account that were neglected in the multiphase porous media flow model (Azevedo and Marchesin, 1995; Isaacson et al., 1990). Since it is the most used criterion in porous media flow, the vanishing viscosity criterion will be used to obtain a numerical solution in this thesis.

Another problem that arises when solving the Riemann problem for non-strictly hyperbolic systems is the possibility of transitional waves which do not belong to either the fast family or the slow family. Transitional shock waves are shock waves that obey the vanishing viscosity criterion but that do not obey the Lax entropy condition (Isaacson et al., 1990). These transitional shock waves are also called undercompressive shock waves (Marchesin and Plohr, 2001) because they have a smaller number of characteristics impinging on the shock than in the classical case causing them to violate Lax entropy condition (LeVeque, 2002). This violation of Lax entropy condition also means that it is unclear whether the shock belongs to the fast or slow family (LeVeque, 2002). Since the transitional shocks obey the vanishing viscosity criterion they are sensitive to the precise form of the diffusion term (Isaacson et al., 1990). This means that qualitatively different solutions might arise when the diffusion term is modelled differently, e.g. due to an incorrect capillary pressure term or due to numerical diffusion (Azevedo et al., 2002; Isaacson et al., 1990; Marchesin and Plohr, 2001).
Transitional rarefaction waves are rarefactions waves that change family. It occurs when a slow-family rarefaction curve joins a fast-family rarefaction curve and if the fast and slow eigenvalues are equal at the point where the rarefaction curves join (Isaacson et al., 1990). This means that this can only happen at an umbilic point or at the edge between the elliptic region and the hyperbolic region. When looking from upstream to downstream, these transitional rarefaction waves start of as a slow-rarefaction wave and switch to a fast-rarefaction wave at the point where the two rarefaction curves join. Since the fast and slow speed are equal at this point the state where they join is not a constant state. Note that it is also possible to have a compositional transitional wave (Isaacon et al., 1992), i.e. a transitional shock wave directly followed by a transitional rarefaction wave or the other way around.
Thirdly, note that rarefactions curves do not enter the elliptic region (Holden, 1987). Furthermore, the use of the vanishing viscosity condition, opposed to using the Liu entropy condition, combined with loss of strict-hyperbolicity implies that the shock curves of state $S$ are no longer necessarily connected to $S$ nor necessarily smooth curves without self-intersections. They might contain loops or detached branches (Holden, 1987; Keyfitz, 1991). If a state $S$ is inside the elliptic region, its RH locus will not be connected to state $S$ itself an it will be completely located outside the elliptic region (Holden, 1987). Therefore, if the upstream and the downstream state are both in the elliptic region, they cannot be connected directly by either a rarefaction wave, shock wave or composite wave. The solution must then always contain at least one state outside the elliptic region (Holden, 1987).

### 5.2.1. Wave-curve method for non-strictly hyperbolic system

For a system that is not strictly hyperbolic more than three constant states can arise, e.g. (Azevedo et al., 2010). This means that the wave-curve method as described in Section 5.1.3 fails, since now multiple constant states must be determined. Currently a general method to determine the Riemann solution for a non-strictly hyperbolic system does not exist. However, the RH loci and the rarefaction curves can still be used to obtain information about the structure of the numerical solution. For instance, the constant states can be obtained from the numerical solution after which the rarefaction curves and the RH locus of this state can be computed. Due to numerical errors, these curves will not be exact and the saturation path can show some deviations from the rarefaction curves or the RH loci. An example is shown in Figure 5.2 and a further zoom in of the saturation path is shown in Figure 5.3. In this second figure it can be seen that there is an

elliptic region and that the saturation path passes through the elliptic region. From Figure 5.2a it can be con-



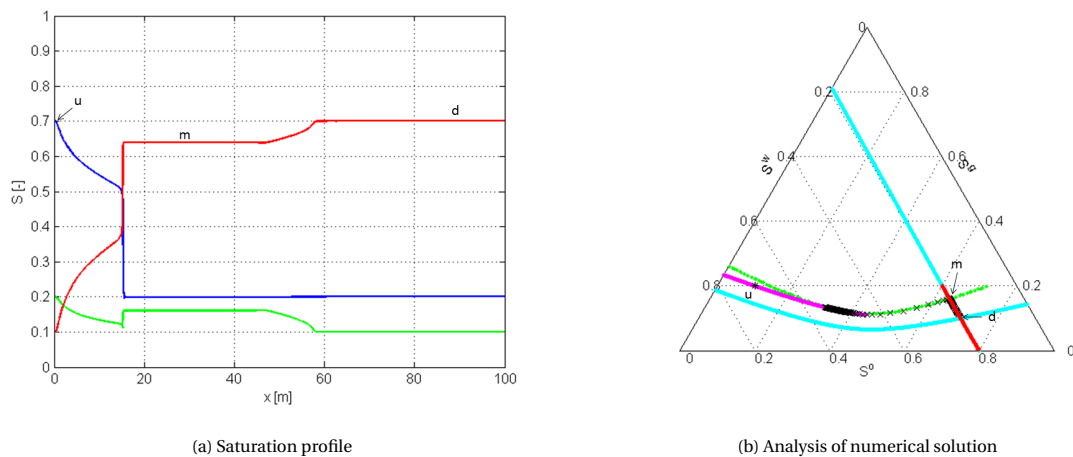(a) Saturation profile                  (b) Analysis of numerical solution
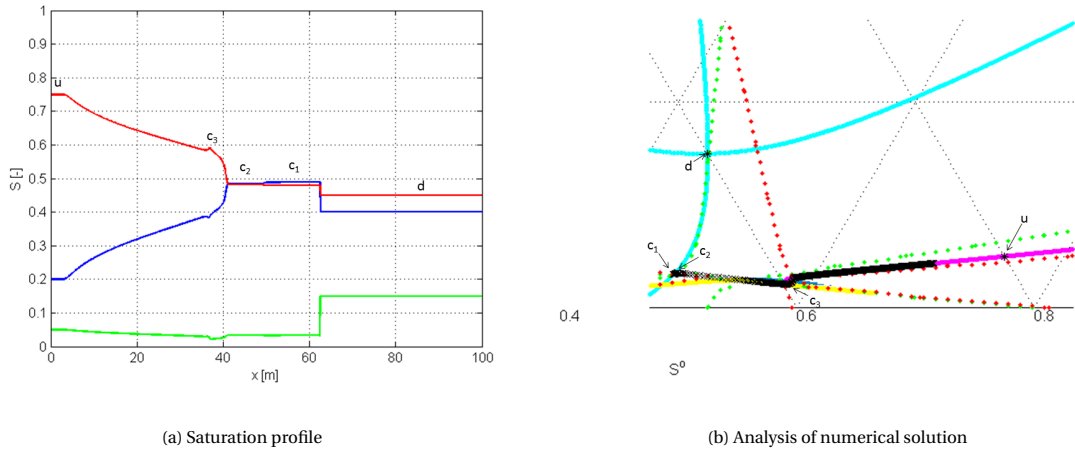
Figure 5.2: Saturation profile at half of the total simulation time (a) and analysis of numerical solution for the total simulation time (b), both using interpolation I. In (a) the water saturation is shown in blue, the gas saturation is shown in green and the oil saturation is shown in red. In (b) the light blue curves shows the RH locus of the downstream state $d$, the green curve shows the RH locus of the second constant state $c_2$, the red curve shows the RH locus of the third constant state $c_3$. The pink line shows the slow integral curve through the upstream state $u$ and the yellow line shows the fast-family integral curve through $c_3$. The saturation path is shown in black and the elliptic region is shown in blue.
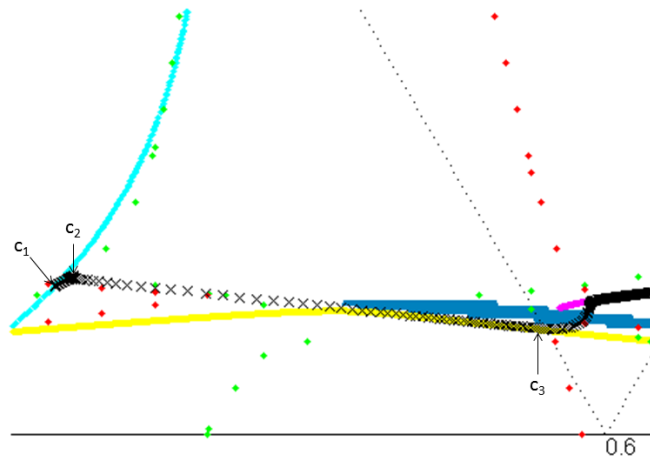


Figure 5.3: Analysis of numerical solution using interpolation I. The light blue curves shows the RH locus of the downstream state $d$, the green curve shows the RH locus of the second constant state $c_2$, the red curve shows the RH locus of the third constant state $c_3$. The pink line shows the slow integral curve through the upstream state $u$ and the yellow line shows the fast-family integral curve through $c_3$. The saturation path is shown in black and the elliptic region is shown in blue.

cluded that there is indeed more than one constant state, meaning that the wave-curve method cannot be used. There are even three constant states aside from the upstream en downstream states, denoted by $c_1$, $c_2$ and $c_3$ when looking from downstream to upstream. These constant states are also shown in the saturation path in Figures 5.2b and 5.3. Knowing these constant states, the RH loci and integral curves of these constant states can be computed in order to determine the structure of the numerical solution. When looking at the wave speeds of the resulting RH loci and integral curves, only one wave-curve remains such that the speed increases from upstream to downstream. Part of this wave-curve is shown in Figures 5.2b and 5.3 from which

it can be concluded that the numerical solution has the following structure from downstream to upstream; the downstream state is connected to the first constant state $c_1$ with a fast-family shock, shown in light blue in Figures 5.2b and 5.3. The constant state $c_1$ is then connected to the second constant state $c_2$ with a shock. Note that this part of the wave-curve is not shown in Figures 5.2b and 5.3 since $c_1$ and $c_2$ are too close to each other. The constant state $c_2$ is then connected to the third constant state $c_3$ by a shock-rarefaction wave, which is shown in green followed by yellow in Figures 5.2b and 5.3. Finally, the constant state $c_3$ is connected to the upstream state by a shock-rarefaction, which is shown in red followed by pink in Figures 5.2b and 5.3. Thus, the full solution has the following structure:

$$S_d \xrightarrow{S_f} S_{c_1} \xrightarrow{S} S_{c_2} \xrightarrow{SR} S_{c_3} \xrightarrow{SR} S_u \tag{5.15}$$

This example clearly shows that multiple constant states can indeed arise when loss of strict hyperbolicity occurs, meaning that the wave-curve method as described in section 5.1.3 cannot be used to obtain the Riemann solution. Furthermore, this example shows that a non-strictly hyperbolic system can result in a more complex structure of the Riemann solution than the Riemann solution of the strictly hyperbolic case.

Now that the structure of a solution can be analysed, the effect of different relative permeability models on the existence of the elliptic region and on the numerical solution can be investigated.

<div style="text-align: right;">

# 6

</div>

# Effect of relative permeability model on the existence and location of the elliptic region

From section 3.4 it can be concluded that it is not easy to detect if the numerical solution is in the elliptic region or is entering the elliptic region during the simulation based on the Jacobian of FIM. As an alternative, analysis to determine the existence and location of the elliptic region can be done before the simulation is started. It is straightforward to make a plot like Figure 3.1 which shows the elliptic region in the ternary diagram. This works well for system with a relative permeability model that results in a large elliptic region. However, for realistic relative permeabilities the elliptic regions are typically small and occupy only 1% of the ternary diagram (Jackson and Blunt (2002) and references therein). Using relative permeability models described in Chapter 4 with realistic Corey-coefficients also results in small elliptic regions. In order to make a plot as in Figure 3.1, the eigenvalues $\eta$ of the Jacobian (3.3) must be determined for every saturation value in the ternary diagram. To compute the eigenvalues numerically only a finite number of discrete saturation values can be used. If the spacing between the discrete saturation values is too large, a small elliptic region might not be visible. Furthermore, a single umbilic point is almost impossible to detect by computing the eigenvalues for a finite number of saturation values. Therefore, different techniques must be used to determine the existence and location of the elliptic region based on the relative permeability model. Multiple methods will be discussed in this chapter. First, rotation in the direction of the eigenvectors on the edges of the ternary diagram might be used to determine the existence of an elliptic region. Secondly, curves through the ternary diagram based on the fractional flow functions can be used to determine the existence and location of the elliptic region. Two sets of these curves will be discussed, namely the curves by Holden (1990) and the two-phase-like flow curves by Medeiros (1992).

To discuss the importance of the rotation of the eigenvectors on the edges of the ternary diagram and the importance of the curves by Holden a distinction is made between removable and non-removable elliptic regions. These terms are introduced by Holden (1990), who states that an elliptic region is called removable if it can be removed from the ternary diagram by a continuous perturbation of the fractional flow functions. A non-removable elliptic region is an elliptic region that can only be shrunk to an umbilic point by a continuous perturbation of the fractional flow functions. It is important to note that Holden (1990) considers only a certain class of relative permeability models. He assumes a Stone-type model and requires certain conditions on the fractional flow functions inside the ternary diagram and on the edges of the ternary diagram on top of the condition that the model must reduce to two-phase flow on the edges. This means that there are elliptic regions that are non-removable in the context of Holden (1990) but that may be removed from the ternary diagram by choosing a different three-phase relative permeability model.

## 6.1. Eigenvectors on edges of ternary diagram

Holden (1990) finds that the ternary diagram contains a non-removable elliptic region if and only if the eigenvectors rotate along a path following the boundary of the three-phase flow region where all three phases are mobile. This means that if the eigenvectors switch direction along one of the edges, i.e rotate 180°, there is a non-removable elliptic region inside the ternary diagram. Furthermore, this means that if the eigenvectors

of one family are parallel to each edge and if the eigenvector points into the ternary diagram for saturations close to the corners, there is a non-removable elliptic region (Holden, 1990; Juanes and Patzek, 2004a). Based on this observation Juanes and Patzek (2004a) derive necessary conditions on the relative permeability model for the system to be strictly hyperbolic, which will be discussed later in this section.

Note that an eigenvector is parallel to the edge on that edge if and only if two-phase flow behavior occurs



(a) Interpolation I                                          (b) Interpolation III
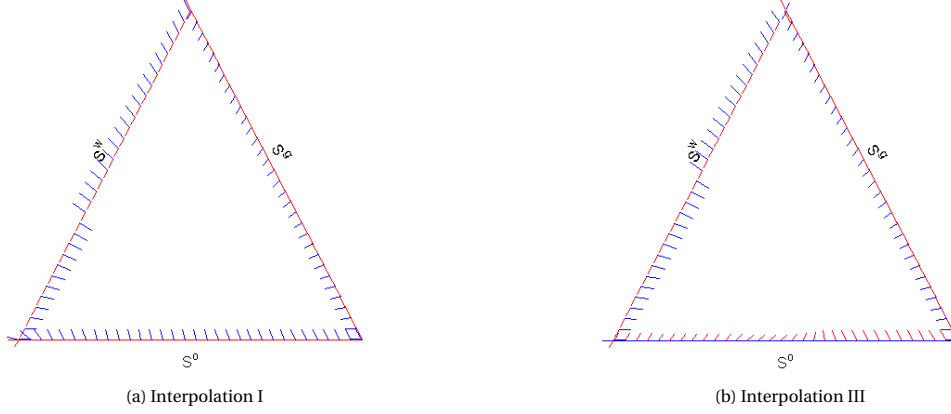
Figure 6.1: Direction of the eigenvectors on the edges of the ternary diagram for interpolation I (a) and III (b). The fast eigenvectors are shown in red and the slow eigenvector is shown in blue.

on the edge. This means that for interpolation I and III at least one of the eigenvectors is parallel to the edge on each edge and it can be determined to which family this eigenvector belongs. Interpolation II will not be considered, since it does not reduce to two-phase behavior on the edges, and therefore none of the eigenvectors is parallel to the edge on any of the edges.
In order to determine for interpolation I and III to which family the parallel eigenvector belongs, first recall that the eigenvectors of the linearized dimensionless system (5.5) are given by:

$$\frac{r^w}{r^g} = \frac{f_g^w}{\eta - f_w^w} = \frac{\eta - f_g^g}{f_w^g} \tag{6.1}$$

where the eigenvalues are given by equation (3.3):

$$\eta = \frac{1}{2}\left[ f_w^w + f_g^g \pm \sqrt{(f_w^w - f_g^g)^2 + 4f_g^w f_w^g} \right]$$

If the eigenvalues are real then the fast eigenvalue $\eta_f$ is equal to $\eta_+$ and the slow eigenvalue $\eta_s$ is equal to $\eta_-$. Note that an eigenvector is parallel to the OW edge if $r = (1\ 0)^T$, parallel to the OG edge if $r = (0\ 1)^T$ and parallel to the WG edge if $r = (1\ -1)^T$.
This section will only give the short version of the proof of which family is parallel to which edge. For the proof in full detail, see Appendix C.

### 6.1.1. Interpolation I

First the eigenvectors on the OW edge will be looked at. The right eigenvector $r = (r^w\ r^g)^T$ will be parallel to the OW edge if $r = (1\ 0)^T$. In other words, using equation (6.1), the right eigenvector is parallel to the OW edge if:

$$\frac{r^g}{r^w} = \frac{\eta - f_w^w}{f_g^w} = 0 \tag{6.2}$$

On the OW edge interpolation I gives $f_w^g, f_g^g = 0$ for all $0 < S^w, S^g < 1$ and $f_g^w, f_w^w \neq 0$ for most $0 < S^w, S^g < 1$. Substituting this and the expression for the eigenvalues in equation (6.2) gives that the large eigenvector will always be parallel to the OW edge.
A similar argument holds on the OG edge. The right eigenvector is parallel to the OG edge if:

$$\frac{r^w}{r^g} = \frac{\eta - f_g^g}{f_w^g} = 0 \tag{6.3}$$

On the OG edge interpolation I gives $f_g^w, f_w^w = 0$ for all $0 < S^w, S^g < 1$ and $f_w^g, f_g^g \neq 0$ for most $0 < S^w, S^g < 1$. Substituting this and the expression for the eigenvalues in equation (6.3) gives that the large eigenvector will always be parallel to the OG edge.

The proof for the WG edge is slightly different but goes along the same lines. The right eigenvector is parallel to the WG edge if:

$$\frac{r^w}{r^g} = \frac{\eta - f_g^g}{f_w^g} = -1 \tag{6.4}$$

On the WG edge interpolation I gives $f_w^g = -f_w^w$ and $f_g^w = -f_g^g$. Substituting this and the expression for the eigenvalues in equation (6.4) gives that the large eigenvector will always be parallel to the WG edge.

So, for interpolation I the fast-family eigenvector is always parallel to the edge on all three edges of the ternary diagram, see Figure 6.1a. In this figure it can also be seen that the small eigenvector switches direction on the WG edge, meaning that a non-removable elliptic region should be present. In figure 6.4 it can be seen that there is indeed a non-removable elliptic region inside the ternary diagram.

### 6.1.2. Interpolation III

Again, the OW edge is considered first. As for interpolation I, the condition for the right eigenvector to be parallel to the OW edge is given by equation (6.2). On the OW edge interpolation III gives $f_w^g = 0$ and $f_w^w, f_g^g, f_g^w \neq 0$. Substituting this in the expression for the eigenvalues gives that the eigenvalues have a $\sqrt{(f_w^w - f_g^g)^2}$ term. This term is either $f_w^w - f_g^g$ or $-(f_w^w - f_g^g)$ depending on the sign of $f_w^w - f_g^g$. Therefore, the following conditions to determine which eigenvector is parallel to the OW edge can be obtained from equation (6.2):

- If $f_w^w - f_g^g > 0$ then the fast-family eigenvector is parallel to the OW edge.

- If $f_w^w - f_g^g < 0$ then the slow-family eigenvector is parallel to the OW edge.

- If $f_w^w - f_g^g = 0$ then both eigenvectors are parallel to the OW edge.

On the OG edge interpolation III gives $f_g^w = 0$ and $f_w^w, f_g^g, f_g^g \neq 0$. Again, this results in a $\sqrt{(f_w^w - f_g^g)^2}$ term in the expression for the eigenvalues. Using this, equation (6.3) results in the following conditions to determine which eigenvector is parallel to the OG edge:

- If $f_w^w - f_g^g < 0$ then the fast-family eigenvector is parallel to the OG edge.

- If $f_w^w - f_g^g > 0$ then the slow-family eigenvector is parallel to the OG edge.

- If $f_w^w - f_g^g = 0$ then both eigenvectors are parallel to the OG edge.

On the WG edge interpolation III gives $f_g^w = -f_g^g - \frac{1}{\lambda_T}\lambda_w^o$ and $f_w^g = -f_w^w - \frac{1}{\lambda_T}\lambda_w^o$ using that $\lambda_w^o = \lambda_g^o$ on the WG edge. After some rewriting this results in a $\sqrt{(f_w^w + f_g^g + 2\frac{1}{\lambda_T}\lambda_w^o)^2} = |f_w^w + f_g^g + 2\frac{1}{\lambda_T}\lambda_w^o|$ term in the eigenvalues. Equation (6.4) then gives the following conditions to determine which eigenvector is parallel to the WG edge:

- If $f_w^w + f_g^g + 2\frac{1}{\lambda_T}\lambda_w^o < 0$ then the fast-family eigenvector is parallel to the WG edge.

- If $f_w^w + f_g^g + 2\frac{1}{\lambda_T}\lambda_w^o > 0$ then the slow-family eigenvector is parallel to the WG edge.

- If $f_w^w + f_g^g + 2\frac{1}{\lambda_T}\lambda_w^o = 0$ then both eigenvectors are parallel to the WG edge.

Thus for interpolation III the eigenvector that is parallel to the edges is not necessarily from the same family on every edge, see Figure 6.1b. In fact, the family might change on an edge such that the fast-family eigenvector is parallel to the edge on part of the edge and the slow-family eigenvector is parallel to the edge on the other part of the edge. This difference with interpolation I is caused by the influence of interpolation II, which introduces a non-zero derivative of the relative permeability on the edge where the saturation is zero.

### 6.1.3. Hyperbolic model

The assumptions that are commonly made on three-phase relative permeability, see e.g. (Holden, 1990) or (Shearer, 1988), will lead to systems where the fast-family eigenvectors are always parallel to the edge on all edges. This means that those type of relative permeability models will generally give rise to an elliptic region (Holden, 1990; Juanes and Patzek, 2004a). In order to avoid the existence of an elliptic region and to obtain a relative permeability model that results in a strictly hyperbolic system Juanes and Patzek (2004a) let go of these common assumptions. They start by assuming that the system is strictly hyperbolic everywhere inside the ternary diagram. This leads to necessary conditions on the relative permeability models for the systems to be strictly hyperbolic. The only assumption on the relative permeability model is that the system must reduce to two-phase flow behavior on the edges of the ternary diagram. From this it directly follows
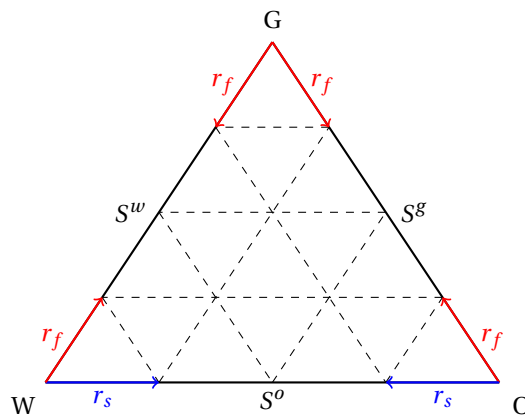


Figure 6.2: Direction of fast eigenvector $r_f$ (red) and slow eigenvector $r_s$ (blue) along all edges to allow strict hyperbolicity inside the ternary diagram.

that on each edge one of the eigenvectors must be parallel to that edge. This means that the systems cannot be strictly hyperbolic on all edges and in all corners. The systems is either strictly hyperbolic in all corners which means that there is at least one edge with an umbilic point, or the system is strictly hyperbolic on all edges and at least one of the corners is an umbilic point. Since the mobility of gas is usually higher than the mobility of the other two phases Juanes and Patzek (2004a) assume that the fast-family eigenvectors are parallel to OG and WG edge and that the slow eigenvector is parallel to the OW edge, see Figure 6.2. This means that the gas corner will be an umbilic point. The necessary conditions for the relative permeabilities on each edge are then derived by requiring that the correct eigenvector is parallel to each edge and that the system is strictly hyperbolic along that edge, i.e. both eigenvalues must be real and distinct. Furthermore, in the W and O corner the eigenvalues are also required to be real and distinct, whereas the eigenvalues are required to be real and equal in the G corner. Assuming a Stone-type model the essential condition is that the gas relative permeability should have a positive derivative with respect to its own saturation at the OW edge. Juanes and Patzek (2004a) show that a positive derivative of the gas relative permeability with respect to gas saturation at small saturation values, i.e. near the OW edge, is in agreement with both two-phase and three-phase relative permeability data. Azevedo et al. (2010) on the other hand state that the positive derivative at the OW edge, which means that the gas relative permeability is essentially linear for small gas saturations, is typically associated with miscible flow.

For the existing relative permeability models described in section 4.1 with Corey-correlations for the two-phase relative permeabilities the derivative of the gas relative permeability with respect to its own saturation is zero. To meet the necessary condition of a positive derivative of the gas relative permeability at the OW edge, a small linear term $\varepsilon$ is introduced in the gas relative permeability for low gas saturation. The modified

gas relative permeability $\hat{k}_r^g$ and its derivative are then given by:

$$\hat{k}_r^g = \begin{cases} k_r^g & \text{for } S^g > S^{g*} \\ k_r^g + \varepsilon S^g & \text{for } S^g < S^{g*} \end{cases} \tag{6.5}$$

$$\frac{\partial \hat{k}_r^g}{\partial S^g} = \begin{cases} \frac{\partial k_r^g}{\partial S^g} & \text{for } S^g > S^{g*} \\ \frac{\partial k_r^g}{\partial S^g} + \varepsilon & \text{for } S^g > S^{g*} \end{cases} \tag{6.6}$$

The value of $\varepsilon$ is determined by the condition on the OW edge, which is given by (Juanes and Patzek, 2004a):

$$\lambda_g^g > \lambda_w^w \tag{6.7}$$

Assuming Corey-correlation with zero residual saturations and endpoints equal to one gives that this condition is met if $\varepsilon > \frac{\mu_g}{\mu_w}$. Note that adding a linear term to the gas relative permeability changes the two-phase gas relative permeability of the water-gas and oil-gas systems. Moreover, depending on the value of $\mu_g$ and $\mu_w$ the added term $\varepsilon$ can be quite large compared to the original gas relative permeability $k_r^g$. If two-phase relative permeability data is available, such a modification is undesirable.

## 6.2. Important curves

A second method to determine if an elliptic region exists is by a set of curves. Two sets of curves will be looked at, namely those defined by Holden (1990) and the curves defined by Medeiros (1992). Holden (1990) defines curves for a certain class of relative permeability models which gives sufficient conditions for the existence of an elliptic region. Medeiros (1992) defines two-phase-like flow curves which can be used to estimate the size of the elliptic region. These two-phase-like-flow curves are defined for the same class of relative permeability models as Holden (1990) considered. In this section the curves from Holden (1990) and Medeiros (1992) will be derived for more general three-phase relative permeability models. Furthermore, the behavior of the curves by Holden for interpolation I, III and the hyperbolic model introduced by Juanes and Patzek (2004a) will be investigated.

### 6.2.1. Curves by Holden



(a) Interpolation I          (b) Interpolation III          (c) Hyperbolic model
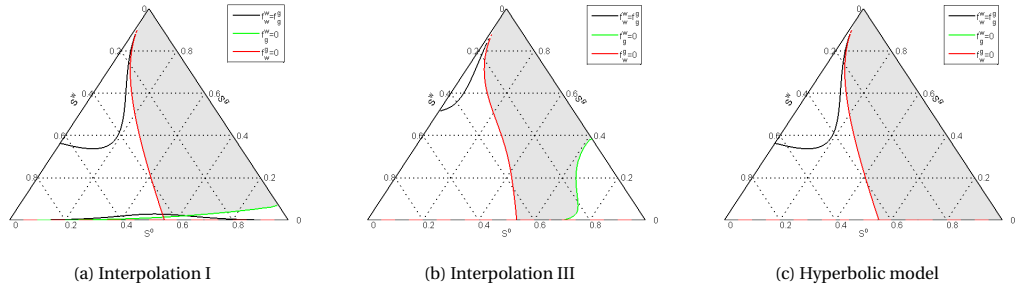
Figure 6.3: Curves by Holden for interpolation I (a), III (b) and for the hyperbolic model (c). The curve $f_g^w = 0$ is shown in green, the curve $f_w^g = 0$ is shown in red and the curve $f_w^w - f_g^g = 0$ is shown in black. The area where $f_g^w f_w^g < 0$ is shown in grey.

To derive the curves defined by Holden (1990) the term in the eigenvalues that determines if they are complex will be looked at and the derivation outlined by Holden (1990) will be followed. Thus the discriminant $d$ of the characteristic equation of the Jacobian, see equation (3.3), will be considered:

$$d = (f_w^w - f_g^g)^2 + 4 f_g^w f_w^g \tag{6.8}$$

The eigenvalues are complex if $d < 0$, real and equal if $d = 0$ and real and distinct if $d > 0$. The first part of the discriminant is always positive due to the square. The second term can be either positive or negative depending on the signs of $f_g^w$ and $f_w^g$. If this second term is positive, the entire discriminant will be positive and hence there will be no elliptic region. If on the other hand this second term is negative the discriminant can become negative. Therefore, two of the curves are given by:

$$f_g^w = 0 \quad \text{and} \quad f_w^g = 0 \tag{6.9}$$
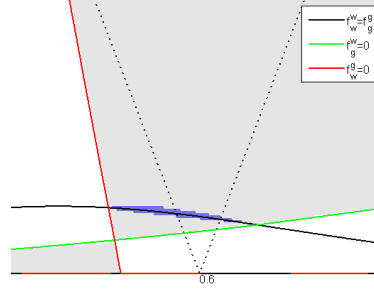
Figure 6.4: Curves by Holden for interpolation I in part of the ternary diagram. The curve $f_g^w = 0$ is shown in green, the curve $f_w^g = 0$ is shown in red, the curve $f_w^w - f_g^g = 0$ is shown in black and the elliptic region is shown in blue. The area where $f_g^w f_w^g < 0$ is shown in grey.

These two curves create a region in the ternary where the last term of the discriminant $f_g^w f_w^g$ is negative. If there is an elliptic region inside the ternary diagram, it will lie inside this negative region created by the two curves. If within this region the first term of the discriminant $(f_w^w - f_g^g)^2$ is zero, then there must be an elliptic region. Therefore, the last curve is given by:

$$f_w^w - f_g^g = 0 \tag{6.10}$$

If the last curves intersects the negative region there is an elliptic region present in the ternary diagram. For the class of relative permeability models that Holden (1990) considers, this last curve always intersects both of the other curves. It therefore either intersects the negative regions, or it intersects the other two curves at the point where they intersect each other. This means that the elliptic region found by the intersection of the third curve and the negative region is a non-removable elliptic region. The elliptic region can be shrunk to an umbilic point by continuously perturbing the fractional flow functions in such a way that the third curve intersects the other two curves at the point where they intersect each other. The umbilic point is then located at the intersection of all three curves. Thus this set of curves can also be used to determine the existence and location of an umbilic point.

For a general three-phase interpolation method the exact form of the three curves will be difficult or even impossible to determine analytically. Using a numerical approach the curves can be plotted and the location of a possible non-removable elliptic region can be determined, see Figures 6.3 and 6.4. These figures give an example of an elliptic region with the three curves shown as well. It can indeed be seen that the elliptic region lies inside the negative region created by the first two curves and that the elliptic region lies around the last curve. Another way to use these curves is to determine the qualitative behavior of the curves based on the derivatives of the fractional flow function on the edges of the ternary diagram (Holden, 1990). The first step in this procedure is to determine the sign of the relevant derivatives on the edges for each curve. For example, for the first curve the sign of $f_g^w$ is determined on all three edges. Based on these signs, the qualitative behavior of the curves can be determined, see Figure 6.5. This procedure will be further explained for interpolation I.

## Interpolation I

In order to determine the qualitative behaviour of the curves, the sign of $f_g^w$, $f_w^g$ and $f_w^w - f_g^g$ for interpolation I must be determined on the three edges of the ternary diagram. First, the sign of $f_g^w$ will be determined on all edges. The detailed expression of the derivatives of the fractional flow functions can be found in Appendix C and expressions for the derivatives of the relative permeabilities on the edges can be found in Appendix B. On the OG edge $f_g^w = 0$ for all Corey-coefficients. On the WG and the OW edge on the other hand $f_g^w$ has a different sign depending on the Corey-coefficients. On the OW edge there are two options. If $n_{og} \ll n_{ow}$ it holds that:

$$\begin{cases} f_g^w > 0 & \text{for } S^w < \hat{S}_{OW}^w \\ f_g^w < 0 & \text{for } S^w > \hat{S}_{OW}^w \end{cases} \tag{6.11}$$

where $\hat{S}_{OW}^w$ is some value of the water saturation for which $f_g^w = 0$ on the OW edge. And for any other combination of $n_{og} > 1$ and $n_{ow} > 1$ it holds that $f_g^w > 0$ for all $0 < S^w < 1$. Similarly, there are two options on the

(a) Curve 1: $f_g^w = 0$



(b) Curve 2: $f_w^g = 0$



(c) Curve 3: $f_w^w - f_g^g = 0$



(d) Curves combined
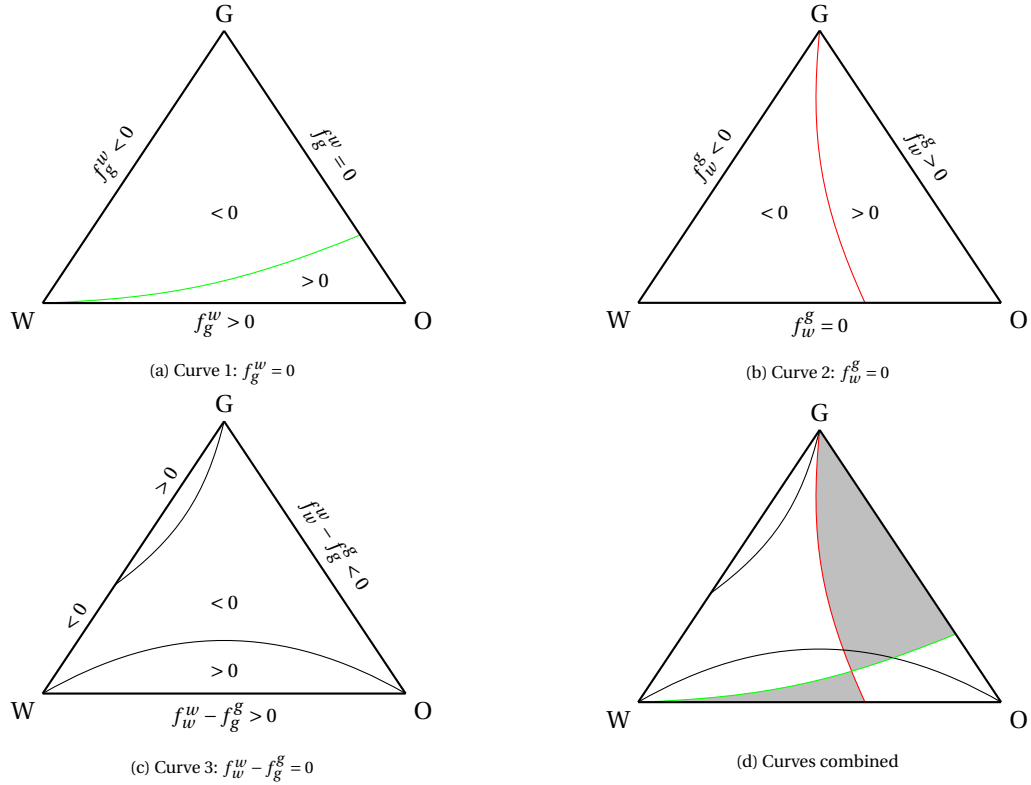
Figure 6.5: Determination of the qualitative behavior of the curves by Holden. The curve $f_g^w = 0$ is shown in green, the curve $f_w^g = 0$ is shown in red and the curve $f_w^w - f_g^g = 0$ is shown in black. The grey area shows the region where the product $f_g^w f_w^g$ is negative.

WG edge. If $n_{go} \ll n_{gw}$ it holds that:

$$\begin{cases} f_g^w > 0 & \text{for } S^w > \hat{S}_{WG}^w \\ f_g^w < 0 & \text{for } S^w < \hat{S}_{WG}^w \end{cases} \tag{6.12}$$

And for any other combination of $n_{go} > 1$ and $n_{gw} > 1$ it holds that $f_g^w < 0$. This means that in total there are four options for the signs of $f_g^w$ on the edges of the ternary diagram.

For $f_w^g$ it holds that $f_w^g = 0$ on the OW edge for all Corey-coefficients. As was the case for $f_g^w$ the sign of $f_w^g$ on the other edges depends on the Corey-coefficients. On the OG edge there are two options. If $n_{ow} \ll n_{og}$ it holds that:

$$\begin{cases} f_w^g > 0 & \text{for } S^g < \hat{S}_{OG}^g \\ f_w^g < 0 & \text{for } S^g > \hat{S}_{OG}^g \end{cases} \tag{6.13}$$

And for any other combination of $n_{ow} > 1$ and $n_{og} > 1$ it holds that $f_w^g > 0$. Similarly, there are two options on the WG edge. If $n_{wo} \ll n_{wg}$ it holds that:

$$\begin{cases} f_w^g > 0 & \text{for } S^w < \hat{S}_{WG}^w \\ f_w^g < 0 & \text{for } S^w > \hat{S}_{WG}^w \end{cases} \tag{6.14}$$

And for any other combination of $n_{wo} > 1$ and $n_{og} > 1$ it holds that $f_w^g < 0$. Thus there are four options for the signs of $f_w^g$ on the edges of the ternary diagram.

Finally for the sign of $f_w^w - f_g^g$ it holds that $f_w^w - f_g^g = f_w^w > 0$ on the OW edge for all Corey coefficients and $f_w^w - f_g^g = -f_g^g < 0$ on the OG edge for all Corey coefficients. Depending on the Corey-coefficients, there are four options on the WG edge. If $n_{wo} \ll n_{wg}$ and $n_{go} \ll n_{gw}$ it holds that:

$$\begin{cases} f_w^w - f_g^g > 0 & \text{for } S^w > \hat{S}_{WG}^w \\ f_w^w - f_g^g < 0 & \text{for } S^w < \hat{S}_{WG}^w \end{cases} \tag{6.15}$$

If only $n_{wo} \ll n_{wg}$ it holds that $f_w^w - f_g^g < 0$ and if only $n_{go} \ll n_{gw}$ it holds that $f_w^w - f_g^g > 0$. For any other combination of $n_{wo}, n_{wg}, n_{go}$ and $n_{gw}$ it holds that:

$$\begin{cases} f_w^w - f_g^g > 0 & \text{for } S^w < \hat{S}_{WG}^w \\ f_w^w - f_g^g < 0 & \text{for } S^w > \hat{S}_{WG}^w \end{cases} \tag{6.16}$$

Since combining the curves can be done in $4^3 = 64$ ways, only one example will be discussed. For the example it will be assumed that $n_{wg} = n_{wo}$ and $n_{gw} = n_{go}$, which results in a Stone-type relative permeability model when using interpolation I. This means that on the WG edge the sign of $f_w^w - f_g^g$ is determined by equation (6.16). For the other two curves it will be assumed that the sign is the same along the entire edge for each edge. It will be assumed that $f_g^w < 0$ on the WG edge, $f_g^w > 0$ on the OW edge, $f_w^g < 0$ on the WG edge and $f_w^g > 0$ on the OG edge, see Figure 6.5. From the signs on the edges the behavior of the curves can be determined. For example, looking at the sign of $f_g^w$ on the edges in Figure 6.5a it can be seen that the curve $f_g^w = 0$ must go from the W corner to the OG edge. Similarly, the $f_w^g = 0$ curve must go from the G corner to the OW edge and the $f_w^w - f_g^g = 0$ curve consists of two separate curves; one from the G corner to the WG edge and one from the W corner to the O corner. The point where a curve meets an edge and the shape of the curve inside the ternary diagram can not be determined by the signs on the edges. Therefore, only the qualitative behavior can be determined. For example, the combination of the curves as shown in Figure 6.5d suggest that there is a non-removable elliptic region inside the upper negative region. But this location depends on the exact shape of the curves inside the ternary diagram, which can not be determined solely using information on the edges. Based on the information on the edges it can however be concluded that there is at least one non-removable elliptic region or umbilic point since the $f_w^w - f_g^g = 0$ curve from W to O will always intersect the negative region or there will be a single intersection point of all three curves. Note that based on the information on the edges it is also possible that the $f_w^w - f_g^g = 0$ curve from G to WG will cross the negative region resulting in a second non-removable elliptic region. Furthermore, there can be one or more removable elliptic regions in the negative region. The qualitative behavior of the curves can therefore be used to determine if a non-removable elliptic region is present, but the location can not be determined.

### Interpolation III

To investigate the qualitative behavior of the three curves for interpolation III, the difference between interpolation III and interpolation I will be exploited. The main difference is that interpolation III has a non-zero derivative of the relative permeability on the edge where the saturation of that phase is zero. This introduces some extra terms to the derivatives of the fractional flow functions on the edges compared to the curves for interpolation I, and the effect of these extra terms on the three curves will be looked at. The detailed expression of the derivatives of the fractional flow functions can be found in Appendix C and expressions for the derivatives of the relative permeabilities on the edges can be found in Appendix B.
For the first curve $f_g^w = 0$ the sign of $f_g^w$ must be determined on all edges, for which the following holds for interpolation III:

$$f_g^{w,III} = f_g^{w,I} - \frac{1}{\lambda_T^2} \lambda^w \lambda_g^g \quad \text{on the OW edge}$$

$$f_g^{w,III} = f_g^{w,I} = 0 \qquad \text{on the OG edge} \tag{6.17}$$

$$f_g^{w,III} = f_g^{w,I} - \frac{1}{\lambda_T^2} \lambda^w \lambda_g^o \quad \text{on the WG edge}$$

where $f_g^{w,I}$ and $f_g^{w,III}$ are used to denote $f_g^w$ obtained using interpolation I and interpolation III respectively. So there are two extra terms compared to interpolation I; $-\frac{1}{\lambda_T^2} \lambda^w \lambda_g^g$ on the OW edge and $-\frac{1}{\lambda_T^2} \lambda^w \lambda_g^o$ on the WG edge. On the OW edge $\lambda^w, \lambda_g^g > 0$ for all $0 < S^w < 1$ and on the WG edge $\lambda^w, \lambda_g^o > 0$ for all $0 < S^w < 1$, for all Corey-coefficients. This means that both extra terms are negative.
For the second curve $f_w^g = 0$ the sign of $f_w^g$ must be determined on all edges, for which the following holds for

interpolation III:

$$f_w^{g,III} = f_w^{g,I} = 0 \qquad\qquad \text{on the OW edge}$$

$$f_w^{g,III} = f_w^{g,I} - \frac{1}{\lambda_T^2}\lambda^g\lambda_w^w \quad \text{on the OG edge} \tag{6.18}$$

$$f_w^{g,III} = f_w^{g,I} - \frac{1}{\lambda_T^2}\lambda^g\lambda_w^o \quad \text{on the WG edge}$$

So there are two extra terms; $-\frac{1}{\lambda_T^2}\lambda^g\lambda_w^w$ on the OG edge and $-\frac{1}{\lambda_T^2}\lambda^g\lambda_w^o$ on the WG edge. On the OG edge $\lambda^g, \lambda_w^w > 0$ for all $0 < S^g < 1$ and on the WG edge $\lambda^g, \lambda_w^o > 0$ for all $0 < S^w < 1$. Thus both extra terms are negative.

For the third curve $f_w^w - f_g^g = 0$ the sign of $f_w^w - f_g^g$ must be determined on all edges, for which the following holds for interpolation III:

$$f_w^{w,III} - f_g^{g,III} = f_w^{w,I} - f_g^{g,III} \qquad\qquad\qquad \text{on the OW edge}$$

$$f_w^{w,III} - f_g^{g,III} = f_w^{w,III} - f_g^{g,I} \qquad\qquad\qquad \text{on the OG edge} \tag{6.19}$$

$$f_w^{w,III} - f_g^{g,III} = f_w^{w,I} - f_g^{g,I} - \frac{1}{\lambda_T^2}\lambda^w\lambda_w^o + \frac{1}{\lambda_T^2}\lambda^g\lambda_g^o \quad \text{on the WG edge}$$

So there are three extra terms; $-f_g^{g,III}$ on the OW edge, $f_w^{w,III}$ on the OG edge and $-\frac{1}{\lambda_T^2}\lambda^w\lambda_w^o + \frac{1}{\lambda_T^2}\lambda^g\lambda_g^o$ on the WG edge. First note that

$$f_g^{g,III} = \frac{1}{\lambda_T^2}\left[\lambda^o + \lambda^w\right]\lambda_g^g \quad \text{on the OW edge}$$

$$f_w^{w,III} = \frac{1}{\lambda_T^2}\left[\lambda^o + \lambda^g\right]\lambda_w^w \quad \text{on the OG edge}$$

On the OW edge $\lambda^o, \lambda^w, \lambda_g^g > 0$ for all $0 < S^w < 1$ and on the OG edge $\lambda^o, \lambda^g, \lambda_w^w > 0$ for all $0 < S^g < 1$. Therefore the extra terms on the OW and OG edge are positive. Since $\lambda_w^o = \lambda_g^o > 0$ on the WG edge the extra term can be rewritten to $\frac{1}{\lambda_T^2}\left[\lambda^g - \lambda^w\right]\lambda_w^o$. Note that $\lambda^g, \lambda^w > 0$ on the WG edge. As $S^w \to 0$ it holds that $k_r^w \to 0$ and $k_r^g \to 1$ such that $\lambda^g > \lambda^w$ if $S^w$ is small. Conversely, as $S^w \to 1$ it holds that $k_r^w \to 1$ and $k_r^g \to 0$ such that $\lambda^g < \lambda^w$ if $S^w$ is large. This means that the extra term on the WG edge is positive if $S^w$ is small and negative if $S^w$ is large, i.e:

$$\begin{cases} \frac{1}{\lambda_T^2}\left[\lambda^g - \lambda^w\right]\lambda_w^o > 0 & \text{if } S^w < \hat{S}_{WG}^{w,III} \\ \frac{1}{\lambda_T^2}\left[\lambda^g - \lambda^w\right]\lambda_w^o < 0 & \text{if } S^w > \hat{S}_{WG}^{w,III} \end{cases}$$

where $\hat{S}_{WG}^{w,III}$ is some water saturation for which the extra term is zero.

Note that the sign of the extra terms is independent of the Corey-coefficients. This means that, given the curves obtained using interpolation I, interpolation III will always influence the sign of the curves on the edges in the same way. In some cases this will alter the qualitative behavior of the curves, while in other cases the influence of the extra terms may be too small to alter the behavior of the curves. The effect of interpolation III is therefore determined by the output of interpolation I which in turn is determined by the two-phase relative permeabilities. As an example of the qualitative behavior of the curves for interpolation III the example for interpolation I from the previous section will be used. Looking at the signs on the edges for interpolation I in Figure 6.5 it can be seen that the extra terms on the OW and OG edge are of opposite sign whereas the extra terms on the WG edge have the same sign as interpolation I. Looking at the sign of $f_w^w - f_g^g$ on the WG edge for interpolation I and at the sign of the extra terms it can be seen that for interpolation III $f_w^w - f_g^g$ will switch sign on the WG edge just like it does for interpolation I, but the point on the WG edge where it switches sign might be different for interpolation I and III. If the extra terms on the OW and OG edges become large enough, the signs of interpolation III will be the opposite of the signs of interpolation I. If on the other other hand the extra terms are small the signs of interpolation III will be the same as the signs of interpolation I.

(a) Interpolation I                                    (b) Interpolation, second option
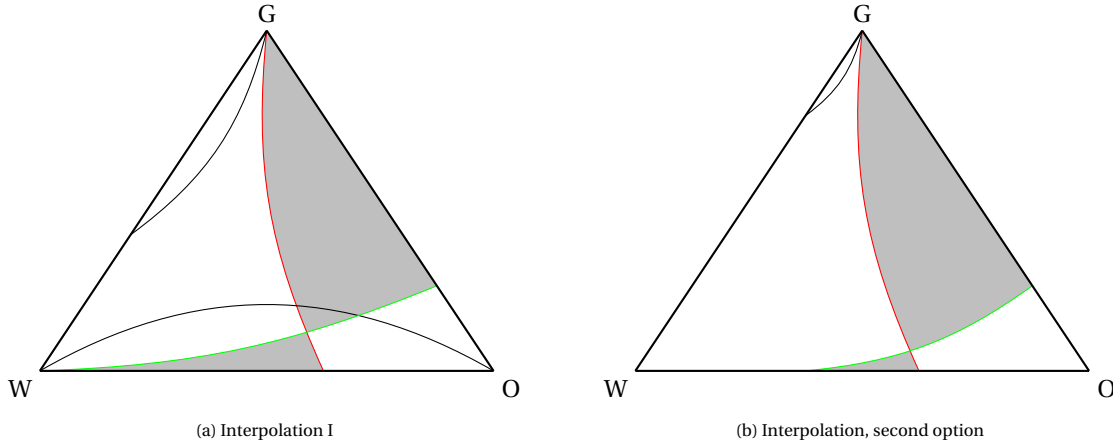
Figure 6.6: Example of the qualitative behavior of the curves by Holden for interpolation I (a) and interpolation III (b). The curve $f_g^w = 0$ is shown in green, the curve $f_w^g = 0$ is shown in red and the curve $f_w^w - f_g^g = 0$ is shown in black. The grey area shows the region where the product $f_g^w f_w^g$ is negative.

Finally, there is also an option in between where the signs of interpolation III will change along an edge while the sign is constant along the edge for interpolation I. As an example a situation will be assumed where on the OW edge $f_w^w - f_g^g$ has opposite sign for interpolation III and interpolation I and it will be assumed that $f_g^w$ will switch sign on the OW edge for interpolation III whereas $f_g^w < 0$ on the OW edge for interpolation I. All the other signs are assumed to be the same for interpolation I and III. This leads to the curves for interpolation III as shown in Figure 6.6b. From this figure it can be concluded that the non-removable elliptic region that is present for interpolation I due to the $f_w^w - f_g^g = 0$ curve from O to W does not exist for interpolation III since there is no $f_w^w - f_g^g$ curve from O to W. This can also be seen in Figures 6.3 and 6.4. Therefore, there are situations where interpolation I shows a non-removable elliptic region which can be removed from the ternary diagram by using interpolation III instead of interpolation I.

### Hyperbolic model

The necessary conditions on the relative permeabilities to result in a strictly hyperbolic system derived by Juanes and Patzek (2004a) are based on assumptions made on eigenvectors on the edges of the ternary diagram. Comparing Figure 6.1a with Figure 6.2 shows that the difference between interpolation I and the hyperbolic model is the family of the eigenvector that is parallel to the OW edge. Therefore, the effect of this different family on the qualitative behavior of the three curves will be investigated. The assumption on the OW edge for the hyperbolic model is that $\lambda^g = 0$ and the necessary condition is that $\lambda_w^g = 0$ and $\lambda_g^g > \lambda_w^w - \lambda_{T,w} \frac{\lambda^w}{\lambda_T}$ (Juanes and Patzek, 2004a). From $\lambda_w^g = 0$ it follows that $f_w^g = 0$ and from the the fact that the small eigenvector is parallel to the OW edge it follows that $f_g^w \neq 0$ on the OW edge, just like for interpolation I. The difference with interpolation I becomes clear when looking at the sign of $f_w^w - f_g^g$. For the hyperbolic model, the small eigenvector is parallel to the OW edge. From equation (6.2) it follows that $\eta_s - f_w^w = 0$ if the small eigenvector is parallel to the OW edge. Substituting $f_w^g = 0$ in the expressions for the eigenvalues gives:

$$\eta_s - f_w^w = \frac{1}{2}\left[ f_w^w + f_g^g - \sqrt{(f_w^w - f_g^g)^2 + 4 f_g^w \cdot 0} \right] - f_w^w$$

$$= \frac{1}{2}\left[ f_g^g - f_w^w - \sqrt{(f_w^w - f_g^g)^2} \right] \tag{6.20}$$

$$= \begin{cases} 0, & f_w^w - f_g^g \leq 0 \\ f_g^g - f_w^w, & f_w^w - f_g^g > 0 \end{cases} \tag{6.21}$$

Since $\eta_s - f_w^w = 0$ it follows that $f_w^w - f_g^g \leq 0$ on the OW edge, while $f_w^w - f_g^g > 0$ on the OW edge for interpolation I. Thus, the curve $f_w^w - f_g^g = 0$ will always be qualitatively different for interpolation I and the hyperbolic model. Furthermore, the curve $f_g^w = 0$ might be qualitatively different. An example is given in Figure 6.3. In this example the hyperbolic model uses the same relative permeability model as obtained by using interpolation I but with an added linear term $\varepsilon = \frac{\mu_w}{\mu_o}$ to the gas relative permeability for gas saturation smaller than

$S^{g*} = 0.1$, see equations (6.5) and (6.6). From Figure 6.3a and 6.3c it follows that both the $f_w^w - f_g^g = 0$ and $f_g^w = 0$ curves are different. In fact, for the hyperbolic model $f_g^w < 0$ throughout the entire ternary diagram. Therefore the negative region is the region between the $f_w^g = 0$ curve and the WG edge.

Since a Stone-type model is considered adding a linear term to the gas relative permeability only changes the gas relative permeability. Furthermore, the isoperms of the gas relative permeability are straight lines parallel to the OW edge. Therefore adding the linear term to the gas relative permeability only changes the eigenvalues in the region of the ternary diagram where $S^g < S^{g*}$. If there would be an elliptic region using interpolation I for greater gas saturations, modifying the gas relative permeability will not remove the elliptic region, see Figure 6.7. Furthermore, modifying the gas relative permeability by adding a linear term for small



(a) Interpolation I                          (b) Hyperbolic model
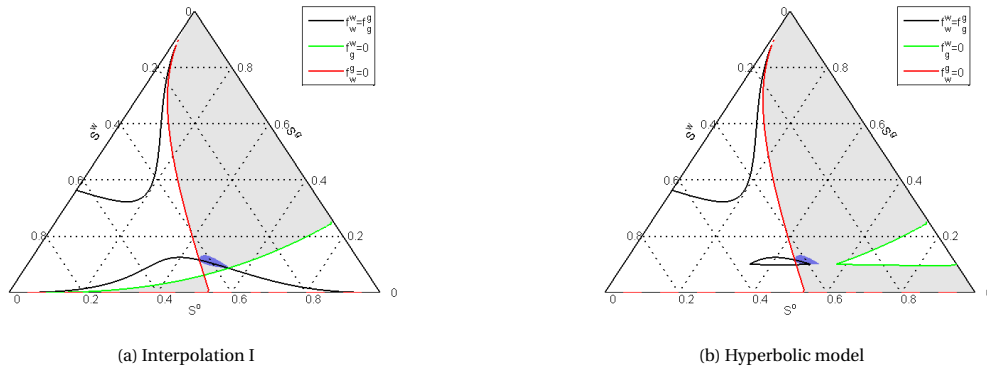
Figure 6.7: Curves by Holden for interpolation I (a) for the hyperbolic model (b). The curve $f_w^w = 0$ is shown in green, the curve $f_w^g = 0$ is shown in red and the curve $f_w^w - f_g^g = 0$ is shown in black. The area where $f_g^w f_w^g < 0$ is shown in grey and the elliptic region is shown in blue.

gas saturation also alters the gas relative permeability in part of the two-phase oil-gas and water-gas systems. In a situation where the two-phase relative permeability data is available this is an undesirable modification if $\varepsilon$ is large compared to the value of the measured gas relative permeability for small gas saturations. Altering the two-phase relative permeability data also contradicts the view that obtaining relative permeabilities that lead to a strictly hyperbolic model must be seen as interpolation problems, since this view takes the two-phase relative permeability as a given. Therefore, this model will not be considered any further.

### 6.2.2. Two-phase-like flow curves



(a) Interpolation I                          (b) Interpolation III
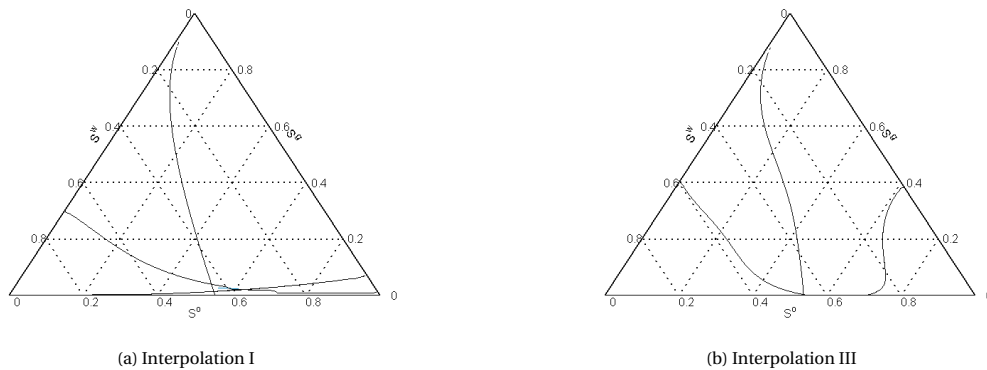
Figure 6.8: Example of two-phase-like flow curves for interpolation I (a) and III (b). The curves are shown in black and the elliptic region is shown in blue.

The second set of curves that can be used to determine if there is an elliptic region is the set of two-phase-like flow curves. A two-phase-like flow curve is characterized as a curve along which one of the eigenvectors of the Jacobian of the system (6.1) is parallel to one of the edges of the ternary diagram $T$ (Medeiros, 1992). This

means that along these curves the system locally shows two-phase flow behaviour instead of three-phase flow. Recall that the eigenvector is parallel to the OW edge if $r = (1\ 0)^T$, parallel to the OG edge if $r = (0\ 1)^T$ and parallel to the WG edge if $r = (1\ -1)^T$. Using equations (6.2), (6.3) and (6.4) the three two-phase-like flow curves are given by:

$$\eta - f_w^w = 0, \quad \text{eigenvector parallel to OW edge}$$
$$\eta - f_g^g = 0, \quad \text{eigenvector parallel to OG edge}$$
$$\eta - f_w^w + f_g^w = 0, \quad \text{eigenvector parallel to WG edge}$$

Substituting the expression for the eigenvalues results in the following curves:

$$f_g^g - f_w^w \pm \sqrt{\left(f_w^w - f_g^g\right)^2 + 4 f_g^w f_w^g} = 0, \quad \text{eigenvector parallel to OW edge} \tag{6.22}$$

$$f_w^w - f_g^g \pm \sqrt{\left(f_w^w - f_g^g\right)^2 + 4 f_g^w f_w^g} = 0, \quad \text{eigenvector parallel to OG edge} \tag{6.23}$$

$$\frac{1}{2}\left[f_g^g - f_w^w \pm \sqrt{\left(f_w^w - f_g^g\right)^2 + 4 f_g^w f_w^g}\right] + f_g^w = 0, \quad \text{eigenvector parallel to WG edge} \tag{6.24}$$

An example of the two-phase-like flow curves for interpolation I and interpolation III is shown in Figure 6.8. For a system without gravity, which is assumed for the system considered in this thesis, two of these curves are the same as two of the curves by Holden (Medeiros, 1992). The two-phase-like flow curves create one or multiple regions in which the elliptic region must be located (Medeiros, 1992). This means that the two-phase-like flow curves can be used to estimate the size and location of the elliptic region, opposed to the curves by Holden which only give sufficient conditions for the existence of an elliptic region. For the specific class of relative permeability models considered by Medeiros (1992) the regions in which the elliptic regions must be located can be determined analytically. However, for general relative permeability models the two-phase-like flow curves (6.22) - (6.24), and subsequently the regions in which the elliptic region must be located, will be difficult if not impossible to determine analytically. Therefore, the two-phase-like flow curves will not be considered any further and the curves by Holden will be used.

# 7

# Numerical experiments

In chapter 6 multiple methods are described to determine if an elliptic region is present in the ternary diagram depending on the three-phase relative permeability model. Chapter 5 explains how the structure of the numerical solution can be obtained. In this chapter the methods described in chapter 5 and 6 are used to analyse the effect of different interpolation methods on loss of strict hyperbolicity. Furthermore, the effect of a different interpolation method on the numerical solution of the three-phase porous media flow model will be investigated.

## 7.1. Loss of strict hyperbolicity for different interpolation methods

To investigate the effect of the relative permeability model on the occurrence of loss of strict hyperbolicity the existing and widely used normalized Stone interpolation will be compared with the newly introduced interpolation I and interpolation III. The current practice is to use an interpolation method to obtain the oil relative permeability only, the water and gas relative permeabilities are assumed to be function of only the water saturation and gas saturation respectively. This means that the three-phase water relative permeability is assumed to be equal to the water relative permeability of the two-phase water-oil system, i.e. $k_r^w(S^w) = k_r^{wo}(S^w)$. Similarly, the gas relative permeability is assumed to be equal to the gas relative permeability of the two-phase oil-gas systems, i.e. $k_r^g(S^g) = k_r^{go}(S^g)$. Note that this can be viewed as that an interpolation method is implicitly used to obtain the water and gas relative permeabilities anyway. As described in section 4.2.1 it is also possible to assume that all three-phase relative permeabilities depend on both the water and gas saturations, meaning that an interpolation method is used explicitly to obtain the relative permeability of all three phases. Due to the construction and assumptions of normalized Stone, see section 3.1, it can only be used to obtain the three-phase relative permeability of oil and not the water and gas relative permeability. Therefore, the following three-phase relative permeability models will be compared; normalized Stone, interpolation I and interpolation III for only the oil relative permeability, and interpolation I and interpolation III for the relative permeability of all three phases. For all interpolation methods Corey-correlations with zero residuals and endpoints one will be assumed for the two-phase relative permeabilities. Furthermore, Corey-coefficients are chosen such that $n_{gw} = n_{go} := n_g$ and $n_{wg} = n_{wo} := n_w$. Recall from chapter 4 that this choice of Corey-coefficients means that interpolation I for all phases will result in a Stone-type relative permeability model whereas interpolation III for all three phases will result in a relative permeability model where all three-phase relative permeabilities will depend on both the water and gas saturation. Note that this means that interpolation I for only oil and interpolation I for all three phases will result in the same relative permeability, i.e. they are equivalent for this choice of two-phase relative permeabilities. This means that normalized Stone, interpolation I for only oil, interpolation I for all three phases and interpolation III for oil will result in a Stone-type model, i.e. $k_r^o = k_r^o(S^w, S^g)$, $k_r^g = k_r^g(S^g)$ and $k_r^w = k_r^w(S^w)$, whereas interpolation III for all phases will result in a new type relative permeability model with $k_r^o = k_r^o(S^w, S^g)$, $k_r^g = k_r^g(S^w, S^g)$ and $k_r^w = k_r^w(S^w, S^g)$

The first example that will be looked at is the same example as used in section 3.3, i.e with the following

(a) Normalized Stone

(b) Interpolation I for only oil and interpolation I for all phases

(c) Interpolation III for only oil

(d) Interpolation III for all phases

Figure 7.1: Curves by Holden for normalized Stone (a), interpolation I (b), interpolation III for only oil (c) and interpolation III for all phases (d). All interpolation methods use two-phase relative permeabilities with $n_{og} = 2$, $n_g = 1.1$, $n_w = 1.1$ and $n_{ow} = 2$ as Corey-coefficients. The grey area shows the region where $f_g^w f_w^g$ is negative and the elliptic region is shown in blue.



(a) Normalized Stone

(b) Interpolation I for only oil and interpolation I for all phases

(c) Interpolation III for only oil

(d) Interpolation III for all phases

Figure 7.2: Zoom in of curves by Holden for normalized Stone (a), interpolation I (b), interpolation III for only oil (c) and interpolation III for all phases (d). All interpolation methods use two-phase relative permeabilities with $n_{og} = 2$, $n_g = 1.1$, $n_w = 1.1$ and $n_{ow} = 2$ as Corey-coefficients. The grey area shows the region where $f_g^w f_w^g$ is negative.

(a) Normalized Stone



(b) Interpolation I for only oil and interpolation I for all phases



(c) Interpolation III for only oil



(d) Interpolation III for all phases

Figure 7.3: Curves by Holden for normalized Stone (a), interpolation I (b), interpolation III for only oil (c) and interpolation III for all phases (d). All interpolation methods use two-phase relative permeabilities with $n_{og} = 2.5$, $n_g = 1.5$, $n_w = 5$ and $n_{ow} = 3.5$ as Corey-coefficients. The grey area shows the region where $f_g^w f_w^g$ is negative and the elliptic region is shown in blue.

Corey-coefficients and viscosities:

$$
\begin{aligned}
n_{og} &= 2 & \mu^w &= 0.4\text{cP} \\
n_g &= 1.1 & \mu^o &= 0.4\text{cP} \\
n_w &= 1.1 & \mu^g &= 0.05\text{cP} \\
n_{ow} &= 2
\end{aligned}
$$

where $1\text{cP} = 1 \cdot 10^{-3} \frac{\text{kg}}{\text{ms}}$. Note that $n_{og} = n_{ow}$ which means that interpolation I will result in a Corey-type model, i.e. $k_r^o = k_r^o(S^o)$, such that a single umbilic point is expected inside the ternary diagram (Trangenstein, 1989). Figure 7.1 shows the curves by Holden and the possible elliptic regions for the different three-phase relative permeability models, and a zoom in is shown in Figure 7.2. Note that to the left of the elliptic region shown in Figure 7.1a the oil is immobile meaning that that region is governed by two-phase flow, see also Figure 3.5b. This means that loss of strict hyperbolicity can not occur in this region. This can also be seen in Figure 7.1a, which shows that $f_g^w f_w^g > 0$ in this region and that the elliptic region indeed stops at the boundary of the two-phase flow region. Figure 7.2 shows that normalized Stone and interpolation III for only oil result in a small elliptic region in the bottom region of the ternary diagram, since the curve $f_w^w - f_g^g = 0$ intersects the region where $f_g^w f_g^w < 0$. This figure also shows that interpolation I results in an umbilic point. Furthermore, it can be seen from Figures 7.1d and 7.2d that using interpolation III for all phases results in a strictly hyperbolic model. Hence, loss of strict hyperbolicity occurs for normalized Stone, interpolation I and interpolation III for only oil. Note that the elliptic region obtained using normalized Stone is substantially larger than the elliptic region obtained using interpolation III for oil, and that normalized Stone results in two elliptic regions.

For the second example the following Corey-coefficients and viscosities will be used:

(a) Normalized Stone



(b) Interpolation I for only oil and interpolation I for all phases



(c) Interpolation III for only oil



(d) Interpolation III for all phases

Figure 7.4: Zoom in of curves by Holden for normalized Stone (a), interpolation I (b), interpolation III for only oil (c) and interpolation III for all phases (d). All interpolation methods use two-phase relative permeabilities with $n_{og} = 2.5$, $n_g = 1.5$, $n_w = 5$ and $n_{ow} = 3.5$ as Corey-coefficients. The grey area shows the region where $f_g^w f_w^g$ is negative.

$$
\begin{aligned}
n_{og} &= 2.5 & \mu^w &= 0.4\text{cP} \\
n_g &= 1.5 & \mu^o &= 0.7\text{cP} \\
n_w &= 5 & \mu^g &= 0.05\text{cP} \\
n_{ow} &= 3.5
\end{aligned}
$$

Figure 7.3 shows the curves by Holden and the possible elliptic regions for the different three-phase relative permeability models, and a zoom in is shown in Figure 7.4. These figures show that, based on the curves by Holden, normalized Stone and interpolation I result in a small elliptic region in the bottom of the ternary diagram. Figures 7.3c and 7.4c show that interpolation III for only oil results in a large elliptic region in the middle of the ternary diagram and, based on the curves by Holden, a small elliptic region in the bottom of the ternary diagram. Finally, Figures 7.3d and 7.4d show that using interpolation III for all phases results in a strictly hyperbolic three-phase porous media flow model throughout the entire ternary diagram. Hence, loss of strict hyperbolicity occurs for normalizes Stone, interpolation I and interpolation III for only oil.

The third example uses the following Corey-coefficients and viscosities:

$$
\begin{aligned}
n_{og} &= 2 & \mu^w &= 0.4\text{cP} \\
n_g &= 2 & \mu^o &= 0.7\text{cP} \\
n_w &= 3.5 & \mu^g &= 0.05\text{cP} \\
n_{ow} &= 3.5
\end{aligned}
$$

The curves by Holden and the possible elliptic regions are shown in Figure 7.5, and a zoom in is shown in Figure 7.6. Figures 7.5a and 7.6a show that normalized Stone results in two small elliptic region in the bottom of the ternary diagram. Figures 7.5b and 7.6b show that interpolation I results in a small elliptic region in the bottom of the ternary diagram. Figures 7.5c and 7.6c show that using interpolation III for only oil results in a large elliptic region at the top of the ternary diagram and a small elliptic region at the bottom of the ternary

(a) Normalized Stone

(b) Interpolation I for only oil and interpolation I for all phases

(c) Interpolation III for only oil
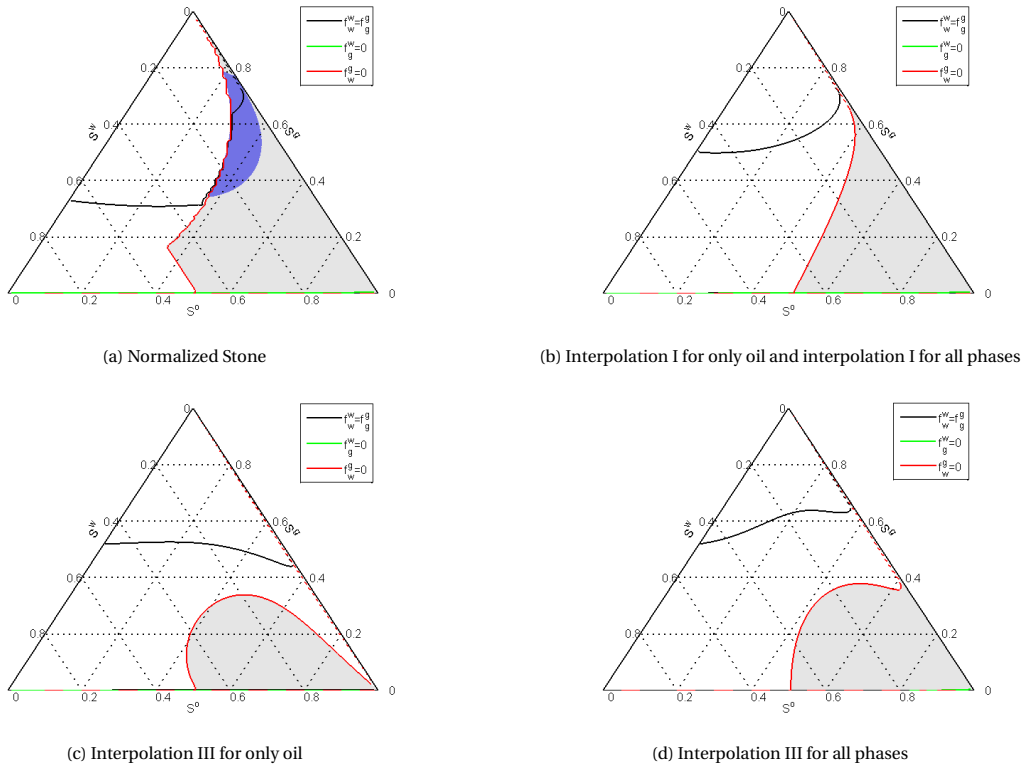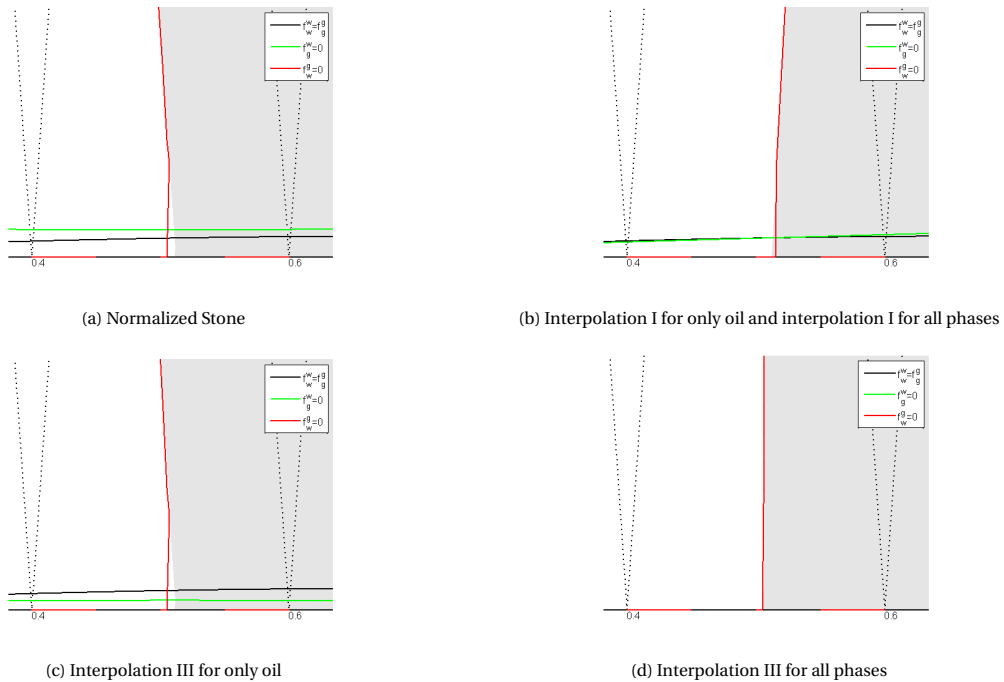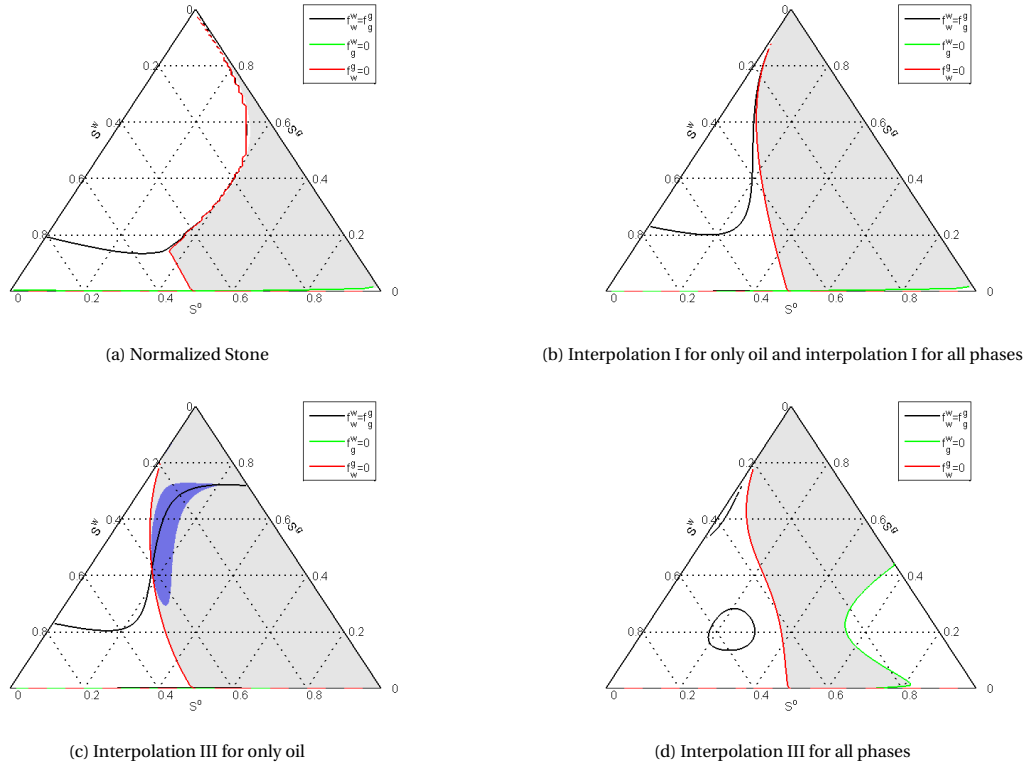
(d) Interpolation III for all phases

Figure 7.5: Curves by Holden for normalized Stone (a), interpolation I (b), interpolation III for only oil (c) and interpolation III for all phases (d). All interpolation methods use two-phase relative permeabilities with $n_{og} = 2$, $n_g = 2$, $n_w = 3.5$ and $n_{ow} = 3.5$ as Corey-coefficients. The grey area shows the region where $f_g^w f_w^g$ is negative and the elliptic region is shown in blue.



(a) Normalized Stone

(b) Interpolation I for only oil and interpolation I for all phases

(c) Interpolation III for only oil

(d) Interpolation III for all phases
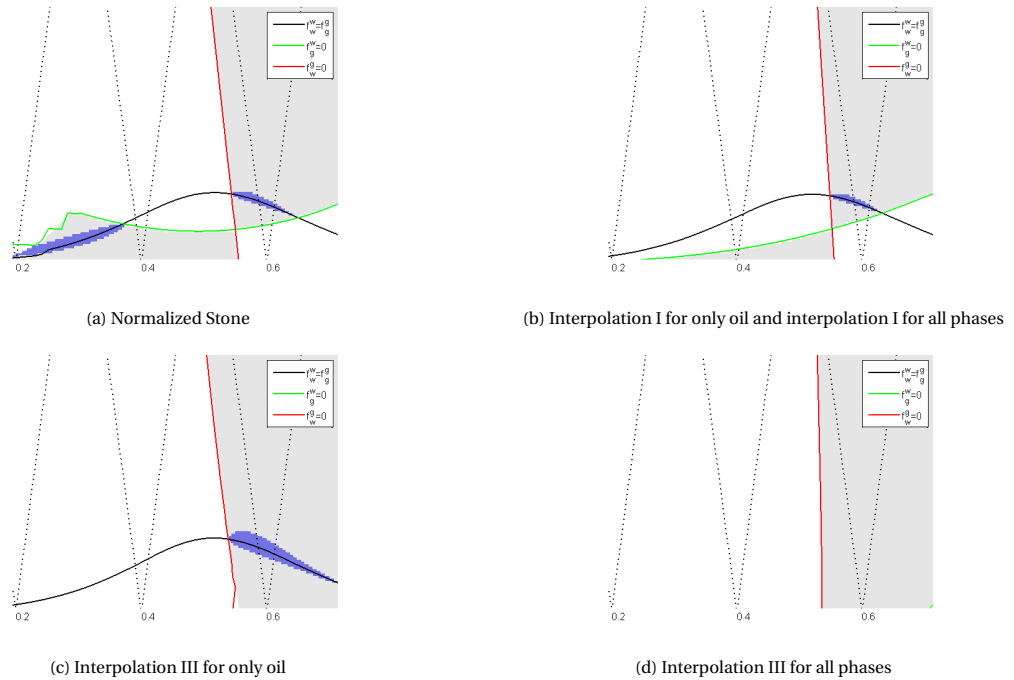
Figure 7.6: Zoom if of curves by Holden for normalized Stone (a), interpolation I (b), interpolation III for only oil (c) and interpolation III for all phases (d). All interpolation methods use two-phase relative permeabilities with $n_{og} = 2$, $n_g = 2$, $n_w = 3.5$ and $n_{ow} = 3.5$ as Corey-coefficients. The grey area shows the region where $f_g^w f_w^g$ is negative and the elliptic region is shown in blue.

(a) Normalized Stone

(b) Interpolation I for only oil and interpolation I for all phases

(c) Interpolation III for only oil

(d) Interpolation III for all phases
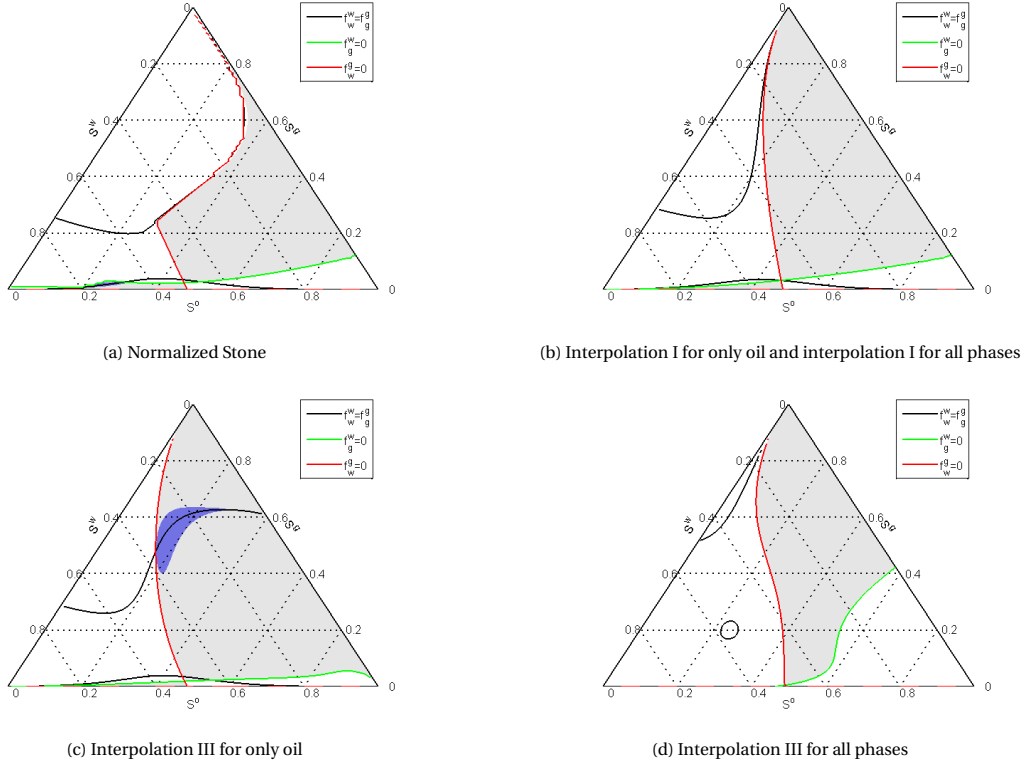
Figure 7.7: Curves by Holden for normalized Stone (a), interpolation I (b), interpolation III for only oil (c) and interpolation III for all phases (d). All interpolation methods use two-phase relative permeabilities with $n_{og} = 3$, $n_g = 2$, $n_w = 5$ and $n_{ow} = 3$ as Corey-coefficients. The grey area shows the region where $f_g^w f_w^g$ is negative and the elliptic region is shown in blue.

diagram. Figures 7.5d and 7.6d, on the other hand, show that using interpolation III for all phases results in strictly hyperbolic model. Therefore, loss of strict hyperbolicity occurs for normalized Stone, interpolation I and interpolation III for only oil, whereas loss of strict hyperbolicity does not occur for interpolation III for all phases.

For the final example the following Corey-coefficients and viscosities will be used:

$$
\begin{aligned}
n_{og} &= 3 & \mu^w &= 0.4\text{cP} \\
n_g &= 2 & \mu^o &= 0.8\text{cP} \\
n_w &= 5 & \mu^g &= 0.08\text{cP} \\
n_{ow} &= 3
\end{aligned}
$$

Note that $n_{og} = n_{ow}$ which means that interpolation I will result in a Corey-type model, i.e. $k_r^o = k_r^o(S^o)$, such that a single umbilic point is expected inside the ternary diagram (Trangenstein, 1989). Figure 7.7 shows the curves by Holden and the possible elliptic regions for all interpolation methods, and a zoom in is shown in Figure 7.8. Figures 7.7a and 7.8a show that normalized Stone results in two relatively small elliptic region at the bottom of the ternary diagram. Figures 7.7b and 7.8b show that interpolation I results in a single umbilic point, as expected based on the Corey-coefficients, located at the intersection of the three curves by Holden. Figures 7.7c and 7.8c show that interpolation III for only oil results in a large elliptic region in the middle of the ternary diagram and a small elliptic region at the bottom of the ternary diagram. Finally, Figures 7.7d and 7.8d show that interpolation III for all phases results in a strictly hyperbolic model. This means that loss of strict hyperbolicity occurs for normalized Stone, interpolation I and interpolation III for only oil and that it does not occur for interpolation III for all phases.

In the examples above the Stone-type models, i.e. normalized Stone, interpolation I and interpolation III for

(a) Normalized Stone



(b) Interpolation I for only oil and interpolation I for all phases



(c) Interpolation III for only oil



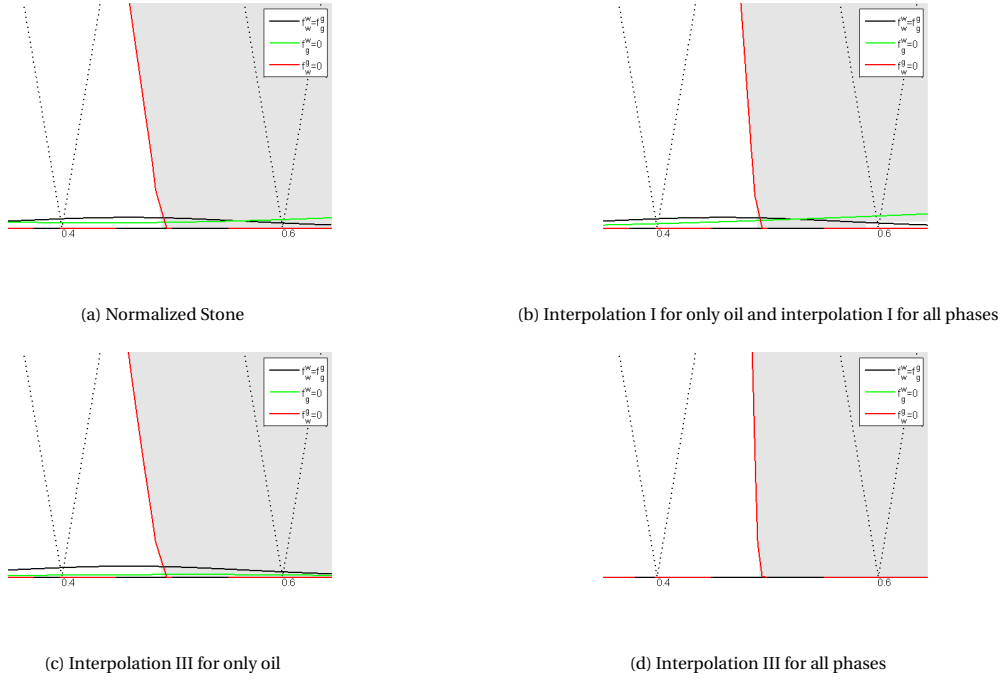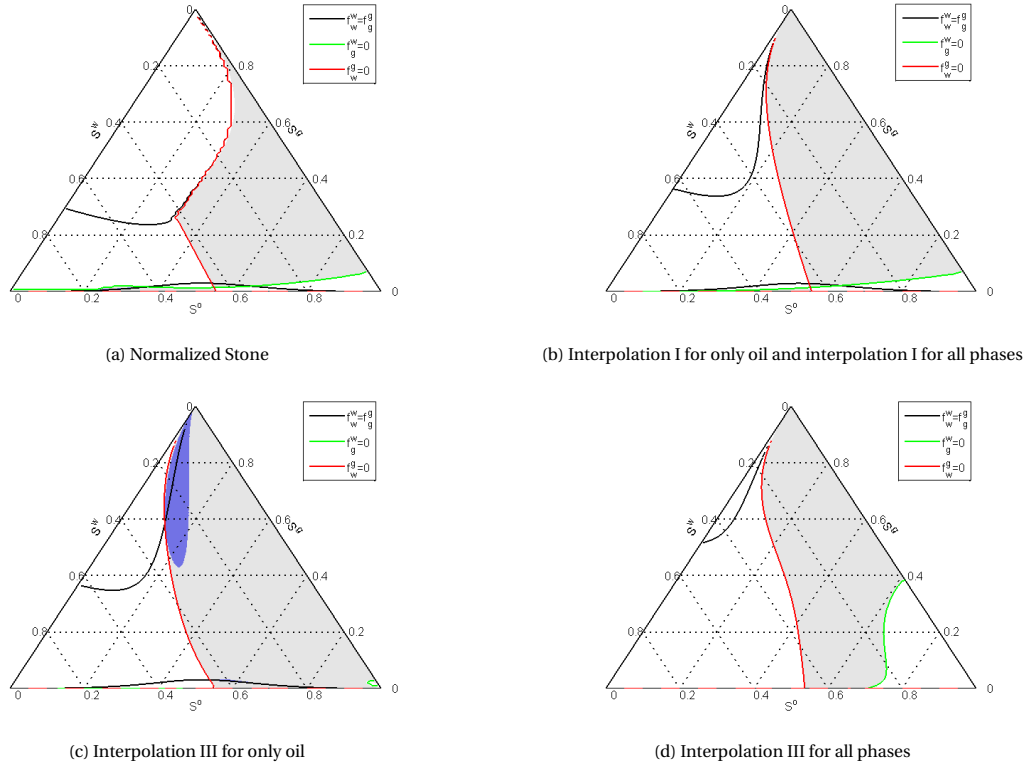(d) Interpolation III for all phases
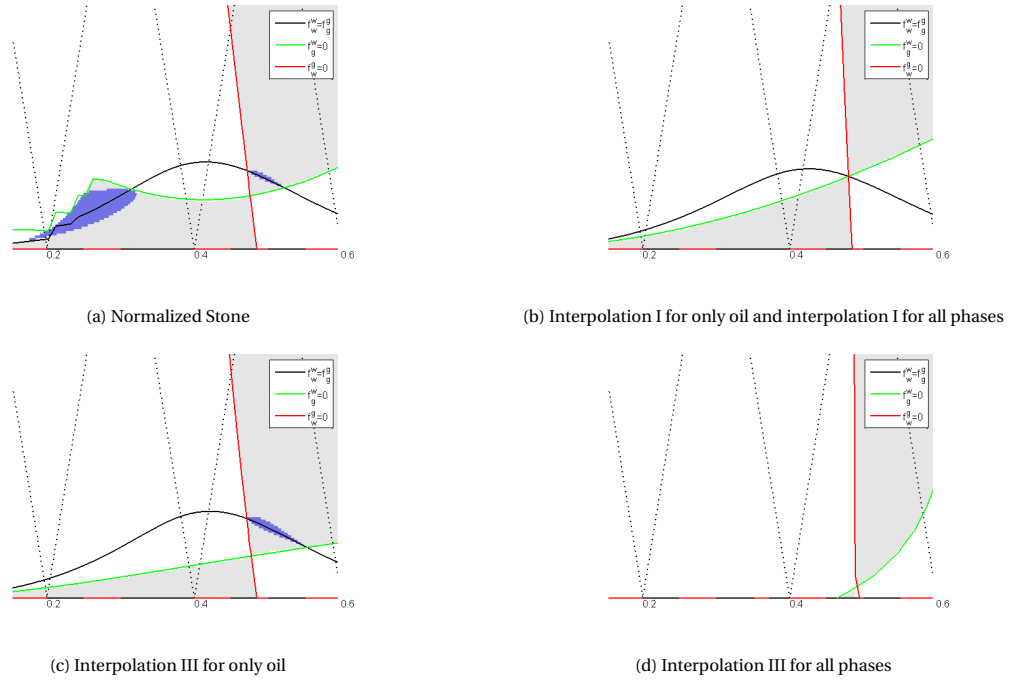
Figure 7.8: Zoom in of curves by Holden for normalized Stone (a), interpolation I (b), interpolation III for only oil (c) and interpolation III for all phases (d). All interpolation methods use two-phase relative permeabilities with $n_{og} = 3$, $n_g = 2$, $n_w = 5$ and $n_{ow} = 3$ as Corey-coefficients. The grey area shows the region where $f_g^w f_w^g$ is negative and the elliptic region is shown in blue.

oil, give rise to loss of strict hyperbolicity, which is in accordance with Trangenstein (1989) who showed that Stone-type models will in general result in an elliptic region. However, interpolation I results in an umbilic point or in a smaller elliptic region than normalized Stone and interpolation III for only oil. Furthermore, it can be seen that interpolation I results in a single umbilic point or single elliptic region for all examples whereas normalized Stone and interpolation III for oil result in two elliptic regions for most examples. Therefore, interpolation I is preferred to normalized Stone and to interpolation III for oil for these examples. At the same time, interpolation III for all phases results in a strictly hyperbolic model for all these examples. From this it can be concluded that letting go of the assumptions of a Corey-type or a Stone-type model, as was done for interpolation III for all phases, can indeed lead to a strictly hyperbolic model whereas Corey-type and Stone-type models in general result in loss of strict hyperbolicity.

Note that the elliptic region that is present at the bottom of the ternary diagram is located in approximately the same part of the ternary diagram for all the interpolation methods if it is present. Finally, note that all the elliptic region lie inside the area where $f_g^w f_w^g < 0$, as expected, but that they also lie around the curve $f_w^w - f_g^g = 0$ meaning that all the elliptic regions in these examples are non-removable elliptic regions.

Since the effect of a relatively large elliptic region on the numerical solution is already investigated in section 3.3 and since interpolation I is preferred to normalized Stone and to interpolation III for only oil based on the size of the elliptic region, normalized Stone and interpolation III for only oil will be not be considered any further. Interpolation I results, for the examples considered, in a single umbilic point or in one small elliptic region. Due to the size of the elliptic region the chance of choosing the injection or reservoir state inside the elliptic region or at the umbilic point is small. However, in section 5.2 it is found that such a small elliptic region still has an effect on the structure of the numerical solution even when both the injection and the reservoir state are chosen outside the elliptic region. Since it is unclear whether the resulting numerical solution is physical, such a small elliptic region or umbilic point should still be avoided. Therefore, the difference in numerical solution using interpolation I and interpolation III for all phases will be investigated, since using interpolation III for all phases results in a strictly hyperbolic model for the examples considered here. More specifically it is investigated if there is a clear difference in numerical solution between a model with a very small elliptic region or umbilic point, and a strictly hyperbolic model.

## 7.2. Difference in numerical solution when using interpolation I and interpolation III

To investigate possible differences in numerical solution two examples from the previous section will be analysed. For the first case, interpolation I gives rise to a small elliptic region in the ternary diagram while interpolation III results in a strictly hyperbolic model, which corresponds to the third example in the previous section. For the second case, using interpolation I results in a single umbilic point inside the ternary diagram. Again, interpolation III results in a strictly hyperbolic model inside the ternary diagram. This case corresponds to the fourth example in the previous section. Recall from the previous section that, for both cases, Corey-correlations with zero residuals and endpoints one are assumed for the two-phase relative permeabilities. Furthermore, Corey-coefficients are chosen such that $n_{gw} = n_{go} := n_g$ and $n_{wg} = n_{wo} := n_w$ and interpolation I and interpolation III will be used to obtain the three-phase relative permeability for all three phases. Also recall that this choice of Corey-coefficients means that interpolation I will result in a Stone-type relative permeability model whereas for interpolation III all three-phase relative permeabilities will depend on both the water and gas saturation. Since interpolation I and interpolation III are not incorporated in the reservoir simulator that was used in section 3.3.2, the numerical experiments in this chapter are obtained using the fractional flow equations and the upwind method as described in section 3.2.2.

### 7.2.1. Case with elliptic region for interpolation I

Recall from the previous section that for the first case, the following Corey-coefficients are used:

$$n_{og} = 2$$
$$n_g = 2$$
$$n_w = 3.5$$
$$n_{ow} = 3.5$$

The curves $f_g^w = 0$, $f_w^g = 0$ and $f_w^w - f_g^g = 0$ are shown in Figure 7.5b for interpolation I and in Figure 7.5d for interpolation III. Since Figure 7.5b shows that the curve $f_w^w - f_g^g = 0$ intersect the region where $f_g^w f_w^g$ is negative, a non-removable elliptic region must be present inside the ternary diagram. A zoom in of the region



(a) Interpolation I          (b) Interpolation III
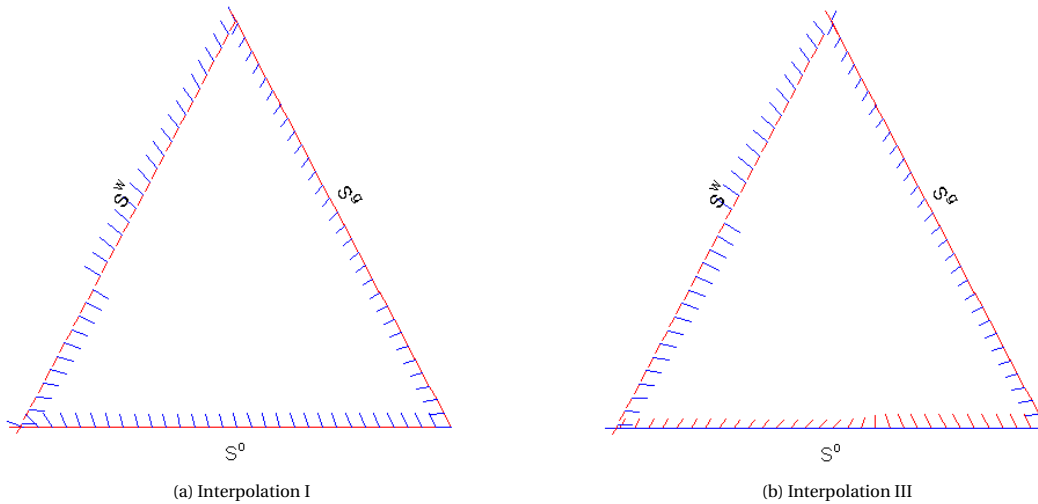
Figure 7.9: Direction of eigenvectors on the edges of the ternary diagram for interpolation I (a) and interpolation III (b). Both interpolation methods use two-phase relative permeabilities with $n_{og} = 2$, $n_g = 2$, $n_w = 3.5$ and $n_{ow} = 3.5$ as Corey-coefficients. The fast eigenvectors are shown in red and the slow eigenvector is shown in blue.

where the curve $f_w^w - f_g^g = 0$ intersects the region where $f_g^w f_w^g$ is negative for interpolation I is shown in Figure 7.6b. In this figure the elliptic region is clearly visible. Figure 7.5d shows that the curve $f_w^w - f_g^g = 0$ does not intersect the area where $f_g^w f_w^g$ is negative or the curves $f_w^g = 0$ and $f_g^w = 0$. Therefore, the elliptic region that is present for interpolation I is not present for interpolation III. Furthermore, Figure 7.9 shows that the fast-family eigenvectors are parallel to the OW edge on that edge for interpolation I whereas for interpolation

III the slow-family eigenvectors are parallel to the OW edge.

For the first example, the injection state $S_u$ is taken inside the elliptic region and the reservoir state $S_d$ is taken outside the elliptic region and above the curve $f_w^w - f_g^g = 0$ from O to W:

$$S_u = \begin{pmatrix} 0.4 \\ 0.025 \end{pmatrix} \quad S_d = \begin{pmatrix} 0.9 \\ 0.1 \end{pmatrix} \tag{7.1}$$

The saturation profile after 1.25 years for both interpolation I and III is shown in Figure 7.10. Comparing



(a) Saturation profile for interpolation I                    (b) Saturation profile for interpolation III

Figure 7.10: Saturation profile for interpolation I (a) and interpolation III (b) after a quarter of the total simulation time of 4.93 years. The blue line shows the water saturation, the red line shows the oil saturation and the green line shows the gas saturation. The downstream state is denoted by d, the middle state is denoted by m and the upstream state is denoted by u. Both interpolation methods use two-phase relative permeabilities with $n_{og} = 2$, $n_g = 2$, $n_w = 3.5$ and $n_{ow} = 3.5$ as Corey-coefficients.

Figures 7.10a and 7.10b shows some differences in the saturation profiles. The first difference is that interpolation III has a different wave speed. The change in saturation that occurs around 30m for interpolation I occurs around 25m for interpolation III. On the other hand, the change in saturation that occurs around 60m for interpolation I occurs around 70m for interpolation III. The second difference is that the change in saturation around 60m for interpolation I is smaller than the change around 70m for interpolation III. This can be explained by looking at the structure of the numerical solution, which is shown in Figure 7.11. A zoom in



(a) Analysis numerical solution interpolation I                    (b) Analysis numerical solution interpolation III

Figure 7.11: Analysis of the numerical solution for interpolation I (a) and interpolation III (b) after the total simulation time of 4.93 years. The RH locus of the upstream state is shown in blue, and the fast integral curve through the downstream state is shown in red. The saturation path is shown in black, and in (a) the elliptic region is shown in light blue.

(a) Analysis numerical solution interpolation I          (b) Analysis numerical solution interpolation III

Figure 7.12: Analysis of the numerical solution for interpolation I (a) and interpolation III (b) after the total simulation time of 4.93 years. The RH locus of the upstream state is shown in blue, and the fast integral curve through the downstream state is shown in red. The saturation path is shown in black. Both figures show the same section of the ternary diagram.

of the structure around the downstream state is shown in Figure 7.12. From Figures 7.11a and 7.12a it follows that the solution for interpolation I, when looking from downstream to upstream, consist of the downstream state followed by a fast-family rarefaction wave to a middle state followed by a shock wave to the upstream state:

$$S_d \xrightarrow{R_f} S_m \xrightarrow{S} S_u \quad \text{for interpolation I} \tag{7.2}$$

Looking at Figures 7.11b and 7.12b it can be seen that the structure of the solution for interpolation III is similar to the structure of the solution for interpolation I. That is, when looking from downstream to upstream, the solution for interpolation III consist of the downstream state followed by a fast-family rarefaction wave to a middle state followed by a slow-family shock wave to the upstream state:

$$S_d \xrightarrow{R_f} S_m \xrightarrow{S_s} S_u \quad \text{for interpolation III} \tag{7.3}$$

The difference seen in the saturation profile is explained by the difference in the RH locus of the upstream state for both interpolation methods. The solution for both methods follow the integral curve from the downstream state until a point on the RH locus of the upstream state is reached. Looking at Figure 7.12 it can be seen that the RH locus of interpolation I intersect the WG edge at a higher water saturation than for interpolation III such that the distance travelled over the integral curve is smaller for interpolation I than for interpolation III. Therefore, the change in saturation due to the rarefaction wave is smaller for interpolation I than for interpolation III. Also note that the RH locus of the upstream state for interpolation III consists of two continuous curves, whereas the RH locus of the upstream state for interpolation I contains disconnected branches. This is due to the fact that the upstream state lies inside an elliptic region for interpolation I whereas the upstream state lies in a strictly hyperbolic region for interpolation III, see section 5.2.

For the second example, the injection state $S_u$ is taken on the WG edge and lies above the curve $f_w^w - f_g^g = 0$ from O to W and the reservoir state $S_d$ is taken on the OW edge and lies beneath the curve $f_w^w - f_g^g = 0$ from O to W:

$$S_u = \begin{pmatrix} 0.9 \\ 0.1 \end{pmatrix} \quad S_d = \begin{pmatrix} 0.3 \\ 0 \end{pmatrix} \tag{7.4}$$

The saturation profile after 1.23 years for both interpolation I and III is shown in Figure 7.13. Comparing Figure 7.13a with Figure 7.13b a clear difference in saturation profile can be seen. This is due to the direction of the eigenvectors on the OW edge and can be explained by looking at the structure of the numerical solution, which is shown in Figure 7.14. Note that for the time simulated, the injection state has not yet reached point 1, where the saturation path is taken. Comparing Figures 7.13a and 7.14a with Figures 7.13b and 7.14b it can be seen that the main difference in the solution is the middle state. For interpolation I, this middle state is located on the OW edge, whereas for interpolation III this state is located inside the ternary diagram. However, for

(a) Saturation profile for interpolation I                      (b) Saturation profile for interpolation III
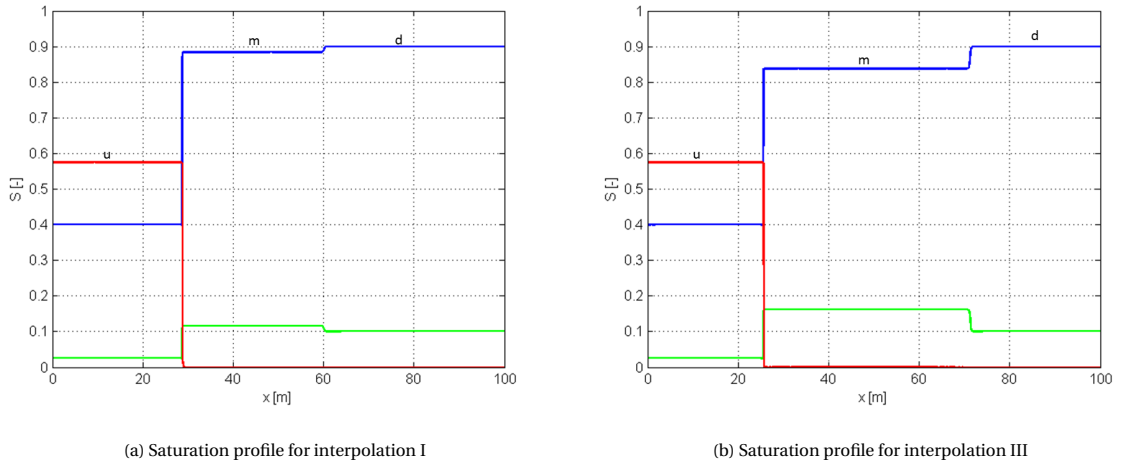
Figure 7.13: Saturation profile for interpolation I (a) and interpolation III (b) after a quarter of the total simulation time of 4.93 years. The blue line shows the water saturation, the red line shows the oil saturation and the green line shows the gas saturation. The downstream state is denoted by d, the middle state is denoted by m and the upstream state is denoted by u. Both interpolation methods use two-phase relative permeabilities with $n_{og} = 2$, $n_g = 2$, $n_w = 3.5$ and $n_{ow} = 3.5$ as Corey-coefficients.



(a) Analysis numerical solution interpolation I                     (b) Analysis numerical solution interpolation III
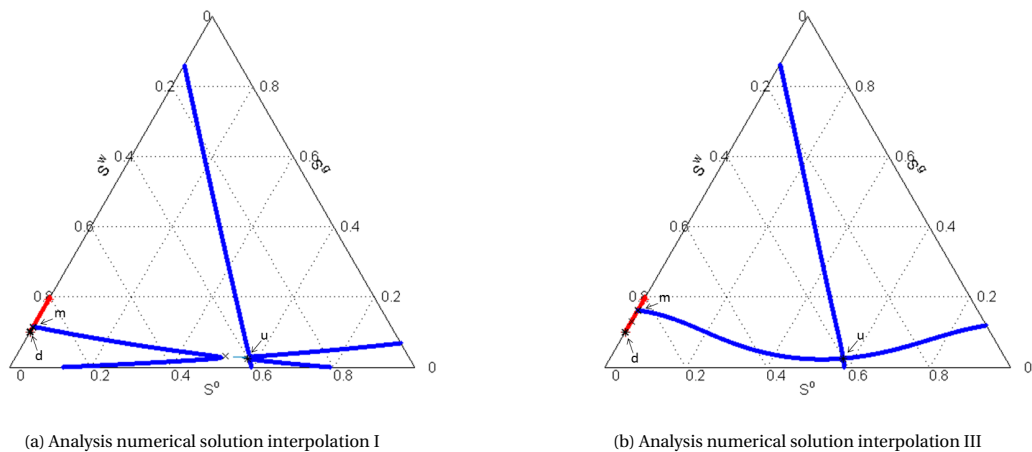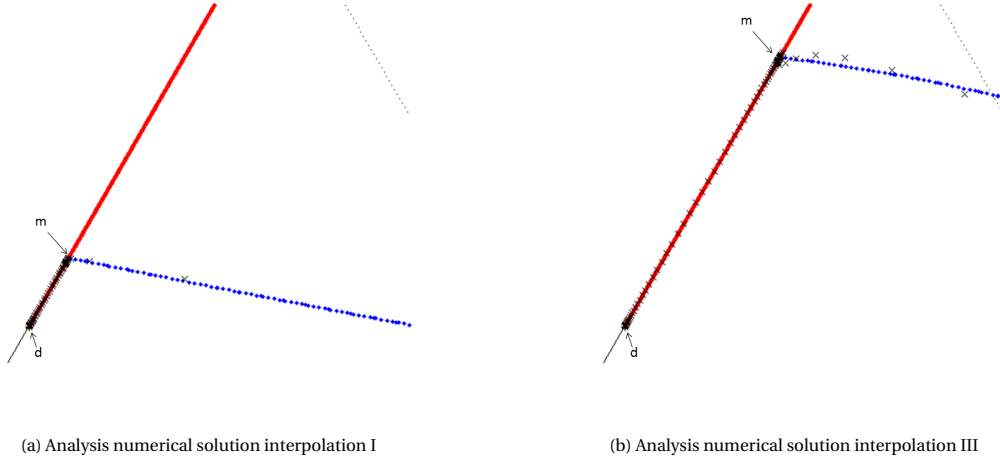
Figure 7.14: Analysis of the numerical solution for interpolation I (a) and interpolation III (b) after the total simulation time of 4.93 years. The RH locus of the downstream state is shown in light blue, and the fast integral curve through the downstream state is shown in red. The slow integral curve through the upstream state is shown in pink. The green curve shows the RH locus of the middle state. The saturation path is shown in black.

both interpolation methods the downstream state is connected to the middle state by a fast-family shock wave after which the middle state is connected to the upstream state by a slow-family shock-rarefaction wave, i.e:

$$S_d \xrightarrow{S_f} S_m \xrightarrow{SR_s} S_u \quad \text{for both interpolation I and III} \tag{7.5}$$

The difference in location of the middle state is caused by the direction of the eigenvectors on the OW edge. Since the wave speed must increase from upstream to downstream, the downstream state must be connected by a fast-family wave to the next state. For interpolation I the fast-family eigenvectors are parallel to the OW edge on the OW edge, whereas for interpolation III the slow-family eigenvectors are parallel to the edge and the fast-family eigenvectors point into the ternary diagram. Therefore, the solution using interpolation I can follow the OW edge resulting in two-phase behaviour for the first wave. This can also be seen in Figure 7.13a, since the gas saturation does not change during the shock wave around 70m. The solution using interpolation III, however, must shock into the ternary diagram resulting in three-phase behaviour for the first wave. This can also be seen in Figure 7.13b since the gas saturation changes during the shock around 95m. Note that the shock-rarefaction connecting the middle state to the upstream state shows three-phase behaviour for both interpolation methods.

### 7.2.2. Case with umbilic point for interpolation I

Recall from the fourth example of the previous section that for the second case, the following Corey-coefficients are used:

$$
\begin{aligned}
n_{og} &= 3 \\
n_g &= 2 \\
n_w &= 5 \\
n_{ow} &= 3
\end{aligned}
$$

The curves $f_g^w = 0$, $f_w^g = 0$ and $f_w^w - f_g^g = 0$ are shown in Figure 7.7b for interpolation I and in Figure 7.7d for interpolation III. Since Figure 7.7b shows that the curves $f_w^w - f_g^g = 0$, $f_g^w = 0$ and $f_w^g = 0$ intersect at one point an umbilic point is present at that point in the ternary diagram. This could also be expected based on the Corey-coefficients. Since $n_{og} = n_{ow}$, and since $n_{gw} = n_{go} := n_g$ and $n_{wg} = n_{wo} := n_w$, interpolation I results in a Corey-type relative permeability model, meaning that there must be an umbilic point inside the ternary diagram. A zoom in of the intersection of the three curves for interpolation I is shown in Figure 7.8b. Figure 7.7d, on the other hand, shows that the curve $f_w^w - f_g^g = 0$ does not intersect the area where $f_g^w f_w^g$ is negative or the curves $f_w^g = 0$ and $f_g^w = 0$. Therefore, the umbilic point that is present for interpolation I is not present for interpolation III. Furthermore, Figure 7.15 shows that the fast-family eigenvectors are parallel to the OW



(a) Interpolation I                    (b) Interpolation III
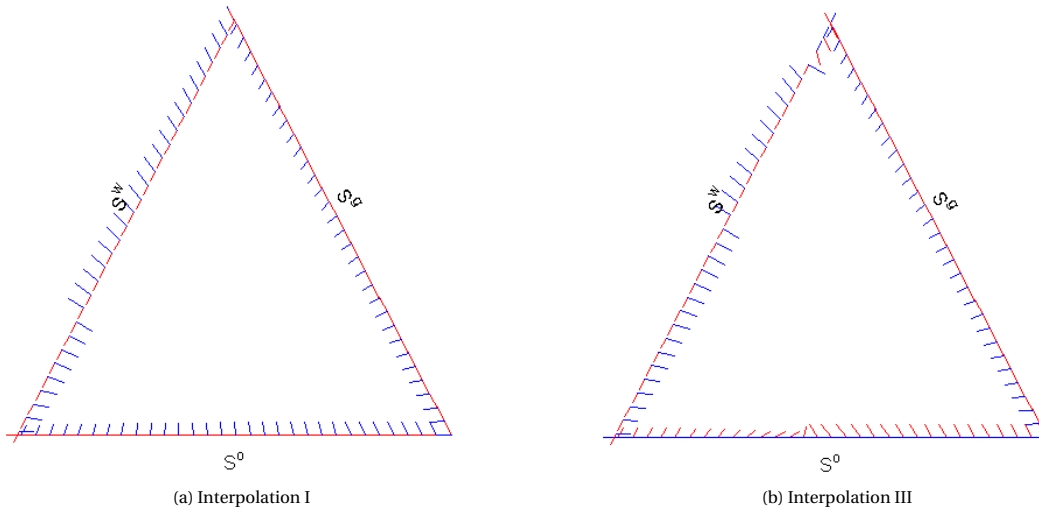
Figure 7.15: Direction of eigenvectors on the edges of the ternary diagram for interpolation I (a) and interpolation III (b). Both interpolation methods use the same two-phase relative permeabilities with $n_{og} = 3$, $n_g = 2$, $n_w = 5$ and $n_{ow} = 3$ as Corey-coefficients. The fast eigenvectors are shown in red and the slow eigenvector is shown in blue.

edge on that edge for interpolation I whereas for interpolation III the slow-family eigenvectors are parallel to the OW edge.

As an example the downstream state is chosen inside the closed curve $f_w^w - f_g^g = 0$, see Figure 7.7d, and the upstream state is chosen such that it lies below the curve $f_g^w = 0$ for both interpolation I and interpolation III:

$$
S_u = \begin{pmatrix} 0.1 \\ 0.05 \end{pmatrix} \quad S_d = \begin{pmatrix} 0.55 \\ 0.2 \end{pmatrix} \tag{7.6}
$$

The saturation profile after 0.49 years for both interpolation I and III is shown in Figure 7.16. Comparing Figure 7.16a with Figure 7.16b shows that there are relatively small differences in the saturation profile. The structure of the numerical solution, on the other hand, shows a clear difference. The structure of the solution using both interpolation I and interpolation III is given in Figure 7.17. The solution for interpolation I consists of the following waves. The downstream state is connected with a fast-family shock-rarefaction to the first constant state $c_1$. This constant state is connected to a second constant state $c_2$ with a shock-rarefaction. Finally the second constant state is connected to the upstream state by a slow-family rarefaction wave. Hence,

(a) Saturation profile for interpolation I
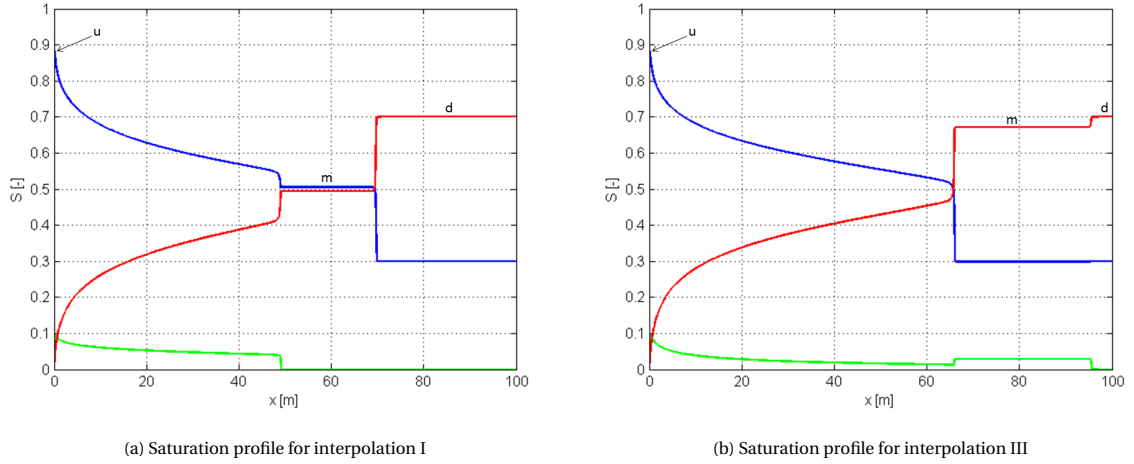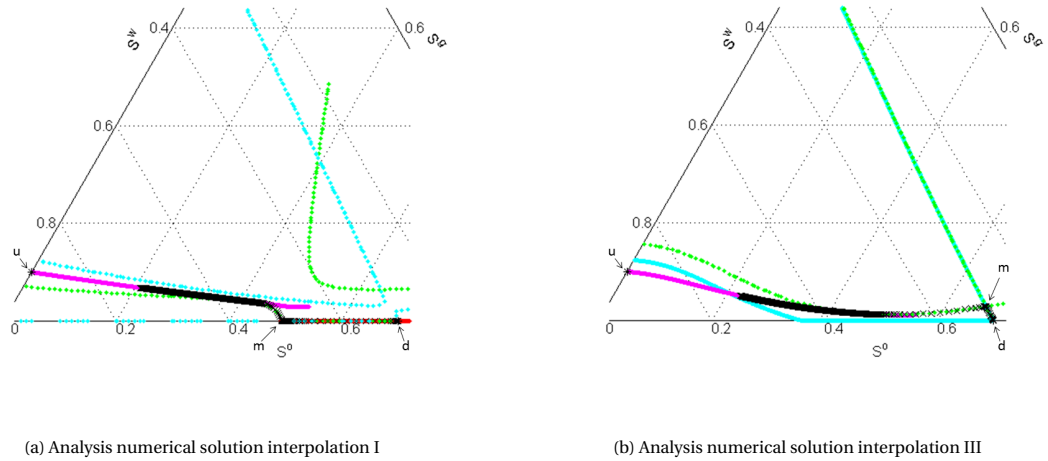


(b) Saturation profile for interpolation III

Figure 7.16: Saturation profile for interpolation I (a) and interpolation III (b) after one tenth of the total simulation time of 4.93 years. The blue line shows the water saturation, the red line shows the oil saturation and the green line shows the gas saturation. The downstream state is denoted by d and the upstream state is denoted by u. In (a) the first constant state is denoted by $c_1$ and the second constant state is denoted by $c_2$. In (b) the middle state is denoted by m. Both interpolation methods use the same two-phase relative permeabilities with $n_{og} = 3$, $n_g = 2$, $n_w = 5$ and $n_{ow} = 3$ as Corey-coefficients.



(a) Analysis numerical solution interpolation I



(b) Analysis numerical solution interpolation III

Figure 7.17: Analysis of the numerical solution for interpolation I (a) and interpolation III (b) after the total simulation time of 4.93 years. The RH locus of the downstream state is shown in light blue, and the fast integral curve through the downstream state is shown in red. The slow integral curve through the upstream state is shown in pink. The green curve in (b) shows the RH locus of the middle state and in (a) the RH locus of the first constant state. In (a) the yellow curve shows the integral curve through the second constant state. The saturation path is shown in black.

the structure of the full solution is given by:

$$S_d \xrightarrow{SR_f} S_{c_1} \xrightarrow{SR} S_{c2} \xrightarrow{R_s} S_u \quad \text{for interpolation I} \tag{7.7}$$

This means that the solution for interpolation I has two constant states besides the downstream and upstream states, which only occurs for non strictly hyperbolic systems. The first constant state after the downstream state $c_1$ can clearly be seen in the saturation profile, approximately between 25m and 50m. The second constant state is less clear and occurs around 20m, see Figure 7.16a. The saturation profile at a later point in time is shown in Figure 7.18. In this figure the second constant state $c_2$ can be seen more clearly, approximately around 70m. Interpolation III results in a strictly hyperbolic system. Therefore, the solution is expected to have only one constant state besides the downstream and upstream state, which is then called the middle state. From Figure 7.17b it follows that the solution using interpolation III consists of the downstream state which is connected with a fast-family shock-rarefaction to the middle state which is in turn connected to the

(a) Saturation profile for interpolation I

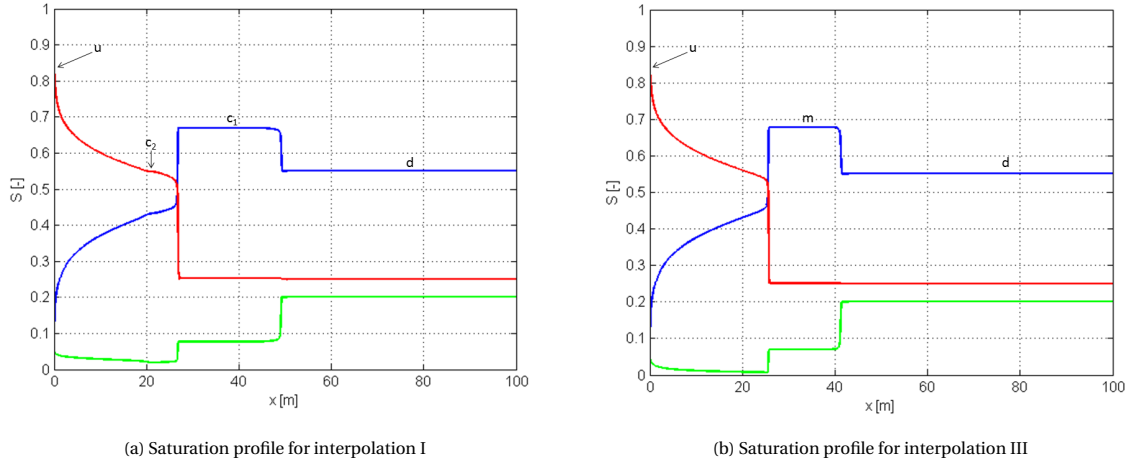(b) Saturation profile for interpolation III
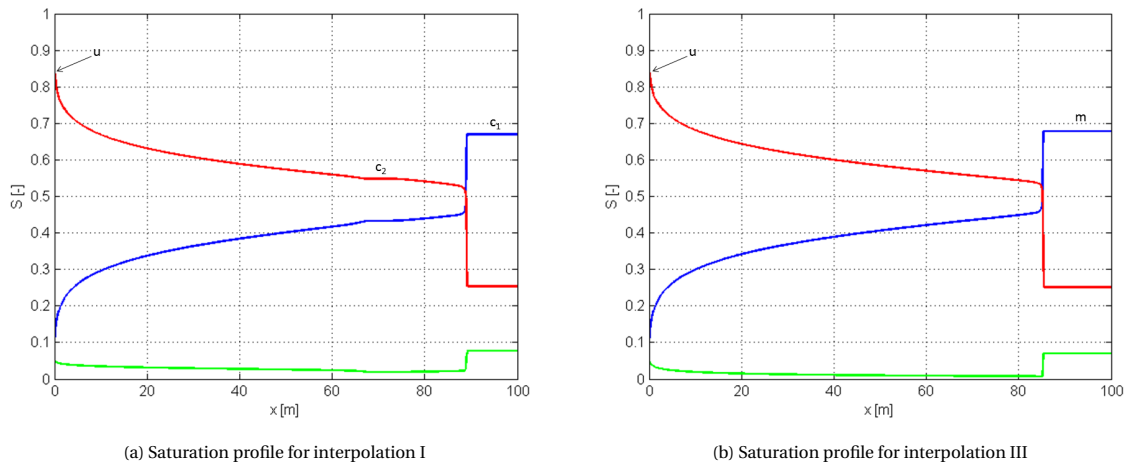
Figure 7.18: Saturation profile for interpolation I (a) and interpolation III (b) after one third of the total simulation time of 4.93 years. The blue line shows the water saturation, the red line shows the oil saturation and the green line shows the gas saturation. The downstream state is denoted by d and the upstream state is denoted by u. In (a) the first constant state is denoted by $c_1$ and the second constant state is denoted by $c_2$. In (b) the middle state is denoted by m. Both interpolation methods use the same two-phase relative permeabilities with $n_{og} = 3$, $n_g = 2$, $n_w = 5$ and $n_{ow} = 3$ as Corey-coefficients.
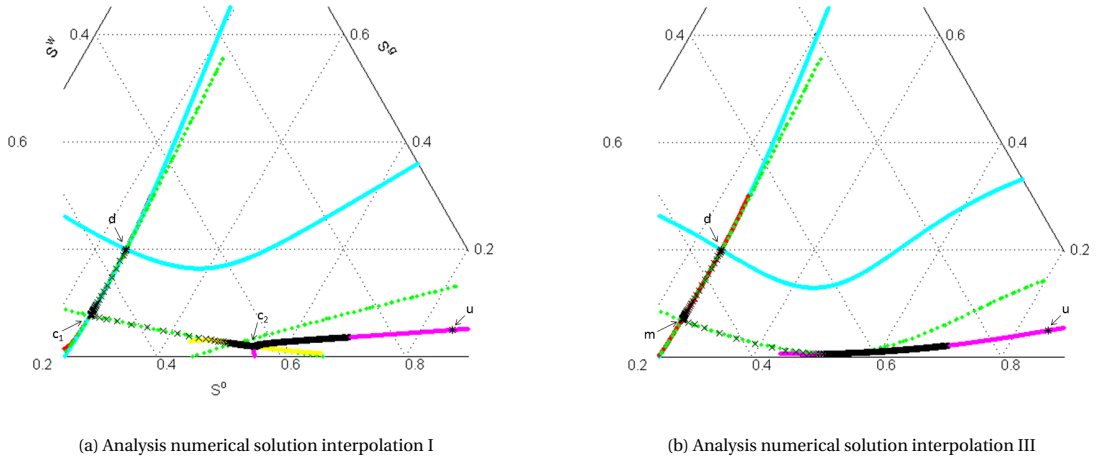
upstream state with a slow-family shock-rarefaction:

$$S_d \xrightarrow{SR_f} S_m \xrightarrow{SR_s} S_u \quad \text{for interpolation III} \tag{7.8}$$

The difference between the structure of the solutions is caused by the curve $f_w^w - f_g^g = 0$. For interpolation I there is such a curve from O to W which is crossed twice by the saturation path. For interpolation III on the other hand, the curve $f_w^w - f_g^g = 0$ from O to W does not exist and has therefore no effect on the solution.

From Figures 7.10, 7.13 and 7.16 it can be concluded that using different three-phase relative permeability models results in significantly different numerical solutions. One of the main differences, which can be seen in all three figures, is that using a different relative permeability model results in different wave speeds. This means for instance that predicted breakthrough time of water will be different for each model. In Figure 7.10 it can be seen that even if the structure of the solution is the same for both interpolation methods, the values of the saturation profile can be different resulting in different predictions of oil recovery. Figures 7.13 and 7.16 show that it is even possible that the solution has a different structure depending on the relative permeability model used. For instance Figures 7.16 and 7.18 shows an extra constant state for interpolation I compared to the solution of interpolation III. This extra constant state is caused by the loss of strict hyperbolicity that occurs for interpolation I due to the umbilic point. Interpolation III results in a strictly hyperbolic system in this example, meaning that the solution can only contain one constant state aside from the upstream and downstream state. This shows that even a single umbilic point can have an effect on the structure of the numerical solution.

From the examples in this chapter it can be concluded that the relative permeability model has a great influence on the solution of the three-phase porous media flow model. The relative permeability model determines if loss of strict hyperbolicity and subsequent effects on the numerical solution occur. Furthermore, the relative permeability model determines the wave speed of the numerical solution as well as the structure of the numerical solution and the saturation path taken. Therefore, extreme care must be taken when choosing the three-phase relative permeability model.

# 8
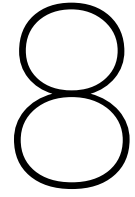
# Conclusion

In this chapter some concluding remarks are made in the first section and some comments one these conclusions are given in the second section. Furthermore, some remarks concerning future work are made in the second section.

## 8.1. Conclusion

First, from section 6 it can be seen that analysis to determine if loss of strict hyperbolicity occurs can be done before simulation by using the curves of Holden or the direction of the eigenvectors on the edges of the ternary diagram. The curves by Holden are a set of three curves based on the derivatives of the fractional flow functions that give sufficient conditions for loss of strict hyperbolicity to occur. If these curves are computed throughout the entire ternary diagram they can be used to determine the location of an elliptic region or umbilic point. If the curves cannot be computed inside the ternary diagram, the sign of the curves on the edges of the ternary diagram can be used to determine if loss of strict hyperbolicity occurs, but a precise location of the elliptic region or umbilic point cannot be determined.

Secondly, it can be concluded that loss of strict hyperbolicity has a great influence on the numerical solution of the three-phase porous media flow model. In section 3.3 it was found that oscillations can occur in the saturation profile if the injection state lies inside the elliptic region. Furthermore, if the injection state lies inside the elliptic region the qualitative structure of the solution as a function of time can be different for different grid cells. Moreover, the qualitative structure of the solution changes depending on the ratio between $\Delta t$ and $\Delta x$ due to the underlying sensitivity of transitional shocks to diffusion. Finally, in chapter 5 and chapter 7 it was found that loss of strict hyperbolicity can result in extra constant states in the numerical solution.

Thirdly, the three-phase relative permeability model is of great influence on the existence of an elliptic region or umbilic point and on the location and size of the elliptic region. For the same two-phase relative permeability, the chosen three-phase relative permeability model determines if loss of strict hyperbolicity occurs or the chosen model can alter the size of the elliptic region. Subsequently, the three-phase relative permeability model is of great influence on the numerical solution, even up to the point where different relative permeability models lead to solutions with a different structure, see chapter 7.
Furthermore, three-phase relative permeability is difficult, time consuming and expensive to measure, meaning that three-phase relative permeability data is scarce. In section 4.2 it was stated that the available data show different behavior for each situation and therefore the relative permeability model should be chosen for each individual situation in order to best match this behaviour. Moreover, the data show multiple situations in which a Corey-type or Stone-type model would be unable to produce the correct isoperms, that is, the gas and water relative permeabilities show dependence on both the water and gas saturation. At the same time, Corey-type and Stone-type models generally result in loss of strict hyperbolicity. Modelling three-phase relative permeability data can thus be seen as an interpolation problem, as described in section 4.2.1, where the relative permeability of each phase is obtained by interpolating between two two-phase systems. This can lead to a new type of relative permeability model where the relative permeability of all phases depend on

both the water and gas saturation, meaning that the relative permeability model is neither of Stone-type nor of Corey-type.

Finally, based on the numerical experiments in this thesis and on the theory and numerical and experimental data available in the literature, loss of strict hyperbolicity and the subsequent solution are deemed unphysical. Using a relative permeability model that ensures strict hyperbolicity can then be seen as an extra constraint that should be imposed on the three-phase porous media flow model. In this thesis a relative permeability model that avoids loss of strict hyperbolicity for all situations has not been found. However, the results in chapter 6 suggest that it is possible to choose a relative permeability model such that loss of strict hyperbolicity is avoided for each situation separately, especially when viewing the relative permeability model as an interpolation problem. This means that imposing the extra constraint that the system must be strictly hyperbolic is feasible.

## 8.2. Further remarks

From the conclusions above it follows that the three-phase relative permeability model should be chosen with great care in order to avoid loss of strict hyperbolicity. But, even if a relative permeability model can be chosen such that loss of strict hyperbolicity does not occur for a given situation, this relative permeability model might not result in the correct three-phase porous media flow model. For instance the breakthrough time of water can be predicted incorrectly, see section 7. Therefore, choosing the correct relative permeability must not only be done by making sure that loss of strict hyperbolicity does not occur, but history matching and three-phase relative permeability data, when available, must also be taking into account. This means that choosing the correct relative permeability model is even more difficult.

The examples investigated in this thesis where chosen such that the effect of loss of strict hyperbolicity and the difference in solution when using different relative permeability models can clearly be observed. These examples, or indeed even the new interpolation methods introduced, where not compared with available three-phase data and it is therefore unclear how realistic these examples are. However, the examples illustrate that loss of strict hyperbolicity has a significant effect on the solution, even if there is only a single umbilic point or a small elliptic region present inside the ternary diagram. This also means that even though the chance of choosing the injection state inside the elliptic region is small, since the elliptic region is generally small for realistic situations, the solution can still be influenced by the loss of strict hyperbolicity. The examples therefore still give valuable information for practical situations.

Section 3.4 states that there is no clear link between the eigenvalues of the Jacobian of the continuous system and the eigenvalues of the submatrices of the Jacobian of FIM. And even if such a link exists, it would be impractical to compute the eigenvalues for each time step for every grid cell during a simulation. However, in EOR the relative permeabilities are sometimes changed during a simulation. This means that analysis before the simulation to determine if loss of strict hyperbolicity occurs would have to be done for all the possible relative permeability models that might arise during the simulation. It would therefore still be interesting to investigate if loss of strict hyperbolicity can be determined during the simulation. One way to make this more practical might be not to do analysis for every time step for each grid cell, but only for those time steps and grid cells in which loss of strict hyperbolicity is expected based on the observed numerical solution. For instance if oscillations start to arise. One way to then perform the analysis might be to obtain the derivatives of the fractional flow for these grid cells and time steps and then directly compute the eigenvalues of the Jacobian of the continuous system.

The results in this thesis were obtained for 1D horizontal, incompressible, immiscible flow trough a homogeneous medium where capillary pressure is neglected. The effect on loss of strict hyperbolicity when adding gravity or capillary pressure or when extending the model to two or three dimension or miscible flow is largely unknown. Guzmán and Fayers (1997a) show that adding gravity changes the size of the elliptic region but they could not find a clear relationship between the gravity coefficient and the size of the elliptic region. Azevedo et al. (2002) show that the region of instability might even enlarge when capillary pressure is included in the model. Therefore, loss of strict hyperbolicity when the model is extended to more dimensions or when gravity or capillary pressure is included might have to be investigated.

The new interpolation methods I, II and III introduced in chapter 4 generally result in linear or concave isoperms. In order to match all shapes of isoperms, an interpolation method that results in convex isoperms might be developed. A combination of this interpolation method and interpolation I, II and III might then be used to construct any shape of isoperms in order to match as many different situations as possible. Also, in chapter 7 only cases with $n_{gw} = n_{go} = n_g$ and $n_{wg} = n_{wo} = n_w$, i.e. with the same Corey-coefficients for water and gas in two-phase systems, are considered. Physical data suggest that in general the two phase behaviour of water is different in a water-gas than in a water-oil system, and similarly, the two-phase behavior of gas in a water-gas system is different than in a oil-gas system. Therefore, a generalization to Corey-coefficients such that $n_{gw} \neq n_{go}$ and $n_{wg} \neq n_{wo}$ may be worthwhile to investigate. Finally, the numerical experiments conducted in this thesis used the same interpolation method for all three phases. However, for some practical situations it might be better to use a different interpolation method or three-phase relative permeability model for each phase.

<div style="text-align: right">

# A

</div>
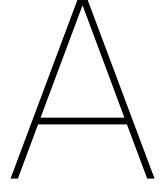
# Derivation of Jacobian for Newton-Raphson

This section gives the derivation of the substituted water saturation residual $R_{\tilde{A}_i^w}$ and the derivation of the entries of the submatrices of the Jacobian for the Newton-Raphson method. First, $R_{\tilde{A}_i^w}$ is determined from equations (3.24) and (3.25). From this and equation (3.25) the entries of the submatrices given by equation (3.31) will be computed.

## A.1. Water saturation residual

First, the phase volume residual (3.24) is rewritten:

$$0 = R_{V_i} = \phi \Delta x \Delta y \Delta z - \sum_\alpha \frac{A_i^\alpha}{\rho^\alpha}$$

$$0 = \phi \Delta x \Delta y \Delta z - \frac{A_i^w}{\rho^w} - \frac{A_i^g}{\rho^g} - \frac{A_i^o}{\rho^o}$$

$$A_i^w = \rho^w \left( \phi \Delta x \Delta y \Delta z - \frac{A_i^g}{\rho^g} - \frac{A_i^o}{\rho^o} \right) \tag{A.1}$$

Substituting this in the residual of the water saturation (3.25) gives:

$$0 = A_i^{w,n+1} - A_i^{w,n} - \frac{\Delta t}{\Delta x} \Delta y \Delta z K \rho^w \frac{1}{\mu^w} \left[ k_{r_i}^{w,n+1}(p_{i+1}^{n+1} - p_i^{n+1}) - k_{r_{i-1}}^{w,n+1}(p_i^{n+1} - p_{i-1}^{n+1}) \right]$$

$$= \rho^w \left[ \phi \Delta x \Delta y \Delta z - \frac{A_i^{g,n+1}}{\rho^g} - \frac{A_i^{o,n+1}}{\rho^o} \right] - \rho^w \left[ \phi \Delta x \Delta y \Delta z - \frac{A_i^{g,n}}{\rho^g} - \frac{A_i^{o,n}}{\rho^o} \right]$$

$$- \frac{\Delta t}{\Delta x} \Delta y \Delta z K \rho^w \frac{1}{\mu^w} \left[ k_{r_i}^{w,n+1}(p_{i+1}^{n+1} - p_i^{n+1}) - k_{r_{i-1}}^{w,n+1}(p_i^{n+1} - p_{i-1}^{n+1}) \right]$$

$$= -\rho^w \frac{A_i^{g,n+1}}{\rho^g} - \rho^w \frac{A_i^{o,n+1}}{\rho^o} - \rho^w \left[ -\frac{A_i^{g,n}}{\rho^g} - \frac{A_i^{o,n}}{\rho^o} \right]$$

$$- \rho^w \frac{\Delta t}{\Delta x} \Delta y \Delta z K \frac{1}{\mu^w} \left[ k_{r_i}^{w,n+1}(p_{i+1}^{n+1} - p_i^{n+1}) - k_{r_{i-1}}^{w,n+1}(p_i^{n+1} - p_{i-1}^{n+1}) \right]$$

Which means that the residual of the substituted water saturation is given by:

$$R_{\tilde{A}_i^w} = -\rho^w \frac{A_i^{g,n+1}}{\rho^g} - \rho^w \frac{A_i^{o,n+1}}{\rho^o} + \rho^w \frac{A_i^{g,n}}{\rho^g} + \rho^w \frac{A_i^{o,n}}{\rho^o} - \rho^w \frac{\Delta t}{\Delta x} \Delta y \Delta z K \frac{1}{\mu^w} \left[ k_{r_i}^{w,n+1}(p_{i+1}^{n+1} - p_i^{n+1}) - k_{r_{i-1}}^{w,n+1}(p_i^{n+1} - p_{i-1}^{n+1}) \right] \tag{A.2}$$

## A.2. Primary variables

In the continuous system the primary variables are $S^w$ and $S^g$ whereas in the discretized system of FIM they are $A^o$ and $A^g$ and $p$. This means that a transformation between these variables must be made. To make

the distinction between the sets of variables clear $S^{\tilde{w}}$ and $S^{\tilde{g}}$ will be used to denote the variables of the continuous system and $S^w$ and $S^o$ for the discretized system. The expressions for the derivatives of the relative permeabilities in the discretized system will be rewritten to the derivatives as found in the continuous system. First recall that:

$$S_i^\alpha \approx \frac{A_i^\alpha}{\phi \Delta x \Delta y \Delta z \rho^\alpha}, \quad \text{for } \alpha \in \{w, o, g\} \tag{A.3}$$

This means that the following holds for each phase:

$$\frac{\partial k_{r_i}^{\alpha_1}}{\partial A_i^{\alpha_2}} = \frac{\partial S_i^{\alpha_2}}{\partial A_i^{\alpha_2}} \frac{\partial k_{r_i}^{\alpha_1}}{\partial S_i^{\alpha_2}} = \frac{1}{\phi \Delta x \Delta y \Delta z \rho^{\alpha_2}} \frac{\partial k_{r_i}^{\alpha_1}}{\partial S_i^{\alpha_2}}, \quad \text{for } \alpha_1, \alpha_2 \in \{w, o, g\} \tag{A.4}$$

This means that only the derivatives of the relative permeabilities with respect to saturation are necessary to do the transformation between the different variables. Note that:

$$\begin{cases} S^{\tilde{w}} = 1 - S^g - S^o \\ S^{\tilde{g}} = S^g \end{cases} \tag{A.5}$$

Therefore, for a Stone-type relative permeability model, $k_r^o = k_r^o(S^o, S^g)$ holds in the discretized system and $k_r^o = k_r^o(S^{\tilde{w}}, S^{\tilde{g}})$ in the continuous system. Furthermore $k_r^w = k_r^w(S^o, S^g)$ and $k_r^g = k_r^g(S^g)$ holds in the discretized system and $k_r^w = k_r^w(S^{\tilde{w}})$ and $k_r^g = k_r^g(S^{\tilde{g}})$ in the continuous system. Starting from the discretized system, the derivatives can be rewritten in term of the variables of the continuous system. First, the derivatives of the oil relative permeability will be looked at:

$$\begin{aligned}
\left.\frac{\partial k_r^o}{\partial S^o}\right|_{S^g} &= \left.\frac{\partial k_r^o}{\partial S^{\tilde{w}}}\right|_{S^{\tilde{g}}} \frac{\partial S^{\tilde{w}}}{\partial S^o} + \left.\frac{\partial k_r^o}{\partial S^{\tilde{g}}}\right|_{S^{\tilde{w}}} \frac{\partial S^{\tilde{g}}}{\partial S^o} \\
&= \left.\frac{\partial k_r^o}{\partial S^{\tilde{w}}}\right|_{S^{\tilde{g}}} \cdot -1 + \left.\frac{\partial k_r^o}{\partial S^{\tilde{g}}}\right|_{S^{\tilde{w}}} \cdot 0 \\
&= -\left.\frac{\partial k_r^o}{\partial S^{\tilde{w}}}\right|_{S^{\tilde{g}}}
\end{aligned} \tag{A.6}$$

$$\begin{aligned}
\left.\frac{\partial k_r^o}{\partial S^g}\right|_{S^o} &= \left.\frac{\partial k_r^o}{\partial S^{\tilde{w}}}\right|_{S^{\tilde{g}}} \frac{\partial S^{\tilde{w}}}{\partial S^g} + \left.\frac{\partial k_r^o}{\partial S^{\tilde{g}}}\right|_{S^{\tilde{w}}} \frac{\partial S^{\tilde{g}}}{\partial S^g} \\
&= \left.\frac{\partial k_r^o}{\partial S^{\tilde{w}}}\right|_{S^{\tilde{g}}} \cdot -1 + \left.\frac{\partial k_r^o}{\partial S^{\tilde{g}}}\right|_{S^{\tilde{w}}} \cdot 1 \\
&= -\left.\frac{\partial k_r^o}{\partial S^{\tilde{w}}}\right|_{S^{\tilde{g}}} + \left.\frac{\partial k_r^o}{\partial S^{\tilde{g}}}\right|_{S^{\tilde{w}}}
\end{aligned} \tag{A.7}$$

Secondly, the water relative permeability will be looked at:

$$\begin{aligned}
\left.\frac{\partial k_r^w}{\partial S^o}\right|_{S^g} &= \left.\frac{\partial k_r^w}{\partial S^{\tilde{w}}}\right|_{S^{\tilde{g}}} \frac{\partial S^{\tilde{w}}}{\partial S^o} \\
&= \left.\frac{\partial k_r^w}{\partial S^{\tilde{w}}}\right|_{S^{\tilde{g}}} \cdot -1 \\
&= -\left.\frac{\partial k_r^w}{\partial S^{\tilde{w}}}\right|_{S^{\tilde{g}}}
\end{aligned} \tag{A.8}$$

$$\begin{aligned}
\left.\frac{\partial k_r^w}{\partial S^g}\right|_{S^o} &= \left.\frac{\partial k_r^w}{\partial S^{\tilde{w}}}\right|_{S^{\tilde{g}}} \frac{\partial S^{\tilde{w}}}{\partial S^g} \\
&= \left.\frac{\partial k_r^w}{\partial S^{\tilde{w}}}\right|_{S^{\tilde{g}}} \cdot -1 \\
&= -\left.\frac{\partial k_r^w}{\partial S^{\tilde{w}}}\right|_{S^{\tilde{g}}}
\end{aligned} \tag{A.9}$$

Finally, the derivatives of the gas relative permeability are rewritten:

$$\begin{aligned}
\left.\frac{\partial k_r^g}{\partial S^o}\right|_{S^g} &= \left.\frac{\partial k_r^g}{\partial S^{\tilde{g}}}\right|_{S^{\tilde{w}}} \frac{\partial S^{\tilde{g}}}{\partial S^o} \\
&= \left.\frac{\partial k_r^g}{\partial S^{\tilde{g}}}\right|_{S^{\tilde{w}}} \cdot 0 \\
&= 0
\end{aligned} \tag{A.10}$$

$$\frac{\partial k_r^g}{\partial S^g}\bigg|_{S^o} = \frac{\partial k_r^g}{\partial S^{\tilde{g}}}\bigg|_{S^{\tilde{w}}} \frac{\partial S^{\tilde{g}}}{\partial S^g}$$

$$= \frac{\partial k_r^g}{\partial S^{\tilde{g}}}\bigg|_{S^{\tilde{w}}} \cdot 1 \tag{A.11}$$

$$= \frac{\partial k_r^g}{\partial S^{\tilde{g}}}\bigg|_{S^{\tilde{w}}}$$

For notational simplicity $(S^w, S^g)$ is used instead of $(S^{\tilde{w}}, S^{\tilde{g}})$ for the variables of the continuous system as well as for the variables of the discretized system from this point on.

## A.3. Entries of the Jacobian matrix

In Section A.1 the phase volume equation was used to eliminate the water phase from the system of equations. This means that a system of three residuals is left, namely $R_{\tilde{A}_i^w}$, $R_{A_i^o}$ and $R_{A_i^g}$. Using these residuals every $3 \times 3$ submatrix $J_{ij}$ of the Jacobian $J$ can be calculated by:

$$J_{ij} = \begin{pmatrix} \frac{\partial R_{\tilde{A}_i^w}}{\partial p_i} & \frac{\partial R_{\tilde{A}_i^w}}{\partial A_i^o} & \frac{\partial R_{\tilde{A}_i^w}}{\partial A_i^g} \\ \frac{\partial R_{A_i^o}}{\partial p_i} & \frac{\partial R_{A_i^o}}{\partial A_i^o} & \frac{\partial R_{A_i^o}}{\partial A_i^g} \\ \frac{\partial R_{A_i^g}}{\partial p_i} & \frac{\partial R_{A_i^g}}{\partial A_i^o} & \frac{\partial R_{A_i^g}}{\partial A_i^g} \end{pmatrix} \tag{A.12}$$

Note that, due to the choice for an upwind scheme, the residuals in grid cell $i$ only depend on accumulations in grid cells $i-1$ and $i$ and. And due to the choice for a central difference scheme, the residual in grid cell $i$ only depend on the pressure in grid cells $i-1$, $i$ and $i+1$. Therefore $J_{ij} \equiv 0$ for $j \neq i-1$, $i$, $i+1$.

First the partial derivatives of the residuals with respect to pressure will be determined. For the substituted water saturation residual (A.2) the following holds:

$$\frac{\partial R_{\tilde{A}_i^w}}{\partial p_{i-1}} = -\frac{\Delta t}{\Delta x} \Delta y \Delta z K \frac{\rho^w}{\mu^w} k_{r_{i-1}}^w \tag{A.13}$$

$$\frac{\partial R_{\tilde{A}_i^w}}{\partial p_i} = -\frac{\Delta t}{\Delta x} \Delta y \Delta z K \frac{\rho^w}{\mu^w} (-k_{r_i}^w - k_{r_{i-1}}^w)$$

$$= \frac{\Delta t}{\Delta x} \Delta y \Delta z K \frac{\rho^w}{\mu^w} (k_{r_i}^w + k_{r_{i-1}}^w) \tag{A.14}$$

$$\frac{\partial R_{\tilde{A}_i^w}}{\partial p_{i+1}} = -\frac{\Delta t}{\Delta x} \Delta y \Delta z K \frac{\rho^w}{\mu^w} k_{r_i}^w \tag{A.15}$$

For the oil saturation residual (3.25) the following holds:

$$\frac{\partial R_{A_i^o}}{\partial p_{i-1}} = -\frac{\Delta t}{\Delta x} \Delta y \Delta z K \frac{\rho^o}{\mu^o} k_{r_{i-1}}^o \tag{A.16}$$

$$\frac{\partial R_{A_i^o}}{\partial p_i} = -\frac{\Delta t}{\Delta x} \Delta y \Delta z K \frac{\rho^o}{\mu^o} (-k_{r_i}^o - k_{r_{i-1}}^o)$$

$$= \frac{\Delta t}{\Delta x} \Delta y \Delta z K \frac{\rho^o}{\mu^o} (k_{r_i}^o + k_{r_{i-1}}^o) \tag{A.17}$$

$$\frac{\partial R_{A_i^o}}{\partial p_{i+1}} = -\frac{\Delta t}{\Delta x} \Delta y \Delta z K \frac{\rho^o}{\mu^o} k_{r_i}^o \tag{A.18}$$

And for the gas saturation residual (3.25) similar expressions as for the substituted water residual are obtained:

$$\frac{\partial R_{A_i^g}}{\partial p_{i-1}} = -\frac{\Delta t}{\Delta x}\Delta y\Delta z K\frac{\rho^g}{\mu^g}k_{r_{i-1}}^g \tag{A.19}$$

$$\frac{\partial R_{A_i^g}}{\partial p_i} = -\frac{\Delta t}{\Delta x}\Delta y\Delta z K\frac{\rho^g}{\mu^g}(-k_{r_i}^g - k_{r_{i-1}}^g)$$

$$= \frac{\Delta t}{\Delta x}\Delta y\Delta z K\frac{\rho^g}{\mu^g}(k_{r_i}^g + k_{r_{i-1}}^g) \tag{A.20}$$

$$\frac{\partial R_{A_i^g}}{\partial p_{i+1}} = -\frac{\Delta t}{\Delta x}\Delta y\Delta z K\frac{\rho^g}{\mu^g}k_{r_i}^g \tag{A.21}$$

Secondly, the partial derivatives of the residuals with respect to the oil accumulation are determined. Using equations (A.4) and (A.8), the following holds for the substituted water saturation residual (A.2):

$$\frac{\partial R_{\tilde{A}_i^w}}{\partial A_{i-1}^o} = -\frac{\Delta t}{\Delta x}\Delta y\Delta z K\frac{\rho^w}{\mu^w}\left[-\frac{1}{\phi\Delta x\Delta y\Delta z\rho^o}\frac{\partial k_{r_{i-1}}^w}{\partial S_{i-1}^o}(p_i - p_{i-1})\right]$$

$$= -\frac{\Delta t}{\Delta x^2}\frac{K}{\phi}\frac{1}{\mu^w}\frac{\rho^w}{\rho^o}(p_i - p_{i-1})\frac{\partial k_{r_{i-1}}^w}{\partial S_{i-1}^w} \tag{A.22}$$

$$\frac{\partial R_{\tilde{A}_i^w}}{\partial A_i^o} = \frac{-\rho^w}{\rho^o} - \frac{\Delta t}{\Delta x}\Delta y\Delta z K\frac{\rho^w}{\mu^w}\frac{1}{\phi\Delta x\Delta y\Delta z\rho^o}\frac{\partial k_{r_i}^w}{\partial S_i^o}(p_{i+1} - p_i)$$

$$= \frac{-\rho^w}{\rho^o} + \frac{\Delta t}{\Delta x^2}\frac{K}{\phi}\frac{1}{\mu^w}\frac{\rho^w}{\rho^o}(p_{i+1} - p_i)\frac{\partial k_{r_i}^w}{\partial S_i^w} \tag{A.23}$$

$$\frac{\partial R_{\tilde{A}_i^w}}{\partial A_{i+1}^o} = 0 \tag{A.24}$$

Using equations (A.4) and (A.6), the following holds for the oil saturation residual (3.25):

$$\frac{\partial R_{A_i^o}}{\partial A_{i-1}^o} = -\frac{\Delta t}{\Delta x}\Delta y\Delta z K\rho^o\frac{1}{\mu^o}\left[-\frac{1}{\phi\Delta x\Delta y\Delta z\rho^o}\frac{\partial k_{r_{i-1}}^o}{\partial S_{i-1}^o}(p_i - p_{i-1})\right]$$

$$= -\frac{\Delta t}{\Delta x^2}\frac{K}{\phi}\frac{1}{\mu^o}(p_i - p_{i-1})\frac{\partial k_{r_{i-1}}^o}{\partial S_{i-1}^w} \tag{A.25}$$

$$\frac{\partial R_{A_i^o}}{\partial A_i^o} = 1 - \frac{\Delta t}{\Delta x}\Delta y\Delta z K\rho^o\frac{1}{\mu^o}\left[\frac{1}{\phi\Delta x\Delta y\Delta z\rho^o}\frac{\partial k_{r_i}^o}{\partial S_i^o}(p_{i+1} - p_i)\right]$$

$$= 1 + \frac{\Delta t}{\Delta x^2}\frac{K}{\phi}\frac{1}{\mu^o}(p_{i+1} - p_i)\frac{\partial k_{r_i}^o}{\partial S_i^w} \tag{A.26}$$

$$\frac{\partial R_{A_i^o}}{\partial A_{i+1}^o} = 0 \tag{A.27}$$

And for the gas saturation residual (3.25) the following is obtained:

$$\frac{\partial R_{A_i^g}}{\partial A_{i-1}^o} = -\frac{\Delta t}{\Delta x} \Delta y \Delta z K \rho^g \frac{1}{\mu^g} \left[ -\frac{1}{\phi \Delta x \Delta y \Delta z \rho^o} \frac{\partial k_{r_{i-1}}^g}{\partial S_{i-1}^o} (p_i - p_{i-1}) \right]$$

$$= \frac{\Delta t}{\Delta x^2} \frac{K}{\phi} \frac{\rho^g}{\rho^o} \frac{1}{\mu^g} (p_i - p_{i-1}) \frac{\partial k_{r_{i-1}}^g}{\partial S_{i-1}^o} \tag{A.28}$$

$$\frac{\partial R_{A_i^g}}{\partial A_i^o} = -\frac{\Delta t}{\Delta x} \Delta y \Delta z K \rho^g \frac{1}{\mu^g} \left[ \frac{1}{\phi \Delta x \Delta y \Delta z \rho^o} \frac{\partial k_{r_i}^g}{\partial S_i^o} (p_{i+1} - p_i) \right]$$

$$= -\frac{\Delta t}{\Delta x^2} \frac{K}{\phi} \frac{\rho^g}{\rho^o} \frac{1}{\mu^o} (p_{i+1} - p_i) \frac{\partial k_{r_i}^g}{\partial S_i^o} \tag{A.29}$$

$$\frac{\partial R_{A_i^g}}{\partial A_{i+1}^o} = 0 \tag{A.30}$$

Finally, the partial derivatives of the residuals with respect to the gas accumulation are determined. Using equations (A.4) and (A.9), the following holds for the substituted water saturation residual (A.2):

$$\frac{\partial R_{\tilde{A}_i^w}}{\partial A_{i-1}^g} = -\frac{\Delta t}{\Delta x} \Delta y \Delta z K \frac{\rho^w}{\mu^w} \left[ -\frac{1}{\phi \Delta x \Delta y \Delta z \rho^g} \frac{\partial k_{r_{i-1}}^w}{\partial S_{i-1}^g} (p_i - p_{i-1}) \right]$$

$$= -\frac{\Delta t}{\Delta x^2} \frac{K}{\phi} \frac{1}{\mu^w} \frac{\rho^w}{\rho^g} (p_i - p_{i-1}) \frac{\partial k_{r_{i-1}}^w}{\partial S_{i-1}^w} \tag{A.31}$$

$$\frac{\partial R_{\tilde{A}_i^w}}{\partial A_i^g} = \frac{-\rho^w}{\rho^g} - \frac{\Delta t}{\Delta x} \Delta y \Delta z K \frac{\rho^w}{\mu^w} \frac{1}{\phi \Delta x \Delta y \Delta z \rho^g} \frac{\partial k_{r_i}^w}{\partial S_i^g} (p_{i+1} - p_i)$$

$$= \frac{-\rho^w}{\rho^g} + \frac{\Delta t}{\Delta x^2} \frac{K}{\phi} \frac{1}{\mu^w} \frac{\rho^w}{\rho^g} (p_{i+1} - p_i) \frac{\partial k_{r_i}^w}{\partial S_i^w} \tag{A.32}$$

$$\frac{\partial R_{\tilde{A}_i^w}}{\partial A_{i+1}^g} = 0 \tag{A.33}$$

Using equations (A.4) and (A.7), the following holds for the oil saturation residual (3.25):

$$\frac{\partial R_{A_i^o}}{\partial A_{i-1}^g} = -\frac{\Delta t}{\Delta x} \Delta y \Delta z K \rho^o \frac{1}{\mu^o} \left[ -\frac{1}{\phi \Delta x \Delta y \Delta z \rho^g} \frac{\partial k_{r_{i-1}}^o}{\partial S_{i-1}^g} (p_i - p_{i-1}) \Big|_{S^o} \right]$$

$$= \frac{\Delta t}{\Delta x^2} \frac{K}{\phi} \frac{\rho^o}{\rho^g} \frac{1}{\mu^o} (p_i - p_{i-1}) \left( \frac{\partial k_{r_{i-1}}^o}{\partial S_{i-1}^g} \Big|_{S^w} - \frac{\partial k_{r_{i-1}}^o}{\partial S_{i-1}^w} \Big|_{S^g} \right) \tag{A.34}$$

$$\frac{\partial R_{A_i^o}}{\partial A_i^g} = -\frac{\Delta t}{\Delta x} \Delta y \Delta z K \rho^o \frac{1}{\mu^o} \left[ \frac{1}{\phi \Delta x \Delta y \Delta z \rho^g} \frac{\partial k_{r_i}^o}{\partial S_i^g} \Big|_{S^o} (p_{i+1} - p_i) \right]$$

$$= -\frac{\Delta t}{\Delta x^2} \frac{K}{\phi} \frac{\rho^o}{\rho^g} \frac{1}{\mu^o} (p_{i+1} - p_i) \left( \frac{\partial k_{r_i}^o}{\partial S_i^g} \Big|_{S^w} - \frac{\partial k_{r_i}^o}{\partial S_i^w} \Big|_{S^g} \right) \tag{A.35}$$

$$\frac{\partial R_{A_i^o}}{\partial A_{i+1}^g} = 0 \tag{A.36}$$

Finally, using equations (A.4) and (A.11), the following holds for the gas saturation residual (3.25):

$$\frac{\partial R_{A_i^g}}{\partial A_{i-1}^g} = -\frac{\Delta t}{\Delta x}\Delta y\Delta z K\rho^g\frac{1}{\mu^g}\left[-\frac{1}{\phi\Delta x\Delta y\Delta z\rho^g}\frac{\partial k_{r_{i-1}}^g}{\partial S_{i-1}^g}(p_i-p_{i-1})\right]$$

$$= \frac{\Delta t}{\Delta x^2}\frac{K}{\phi}\frac{1}{\mu^g}(p_i-p_{i-1})\frac{\partial k_{r_{i-1}}^g}{\partial S_{i-1}^g} \tag{A.37}$$

$$\frac{\partial R_{A_i^g}}{\partial A_i^g} = 1 - \frac{\Delta t}{\Delta x}\Delta y\Delta z K\rho^g\frac{1}{\mu^g}\left[\frac{1}{\phi\Delta x\Delta y\Delta z\rho^g}\frac{\partial k_{r_i}^g}{\partial S_i^g}(p_{i+1}-p_i)\right]$$

$$= 1 - \frac{\Delta t}{\Delta x^2}\frac{K}{\phi}\frac{1}{\mu^g}(p_{i+1}-p_i)\frac{\partial k_{r_i}^g}{\partial S_i^g} \tag{A.38}$$

$$\frac{\partial R_{A_i^g}}{\partial A_{i+1}^g} = 0 \tag{A.39}$$

# Relatives permeabilities and their derivatives for interpolation I, II and III

In this appendix the derivation of the expressions for the three-phase relative permeability of all three phases using interpolation I, II and III are given. Sections 4.3.1, 4.3.2 and 4.3.3 describe how this derivation works for the oil relative permeability. For the other two phases the derivation is similar. This means that the saturations $\tilde{S}$ on the two-phase edges have to be determined after which linear interpolation between the relative permeabilities for these saturations is used to obtain the three-phase relative permeability. For oil relative permeability interpolation is done between the two-phase relative permeabilities of a water-oil and oil-gas system. Similarly, to obtain the water relative permeability interpolation is used between the two-phase relative permeabilities of a water-oil and water-gas system. And for the gas relative permeability interpolation is used between the two-phase relative permeabilities of a oil-gas and water-gas system. For the two-phase relative permeabilities the following is assumed:

$$k_r^{wo} = k_r^{wo}(S^w)$$
$$k_r^{ow} = k_r^{ow}(S^w)$$
$$k_r^{go} = k_r^{go}(S^g)$$
$$k_r^{og} = k_r^{og}(S^g)$$
$$k_r^{wg} = k_r^{wg}(S^w)$$
$$k_r^{gw} = k_r^{gw}(S^w)$$

Here $k_r^{\alpha_1 \alpha_2}$ is used to denote the relative permeability of phase $\alpha_1$ in a $\alpha_1$-$\alpha_2$ system, e.g. $k_r^{wg}$ denotes the relative permeability of water in a water-gas system. Furthermore, if for all two-phase relative permeabilities Corey-correlations with zero residual saturations and endpoint equal to one are assumed, the two-phase relative permeabilities are given:

$$k_r^{wo} = k_r^{wo}(S^w) = (S^w)^{n_{wo}} \tag{B.1}$$
$$k_r^{ow} = k_r^{ow}(S^w) = (1 - S^w)^{n_{ow}} \tag{B.2}$$
$$k_r^{go} = k_r^{go}(S^g) = (S^g)^{n_{go}} \tag{B.3}$$
$$k_r^{og} = k_r^{og}(S^g) = (1 - S^g)^{n_{og}} \tag{B.4}$$
$$k_r^{wg} = k_r^{wg}(S^w) = (S^w)^{n_{wg}} \tag{B.5}$$
$$k_r^{gw} = k_r^{gw}(S^w) = (1 - S^w)^{n_{gw}} \tag{B.6}$$

## B.1. Interpolation I

For interpolation I the two-phase relative permeabilities are taken at the saturations $\tilde{S}$ that lie on the isosaturation line through the point in the interior at which the three-phase relative permeability is to be computed, see Figure B.1. Note that for the interpolation of the gas and water relative permeabilities the oil saturation

is used. But the relative permeabilities can be rewritten as functions of $S^w$ and $S^g$ using that the saturations sum up to one.



(a) Oil relative permeability          (b) Water relative permeability          (c) Gas relative permeability

Figure B.1: Construction of interpolation I to obtain three-phase relative permeability for oil (a), water (b) and gas (c). The isosaturation is shown in red.

### B.1.1. Oil

To obtain the three-phase relative permeability of oil $\tilde{S}^w$ and $\tilde{S}^g$ have to be determined and then linear interpolation has to be used, see Figure B.1a. Since $S^o = 1 - S^w - S^g$ and since $\tilde{S}^w$ and $\tilde{S}^g$ lie on the oil isosaturion and on the OW edge and OG edge respectively, the following holds:

$$S^o = 1 - \tilde{S}^g$$
$$S^o = 1 - \tilde{S}^w$$
$$S^o = 1 - S^w - S^g$$

Therefore,

$$\tilde{S}^w = \tilde{S}^g = S^w + S^g$$

Then, linear interpolation is used between the oil relative permeabilities in $\tilde{S}^w$ and $\tilde{S}^g$ on the two edges to obtain the oil relative permeability for the interior point $(S^w, S^g)$. Note that $\tilde{S}^w$ and $\tilde{S}^g$ lie on the oil-water and oil-gas edge respectively. Therefore the oil relative permeability in these points is given by the two-phase relative permeabilities $k_r^{ow}(\tilde{S}^w)$ and $k_r^{og}(\tilde{S}^g)$. The three-phase oil relative permeability is then given by:

$$k_r^o(S^w, S^g) = \frac{S^w}{S^w + S^g} k_r^{ow}(\tilde{S}^w) + \frac{S^g}{S^w + S^g} k_r^{og}(\tilde{S}^g)$$

$$= \frac{S^w}{S^w + S^g} k_r^{ow}(S^w + S^g) + \frac{S^g}{S^w + S^g} k_r^{og}(S^w + S^g) \tag{B.7}$$

### B.1.2. Water

To find the water relative permeability interpolation is done between the relative permeabilities in the water-gas and water-oil system. This means $\tilde{S}^o$ and $\tilde{S}^g$ have to be determined and subsequently linear interpolation is used, see Figure B.1b. Since $S^w = 1 - S^o - S^g$ and since $\tilde{S}^o$ and $\tilde{S}^g$ lie on the water isosaturion and on the OW and WG edge respectively, the following holds:

$$S^w = 1 - \tilde{S}^g$$
$$S^w = 1 - \tilde{S}^o$$
$$S^w = 1 - S^o - S^g$$

Therefore,

$$\tilde{S}^o = \tilde{S}^g = S^o + S^g$$

The two-phase relative permeabilities can be written in term of $\tilde{S}^g$ and $\tilde{S}^o$ as follows:

$$k_r^{wg} = k_r^{wg}(S^w) = k_r^{wg}(1 - \tilde{S}^g) \tag{B.8}$$
$$k_r^{wo} = k_r^{wo}(S^w) = k_r^{wo}(1 - \tilde{S}^o) \tag{B.9}$$

The three-phase water relative permeability is then given by:

$$k_r^w(S^o, S^g) = \frac{S^o}{S^o + S^g} k_r^{wo}(1 - \tilde{S}^o) + \frac{S^g}{S^o + S^g} k_r^{wg}(1 - \tilde{S}^g)$$

$$= \frac{S^o}{S^o + S^g} k_r^{wo}(1 - S^o - S^g) + \frac{S^g}{S^o + S^g} k_r^{wg}(1 - S^o - S^g) \tag{B.10}$$

Using that the sum of the saturation is one, such that $S^o = 1 - S^w - S^g$, the relative permeability $k_r^w$ can be rewritten as function of $S^w$ and $S^g$:

$$k_r^w(S^w, S^g) = \frac{1 - S^w - S^g}{1 - S^w - S^g + S^g} k_r^{wo}(1 - (1 - S^w - S^g) - S^g) + \frac{S^g}{1 - S^w - S^g + S^g} k_r^{wg}(1 - (1 - S^w - S^g) - S^g)$$

$$= \frac{1 - S^w - S^g}{1 - S^w} k_r^{wo}(S^w) + \frac{S^g}{1 - S^w} k_r^{wg}(S^w) \tag{B.11}$$

### B.1.3. Gas

To find the gas relative permeability interpolation must be done between the relative permeabilities in the water-gas and oil-gas system. This means $\tilde{S}^o$ and $\tilde{S}^w$ have to be determined and subsequently linear interpolation has to be used, see Figure B.1c. Since $S^g = 1 - S^o - S^w$ and since $\tilde{S}^o$ and $\tilde{S}^w$ lie on the gas isosaturion and on the OG edge and WG edge respectively the following holds:

$$S^g = 1 - \tilde{S}^w$$
$$S^g = 1 - \tilde{S}^o$$
$$S^g = 1 - S^o - S^w$$

Therefore,

$$\tilde{S}^o = \tilde{S}^w = S^o + S^w$$

For the two-phase relative permeabilities this means that:

$$k_r^{gw} = k_r^{gw}(\tilde{S}^w) \tag{B.12}$$
$$k_r^{go} = k_r^{go}(S^g) = k_r^{go}(1 - \tilde{S}^o) \tag{B.13}$$

The three-phase gas relative permeability is then given by:

$$k_r^g(S^w, S^o) = \frac{S^o}{S^o + S^w} k_r^{go}(1 - \tilde{S}^o) + \frac{S^g}{S^o + S^w} k_r^{gw}(\tilde{S}^w)$$

$$= \frac{S^o}{S^o + S^w} k_r^{go}(1 - S^o - S^w) + \frac{S^g}{S^o + S^w} k_r^{gw}(S^o + S^w) \tag{B.14}$$

Using that the sum of the saturation is one, such that $S^o = 1 - S^w - S^g$, the relative permeability $k_r^g$ can be rewritten as function of $S^w$ and $S^g$:

$$k_r^g(S^w, S^g) = \frac{1 - S^w - S^g}{1 - S^w - S^g + S^w} k_r^{go}(1 - (1 - S^w - S^g) - S^w) + \frac{S^g}{1 - S^w - S^g + S^w} k_r^{gw}(1 - S^w - S^g + S^w)$$

$$= \frac{1 - S^w - S^g}{1 - S^g} k_r^{go}(S^g) + \frac{S^w}{1 - S^g} k_r^{gw}(1 - S^g) \tag{B.15}$$

## B.2. Interpolation II

For interpolation II the two-phase relative permeabilities are taken at the saturations $\tilde{S}$ that lie on a circle, with the origin as the centre, through the point of interest in the interior at which the three-phase relative permeability is to be computed, see Figure B.2. Note that for the gas and water relative permeabilities the oil saturation is used. But the relative permeabilities can be rewritten as functions of $S^w$ and $S^g$ using that the saturations sum up to one.
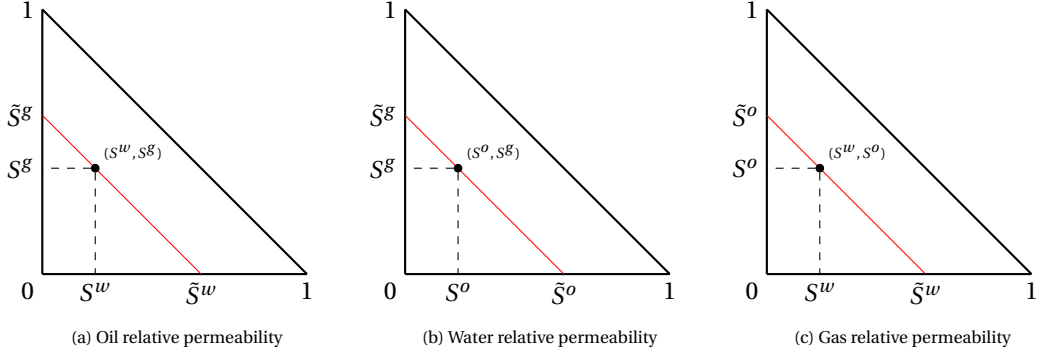
(a) Oil relative permeability      (b) Water relative permeability      (c) Gas relative permeability
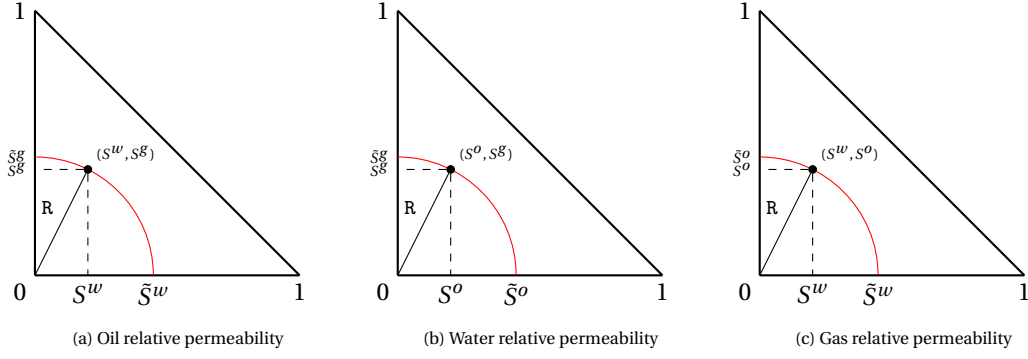
Figure B.2: Construction of interpolation II to obtain three-phase relative permeability for oil (a), water (b) and gas (c). The circle through the interior point for which the relative permeability is computed is shown in red.

### B.2.1. Oil

To obtain the three-phase relative permeability of oil $\tilde{S}^w$ and $\tilde{S}^g$ must be determine and subsequently linear interpolation is used. From Figure B.2a it follows that $\tilde{S}^w = \tilde{S}^g = \text{R} = \sqrt{(S^w)^2 + (S^g)^2}$. Then linear interpolation is used between the oil relative permeabilities in $\tilde{S}^w$ and $\tilde{S}^g$ on the two edges to obtain the oil relative permeability for the interior point $(S^w, S^g)$. Note that $\tilde{S}^w$ and $\tilde{S}^g$ lie on the water-oil and oil-gas edge respectively. Therefore the oil relative permeability in these points is given by the two-phase relative permeabilities $k_r^{ow}(\tilde{S}^w)$ and $k_r^{og}(\tilde{S}^g)$. The three-phase oil relative permeability is then given by:

$$
\begin{aligned}
k_r^o(S^w, S^g) &= \frac{S^w}{S^w + S^g} k_r^{ow}(\tilde{S}^w) + \frac{S^g}{S^w + S^g} k_r^{og}(\tilde{S}^g) \\
&= \frac{S^w}{S^w + S^g} k_r^{ow}\left(\sqrt{(S^w)^2 + (S^g)^2}\right) + \frac{S^g}{S^w + S^g} k_r^{og}\left(\sqrt{(S^w)^2 + (S^g)^2}\right)
\end{aligned}
\tag{B.16}
$$

### B.2.2. Water

From Figure B.2b it follows that $\tilde{S}^o = \tilde{S}^g = \text{R} = \sqrt{(S^o)^2 + (S^g)^2}$. Then linear interpolation is used between the water relative permeabilities in $\tilde{S}^o$ and $\tilde{S}^g$ on the two edges to obtain the water relative permeability for the interior points. For the two-phase relative permeabilities $k_r^{wg}$ and $k_r^{wo}$ are assumed to be functions of $S^w$, so:

$$
k_r^{wg} = k_r^{wg}(1 - \tilde{S}^g) \tag{B.17}
$$
$$
k_r^{wo} = k_r^{wo}(1 - \tilde{S}^o) \tag{B.18}
$$

The three-phase water relative permeability is then given by:

$$
\begin{aligned}
k_r^w(S^o, S^g) &= \frac{S^o}{S^o + S^g} k_r^{wo}(1 - \tilde{S}^o) + \frac{S^g}{S^o + S^g} k_r^{wg}(1 - \tilde{S}^g) \\
&= \frac{S^o}{S^o + S^g} k_r^{wo}\left(1 - \sqrt{(S^o)^2 + (S^g)^2}\right) + \frac{S^g}{S^o + S^g} k_r^{wg}\left(1 - \sqrt{(S^o)^2 + (S^g)^2}\right)
\end{aligned}
\tag{B.19}
$$

Using that the sum of the saturations is one, such that $S^o = 1 - S^w - S^g$, the relative permeability $k_r^w$ can be rewritten as function of $S^w$ and $S^g$:

$$
\begin{aligned}
k_r^w(S^w, S^g) &= \frac{1 - S^w - S^g}{1 - S^w - S^g + S^g} k_r^{wo}\left(1 - \sqrt{(S^o)^2 + (S^g)^2}\right) + \frac{S^g}{1 - S^w - S^g + S^g} k_r^{wg}\left(1 - \sqrt{(S^o)^2 + (S^g)^2}\right) \\
&= \frac{1 - S^w - S^g}{1 - S^w} k_r^{wo}\left(1 - \sqrt{(S^o)^2 + (S^g)^2}\right) + \frac{S^g}{1 - S^w} k_r^{wg}\left(1 - \sqrt{(S^o)^2 + (S^g)^2}\right)
\end{aligned}
\tag{B.20}
$$

with

$$
\begin{aligned}
(S^o)^2 + (S^g)^2 &= (1 - S^w - S^g)^2 + (S^g)^2 \\
&= 1 - 2S^w - 2S^g + 2S^w S^g + (S^w)^2 + 2(S^g)^2
\end{aligned}
$$

### B.2.3. Gas

From Figure B.2c it follows that $\tilde{S}^o = \tilde{S}^w = \mathrm{R} = \sqrt{(S^o)^2 + (S^w)^2}$. Then linear interpolation is used between the gas relative permeabilities in $\tilde{S}^o$ and $\tilde{S}^w$ on the two edges to obtain the gas relative permeability for the interior points. For the two-phase relative permeabilities $k_r^{gw}$ is assumed to be a function of $S^w$ and $k_r^{go}$ to be a function of $S^g$, which means that:

$$k_r^{gw} = k_r^{gw}(\tilde{S}^w) \tag{B.21}$$

$$k_r^{go} = k_r^{go}(1 - \tilde{S}^o) \tag{B.22}$$

The three-phase gas relative permeability is then given by:

$$k_r^g(S^w, S^o) = \frac{S^o}{S^o + S^w} k_r^{go}(1 - \tilde{S}^o) + \frac{S^w}{S^o + S^w} k_r^{gw}(\tilde{S}^w)$$

$$= \frac{S^o}{S^o + S^w} k_r^{go}\left(1 - \sqrt{(S^o)^2 + (S^w)^2}\right) + \frac{S^w}{S^o + S^w} k_r^{gw}\left(\sqrt{(S^o)^2 + (S^w)^2}\right) \tag{B.23}$$

Using that the sum of the saturation is one, such that $S^o = 1 - S^w - S^g$, the relative permeability $k_r^g$ can be rewritten as function of $S^w$ and $S^g$:

$$k_r^g(S^w, S^g) = \frac{1 - S^w - S^g}{1 - S^w - S^g + S^w} k_r^{go}\left(1 - \sqrt{(S^o)^2 + (S^w)^2}\right) + \frac{S^w}{1 - S^w - S^g + S^w} k_r^{gw}\left(\sqrt{(S^o)^2 + (S^w)^2}\right)$$

$$= \frac{1 - S^w - S^g}{1 - S^g} k_r^{go}\left(1 - \sqrt{(S^o)^2 + (S^w)^2}\right) + \frac{S^w}{1 - S^g} k_r^{gw}\left(\sqrt{(S^o)^2 + (S^w)^2}\right) \tag{B.24}$$

with

$$(S^o)^2 + (S^w)^2 = (1 - S^w - S^g)^2 + (S^w)^2$$

$$= 1 - 2S^w - 2S^g + 2S^w S^g + 2(S^w)^2 + (S^g)^2$$

## B.3. Interpolation III

Interpolation III is a combination of interpolation I and interpolation II. Interpolation I is used for the low saturation values to ensure that the relative permeability goes to zero when the saturation goes to zero. Interpolation II is used for the smaller saturation values to obtain more concave isoperms for this region. Writing $k_r^{\alpha,I}$ and $k_r^{\alpha,II}$ for the relative permeability of phase $\alpha$ obtained from interpolation I and interpolation II respectively the relative permeabilities obtained using interpolation III are given by:

$$k_r^o(S^w, S^g) = S^o k_r^{o,II}(S^w, S^g) + (1 - S^o) k_r^{o,I}(S^w, S^g)$$

$$= (1 - S^w - S^g) k_r^{o,II}(S^w, S^g) + (S^w + S^g) k_r^{o,I}(S^w, S^g) \tag{B.25}$$

$$k_r^w(S^w, S^g) = S^w k_r^{w,II}(S^w, S^g) + (1 - S^w) k_r^{w,I}(S^w, S^g) \tag{B.26}$$

$$k_r^g(S^w, S^g) = S^g k_r^{g,II}(S^w, S^g) + (1 - S^g) k_r^{g,I}(S^w, S^g) \tag{B.27}$$

## B.4. Derivatives of the relative permeabilities

In this section the derivatives of the relative permeabilities with respect to the water saturation and gas saturation are determined. These derivative are used to determine the qualitative behavior of the curves by Holden and to determine the direction of the eigenvectors on the edges of the ternary diagram.

### B.4.1. Interpolation I

#### Oil

Equation (B.7) gives the following for the oil relative permeability:

$$k_r^o = \frac{S^w k_r^{ow}(\tilde{S}_o^I) + S^g k_r^{og}(\tilde{S}_o^I)}{S^w + S^g} \tag{B.28}$$

where $\tilde{S}_o^I$ is used to denote the $\tilde{S}$ used for interpolation I to obtain the oil relative permeability and is given by $\tilde{S}_o^I = S^w + S^g$. This gives:

$$\frac{\partial \tilde{S}_o^I}{\partial S^w} = \frac{\partial \tilde{S}_o^I}{\partial S^g} = 1$$

This means that the following holds for the derivatives of the oil relative permeability:

$$
\frac{\partial S^o}{\partial S^w} = \frac{\left(S^w + S^g\right)\left[k_r^{ow}(\tilde{S}_o^I) + S^w k_r^{ow\prime}(\tilde{S}_o^I) + S^g k_r^{og\prime}(\tilde{S}_o^I)\right] - \left[S^w k_r^{ow}(\tilde{S}_o^I) + S^g k_r^{og}(\tilde{S}_o^I)\right] \cdot 1}{(S^w + S^g)^2}
$$

$$
= \frac{1}{S^w + S^g}\left[k_r^{ow}(\tilde{S}_o^I) + S^w k_r^{ow\prime}(\tilde{S}_o^I) + S^g k_r^{og\prime}(\tilde{S}_o^I) - k_r^o(S^w, S^g)\right]
$$

$$
= \frac{(S^w + S^g)\left[S^w k_r^{ow\prime}(\tilde{S}_o^I) + S^g k_r^{og\prime}(\tilde{S}_o^I)\right] + S^g\left[k_r^{ow}(\tilde{S}_o^I) - k_r^{og}(\tilde{S}_o^I)\right]}{(S^w + S^g)^2} \tag{B.29}
$$

$$
\frac{\partial S^o}{\partial S^g} = \frac{\left(S^w + S^g\right)\left[S^w k_r^{ow\prime}(\tilde{S}_o^I) + k_r^{og}(\tilde{S}_o^I) + S^g k_r^{og\prime}(\tilde{S}_o^I)\right] - \left[S^w k_r^{ow}(\tilde{S}_o^I) + S^g k_r^{og}(\tilde{S}_o^I)\right] \cdot 1}{(S^w + S^g)^2}
$$

$$
= \frac{1}{S^w + S^g}\left[S^w k_r^{ow\prime}(\tilde{S}_o^I) + k_r^{og}(\tilde{S}_o^I) + S^g k_r^{og\prime}(\tilde{S}_o^I) - k_r^o(S^w, S^g)\right]
$$

$$
= \frac{(S^w + S^g)\left[S^w k_r^{ow\prime}(\tilde{S}_o^I) + S^g k_r^{og\prime}(\tilde{S}_o^I)\right] + S^w\left[k_r^{og}(\tilde{S}_o^I) - k_r^{ow}(\tilde{S}_o^I)\right]}{(S^w + S^g)^2} \tag{B.30}
$$

Where $k_r^{ow\prime} = \frac{dk_r^{ow}}{dS^w}$ and $k_r^{og\prime} = \frac{dk_r^{og}}{dS^g}$.

### Water

To obtain the derivatives of the water relative permeability, equation (B.11) is used:

$$
k_r^w = \frac{(1 - S^w - S^g)k_r^{wo}(S^w) + S^g k_r^{wg}(S^w)}{1 - S^w} \tag{B.31}
$$

The derivatives of the water relative permeability to water and gas saturation are then given by:

$$
\frac{\partial k_r^w}{\partial S^w} = \frac{(1 - S^w)\left[-k_r^{wo}(S^w) + (1 - S^w - S^g)k_r^{wo\prime}(S^w) + S^g k_r^{wg\prime}(S^w)\right] - \left[(1 - S^w - S^g)k_r^{wo}(S^w) + S^g k_r^{wg}(S^w)\right] \cdot (-1)}{(1 - S^w)^2}
$$

$$
= \frac{1}{1 - S^w}\left[-k_r^{wo}(S^w) + (1 - S^w - S^g)k_r^{wo\prime}(S^w) + S^g k_r^{wg\prime}(S^w) + k_r^w(S^w, S^g)\right]
$$

$$
= \frac{(1 - S^w)\left[(1 - S^w - S^g)k_r^{wo\prime}(S^w) + S^g k_r^{wg\prime}(S^w)\right] + S^g\left[k_r^{wg}(S^w) - k_r^{wo}(S^w)\right]}{(1 - S^w)^2} \tag{B.32}
$$

$$
\frac{\partial k_r^w}{\partial S^g} = \frac{-1 \cdot k_r^{wo}(S^w) + k_r^{wg}(S^w)}{1 - S^w}
$$

$$
= \frac{k_r^{wg}(S^w) - k_r^{wo}(S^w)}{1 - S^w} \tag{B.33}
$$

Where $k_r^{wg\prime} = \frac{dk_r^{wg}}{dS^w}$ and $k_r^{wo\prime} = \frac{dk_r^{wo}}{dS^w}$

### Gas

Finally, for the gas relative permeability, equation (B.15) is used:

$$
k_r^g = \frac{(1 - S^w - S^g)k_r^{go}(S^g) + S^w k_r^{gw}(1 - S^g)}{1 - S^g} \tag{B.34}
$$

This means that the following holds for the derivatives of the gas relative permeability:

$$\frac{\partial k_r^g}{\partial S^w} = \frac{1}{1-S^g}\left[-k_r^{go}(S^g)+k_r^{gw}(1-S^g)\right]$$

$$= \frac{k_r^{gw}(1-S^g)-k_r^{go}(S^g)}{1-S^g} \tag{B.35}$$

$$\frac{\partial k_r^g}{\partial S^g} = \frac{(1-S^g)\left[-k_r^{go}(S^g)+(1-S^w-S^g)k_r^{go\prime}(S^g)+S^w k_r^{gw\prime}(1-S^g)\cdot(-1)\right]-\left[(1-S^w-S^g)k_r^{go}(S^g)+S^w k_r^{gw}(1-S^g)\right]\cdot(-1)}{(1-S^g)^2}$$

$$= \frac{1}{1-S^g}\left[-k_r^{go}(S^g)+(1-S^w-S^g)k_r^{go\prime}(S^g)-S^w k_r^{gw\prime}(1-S^g)+k_r^g(S^w,S^g)\right]$$

$$= \frac{(1-S^g)\left[(1-S^w-S^g)k_r^{go\prime}(S^g)-S^w k_r^{gw\prime}(1-S^g)\right]+S^w\left[k_r^{gw}(1-S^g)-k_r^{go}(S^g)\right]}{(1-S^g)^2} \tag{B.36}$$

Where $k_r^{go\prime}=\frac{dk_r^{go}}{dS^g}$ and $k_r^{gw\prime}=\frac{dk_r^{gw}}{dS^w}$.

## B.4.2. Interpolation II

### Oil

To determine the derivatives of the oil relative permeability recall that for interpolation II the following holds, see equation (B.16):

$$k_r^o = \frac{S^w k_r^{ow}(\tilde{S}_o^{II})+S^g k_r^{og}(\tilde{S}_o^{II})}{S^w+S^g} \tag{B.37}$$

where $\tilde{S}_o^{II}=\sqrt{(S^w)^2+(S^g)^2}$, which means that:

$$\frac{\partial \tilde{S}_o^{II}}{\partial S^w} = \frac{1}{2\sqrt{(S^w)^2+(S^g)^2}}\cdot 2S^w = \frac{S^w}{\sqrt{(S^w)^2+(S^g)^2}} = \frac{S^w}{\tilde{S}_o^{II}}$$

$$\frac{\partial \tilde{S}_o^{II}}{\partial S^g} = \frac{1}{2\sqrt{(S^w)^2+(S^g)^2}}\cdot 2S^g = \frac{S^g}{\sqrt{(S^w)^2+(S^g)^2}} = \frac{S^g}{\tilde{S}_o^{II}}$$

Using these expressions, the derivatives of the oil relative permeability to the water and gas saturation are given by:

$$\frac{\partial k_r^o}{\partial S^w} = \frac{(S^w+S^g)\left[k_r^{ow}(\tilde{S}_o^{II})+S^w k_r^{ow\prime}(\tilde{S}_o^{II})\frac{\partial \tilde{S}_o^{II}}{\partial S^w}+S^g k_r^{og\prime}(\tilde{S}_o^{II})\frac{\partial \tilde{S}_o^{II}}{\partial S^w}\right]-\left[S^w k_r^{ow}(\tilde{S}_o^{II})+S^g k_r^{og}(\tilde{S}_o^{II})\right]\cdot 1}{(S^w+S^g)^2}$$

$$= \frac{1}{S^w+S^g}\left[k_r^{ow}(\tilde{S}_o^{II})+S^w k_r^{ow\prime}(\tilde{S}_o^{II})\frac{S^w}{\tilde{S}_o^{II}}+S^g k_r^{og\prime}(\tilde{S}_o^{II})\frac{S^w}{\tilde{S}_o^{II}}-k_r^o(S^w,S^g)\right]$$

$$= \frac{(S^w+S^g)\frac{S^w}{\tilde{S}_o^{II}}\left[S^w k_r^{ow\prime}(\tilde{S}_o^{II})+S^g k_r^{og\prime}(\tilde{S}_o^{II})\right]+S^g\left[k_r^{ow}(\tilde{S}_o^{II})-k_r^{og}(\tilde{S}_o^{II})\right]}{(S^w+S^g)^2} \tag{B.38}$$

$$\frac{\partial k_r^o}{\partial S^g} = \frac{(S^w+S^g)\left[S^w k_r^{ow\prime}(\tilde{S}_o^{II})\frac{\partial \tilde{S}_o^{II}}{\partial S^g}+k_r^{og}(\tilde{S}_o^{II})+S^g k_r^{og\prime}(\tilde{S}_o^{II})\frac{\partial \tilde{S}_o^{II}}{\partial S^g}\right]-\left[S^w k_r^{ow}(\tilde{S}_o^{II})+S^g k_r^{og}(\tilde{S}_o^{II})\right]\cdot 1}{(S^w+S^g)^2}$$

$$= \frac{1}{S^w+S^g}\left[S^w k_r^{ow\prime}(\tilde{S}_o^{II})\frac{S^g}{\tilde{S}_o^{II}}+k_r^{og}(\tilde{S}_o^{II})+S^g k_r^{og\prime}(\tilde{S}_o^{II})\frac{S^g}{\tilde{S}_o^{II}}-k_r^o(S^w,S^g)\right]$$

$$= \frac{(S^w+S^g)\frac{S^g}{\tilde{S}_o^{II}}\left[S^w k_r^{ow\prime}(\tilde{S}_o^{II})+S^g k_r^{og\prime}(\tilde{S}_o^{II})\right]+S^w\left[k_r^{og}(\tilde{S}_o^{II})-k_r^{ow}(\tilde{S}_o^{II})\right]}{(S^w+S^g)^2} \tag{B.39}$$

### Water

To obtain the derivatives of the water relative permeability recall that for interpolation II the following holds, see equation (B.20):

$$k_r^w = \frac{(1-S^w-S^g)k_r^{wo}(1-\tilde{S}_w^{II})+S^g k_r^{wg}(1-\tilde{S}_w^{II})}{1-S^w} \tag{B.40}$$

with $\tilde{S}_w^{II} = \sqrt{(S^o)^2 + (S^g)^2} = \sqrt{1 - 2S^w - 2S^g + 2S^w S^g + (S^w)^2 + 2(S^g)^2}$, so:

$$\frac{\partial \tilde{S}_w^{II}}{\partial S^w} = \frac{1}{2\sqrt{(S^o)^2 + (S^g)^2}}(-2 + 2S^g + 2S^w) = \frac{-1 + S^w + S^g}{\sqrt{(S^o)^2 + (S^g)^2}} = \frac{-S^o}{\sqrt{(S^o)^2 + (S^g)^2}}$$

$$\frac{\partial \tilde{S}_w^{II}}{\partial S^g} = \frac{1}{2\sqrt{(S^w)^2 + (S^g)^2}}(-2 + 2S^w + 4S^g) = \frac{-1 + S^w + 2S^g}{\sqrt{(S^w)^2 + (S^g)^2}} = \frac{S^g - S^o}{\sqrt{(S^o)^2 + (S^g)^2}}$$

Therefore the derivatives of the water relative permeability to water and gas saturation are given by:

$$\frac{\partial k_r^w}{\partial S^w} = \frac{1}{(1-S^w)^2}\left\{(1-S^w)\left[-k_r^{wo}(1-\tilde{S}_w^{II}) + (1-S^w-S^g)k_r^{wo\prime}(1-\tilde{S}_w^{II})\cdot\frac{-\partial \tilde{S}_w^{II}}{\partial S^w} + S^g k_r^{wg\prime}(1-\tilde{S}_w^{II})\cdot\frac{-\partial \tilde{S}_w^{II}}{\partial S^w}\right]\right.$$

$$\left. - \left[(1-S^w-S^g)k_r^{wo}(1-\tilde{S}_w^{II}) + S^g k_r^{wg}(1-\tilde{S}_w^{II})\right]\cdot(-1)\right\}$$

$$= \frac{1}{1-S^w}\left[-k_r^{wo}(1-\tilde{S}_w^{II}) - (1-S^w-S^g)k_r^{wo\prime}(1-\tilde{S}_w^{II})\frac{\partial \tilde{S}_w^{II}}{\partial S^w} - S^g k_r^{wg\prime}(1-\tilde{S}_w^{II})\frac{\partial \tilde{S}_w^{II}}{\partial S^w} + k_r^w(S^w,S^g)\right]$$

$$= \frac{-(1-S^w)\frac{\partial \tilde{S}_w^{II}}{\partial S^w}\left[(1-S^w-S^g)k_r^{wo\prime}(1-\tilde{S}_w^{II}) + S^g k_r^{wg\prime}(1-\tilde{S}_w^{II})\right] + S^g\left[k_r^{wg}(1-\tilde{S}_w^{II}) - k_r^{wo}(1-\tilde{S}_w^{II})\right]}{(1-S^w)^2} \quad \text{(B.41)}$$

$$\frac{\partial k_r^w}{\partial S^g} = \frac{-1\cdot k_r^{wo}(1-\tilde{S}_w^{II}) + (1-S^w-S^g)k_r^{wo\prime}(1-\tilde{S}_w^{II})\frac{-\partial \tilde{S}_w^{II}}{\partial S^g} + k_r^{wg}(1-\tilde{S}_w^{II}) + S^g k_r^{wg\prime}(1-\tilde{S}_w^{II})\frac{-\partial \tilde{S}_w^{II}}{\partial S^g}}{1-S^w}$$

$$= \frac{\frac{-\partial \tilde{S}_w^{II}}{\partial S^g}\left\{(1-S^w-S^g)k_r^{wo\prime}(1-\tilde{S}_w^{II}) + S^g k_r^{wg\prime}(1-\tilde{S}_w^{II})\right\} + k_r^{wg}(1-\tilde{S}_w^{II}) - k_r^{wo}(1-\tilde{S}_w^{II})}{1-S^w} \quad \text{(B.42)}$$

## Gas

Finally, for the gas relative permeability recall that for interpolation II the following holds, see equation (B.24):

$$k_r^g = \frac{(1-S^g-S^w)k_r^{go}(1-\tilde{S}_g^{II}) + S^w k_r^{gw}(\tilde{S}_g^{II})}{1-S^g} \quad \text{(B.43)}$$

with $\tilde{S}_g^{II} = \sqrt{(S^o)^2 + (S^w)^2} = \sqrt{1 - 2S^w - 2S^g + 2S^w S^g + 2(S^w)^2 + (S^g)^2}$, which gives:

$$\frac{\partial \tilde{S}_g^{II}}{\partial S^w} = \frac{1}{2\sqrt{(S^o)^2 + (S^w)^2}}(-2 + 2S^g + 4S^w) = \frac{-1 + 2S^w + S^g}{\sqrt{(S^o)^2 + (S^w)^2}} = \frac{S^w - S^o}{\sqrt{(S^o)^2 + (S^w)^2}}$$

$$\frac{\partial \tilde{S}_g^{II}}{\partial S^g} = \frac{1}{2\sqrt{(S^o)^2 + (S^w)^2}}(-2 + 2S^w + 2S^g) = \frac{-1 + S^w + S^g}{\sqrt{(S^o)^2 + (S^w)^2}} = \frac{-S^o}{\sqrt{(S^o)^2 + (S^w)^2}}$$

This means that the following holds for the derivatives of the gas relative permeability:

$$\frac{\partial k_r^g}{\partial S^w} = \frac{-k_r^{go}(1-\tilde{S}_g^{II}) + (1-S^w-S^g)k_r^{go\prime}(1-\tilde{S}_g^{II})\frac{-\partial \tilde{S}_g^{II}}{\partial S^w} + k_r^{gw}(\tilde{S}_g^{II}) + S^w k_r^{gw\prime}(\tilde{S}_g^{II})\frac{\partial \tilde{S}_g^{II}}{\partial S^w}}{1-S^g}$$

$$= \frac{\frac{\partial \tilde{S}_g^{II}}{\partial S^w}\left[S^w k_r^{gw\prime}(\tilde{S}_g^{II}) - (1-S^w-S^g)k_r^{go\prime}(1-\tilde{S}_g^{II})\right] + k_r^{gw}(\tilde{S}_g^{II}) - k_r^{go}(1-\tilde{S}_g^{II})}{1-S^g} \tag{B.44}$$

$$\frac{\partial k_r^g}{\partial S^g} = \frac{1}{(1-S^g)^2}\left\{(1-S^g)\left[-k_r^{go}(1-\tilde{S}_g^{II}) + (1-S^w-S^g)k_r^{go\prime}(1-\tilde{S}_g^{II})\frac{-\partial \tilde{S}_g^{II}}{\partial S^g} + S^w k_r^{gw\prime}(\tilde{S}_g^{II})\frac{\partial \tilde{S}_g^{II}}{\partial S^g}\right]\right.$$

$$\left. - \left[(1-S^w-S^g)k_r^{go}(1-\tilde{S}_g^{II}) + S^w k_r^{gw}(\tilde{S}_g^{II})\right]\cdot(-1)\right\}$$

$$= \frac{1}{1-S^g}\left[-k_r^{go}(1-\tilde{S}_g^{II}) - (1-S^w-S^g)k_r^{go\prime}(1-\tilde{S}_g^{II})\frac{\partial \tilde{S}_g^{II}}{\partial S^g} + S^w k_r^{gw\prime}(\tilde{S}_g^{II})\frac{\partial \tilde{S}_g^{II}}{\partial S^g} + k_r^g(S^w,S^g)\right]$$

$$= \frac{(1-S^g)\frac{\partial \tilde{S}_g^{II}}{\partial S^g}\left[S^w k_r^{gw\prime}(\tilde{S}_g^{II}) - (1-S^w-S^g)k_r^{go\prime}(1-\tilde{S}_g^{II})\right] + S^w\left[k_r^{gw}(\tilde{S}_g^{II}) - k_r^{go}(1-\tilde{S}_g^{II})\right]}{(1-S^g)^2} \tag{B.45}$$

### B.4.3. Interpolation III

To determine the derivatives of the relative permeabilities, equations (B.25), (B.26) and (B.27) are used:

$$k_r^o(S^w,S^g) = (1-S^w-S^g)k_r^{o,II}(S^w,S^g) + (S^w+S^g)k_r^{o,I}(S^w,S^g)$$

$$k_r^w(S^w,S^g) = S^w k_r^{w,II}(S^w,S^g) + (1-S^w)k_r^{w,I}(S^w,S^g)$$

$$k_r^g(S^w,S^g) = S^g k_r^{g,II}(S^w,S^g) + (1-S^g)k_r^{g,I}(S^w,S^g)$$

Recall that $k_r^{\alpha,I}$ and $k_r^{\alpha,II}$ are used to denote the relative permeability of phase $\alpha$ obtained using interpolation I and interpolation II respectively. This gives the following for the derivatives:

$$\frac{\partial k_r^o}{\partial S^w} = -k_r^{o,II} + (1-S^w-S^g)\frac{\partial k_r^{o,II}}{\partial S^w} + k_r^{o,I} + (S^w+S^g)\frac{\partial k_r^{o,I}}{\partial S^w} \tag{B.46}$$

$$\frac{\partial k_r^o}{\partial S^g} = -k_r^{o,II} + (1-S^w-S^g)\frac{\partial k_r^{o,II}}{\partial S^g} + k_r^{o,I} + (S^w+S^g)\frac{\partial k_r^{o,I}}{\partial S^g} \tag{B.47}$$

$$\frac{\partial k_r^w}{\partial S^w} = k_r^{w,II} + S^w\frac{\partial k_r^{w,II}}{\partial S^w} - k_r^{w,I} + (1-S^w)\frac{\partial k_r^{w,I}}{\partial S^w} \tag{B.48}$$

$$\frac{\partial k_r^w}{\partial S^g} = S^w\frac{\partial k_r^{w,II}}{\partial S^g} + (1-S^w)\frac{\partial k_r^{w,I}}{\partial S^g} \tag{B.49}$$

$$\frac{\partial k_r^g}{\partial S^w} = S^g\frac{\partial k_r^{g,II}}{\partial S^w} + (1-S^g)\frac{\partial k_r^{g,I}}{\partial S^w} \tag{B.50}$$

$$\frac{\partial k_r^g}{\partial S^g} = k_r^{g,II} + S^g\frac{\partial k_r^{g,II}}{\partial S^g} - k_r^{g,I} + (1-S^g)\frac{\partial k_r^{g,I}}{\partial S^g} \tag{B.51}$$

### B.4.4. Derivatives at edges of ternary diagram

At the edges of the ternary diagram it is possible to be more explicit since the two-phase relative permeabilities are known. Recall that Corey-Correlations with zero residual saturations and endpoint equal to one are assumed for all the two-phase relative permeabilities. The derivatives for all phases at all edges for interpolation I and III are given in Table B.1. In this section the derivation of these expressions is worked out in full detail for the OW edge. Note that only the edges will be considered and not the corners, i.e. $0 < S^w, S^o < 1$. The derivation for the expressions on the other two edges is similar and is therefore omitted.

Oil

At the OW edge the gas saturation is zero such that $S^g = 0$ and $S^o = 1 - S^w$. Therefore:

$$\tilde{S}_o^I = S^w + S^g \qquad\qquad = S^w \tag{B.52}$$

$$\tilde{S}_o^{II} = \sqrt{(S^w)^2 + (S^g)^2} = S^w \tag{B.53}$$

Substituting this in the equations (B.7), (B.29) and (B.30) the oil relative permeability and its derivatives using interpolation I reduce to:

$$k_r^{o,I} = k_r^{ow}(S^w) \tag{B.54}$$

$$\frac{\partial k_r^{o,I}}{\partial S^w} = \frac{(S^w + 0)\left[S^w k_r^{ow\prime}(S^w) + 0 \cdot k_r^{og\prime}(S^w)\right] + 0 \cdot \left[k_r^{ow}(S^w) - k_r^{og}(S^w)\right]}{(S^w)^2}$$

$$= k_r^{ow\prime}(S^w) \tag{B.55}$$

$$\frac{\partial k_r^{o,I}}{\partial S^g} = \frac{(S^w + 0)\left[S^w k_r^{ow\prime}(S^w) + 0 \cdot k_r^{og\prime}(S^w)]\right] + S^w \left[k_r^{og}(S^w) - k_r^{ow}(S^w)\right]}{(S^w)^2}$$

$$= k_r^{ow\prime}(S^w) + \frac{1}{S^w}\left[k_r^{og}(S^w) - k_r^{ow}(S^w)\right] \tag{B.56}$$

For interpolation II first note that:

$$\frac{\partial \tilde{S}_o^{II}}{\partial S^w} = \frac{S^w}{\sqrt{(S^w)^2 + 0^2}} = 1$$

$$\frac{\partial \tilde{S}_o^{II}}{\partial S^g} = \frac{0}{\sqrt{(S^w)^2 + 0^2}} = 0$$

Then substituting these expressions and equation (B.53) in equations (B.16), (B.38) and (B.39) gives:

$$k_r^{o,II} = k_r^{ow}(S^w) \tag{B.57}$$

$$\frac{\partial k_r^{o,II}}{\partial S^w} = \frac{(S^w + 0) \cdot 1 \cdot \left[S^w k_r^{ow\prime}(S^w) + 0 \cdot k_r^{og\prime}(S^w)\right] + 0 \cdot \left[k_r^{ow}(S^w) - k_r^{og}(S^w)\right]}{(S^w)^2}$$

$$= k_r^{ow\prime}(S^w) \tag{B.58}$$

$$\frac{\partial k_r^{o,II}}{\partial S^g} = \frac{(S^w + 0) \cdot 0 \cdot \left[S^w k_r^{ow\prime}(S^w) + 0 \cdot k_r^{og\prime}(S^w)\right] + S^w \left[k_r^{og}(S^w) - k_r^{ow}(S^w)\right]}{(S^w)^2}$$

$$= \frac{1}{S^w}\left[k_r^{og}(S^w) - k_r^{ow}(S^w)\right] \tag{B.59}$$

To obtain the behavior of the interpolation III on the OW edge, the expressions for interpolation I and interpolation II are substituted in equations (B.25), (B.46) and (B.47). Therefore:

$$k_r^{o,III} = (1 - S^w)k_r^{o,II} + S^w k_r^{o,I}$$
$$= (1 - S^w)k_r^{ow} + S^w k_r^{ow}$$
$$= k_r^{ow} \tag{B.60}$$

$$\frac{\partial k_r^{o,III}}{\partial S^w} = -k_r^{o,II} + (1 - S^w)\frac{\partial k_r^{o,II}}{\partial S^w} + k_r^{o,I} + S^w \frac{\partial k_r^{o,I}}{\partial S^w}$$
$$= -k_r^{ow} + (1 - S^w)k_r^{ow\prime}(S^w) + k_r^{ow} + S^w k_r^{ow\prime}(S^w)$$
$$= k_r^{ow\prime}(S^w) \tag{B.61}$$

$$\frac{\partial k_r^{o,III}}{\partial S^g} = -k_r^{o,II} + (1 - S^w)\frac{\partial k_r^{o,II}}{\partial S^g} + k_r^{o,I} + S^w \frac{\partial k_r^{o,I}}{\partial S^g}$$
$$= -k_r^{ow} + (1 - S^w)\frac{1}{S^w}\left[k_r^{og}(S^w) - k_r^{ow}(S^w)\right] + k_r^{ow} + S^w \left\{k_r^{ow\prime}(S^w) + \frac{1}{S^w}\left[k_r^{og}(S^w) - k_r^{ow}(S^w)\right]\right\}$$
$$= S^w k_r^{ow\prime}(S^w) + \frac{1}{S^w}\left[k_r^{og}(S^w) - k_r^{ow}(S^w)\right] \tag{B.62}$$

## Water

A similar derivations holds for the water relative permeability. On the OW edge the following holds:

$$\tilde{S}_w^I = S^o + S^g \qquad = S^0 \qquad = 1 - S^w \tag{B.63}$$

$$\tilde{S}_w^{II} = \sqrt{(S^o)^2 + (S^g)^2} = \sqrt{(1 - S^w)^2} = 1 - S^w \tag{B.64}$$

Substituting equation (B.63) into the expression for the water relative permeability and its derivatives, see equations (B.11), (B.32) and (B.33) gives:

$$
\begin{aligned}
k_r^{w,I} &= \frac{(1 - S^w - 0)\,k_r^{wo}(S^w) + 0 \cdot k_r^{wg}(S^w)}{1 - S^w} \\
&= k_r^{wo}(S^w)
\end{aligned}
\tag{B.65}
$$

$$
\begin{aligned}
\frac{\partial k_r^{w,I}}{\partial S^w} &= \frac{(1 - S^w)\left[(1 - S^w - 0)\,k_r^{wo\prime}(S^w) + 0 \cdot k_r^{wg\prime}(S^w)\right] + 0 \cdot \left[k_r^{wg}(S^w) - k_r^{wo}(S^w)\right]}{(1 - S^w)^2} \\
&= k_r^{wo\prime}(S^w)
\end{aligned}
\tag{B.66}
$$

$$
\frac{\partial k_r^{w,I}}{\partial S^g} = \frac{1}{1 - S^w}\left[k_r^{wg}(S^w) - k_r^{wo}(S^w)\right]
\tag{B.67}
$$

For interpolation II, first note that:

$$
\frac{\partial \tilde{S}_w^{II}}{\partial S^w} = \frac{-S^o}{\sqrt{(S^o)^2 + 0^2}} = \frac{-(1 - S^w)}{1 - S^w} \quad = -1
$$

$$
\frac{\partial \tilde{S}_w^{II}}{\partial S^g} = \frac{0 - S^o}{\sqrt{(S^o)^2 + 0^2}} = \frac{0 - (1 - S^w)}{1 - S^w} = -1
$$

Then, substituting the above expressions and equation (B.64) in equation (B.20), (B.41) and (B.42) gives:

$$
\begin{aligned}
k_r^{w,II} &= k_r^{wo}(1 - \tilde{S}_w^{II}) \\
&= k_r^{wo}(S^w)
\end{aligned}
\tag{B.68}
$$

$$
\begin{aligned}
\frac{\partial k_r^{w,II}}{\partial S^w} &= \frac{-(1 - S^w) \cdot -1 \cdot \left[(1 - S^w - 0)\,k_r^{wo\prime}(1 - \tilde{S}_w^{II}) + 0 \cdot k_r^{wg\prime}(1 - \tilde{S}_w^{II})\right] + 0 \cdot \left[k_r^{wg}(1 - \tilde{S}_w^{II}) - k_r^{wo}(1 - \tilde{S}_w^{II})\right]}{(1 - S^w)^2} \\
&= k_r^{wo\prime}(S^w)
\end{aligned}
\tag{B.69}
$$

$$
\begin{aligned}
\frac{\partial k_r^{w,II}}{\partial S^g} &= \frac{1}{1 - S^w}\left[--1\left\{(1 - S^w - 0)\,k_r^{wo\prime}(1 - \tilde{S}_w^{II}) + 0 \cdot k_r^{wg\prime}(1 - \tilde{S}_w^{II})\right\} + k_r^{wg}(1 - \tilde{S}_w^{II}) - k_r^{wo}(1 - \tilde{S}_w^{II})\right] \\
&= k_r^{wo\prime}(S^w) + \frac{1}{1 - S^w}\left[k_r^{wg}(S^w) - k_r^{wo}(S^w)\right]
\end{aligned}
\tag{B.70}
$$

$$\tag{B.71}$$

To obtain the behavior of the interpolation III on the OW edge, the expressions for interpolation I and interpolation II are substituted in equations (B.26), (B.48) and (B.49). Therefore:

$$
\begin{aligned}
k_r^{w,III} &= S^w k_r^{w,II} + (1 - S^w) k_r^{w,I} \\
&= S^w k_r^{wo} + (1 - S^w) k_r^{wo} \\
&= k_r^{wo}
\end{aligned}
\tag{B.72}
$$

$$
\begin{aligned}
\frac{\partial k_r^{w,III}}{\partial S^w} &= k_r^{w,II} + S^w \frac{\partial k_r^{w,II}}{\partial S^w} - k_r^{w,I} + (1 - S^w) \frac{\partial k_r^{w,I}}{\partial S^w} \\
&= k_r^{wo}(S^w) + S^w k_r^{wo\prime}(S^w) - k_r^{wo}(S^w) + (1 - S^w) k_r^{wo\prime}(S^w) \\
&= k_r^{wo\prime}(S^w)
\end{aligned}
\tag{B.73}
$$

$$
\begin{aligned}
\frac{\partial k_r^{w,III}}{\partial S^g} &= S^w \frac{\partial k_r^{w,II}}{\partial S^g} + (1 - S^w) \frac{\partial k_r^{w,I}}{\partial S^g} \\
&= S^w \left[k_r^{wo\prime}(S^w) + \frac{1}{1 - S^w}\left(k_r^{wg}(S^w) - k_r^{wo}(S^w)\right)\right] + (1 - S^w) \frac{1}{1 - S^w}\left[k_r^{wg}(S^w) - k_r^{wo}(S^w)\right] \\
&= S^w k_r^{wo\prime}(S^w) + \frac{1}{1 - S^w}\left[k_r^{wg}(S^w) - k_r^{wo}(S^w)\right]
\end{aligned}
\tag{B.74}
$$

### Gas

Finally, the derivatives of the gas relative permeability on the OW edge are determined. On the OW edge the following holds:

$$\tilde{S}_g^I = S^o + S^w \qquad = 1 - S^w + S^w \qquad = 1 \tag{B.75}$$

$$\tilde{S}_g^{II} = \sqrt{(S^o)^2 + (S^w)^2} = \sqrt{(1-S^w)^2 + (S^w)^2} = \sqrt{2(S^w)^2 - 2S^w + 1} \tag{B.76}$$

Note that $k_r^{go}(0) = k_r^{gw}(1) = k_r^{go\prime}(0) = k_r^{gw\prime}(1) = 0$ since Corey-correlations with zero residual saturations and endpoints equal to one are assumed for the two-phase relative permeabilities. Substituting equation (B.75) in equations (B.15), (B.35) and (B.36) gives:

$$k_r^{g,I} = \frac{(1-S^w)k_r^{go}(0) + S^w k_r^{gw}(1-0)}{1-0} \qquad = 0 \tag{B.77}$$

$$\frac{\partial k_r^{g,I}}{\partial S^w} = \frac{k_r^{gw}(1-0) - k_r^{go}(0)}{1-0} \qquad = 0 \tag{B.78}$$

$$\frac{\partial k_r^{g,I}}{\partial S^g} = \frac{(1-0)\left[(1-S^w)k_r^{go\prime}(0) - S^w k_r^{gw\prime}(1-0)\right] + S^w\left[k_r^{gw}(1-0) - k_r^{go}(0)\right]}{(1-0)^2} = 0 \tag{B.79}$$

For interpolation II, first note that:

$$\frac{\partial \tilde{S}_g^{II}}{\partial S^w} = \frac{S^w - S^o}{\sqrt{(S^o)^2 + (S^w)^2}}, \quad = \frac{S^w - (1-S^w)}{\sqrt{2(S^w)^2 - 2S^w + 1}} = \frac{2S^w - 1}{\sqrt{2(S^w)^2 - 2S^w + 1}}$$

$$\frac{\partial \tilde{S}_g^{II}}{\partial S^g} = \frac{-S^o}{\sqrt{(S^o)^2 + (S^w)^2}}, \quad = \frac{-(1-S^w)}{\sqrt{2(S^w)^2 - 2S^w + 1}}$$

Substituting this in equations (B.24), (B.44) and (B.45) gives:

$$k_r^{g,II} = \frac{(1-S^w-0)k_r^{go}(1-\tilde{S}_g^{II}) + S^w k_r^{gw}(\tilde{S}_g^{II})}{1-0}$$
$$= (1-S^w)k_r^{go}(1-\tilde{S}_g^{II}) + S^w k_r^{gw}(\tilde{S}_g^{II}) \tag{B.80}$$

$$\frac{\partial k_r^{g,II}}{\partial S^w} = \frac{1}{1-0}\left[\frac{2S^w-1}{\sqrt{2(S^w)^2 - 2S^w + 1}}\left\{S^w k_r^{gw\prime}(\tilde{S}_g^{II}) - (1-S^w-0)k_r^{go\prime}(1-\tilde{S}_g^{II})\right\} + k_r^{gw}(\tilde{S}_g^{II}) - k_r^{go}(1-\tilde{S}_g^{II})\right]$$
$$= \frac{2S^w-1}{\sqrt{2(S^w)^2 - 2S^w + 1}}\left[S^w k_r^{gw\prime}(\tilde{S}_g^{II}) - (1-S^w)k_r^{go\prime}(1-\tilde{S}_g^{II})\right] + k_r^{gw}(\tilde{S}_g^{II}) - k_r^{go}(1-\tilde{S}_g^{II}) \tag{B.81}$$

$$\frac{\partial k_r^{g,II}}{\partial S^g} = \frac{(1-0)\frac{-(1-S^w)}{\sqrt{2(S^w)^2-2S^w+1}}\left[S^w k_r^{gw\prime}(\tilde{S}_g^{II}) - (1-S^w-0)k_r^{go\prime}(1-\tilde{S}_g^{II})\right] + S^w\left[k_r^{gw}(\tilde{S}_g^{II}) - k_r^{go}(1-\tilde{S}_g^{II})\right]}{(1-0)^2}$$
$$= \frac{-(1-S^w)}{\sqrt{2(S^w)^2 - 2S^w + 1}}\left[S^w k_r^{gw\prime}(\tilde{S}_g^{II}) - (1-S^w)k_r^{go\prime}(1-\tilde{S}_g^{II})\right] + S^w\left[k_r^{gw}(\tilde{S}_g^{II}) - k_r^{go}(1-\tilde{S}_g^{II})\right] \tag{B.82}$$

Where $\tilde{S}_g^{II}$ is given by equation (B.76). Note that $k_r^{g,II}$ is in general not equal to zero, meaning that the second interpolation does not result in a zero relative permeability when the saturation goes to zero.
To obtain the behavior of the interpolation III on the OW edge, the expressions for interpolation I and inter-

polation II are substituted in equations (B.27), (B.50) and (B.51). Therefore:

$$
\begin{aligned}
k_r^{g,III} &= 0 \cdot k_r^{g,II} + (1-0)k_r^{g,I} \\
&= k_r^{g,I} \\
&= 0
\end{aligned}
\tag{B.83}
$$

$$
\begin{aligned}
\frac{\partial k_r^{g,III}}{\partial S^w} &= 0 \cdot \frac{\partial k_r^{g,II}}{\partial S^w} + (1-0)\frac{\partial k_r^{g,I}}{\partial S^w} \\
&= \frac{\partial k_r^{g,I}}{\partial S^w} \\
&= 0
\end{aligned}
\tag{B.84}
$$

$$
\begin{aligned}
\frac{\partial k_r^{g,III}}{\partial S^g} &= k_r^{g,II} + 0 \cdot \frac{\partial k_r^{g,II}}{\partial S^g} - k_r^{g,I} + (1-0)\frac{\partial k_r^{g,I}}{\partial S^g} \\
&= k_r^{g,II} - k_r^{g,I} + \frac{\partial k_r^{g,I}}{\partial S^g} \\
&= (1-S^w)k_r^{go}(1-\tilde{S}_g^{II}) + S^w k_r^{gw}(\tilde{S}_g^{II})
\end{aligned}
\tag{B.85}
$$

Table B.1: Relative permeability and its derivatives with respect to water and gas saturation of all phases on the edges of the ternary diagram. All derivatives are expressed in terms of the two-phase relative permeabilities $k_r^{\alpha_1 \alpha_2}$ on each edge.

| | | **I** | **III** |
|---|---|---|---|
| **OW edge** | oil | $k_r^o = k_r^{ow}(S^w)$ | $k_r^o = k_r^{ow}(S^w)$ |
| | | $\frac{\partial k_r^o}{\partial S^w} = k_r^{ow\prime}(S^w)$ | $\frac{\partial k_r^o}{\partial S^w} = k_r^{ow\prime}(S^w)$ |
| | | $\frac{\partial k_r^o}{\partial S^g} = k_r^{ow\prime}(S^w) + \frac{1}{S^w}\left[k_r^{og}(S^w) - k_r^{ow}(S^w)\right]$ | $\frac{\partial k_r^o}{\partial S^g} = S^w k_r^{ow\prime}(S^w) + \frac{1}{S^w}\left[k_r^{og}(S^w) - k_r^{ow}(S^w)\right]$ |
| | water | $k_r^w = k_r^{wo}(S^w)$ | $k_r^w = k_r^{wo}(S^w)$ |
| | | $\frac{\partial k_r^w}{\partial S^w} = k_r^{wo\prime}(S^w)$ | $\frac{\partial k_r^w}{\partial S^w} = k_r^{wo\prime}(S^w)$ |
| | | $\frac{\partial k_r^w}{\partial S^g} = \frac{1}{1-S^w}\left[k_r^{wg}(S^w) - k_r^{wo}(S^w)\right]$ | $\frac{\partial k_r^w}{\partial S^g} = S^w k_r^{wo\prime}(S^w) + \frac{1}{1-S^w}\left[k_r^{wg}(S^w) - k_r^{wo}(S^w)\right]$ |
| | gas | $k_r^g = 0$ | $k_r^g = 0$ |
| | | $\frac{\partial k_r^g}{\partial S^w} = 0$ | $\frac{\partial k_r^g}{\partial S^w} = 0$ |
| | | $\frac{\partial k_r^g}{\partial S^g} = 0$ | $\frac{\partial k_r^g}{\partial S^g} = (1-S^w)k_r^{go}(1-\tilde{S}_g^{II}) + S^w k_r^{gw}(\tilde{S}_g^{II})$ |
| | | | with $\tilde{S}_g^{II} = \sqrt{2(S^w)^2 - 2S^w + 1}$ |
| **OG edge** | oil | $k_r^o = k_r^{og}(S^g)$ | $k_r^o = k_r^{og}(S^g)$ |
| | | $\frac{\partial k_r^o}{\partial S^w} = k_r^{og\prime}(S^g) + \frac{1}{S^g}\left[k_r^{ow}(S^g) - k_r^{og}(S^g)\right]$ | $\frac{\partial k_r^o}{\partial S^w} = S^g k_r^{og\prime}(S^g) + \frac{1}{S^g}\left[k_r^{ow}(S^g) - k_r^{og}(S^g)\right]$ |
| | | $\frac{\partial k_r^o}{\partial S^g} = k_r^{og\prime}(S^g)$ | $\frac{\partial k_r^o}{\partial S^g} = k_r^{og\prime}(S^g)$ |
| | water | $k_r^w = 0$ | $k_r^w = 0$ |
| | | $\frac{\partial k_r^w}{\partial S^w} = 0$ | $\frac{\partial k_r^w}{\partial S^w} = (1-S^g)k_r^{wo}(1-\tilde{S}_w^{II}) + S^g k_r^{wg}(1-\tilde{S}_w^{II})$ |
| | | | with $\tilde{S}_w^{II} = \sqrt{2(S^g)^2 - 2S^g + 1}$ |
| | | $\frac{\partial k_r^w}{\partial S^g} = 0$ | $\frac{\partial k_r^w}{\partial S^g} = 0$ |
| | gas | $k_r^g = k_r^{go}(S^g)$ | $k_r^g = k_r^{go}(S^g)$ |
| | | $\frac{\partial k_r^g}{\partial S^w} = \frac{1}{1-S^g}\left[k_r^{gw}(1-S^g) - k_r^{go}(S^g)\right]$ | $\frac{\partial k_r^g}{\partial S^w} = S^g k_r^{go\prime}(S^g) + \frac{1}{1-S^g}\left[k_r^{gw}(1-S^g) - k_r^{go}(S^g)\right]$ |
| | | $\frac{\partial k_r^g}{\partial S^g} = k_r^{go\prime}(S^g)$ | $\frac{\partial k_r^g}{\partial S^g} = k_r^{go\prime}(S^g)$ |
| **WG edge** | oil | $k_r^o = 0$ | $k_r^o = 0$ |
| | | $\frac{\partial k_r^o}{\partial S^w} = 0$ | $\frac{\partial k_r^o}{\partial S^w} = -S^w k_r^{ow}(\tilde{S}_o^{II}) - S^g k_r^{og}(\tilde{S}_o^{II})$ |
| | | $\frac{\partial k_r^o}{\partial S^g} = 0$ | $\frac{\partial k_r^o}{\partial S^g} = -S^w k_r^{ow}(\tilde{S}_o^{II}) - S^g k_r^{og}(\tilde{S}_o^{II})$ |
| | | | with $\tilde{S}_o^{II} = \sqrt{2(S^w)^2 - 2S^w + 1} = \sqrt{2(S^g)^2 - 2S^g + 1}$ |
| | water | $k_r^w = k_r^{wg}(S^w)$ | $k_r^w = k_r^{wg}(S^w)$ |
| | | $\frac{\partial k_r^w}{\partial S^w} = k_r^{wg\prime}(S^w) + \frac{1}{1-S^w}\left[k_r^{wg}(S^w) - k_r^{wo}(S^w)\right]$ | $\frac{\partial k_r^w}{\partial S^w} = (1-S^w)k_r^{wg\prime}(S^w) + \frac{1}{1-S^w}\left[k_r^{wg}(S^w) - k_r^{wo}(S^w)\right]$ |
| | | $\frac{\partial k_r^w}{\partial S^g} = \frac{1}{1-S^w}\left[k_r^{wg}(S^w) - k_r^{wo}(S^w)\right]$ | $\frac{\partial k_r^w}{\partial S^g} = -S^w k_r^{wg\prime}(S^w) + \frac{1}{1-S^w}\left[k_r^{wg}(S^w) - k_r^{wo}(S^w)\right]$ |
| | gas | $k_r^g = k_r^{gw}(1-S^g)$ | $k_r^g = k_r^{gw}(1-S^g)$ |
| | | $\frac{\partial k_r^g}{\partial S^w} = \frac{1}{1-S^g}\left[k_r^{gw}(1-S^g) - k_r^{go}(S^g)\right]$ | $\frac{\partial k_r^g}{\partial S^w} = S^g k_r^{gw\prime}(1-S^g) + \frac{1}{1-S^g}\left[k_r^{gw}(1-S^g) - k_r^{go}(S^g)\right]$ |
| | | $\frac{\partial k_r^g}{\partial S^g} = -k_r^{gw\prime}(1-S^g) + \frac{1}{1-S^g}\left[k_r^{gw}(1-S^g) - k_r^{go}(S^g)\right]$ | $\frac{\partial k_r^g}{\partial S^g} = -(1-S^g)k_r^{gw\prime}(1-S^g) + \frac{1}{1-S^g}\left[k_r^{gw}(1-S^g) - k_r^{go}(S^g)\right]$ |

$$C$$
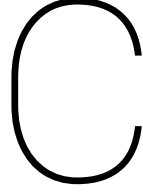
# Eigenvectors on the edges of the ternary diagram for interpolation I and III

In this appendix the direction of both the fast eigenvector and the slow eigenvector along the three edges of the ternary diagram are looked at for interpolation I and III. For both interpolations the flow reduces to two-phase flow on the edges of the ternary diagram. This means that to each edge one of the eigenvectors must be parallel. In this appendix it is determined for every edge whether the fast or the slow eigenvector is parallel to that edge. Corey-correlations with zero residual saturation and endpoints equal to one are assumed for all two-phase relative permeabilities in order to use the results from Table B.1. Furthermore, it is assumed that interpolation I or interpolation III is used to obtain the three-phase relative permeabilities for water, oil and gas. Only the edges of the ternary diagram will be looked at and not the corners, i.e. $0 < S^w, S^o < 1$ on the OW edge, $0 < S^g, S^o < 1$ on the OG edge and $0 < S^w, S^g < 1$ on the WG edge

First recall equation (1.12) which gives the Jacobian matrix of the governing system:

$$\frac{\partial f}{\partial S} := \begin{pmatrix} f_w^w & f_g^w \\ f_w^g & f_g^g \end{pmatrix} \tag{C.1}$$

And recall that the eigenvalues are given by (3.3):

$$\eta = \frac{f_w^w + f_g^g \pm \sqrt{(f_w^w + f_g^g)^2 - 4(f_w^w f_g^g - f_g^w f_w^g)}}{2}$$

$$= \frac{f_w^w + f_g^g \pm \sqrt{(f_w^w - f_g^g)^2 + 4 f_g^w f_w^g}}{2} \tag{C.2}$$

If the eigenvalues are real, $\eta_+ \geq \eta_-$ such that $\eta_+ := \eta_f$ is the eigenvalue corresponding to the fast family and $\eta_- := \eta_s$ is the eigenvalue corresponding tot the slow family. Recall that the fractional flow $f^\alpha$ of phase $\alpha$ is given by:

$$f^\alpha = \frac{\lambda^\alpha}{\lambda_T}$$

Therefore the following holds for the derivatives of the fractional flow functions:

$$f_w^w = \frac{1}{\lambda_T^2} \left[ \lambda_T \lambda_w^w - \lambda^w \lambda_{T,w} \right] \tag{C.3}$$

$$f_g^w = \frac{1}{\lambda_T^2} \left[ \lambda_T \lambda_g^w - \lambda^w \lambda_{T,g} \right] \tag{C.4}$$

$$f_w^g = \frac{1}{\lambda_T^2} \left[ \lambda_T \lambda_w^g - \lambda^g \lambda_{T,w} \right] \tag{C.5}$$

$$f_g^g = \frac{1}{\lambda_T^2} \left[ \lambda_T \lambda_g^g - \lambda^g \lambda_{T,g} \right] \tag{C.6}$$

89

For the right eigenvector $r = \left( r^w \ r^g \right)^T$ the following holds (Juanes and Patzek, 2004a)

$$\frac{r^w}{r^g} = \frac{f_g^w}{\eta - f_w^w} = \frac{\eta - f_g^g}{f_w^g} \tag{C.7}$$

## C.1. OW edge

Note that the right eigenvector is parallel to the OW edge if $r = (1 \ 0)^T$. In other words, the right eigenvector is parallel to the OW edge if:

$$\frac{r^g}{r^w} = \frac{\eta - f_w^w}{f_g^w} = \frac{f_w^g}{\eta - f_g^g} = 0 \tag{C.8}$$

### C.1.1. Interpolation I

From Table B.1 it can be concluded that on the OW edge the mobilities and its derivatives for oil and water are non-zero in general and that the following holds for the gas mobility:

$$\lambda^g = \lambda_w^g = \lambda_g^g = 0 \tag{C.9}$$

such that:

$$\lambda_T = \lambda^o + \lambda^w \quad \text{and} \quad \lambda_{T,w} = \lambda_w^o + \lambda_w^w \quad \text{and} \quad \lambda_{T,g} = \lambda_g^o + \lambda_g^w \tag{C.10}$$

This gives:

$$f_g^w = \frac{1}{\lambda_T^2} \left[ \left( \lambda^o + \lambda^w \right) \lambda_g^w - \lambda^w \left( \lambda_g^o + \lambda_g^w \right) \right]$$

$$= \frac{1}{\lambda_T^2} \left[ \lambda^o \lambda_g^w - \lambda^w \lambda_g^o \right]$$

$$f_w^g = \frac{1}{\lambda_T^2} \left[ \left( \lambda^o + \lambda^w \right) \cdot 0 - 0 \cdot \left( \lambda_w^o + \lambda_w^w \right) \right]$$

$$= 0$$

So $f_w^g = 0$ on the OW edge whereas in general $f_g^w \neq 0$ on the OW edge. From equation (C.8) it follows that the right eigenvector will be parallel to the OW edge if:

$$\eta - f_w^w = 0 \tag{C.11}$$

Substituting the mobilities, i.e. equations (C.9) and (C.10), in the derivatives of the fractional flow functions, i.e. equations (C.3) and (C.6), gives:

$$f_w^w = \frac{1}{\lambda_T^2} \left[ \left( \lambda^o + \lambda^w \right) \lambda_w^w - \lambda^w \left( \lambda_w^o + \lambda_w^w \right) \right]$$

$$= \frac{1}{\lambda_T^2} \left[ \lambda^o \lambda_w^w - \lambda^w \lambda_w^o \right]$$

$$f_g^g = \frac{1}{\lambda_T^2} \left[ \left( \lambda^o + \lambda^w \right) \cdot 0 - 0 \cdot \left( \lambda_g^o + \lambda_g^w \right) \right]$$

$$= 0$$

So $f_g^g = 0$ on the OW edge whereas $f_w^w > 0$ on the OW edge since $\lambda_w^w > 0$ and $\lambda_w^o < 0$ on the OW edge. Substituting $f_g^g = 0$ and $f_w^g = 0$ in equation (C.2) the eigenvalues reduce to:

$$\eta = \frac{f_w^w + 0 \pm \sqrt{\left( f_w^w - 0 \right)^2 + 4 f_g^w \cdot 0}}{2} \tag{C.12}$$

$$= \frac{1}{2} \left[ f_w^w \pm \sqrt{\left( f_w^w \right)^2} \right] \tag{C.13}$$

$$= \frac{1}{2} \left[ f_w^w \pm f_w^w \right] \tag{C.14}$$

Therefore $\eta_f = f_w^w$ and $\eta_s = 0$. Looking at equation (C.11), which determines when the right eigenvector is parallel to the OW edge, it follows that:

$$\eta_f - f_w^w = 0 \tag{C.15}$$

$$\eta_s - f_w^w = -f_w^w \tag{C.16}$$

Since $f_w^w > 0$ on the OW edge, the fast eigenvector is parallel to the OW edge for interpolation I.

### C.1.2. Interpolation III

For interpolation III the derivation is similar to that of interpolation I, but some of the derivatives of the gas mobility are slightly different. From Table B.1 it follows that in general:

$$\lambda^g = \lambda_w^g = 0 \quad \text{and} \quad \lambda_g^g \neq 0 \tag{C.17}$$

such that:

$$\lambda_T = \lambda^o + \lambda^w \quad \text{and} \quad \lambda_{T,w} = \lambda_w^o + \lambda_w^w \quad \text{and} \quad \lambda_{T,g} = \lambda_g^o + \lambda_g^w + \lambda_g^g \tag{C.18}$$

This gives:

$$f_g^w = \frac{1}{\lambda_T^2} \left[ \left( \lambda^o + \lambda^w \right) \lambda_g^w - \lambda^w \left( \lambda_g^o + \lambda_g^w + \lambda_g^g \right) \right]$$

$$= \frac{1}{\lambda_T^2} \left[ \lambda^o \lambda_g^w - \lambda^w \left( \lambda_g^o + \lambda_g^g \right) \right]$$

$$f_w^g = \frac{1}{\lambda_T^2} \left[ \left( \lambda^o + \lambda^w \right) \cdot 0 - 0 \cdot \left( \lambda_w^o + \lambda_w^w \right) \right]$$

$$= 0$$

So $f_w^g = 0$ on the OW edge whereas in general $f_g^w \neq 0$ on the OW edge, which was also the case for interpolation I. Therefore equation (C.8) gives that the right eigenvector will be parallel to the OW edge if:

$$\eta - f_w^w = 0 \tag{C.19}$$

Substituting the mobilities, i.e. equations (C.17) and (C.18), in the the fractional flow functions, i.e. equations (C.3) and (C.6), gives:

$$f_w^w = \frac{1}{\lambda_T^2} \left[ \left( \lambda^o + \lambda^w \right) \lambda_w^w - \lambda^w \left( \lambda_w^o + \lambda_w^w \right) \right]$$

$$= \frac{1}{\lambda_T^2} \left[ \lambda^o \lambda_w^w - \lambda^w \lambda_w^o \right]$$

$$f_g^g = \frac{1}{\lambda_T^2} \left[ \left( \lambda^o + \lambda^w \right) \lambda_g^g - 0 \cdot \left( \lambda_g^o + \lambda_g^w + \lambda_g^g \right) \right]$$

$$= \frac{1}{\lambda_T^2} \left[ \lambda^o + \lambda^w \right] \lambda_g^g$$

So in general $f_w^w \neq 0$ and $f_g^g \neq 0$ on the OW edge, whereas for interpolation I it holds that $f_g^g = 0$. Substituting $f_w^g = 0$ in equation (C.2) the eigenvalues reduce to:

$$\eta = \frac{f_w^w + f_g^g \pm \sqrt{\left( f_w^w - f_g^g \right)^2 + 4 f_g^w \cdot 0}}{2} \tag{C.20}$$

$$= \frac{1}{2} \left[ f_w^w + f_g^g \pm \sqrt{\left( f_w^w - f_g^g \right)^2} \right] \tag{C.21}$$

$$= \begin{cases} \frac{1}{2} \left[ f_w^w + f_g^g \pm \left( f_w^w - f_g^g \right) \right] & \text{if } f_w^w - f_g^g > 0 \\ \frac{1}{2} \left[ f_w^w + f_g^g \pm - \left( f_w^w - f_g^g \right) \right] & \text{if } f_w^w - f_g^g < 0 \\ \frac{1}{2} \left[ f_w^w + f_g^g \right] & \text{if } f_w^w - f_g^g = 0 \end{cases} \tag{C.22}$$

Note that $f_w^w - f_g^g = 0$ if and only if $f_w^w = f_g^g$. Therefore:

$$
\eta_f = \begin{cases} f_w^w & \text{if } f_w^w - f_g^g > 0 \\ f_g^g & \text{if } f_w^w - f_g^g < 0 \\ \frac{1}{2}\left[f_w^w + f_g^g\right] = f_w^w = f_g^g & \text{if } f_w^w - f_g^g = 0 \end{cases} \quad \text{and} \quad \eta_s = \begin{cases} f_g^g & \text{if } f_w^w - f_g^g > 0 \\ f_w^w & \text{if } f_w^w - f_g^g < 0 \\ \frac{1}{2}\left[f_w^w + f_g^g\right] = f_w^w = f_g^g & \text{if } f_w^w - f_g^g = 0 \end{cases}
$$

Looking at equation (C.19), which determine when the right eigenvector is parallel to the OW edge, it follows that:

$$
\eta_f - f_w^w = \begin{cases} 0 & \text{if } f_w^w - f_g^g > 0 \\ f_g^g - f_w^w & \text{if } f_w^w - f_g^g < 0 \\ 0 & \text{if } f_w^w - f_g^g = 0 \end{cases} \quad \text{and} \quad \eta_s = \begin{cases} f_g^g - f_w^w & \text{if } f_w^w - f_g^g > 0 \\ 0 & \text{if } f_w^w - f_g^g < 0 \\ 0 & \text{if } f_w^w - f_g^g = 0 \end{cases} \tag{C.23}
$$

Therefore, the following conditions to determine which eigenvector is parallel to the OW edge hold:

- If $f_w^w - f_g^g > 0$ then the fast-family eigenvector is parallel to the OW edge.

- If $f_w^w - f_g^g < 0$ then the slow-family eigenvector is parallel to the OW edge.

- If $f_w^w - f_g^g = 0$ then both eigenvectors are parallel to the OW edge.

## C.2. OG edge

The right eigenvector $r$ is parallel to the OG edge if $r = (0\ 1)^T$. In other words, the right eigenvector is parallel to the OG edge if:

$$
\frac{r^w}{r^g} = \frac{f_g^w}{\eta - f_w^w} = \frac{\eta - f_g^g}{f_w^g} = 0 \tag{C.24}
$$

### C.2.1. Interpolation I

From Table B.1 it follows that on the OG edge the mobilities of gas and oil and their derivatives are in general non-zero. From this table it can be seen that the following holds for the water mobility and derivatives of the mobility:

$$
\lambda^w = \lambda_w^w = \lambda_g^w = 0 \tag{C.25}
$$

such that:

$$
\lambda_T = \lambda^o + \lambda^g \quad \text{and} \quad \lambda_{T,w} = \lambda_w^o + \lambda_w^g \quad \text{and} \quad \lambda_{T,g} = \lambda_g^o + \lambda_g^g \tag{C.26}
$$

This means that the following holds for the fractional flow functions:

$$
\begin{aligned}
f_g^w &= \frac{1}{\lambda_T^2}\left[\left(\lambda^o + \lambda^g\right)\cdot 0 - 0\cdot\left(\lambda_g^o + \lambda_g^g\right)\right] \\
&= 0 \\
f_w^g &= \frac{1}{\lambda_T^2}\left[\left(\lambda^o + \lambda^g\right)\lambda_w^g - \lambda^g\left(\lambda_w^o + \lambda_w^g\right)\right] \\
&= \frac{1}{\lambda_T^2}\left[\lambda^o\lambda_w^g - \lambda^g\lambda_w^o\right]
\end{aligned}
$$

So $f_g^w = 0$ on the OG edge whereas in general $f_w^g \neq 0$ on the OG edge. From equation (C.24) it then follows that the right eigenvector will be parallel to the OG edge if:

$$
\eta - f_g^g = 0 \tag{C.27}
$$

Substituting the mobilities, i.e. equations (C.25) and (C.26), in the the fractional flow functions, i.e. equations (C.3) and (C.6), gives:

$$f_w^w = \frac{1}{\lambda_T^2} \left[ \left( \lambda^o + \lambda^g \right) \cdot 0 - 0 \cdot \left( \lambda_w^o + \lambda_w^g \right) \right]$$

$$= 0$$

$$f_g^g = \frac{1}{\lambda_T^2} \left[ \left( \lambda^o + \lambda^g \right) \lambda_g^g - \lambda^g \left( \lambda_g^o + \lambda_g^g \right) \right]$$

$$= \frac{1}{\lambda_T^2} \left[ \lambda^o \lambda_g^g - \lambda^g \lambda_g^o \right]$$

So $f_w^w = 0$ on the OG edge whereas $f_g^g > 0$ on the OG edge since $\lambda_g^g > 0$ and $\lambda_g^o < 0$ on the OG edge. Substituting $f_w^w = 0$ and $f_g^w = 0$ in equation (C.2) the eigenvalues reduce to:

$$\eta = \frac{0 + f_g^g \pm \sqrt{(0 - f_g^g)^2 + 4 f_w^g \cdot 0}}{2} \tag{C.28}$$

$$= \frac{1}{2} \left[ f_g^g \pm \sqrt{(-f_g^g)^2} \right] \tag{C.29}$$

$$= \frac{1}{2} \left[ f_g^g \pm f_g^g \right] \tag{C.30}$$

Therefore $\eta_f = f_g^g$ and $\eta_s = 0$. Looking at equation (C.27), which determines when the right eigenvector is parallel to the OG edge, it follows that :

$$\eta_f - f_g^g = 0 \tag{C.31}$$

$$\eta_s - f_g^g = -f_g^g \tag{C.32}$$

Since $f_g^g > 0$ on the OG edge, the fast eigenvector is parallel to the OG edge for interpolation I.

### C.2.2. Interpolation III

For interpolation III the derivation is similar to that of interpolation I, but some of the derivatives of the water mobility are slightly different. From Table B.1 it can be seen that in general:

$$\lambda^w = \lambda_g^w = 0 \quad \text{and} \quad \lambda_w^w \neq 0 \tag{C.33}$$

such that:

$$\lambda_T = \lambda^o + \lambda^g \quad \text{and} \quad \lambda_{T,w} = \lambda_w^o + \lambda_w^g + \lambda_w^w \quad \text{and} \quad \lambda_{T,g} = \lambda_g^o + \lambda_g^g \tag{C.34}$$

This gives:

$$f_g^w = \frac{1}{\lambda_T^2} \left[ \left( \lambda^o + \lambda^g \right) \cdot 0 - 0 \cdot \left( \lambda_g^o + \lambda_g^g \right) \right]$$

$$= 0$$

$$f_w^g = \frac{1}{\lambda_T^2} \left[ \left( \lambda^o + \lambda^g \right) \lambda_w^g - \lambda^g \left( \lambda_w^o + \lambda_w^w + \lambda_w^g \right) \right]$$

$$= \frac{1}{\lambda_T^2} \left[ \lambda^o \lambda_w^g - \lambda^g \left( \lambda_w^o + \lambda_w^w \right) \right]$$

So $f_w^w = 0$ on the OG edge whereas in general $f_w^g \neq 0$ on the OG edge, which was also the case for interpolation I. Therefore equation (C.24) again gives that the right eigenvector will be parallel to the OG edge if:

$$\eta - f_g^g = 0 \tag{C.35}$$

Substituting the mobilities, i.e. equations (C.33) and (C.34), in the the fractional flow functions, i.e. equations (C.3) and (C.6), gives:

$$
\begin{aligned}
f_w^w &= \frac{1}{\lambda_T^2} \left[ \left( \lambda^o + \lambda^g \right) \lambda_w^w - 0 \cdot \left( \lambda_w^o + \lambda_w^w + \lambda_w^g \right) \right] \\
&= \frac{1}{\lambda_T^2} \left[ \lambda^o + \lambda^g \right] \lambda_w^w \\
f_g^g &= \frac{1}{\lambda_T^2} \left[ \left( \lambda^o + \lambda^g \right) \lambda_g^g - \lambda^g \left( \lambda_g^o + \lambda_g^g \right) \right] \\
&= \frac{1}{\lambda_T^2} \left[ \lambda^o \lambda_g^g - \lambda^g \lambda_g^o \right]
\end{aligned}
$$

So in general $f_w^w \neq 0$ and $f_g^g \neq 0$ on the OG edge, whereas for interpolation I $f_w^w = 0$ holds. Substituting $f_g^w = 0$ in equation (C.2) the eigenvalues reduce to:

$$
\eta = \frac{f_w^w + f_g^g \pm \sqrt{\left( f_w^w - f_g^g \right)^2 + 4 f_w^g \cdot 0}}{2} \tag{C.36}
$$

$$
= \frac{1}{2} \left[ f_w^w + f_g^g \pm \sqrt{\left( f_w^w - f_g^g \right)^2} \right] \tag{C.37}
$$

$$
= \begin{cases}
\frac{1}{2} \left[ f_w^w + f_g^g \pm \left( f_w^w - f_g^g \right) \right] & \text{if } f_w^w - f_g^g > 0 \\
\frac{1}{2} \left[ f_w^w + f_g^g \pm -\left( f_w^w - f_g^g \right) \right] & \text{if } f_w^w - f_g^g < 0 \\
\frac{1}{2} \left[ f_w^w + f_g^g \right] & \text{if } f_w^w - f_g^g = 0
\end{cases} \tag{C.38}
$$

Note that $f_w^w - f_g^g = 0$ if and only if $f_w^w = f_g^g$. Therefore:

$$
\eta_f = \begin{cases}
f_w^w & \text{if } f_w^w - f_g^g > 0 \\
f_g^g & \text{if } f_w^w - f_g^g < 0 \\
\frac{1}{2} \left[ f_w^w + f_g^g \right] = f_w^w = f_g^g & \text{if } f_w^w - f_g^g = 0
\end{cases}
\quad \text{and} \quad
\eta_s = \begin{cases}
f_g^g & \text{if } f_w^w - f_g^g > 0 \\
f_w^w & \text{if } f_w^w - f_g^g < 0 \\
\frac{1}{2} \left[ f_w^w + f_g^g \right] = f_w^w = f_g^g & \text{if } f_w^w - f_g^g = 0
\end{cases}
$$

Looking at equation (C.35), which determines when the right eigenvector is parallel to the OG edge, it follows that:

$$
\eta_f - f_g^g = \begin{cases}
f_w^w - f_g^g & \text{if } f_w^w - f_g^g > 0 \\
0 & \text{if } f_w^w - f_g^g < 0 \\
0 & \text{if } f_w^w - f_g^g = 0
\end{cases}
\quad \text{and} \quad
\eta_s - f_g^g = \begin{cases}
0 & \text{if } f_w^w - f_g^g > 0 \\
f_w^w - f_g^g & \text{if } f_w^w - f_g^g < 0 \\
0 & \text{if } f_w^w - f_g^g = 0
\end{cases} \tag{C.39}
$$

This means that the following conditions to determine which eigenvector is parallel to the OG edge are obtained:

- If $f_w^w - f_g^g < 0$ then the fast-family eigenvector is parallel to the OG edge.

- If $f_w^w - f_g^g > 0$ then the slow-family eigenvector is parallel to the OG edge.

- If $f_w^w - f_g^g = 0$ then both eigenvectors are parallel to the OG edge.

## C.3. WG edge

The right eigenvector $r$ is parallel to the WG edge if $r = (1 \ -1)^T$. In other words, the right eigenvector is parallel to the WG edge if:

$$
\frac{r^w}{r^g} = \frac{f_g^w}{\eta - f_w^w} = \frac{\eta - f_g^g}{f_w^g} = -1 \tag{C.40}
$$

### C.3.1. Interpolation I

From Table B.1 it follows that on the WG edge the mobilities of gas and water and their derivatives are in general non-zero. From this table it can also be seen that the following holds for the oil mobility and derivatives of the mobility:

$$\lambda^o = \lambda_w^o = \lambda_g^o = 0 \tag{C.41}$$

such that:

$$\lambda_T = \lambda^w + \lambda^g \quad \text{and} \quad \lambda_{T,w} = \lambda_w^w + \lambda_w^g \quad \text{and} \quad \lambda_{T,g} = \lambda_g^w + \lambda_g^g \tag{C.42}$$

This means that the following holds for the fractional flow functions:

$$f_g^w = \frac{1}{\lambda_T^2} \left[ \left( \lambda^w + \lambda^g \right) \lambda_g^w - \lambda^w \left( \lambda_g^w + \lambda_g^g \right) \right]$$

$$= \frac{1}{\lambda_T^2} \left[ \lambda^g \lambda_g^w - \lambda^w \lambda_g^g \right]$$

$$f_w^g = \frac{1}{\lambda_T^2} \left[ \left( \lambda^w + \lambda^g \right) \lambda_w^g - \lambda^g \left( \lambda_w^w + \lambda_w^g \right) \right]$$

$$= \frac{1}{\lambda_T^2} \left[ \lambda^w \lambda_w^g - \lambda^g \lambda_w^w \right]$$

So in general $f_g^w \neq 0$ and $f_w^g \neq 0$ on the WG edge. From equation (C.40) it follows that the right eigenvector will be parallel to the WG edge if:

$$\eta - f_g^g + f_w^g = 0 \tag{C.43}$$

Substituting the mobilities, i.e. equations (C.41) and (C.42), in the the fractional flow functions, i.e. equations (C.3) and (C.6), gives:

$$f_w^w = \frac{1}{\lambda_T^2} \left[ \left( \lambda^w + \lambda^g \right) \lambda_w^w - \lambda^w \left( \lambda_w^w + \lambda_w^g \right) \right]$$

$$= \frac{1}{\lambda_T^2} \left[ \lambda^g \lambda_w^w - \lambda^w \lambda_w^g \right]$$

$$= -f_w^g$$

$$f_g^g = \frac{1}{\lambda_T^2} \left[ \left( \lambda^w + \lambda^g \right) \lambda_g^g - \lambda^g \left( \lambda_g^w + \lambda_g^g \right) \right]$$

$$= \frac{1}{\lambda_T^2} \left[ \lambda^w \lambda_g^g - \lambda^g \lambda_g^w \right]$$

$$= -f_g^w$$

So $f_w^g = -f_w^w$ and $f_g^w = -f_g^g$ on the WG edge. Substituting this in the first expression of equation (C.2) the eigenvalues reduce to:

$$\eta = \frac{f_w^w + f_g^g \pm \sqrt{\left( f_w^w + f_g^g \right)^2 - 4 \left( f_w^w f_g^g - (-f_w^w)(-f_g^g) \right)}}{2} \tag{C.44}$$

$$= \frac{1}{2} \left[ f_w^w + f_g^g \pm \sqrt{\left( f_w^w + f_g^g \right)^2} \right] \tag{C.45}$$

$$= \frac{1}{2} \left[ f_w^w + f_g^g \pm \left( f_w^w + f_g^g \right) \right] \tag{C.46}$$

Here it was used that $f_w^w + f_g^g \geq 0$ since $\lambda_w^w, \lambda_g^g > 0$ and $\lambda_w^g, \lambda_g^w < 0$ on the WG edge. Therefore $\eta_f = f_w^w + f_g^g$ and $\eta_s = 0$. Looking at equation (C.43), which determines when the right eigenvector is parallel to the WG

edge, and using that $f_w^g = -f_w^w$ and $f_g^w = -f_g^g$ the following holds:

$$
\begin{aligned}
\eta_f - f_g^g + f_w^g &= f_w^w + f_g^g - f_g^g + f_w^g \\
&= f_w^w + f_w^g \\
&= -f_w^g + f_w^g \\
&= 0
\end{aligned}
\tag{C.47}
$$

$$
\begin{aligned}
\eta_s - f_g^g + f_w^g &= -f_g^g + f_w^g \\
&= f_g^w + f_w^g
\end{aligned}
\tag{C.48}
$$

Since $f_g^w + f_w^g = -f_g^g - f_w^w < 0$ on the WG edge, the fast eigenvector is parallel to the WG edge for interpolation I.

## C.3.2. Interpolation III

For interpolation III the derivation is similar to that of interpolation I, but some of the derivatives of the oil mobility are slightly different. From Table B.1 it follows that in general:

$$
\lambda^o = 0 \quad \text{and} \quad \lambda_w^w \neq 0 \quad \text{and} \quad \lambda_g^w \neq 0
\tag{C.49}
$$

such that:

$$
\lambda_T = \lambda^w + \lambda^g \quad \text{and} \quad \lambda_{T,w} = \lambda_w^o + \lambda_w^g + \lambda_w^w \quad \text{and} \quad \lambda_{T,g} = \lambda_g^o + \lambda_g^g + \lambda_g^w
\tag{C.50}
$$

This means that:

$$
\begin{aligned}
f_g^w &= \frac{1}{\lambda_T^2}\left[\left(\lambda^w + \lambda^g\right)\lambda_g^w - \lambda^w\left(\lambda_g^o + \lambda_g^w + \lambda_g^g\right)\right] \\
&= \frac{1}{\lambda_T^2}\left[\lambda^g \lambda_g^w - \lambda^w\left(\lambda_g^o + \lambda_g^g\right)\right] \\
&= \frac{1}{\lambda_T^2}\left[\lambda^g \lambda_g^w - \lambda^w \lambda_g^g\right] - \frac{1}{\lambda_T^2}\lambda^w \lambda_g^o
\end{aligned}
\tag{C.51}
$$

$$
\begin{aligned}
f_w^g &= \frac{1}{\lambda_T^2}\left[\left(\lambda^w + \lambda^g\right)\lambda_w^g - \lambda^g\left(\lambda_w^o + \lambda_w^w + \lambda_w^g\right)\right] \\
&= \frac{1}{\lambda_T^2}\left[\lambda^w \lambda_w^g - \lambda^g\left(\lambda_w^o + \lambda_w^w\right)\right] \\
&= \frac{1}{\lambda_T^2}\left[\lambda^w \lambda_w^g - \lambda^g \lambda_w^w\right] - \frac{1}{\lambda_T^2}\lambda^g \lambda_w^o
\end{aligned}
\tag{C.52}
$$

So in general $f_g^w \neq 0$ and $f_w^g \neq 0$ on the WG edge. From equation (C.40) it follows that the right eigenvector will be parallel to the WG edge if:

$$
\eta - f_g^g + f_w^g = 0
\tag{C.53}
$$

Substituting the mobilities, i.e. equations (C.49) and (C.50), in the the fractional flow functions, i.e. equations (C.3) and (C.6), gives:

$$
\begin{aligned}
f_w^w &= \frac{1}{\lambda_T^2}\left[\left(\lambda^w + \lambda^g\right)\lambda_w^w - \lambda^w\left(\lambda_w^o + \lambda_w^w + \lambda_w^g\right)\right] \\
&= \frac{1}{\lambda_T^2}\left[\lambda^g \lambda_w^w - \lambda^w\left(\lambda_w^o + \lambda_w^g\right)\right] \\
&= \frac{1}{\lambda_T^2}\left[\lambda^g \lambda_w^w - \lambda^w \lambda_w^g\right] - \frac{1}{\lambda_T^2}\lambda^w \lambda_w^o
\end{aligned}
\tag{C.54}
$$

$$
\begin{aligned}
f_g^g &= \frac{1}{\lambda_T^2}\left[\left(\lambda^w + \lambda^g\right)\lambda_g^g - \lambda^g\left(\lambda_g^o + \lambda_g^w + \lambda_g^g\right)\right] \\
&= \frac{1}{\lambda_T^2}\left[\lambda^w \lambda_g^g - \lambda^g\left(\lambda_g^o + \lambda_g^w\right)\right] \\
&= \frac{1}{\lambda_T^2}\left[\lambda^w \lambda_g^g - \lambda^g \lambda_g^w\right] - \frac{1}{\lambda_T^2}\lambda^g \lambda_g^o
\end{aligned}
\tag{C.55}
$$

So in general $f_w^w \neq 0$ and $f_g^g \neq 0$ on the WG edge. Furthermore, comparing equation (C.51) with equation (C.55) and comparing equation (C.52) with (C.54) gives:

$$f_g^w = -f_g^g - \frac{1}{\lambda_T^2} \lambda_g^o \left( \lambda^w + \lambda^g \right) \tag{C.56}$$

$$f_w^g = -f_w^w - \frac{1}{\lambda_T^2} \lambda_w^o \left( \lambda^w + \lambda^g \right) \tag{C.57}$$

Table B.1 gives that $\frac{\partial k_r^o}{\partial S^w} = \frac{\partial k_r^o}{\partial S^g}$ for interpolation III on the WG edge, and therefore $\lambda_w^o = \lambda_g^o$ on the WG edge. This means that:

$$
\begin{aligned}
f_g^w f_w^g &= f_g^g f_w^w + f_g^g \frac{1}{\lambda_T^2} \lambda_w^o \left( \lambda^w + \lambda^g \right) + f_w^w \frac{1}{\lambda_T^2} \lambda_g^o \left( \lambda^w + \lambda^g \right) + \frac{1}{\lambda_T^4} \lambda_g^o \lambda_w^o \left( \lambda^w + \lambda^g \right)^2 \\
&= f_g^g f_w^w + \frac{1}{\lambda_T^2} \lambda_w^o \left( \lambda^w + \lambda^g \right) \left( f_w^w + f_g^g \right) + \frac{1}{\lambda_T^4} \left( \lambda_w^o \right)^2 \left( \lambda^w + \lambda^g \right)^2 \\
&= f_g^g f_w^w + \frac{1}{\lambda_T} \lambda_w^o \left( f_w^w + f_g^g \right) + \frac{1}{\lambda_T^2} \left( \lambda_w^o \right)^2 \tag{C.58}
\end{aligned}
$$

where in the last step it was used that $\lambda_T = \lambda^g + \lambda^w$ on the WG edge. Substituting this in the first expression of equation (C.2) gives:

$$
\begin{aligned}
\eta &= \frac{f_w^w + f_g^g \pm \sqrt{\left( f_w^w + f_g^g \right)^2 - 4\left[ f_w^w f_g^g - \left( f_g^g f_w^w + \frac{1}{\lambda_T} \lambda_w^o \left( f_w^w + f_g^g \right) + \frac{1}{\lambda_T^2} \left( \lambda_w^o \right)^2 \right) \right]}}{2} \\
&= \frac{1}{2} \left[ f_w^w + f_g^g \pm \sqrt{\left( f_w^w + f_g^g \right)^2 + 4\frac{1}{\lambda_T} \lambda_w^o \left( f_w^w + f_g^g \right) + 4\frac{1}{\lambda_T^2} \left( \lambda_w^o \right)^2} \right] \\
&= \frac{1}{2} \left[ f_w^w + f_g^g \pm \sqrt{\left( \left( f_w^w + f_g^g \right) + 2\frac{1}{\lambda_T} \left( \lambda_w^o \right) \right)^2} \right] \\
&= \begin{cases} \frac{1}{2} \left[ f_w^w + f_g^g \pm \left( f_w^w + f_g^g + 2\frac{1}{\lambda_T} \lambda_w^o \right) \right] & \text{if } f_w^w + f_g^g + 2\frac{1}{\lambda_T} \lambda_w^o > 0 \\ \frac{1}{2} \left[ f_w^w + f_g^g \pm - \left( f_w^w + f_g^g + 2\frac{1}{\lambda_T} \lambda_w^o \right) \right] & \text{if } f_w^w + f_g^g + 2\frac{1}{\lambda_T} \lambda_w^o < 0 \\ \frac{1}{2} \left[ f_w^w + f_g^g \right] & \text{if } f_w^w + f_g^g + 2\frac{1}{\lambda_T} \lambda_w^o = 0 \end{cases} \tag{C.59}
\end{aligned}
$$

Which gives the following for the large and small eigenvalues:

$$
\eta_f = \begin{cases} f_w^w + f_g^g + \frac{1}{\lambda_T} \lambda_w^o & \text{if } f_w^w + f_g^g + 2\frac{1}{\lambda_T} \lambda_w^o > 0 \\ -\frac{1}{\lambda_T} \lambda_w^o & \text{if } f_w^w + f_g^g + 2\frac{1}{\lambda_T} \lambda_w^o < 0 \\ \frac{1}{2} \left[ f_w^w + f_g^g \right] & \text{if } f_w^w + f_g^g + 2\frac{1}{\lambda_T} \lambda_w^o = 0 \end{cases} \quad \text{and} \quad \eta_s = \begin{cases} \frac{1}{\lambda_T} \lambda_w^o & \text{if } f_w^w + f_g^g + 2\frac{1}{\lambda_T} \lambda_w^o > 0 \\ f_w^w + f_g^g + \frac{1}{\lambda_T} \lambda_w^o & \text{if } f_w^w + f_g^g + 2\frac{1}{\lambda_T} \lambda_w^o < 0 \\ \frac{1}{2} \left[ f_w^w + f_g^g \right] & \text{if } f_w^w + f_g^g + 2\frac{1}{\lambda_T} \lambda_w^o = 0 \end{cases} \tag{C.60}
$$

Substituting $\lambda_w^o = \lambda_g^o$ and $\lambda_T = \lambda^w + \lambda^g$ in equations (C.56) and (C.57) gives:

$$f_g^w = -f_g^g - \frac{1}{\lambda_T} \lambda_w^o$$

$$f_w^g = -f_w^w - \frac{1}{\lambda_T} \lambda_w^o$$

Looking at equation (C.53), which determines when the right eigenvector is parallel to the WG edge, it follows that:

$$
\begin{aligned}
\eta_f - f_g^g + f_w^g &= f_w^w + \frac{1}{\lambda_T} \lambda_w^o + f_w^g \\
&= -f_w^g + f_w^g \\
&= 0 \\
\eta_s - f_g^g + f_w^g &= -\frac{1}{\lambda_T} \lambda_w^o - f_g^g + f_w^g \\
&= f_g^w + f_w^g
\end{aligned}
$$

if $f_w^w + f_g^g + 2\frac{1}{\lambda_T}\lambda_w^o > 0$. In the case $f_w^w + f_g^g + 2\frac{1}{\lambda_T}\lambda_w^o < 0$ equation (C.53) gives:

$$\eta_f - f_g^g + f_w^g = -\frac{1}{\lambda_T}\lambda_w^o - f_g^g + f_w^g$$

$$= f_g^w + f_w^g$$

$$\eta_s - f_g^g + f_w^g = f_w^w + \frac{1}{\lambda_T}\lambda_w^o + f_w^g$$

$$= -f_w^g + f_w^g$$

$$= 0$$

Note that $f_w^w + f_g^g + 2\frac{1}{\lambda_T}\lambda_w^o = 0$ if and only if $f_w^w + f_g^g = -2\frac{1}{\lambda_T}\lambda_w^o$. Therefore, in the case that $f_w^w + f_g^g + 2\frac{1}{\lambda_T}\lambda_w^o = 0$ the eigenvalues reduce to $\eta_f = \eta_s = -\frac{1}{\lambda_T}\lambda_w^o$. Substituting this in equation (C.53) gives:

$$\eta_f - f_g^g + f_w^g = \eta_s - f_g^g + f_w^g = -\frac{1}{\lambda_T}\lambda_w^o - f_g^g + f_w^g$$

$$= -\frac{1}{\lambda_T}\lambda_w^o - f_g^g - f_w^w - \frac{1}{\lambda_T}\lambda_w^o$$

$$= -2\frac{1}{\lambda_T}\lambda_w^o - (f_g^g + f_w^w)$$

$$= -2\frac{1}{\lambda_T}\lambda_w^o + 2\frac{1}{\lambda_T}\lambda_w^o$$

$$= 0$$

This means that the following conditions to determine which eigenvector is parallel to the WG edge are obtained:

- If $f_w^w + f_g^g + 2\frac{1}{\lambda_T}\lambda_w^o < 0$ then the fast-family eigenvector is parallel to the WG edge.

- If $f_w^w + f_g^g + 2\frac{1}{\lambda_T}\lambda_w^o > 0$ then the slow-family eigenvector is parallel to the WG edge.

- If $f_w^w + f_g^g + 2\frac{1}{\lambda_T}\lambda_w^o = 0$ then both eigenvectors are parallel to the WG edge.

# Bibliography

M. Akhlaghinia, F. Torabi, and C.W. Chan. Experimental investigation of temperature effect on three-phase relative permeability isoperms in heavy oil systems. *Fuel*, 118:281–290, 2014.

A.H. Alizadeh and M. Piri. Three-phase flow in porous media: A review of experimental studies on relative permeability. *Rev. Geophys.*, 52:468–521, 2014. doi: 10.1002/2013RG000433.

A.V. Azevedo and D. Marchesin. Multiple viscous solutions for systems of conservation laws. *Transactions of the American Mathematical Society*, 347:3061–3077, 1995.

A.V. Azevedo, D. Marchesin, B. Plohr, and K. Zumbrum. Capillary instability in models for three-phase flow. *Zeitschrift für angewandte Mathematik und Physik*, 53:713–746, 2002.

A.V. Azevedo, A.J. De Souza, F Furtado, D Marchesin, and B Plohr. The solution by the wave curve method of three-phase flow in virgin reservoirs. *Transport in Porous Media*, 83:99–125, 2010. doi: 10.1007/s11242-009-9508-9.

K. Aziz and A. Settari. *Petroleum Reservoir Simulation*. Applied Science Publisher LTD, 1979.

L.E. Baker. Three-phase relative permeability correlations. *SPE Conference Paper*, 1988. doi: 10.2118/17369-MS.

J.B. Bell, J.A. Trangenstein, and G.R. Shubin. Conservation laws of mixed type describing three-phase flow in porous media. *SIAM Journal on Applied Mathematics*, 46:1000–1017, 1986.

S. Čanić. Nonexistence of riemann solutions for a quadratic model deriving from petroleum engineering. *Nonlinear Analysis:Real World Applications*, 4:373–408, 2003.

A.H. Falls and W.M. Schulte. Theory of three-component, three-phase displacement in porous media. *SPE Reservoir Engineering*, 1992.

F.J. Fayers. Extension of stone's method 1 and conditions for real characteristics in three-phase flow. *SPE Reservoir Engineering*, 1989.

R.E. Guzmán and F.J. Fayers. Mathematical properties of three-phase flow equation. *SPE journal*, 2, 1997a.

R.E. Guzmán and F.J. Fayers. Solutions to the three-phase buckley-leverett problem. *SPE journal*, 2, 1997b.

H. Holden. On the riemann problem for a prototype of a mixed type conservation law. *Communications on Pure and Applied Mathematics*, 40:229–264, 1987. doi: 10.1002/cpa.3160400206.

L. Holden. On the strict hyperbolicity of the buckley-leverett equations for three-phase flow in a porous medium. *SIAM Journal on Applied Mathematics*, 50:667–682, 1990.

E.L. Isaacon, D. Marchesin, B.J. Plohr, and J.B. Temple. Multiphase flow models with singular riemann problems. *Mat.Aplic.Comp.*, 11:147–166, 1992.

E.L. Isaacson, D. Marchesin, and B.J. Plohr. Transitional waves for conservation laws. *SIAM J. Math. Anal.*, 21:837–866, 1990.

M. D. Jackson and M.J. Blunt. Elliptic regions and stable solutions for three-phase flow in porous media. *Transport in Porous Media*, 48:249–269, 2002.

R. Juanes and T.W. Patzek. Relative permeability for strictly hyperbolic models of three-phase flow in porous media. *Transport in Porous Media*, 57:125–152, 2004a.

R. Juanes and T.W. Patzek. Analytical solution to the riemann problem of three-phase flow in porous media. *Transport in Porous Media*, 55:47–70, 2004b.

B.L. Keyfitz. Admissibility conditions for shocks in conservation laws that change type. *SIAM. J. Math. Anal.*, 22:1284–1292, 1991.

A. Kianinejad and D.A. DiCarlo. Three-phase oil relative permeability in water-wet media: A comprehensive study. *Transport in Porous Media*, 112:665–687, 2016. doi: 10.1007/s11242-016-0669-z.

L.W. Lake, R.T. Johns, W.R. Rossen, and G.A. Pope. *Fundamentals of Enhanced Oil Recovery*. Society of Petroleum Engineers, 2014.

R.J. LeVeque. *Finite Volume Methods for Hyperbolic Problems*. Cambridge University Press, 2002.

T.P. Liu. The riemann problem for general 2x2 conservation laws. *Trans. Amer. Math. Soc.*, 199:89–112, 1974.

W. Lü, Q. Liu, Z. Zhang, D. Ma, K. Wu, and Z. Leng. Measurement of three-phase relative permeabilities. *Petrol. Explor. Develop.*, 39:758–763, 2012.

D. Marchesin and B.J. Plohr. Wave structure in wag recovery. *SPE journal*, 2001.

H.B. Medeiros. Stable hyperbolic singularities for three-phase flow models in oil reservoir simulation. *Acta Applicandae Mathematicae*, 28:135–159, 1992.

M. Shearer. Loss of strict hyperbolicity of the buckley-leverett equations for three phase flow in a porous medium. In *Numerical Simulation in Oil Recovery*, volume 11 of *The IMA Volumes in Mathematics and Its Applications*, pages 263–283, New York, 1988. Springer-Verlag.

M. Shearer and J.A. Trangenstein. Loss of real characteristics for models of three-phase flow in a porous medium. *Tranport in Porous Media*, 4:499–525, 1989.

M. Shearer, D.G. Schaeffer, D. Marchesin, and P.L. Paes-Leme. Solution of the riemann problem for a prototype $2 \times 2$ system of non-strictly hyperbolic conservation laws. *Archive for Rational Mechanics and Analysis*, 97:229–320, 1987.

H.L. Stone. Probability model for estimating three-phase relative permeability. *Journal of Petroleum Technology*, 1970.

H.L. Stone. Estimation of three-phase relative permeability and residual oil data. *Journal of Canadian Petroleum Technology*, 1973.

J.A. Trangenstein. Three-phase flow with gravity. In *Current Progress in Hyperbolic Systems: Riemann Problems and Computations*, volume 100 of *Contemporary Mathematics*, pages 147–159. American Mathematical Society, 1989.